Signalling circuitry controlling fungal virulence in the rice blast fungus *Magnaporthe oryzae*

Submitted by Míriam Osés-Ruiz

to the University of Exeter as a thesis for the degree of
Doctor of Philosophy in Biological Sciences
September 2014

I certify that all material in this thesis which is not my own work has been identified and that no material has previously been submitted and approved for the award of a degree by this or any other University.

Míriam Osés-Ruiz

ABSTRACT

Rice blast disease is caused by the filamentous ascomycete fungus *Magnaporthe oryzae* and is the most destructive disease of cultivated rice. The pathogen elaborates a specialized infection structure called the appressorium. The morphological and physiological transitions that lead to appressorium formation of *M. oryzae* are stimulated through perception of environmental signals and are tightly regulated by cell cycle checkpoints. External stimuli are internalized by a variety of intracellular MAP kinase signaling pathways, and the major pathway regulating appressorium morphogenesis and plant infection is the Pmk1 MAP kinase signaling pathway. The central kinase, Pmk1, is required for appressorium morphogenesis and the homeobox and C2/H2 Zn-finger domain transcription factor, called Mst12, is required for appressorium formation and tissue invasion. The Mst12 null mutant is able to form melanised appressoria, but it is non-pathogenic. To understand the mechanism of appressorium morphogenesis and penetration peg formation, genome-wide comparative transcriptional profiling analysis was performed for the *Δpmk1* and *Δmst12* mutant using RNA-seq and HiSeq 2000 sequencing. This thesis reports the identification of gene sets regulated by the Pmk1 signalling pathway and defines the sub-set of these genes regulated by Mst12. I show that a hierarchy of transcription factors is likely to operate downstream of Pmk1 to regulate the main processes required for appressorium morphogenesis and plant infection. I also report the role of Mst12 in cytoskeletal re-organisation and show that it is necessary for septin-dependent F-actin polymerisation at the base on the appressorium prior to plant infection. This is consistent with the major transcriptional changes observed by RNA-seq. The thesis also reports experiments that strongly

suggest that appressorium mediated plant penetration is regulated by an S-phase checkpoint which operates independently of the conventional DNA damage and repair response, and the Cds1 and Chk1 checkpoint kinases. Transcriptional profiling results are consistent with the S-phase checkpoint operating downstream of the Pmk1 MAP kinase signalling pathway. An integrated model for the operation of the Pmk1/Mst12 signalling pathways and the hierarchical control of appressorium morphogenesis in the rice blast fungus is presented.

Table of Contents

List of Figures

List of Tables

Acknowledgements

I would first like to thank Marie Curie Actions for providing me with the funding to carry out this research and the opportunity of attending high standard scientific courses, conferences and workshops during my PhD. I would also like to thank to all my colleges and PIs of the ARIADNE consortium for sharing this experience with me, professionally and personally.

I would like to thank my supervisor Nick Talbot for everything that he has done for me. I am extremely grateful to him for providing me with this great opportunity, for the support, freedom and encouragement, the scientific discussions and for letting me learn from one of the best scientists I have ever met. Gracias por todo Nick.

All the things I have learned these last 4 years they have been possible thanks to all the professionals and laboratory colleagues from whom I learned so much from. I would first like to thank Mick Kershaw whose support, encouragement and friendship have been really important to me since the very early times in Exeter. Thanks also to Darren Soanes for all the support with the bioinformatics part and Tina Penn to take care of the lab. Special thanks also to Marta de Torres-Zabala, Yasin Dagdas, Wasin Salkukoo, Lauren Ryder and Magdalena Martin-Urdiroz who are great colleagues and have helped me very much at various stages during my PhD. I would also like to thank all the past and current member of the Halpin Lab including George, Xia, Nick Tongue, Romain, Tom, Termizi, Min, Mohammad, Yogesh, Magdalena Basciewicz, Muhammad Badaruddin, Vincent, David, Antonio, Angus and Barbara, to the rest of members of lab 301, and to members of Ken Hayne's lab and Gero Steinberg's lab for his help.

Many thanks also to my good friends in Exeter, who have made my time here really special. Special thanks to Sofia for being my rock, to Dan for all the fun moments and to Garou for being there since the early days. Thanks to my "ibericas", Magdalena and Laura, for make me laugh so hard. Also to Afsoon, Trupti, Joana, Eugenia, Nuria and Kae, and my "salsa familia", who made my days happy, for all the fun and for making me feel in my second home.

I have also to thank my people back home. Thanks to my university friends, “Agrogolfos”, for all the great moments and to my Wageningen friends, who I have missed so much during this time. I wish also to thank my girls in Pamplona. To Maite for our twenty years of friendship, to Enara for being always there, to Carol for all her love, to Marta for all the fun, and especially to Vio, from which was really hard to get separated from after all the things we have shared together.

Finally, my special thanks to my mum, Ana, and my sisters, Claudia and Amaia, because they are the greatest thing for me. Thanks to my mum for being my best friend, and for her patience, effort and support. Thanks to my amazing sisters, because I am so proud of them and they are the music of my life. And last but not least, thanks to Hector, for everything. Thanks for supporting me with this decision and for all your love. Thanks to the four of you that always believed in me, even in the moments I didn’t. I could not have done this without you.

Abbreviations

bp	base pair
cAMP	cyclic 3', 5'-adenosine monophosphate
cDNA	complementary deoxyribonucleic acid
CM	complete medium
CTAB	hexadecyltrimethylammonium bromide
℃	degrees Celcius
ds cDNA	double strand complementary deoxyribonucleic acid
DNA	deoxyribonucleic acid
EDTA	ethylenediaminetetraacetic acid
GFP	green fluorescent protein
g	grams
gL^{-1}	grams per litre
Kb	kilobase
HU	hydroxyurea
L	litre
µg	microgram
µL	microlitre
µm	micrometre
mM	millimolar
M	molar
MAPK	mitogen-activated protein kinase
mod_lfc	moderated log2 fold change value
mRNA	messenger ribonucleic acid
nt	nucleotide
ORF	open-reading frame
p-adj	adjusted p-value
PCR	polymerase chain reaction
RFP	red fluorescent protein
RNA	ribonucleic acid
RNase	ribonuclease
ROS	reactive oxygen species
Rpm	revolutions per minute
v/v	volume to volume
w/v	weight per volume

1 General Introduction

1.1 Global Food Security

In order to feed the growing world population expansion, which will be 9 billion by 2050, global food production has to increase at least three-fold over the next three decades (Godfray *et al.,* 2010). It is estimated that at least 800 million of the world's population live with insufficient nutrition and at least 10% of the world's food crop production is lost due to plant diseases and infection (Strange and Scott, 2005). One of the most world's most important crops is rice (*Oryza sativa*) upon which half of the world's population's relies (Strange and Scott, 2005), and which supplies 23% of the total calorific intake of humankind. Global rice production is 874 million tonnes per annum (FAO Figures 2012-13) each year, but as the world population grows, it is predicted that rice yields will have to double by 2050 in order to meet increasing demand, and projected population growth, particularly across Asia (Godfray *et al.,* 2010).

Among the most devastating and economically important plant diseases worldwide is rice blast disease. Rice blast is caused by the heterothallic ascomycete fungus *Magnaporthe oryzae* (Couch) Barr [anamorph: *Pyricularia oryzae* Sacc] (Barr, 1977; Couch and Kohn, 2002). *M. oryzae* is estimated to be responsible for up to 30% the annual losses in the rice harvest (Talbot, 2003; Thinlay *et al.,* 2000). *M. oryzae* also, however, affects other important crops, such as barley (*Hordeum vulgare*), finger millet (*Eleusine coracana*) and wheat (*Triticum aestivum*) (Talbot, 2003). Furthermore, blast disease of wheat (called 'Brusone' disease) is an emerging problem across South

America, most notably in Brazil. The disease was first reported in 1985 in the northern state of Paraná, in Brazil, and due to the lack of effective fungicides, has led to serious outbreaks in the last few years, across Brazil, Paraguay and Bolivia (Maciel *et al.,* 2014).

Rice blast disease is believed to have originated in the Yangste Valley of China and has been known since rice cultivation began almost 7000 years ago (Ou, 1985). The disease was originally known as rice fever disease in China and, only later, did it become widely known as the Rice Blast due to the rapid development of the disease in the field, causing 'blasting' of whole fields (Ou, 1985). Control of rice blast by fungicide treatment, the development of genetic modified varieties or disease resistant cultivars by plant breeding, have only met with limited success because of the rapid emergence of new pathotypes, fungicide-resistant strains and the high genetic variability of *M. oryzae* in the field (Latterell, 1986).

M. oryzae has emerged as, arguably, the most important model fungus for studying plant pathogen interactions based on both scientific and economic importance (Dean *et al.,* 2012). *M oryzae* possesses many important attributes that have allowed it to be studied as a model organism for understanding fungal-pathogen interactions, including the fact that the fungus grows in axenic culture away from its host and it has a high level of genetic tractability, allowing transformation and use of reporter gene fusions, coupled with the availability of the complete genome sequence of both the pathogen and its host, rice (Perez-Nadales *et al.,* 2014; Talbot, 2003; Wilson and Talbot, 2009).

1.2 The life cycle of *M. oryzae*

M. oryzae is a hemi-biotrophic fungus, and its reproduction in natural field conditions occurs very predominantly by asexual propagation. In fact the sexual stage of the fungus, which can be induced in the laboratory, has not been reported from cultivated rice fields (Talbot, 2003). The disease cycle starts when a three-celled spore, called a conidium, lands on a surface of a rice leaf and attaches to it by secreting spore tip mucilage found in an apical compartment of the conidium (Hamer, 1988). A highly polarized germ tube emerges from the apical cell and elongates to become flattened against the plant surface and, after 4-6 h, changes direction to form a hook (Bourett, 1990). Hooking is considered to be a recognition stage of development, in which physical properties of the leaf surface such as hydrophobicity, surface hardness, and cutin monomers, are perceived by the fungus (Talbot *et al.,* 1993). When these surface characteristics are appropriate, the inductive signals lead to a signal transduction cascade which leads to formation of the specialised infection structure of the fungus, called an appressorium (Talbot *et al.,* 1993). The appressorium is a dome-shaped cell, which generates a melanin layer in the inner part of the chitin-rich cell wall (Bourett, 1990). The melanin layer confers the ability to take up external water into the appressorium as a consequence of high osmotic gradient generated inside the dome by accumulation of glycerol (de Jong *et al.,* 1997; Talbot, 2003). This mechanism allows generation of high turgor inside the appressorium of up to 8.0 MPa, which is translated into mechanical force to pierce the tough cuticle of the leaf (de Jong *et al.,* 1997; Howard *et al.,* 1991; Howard and Valent, 1996; Talbot, 2003). The melanin layer is therefore defined as a virulence determinant, and melanin-deficient mutants, such as

those lacking the melanin biosynthetic enzymes, *albino*, *buff*, and *rosy*, are unable to penetrate the host (Valent and Chumley, 1991). Accumulation of turgor is accompanied by re-location of storage products from the conidium to the incipient appressorium, followed by autophagic-cell death of the conidium (Kershaw and Talbot, 2009; Thines *et al.,* 2000). To pierce the cuticle of the leaf, the fungus develops a penetration peg, which is a specialized narrow hypha that emerges from the appressorium pore (Bourett, 1990). The appressorium pore is the direct contact area between the host and the fungus, which has a limited or absent cell wall at this contact point (de Jong *et al.,* 1997; Howard *et al.,* 1991; Howard and Valent, 1996; Talbot, 2003). Once penetration has occurred, the primary invasive hypha develops into bulbous hyphae to invade and colonise the initial epidermal cell and adjacent tissues. After 3 days, small oval lesions appear on the leaf and become necrotic, and after 5 days they develop aerial conidiophores which sporulate profusely, yielding 20,000-50,000 spores per day (Talbot, 2003).

1.3 Genetic control of appressorium-mediated plant infection

1.3.1 The cAMP Signalling pathway

The cyclic AMP (cAMP) response pathway is triggered at early stages of development, soon after conidial germination, as a result of the perception of surface signals, (reviewed in (Talbot, 2003)). Addition of exogenous cAMP can induce appressorium formation on non-inductive conditions, such as on a hydrophilic surface (Choi and Dean, 1997; Lee and Dean, 1993). Recently, it has been shown that 3200 total proteins are affected by addition of cAMP during appressorium formation (Franck

et al., 2013). The central enzyme involved in production of cAMP is adenylate cyclase, encoded by Mac1 (Adachi and Hamer, 1998; Choi and Dean, 1997). Null mutants of *MAC1* are unable to form appressoria and infect the host, but appressorium development can be restored by addition of exogenous cAMP (Choi and Dean, 1997). It is thought that the cAMP pathway is activated upon contact of the *M. oryzae* germ tube with a hard, hydrophobic surface (Choi and Dean, 1997). During germ tube extension, the cAMP response pathway has been shown to regulate production of the secreted hydrophobin Mpg1 to increase the ability of the fungus to attach to the surface (Soanes *et al.,* 2002; Talbot *et al.,* 1996) The hydrophobin is thought to act as a primer for other attachment factors self-assembling at the hydrophobic surface (Talbot *et al.,* 1996). Consistent with this idea, Δ*mpg1* mutants are reduced in their ability to develop appressoria, but the addition of exogenous cAMP restores appressorium formation, suggesting that surface attachment is necessary for successful induction of their development (Talbot *et al.,* 1993). It is currently unclear which receptors specifically activate cAMP signalling, but Pth11 is one potential candidate. Pth11 is a membrane-localised CFEM domain-containing protein and null mutants are unable to form appressoria but this can be restored by exogenous cAMP (DeZwaan *et al.,* 1999; Kulkarni *et al.,* 2005). CFEM domain proteins belong to a fungal-specific family of G-protein-coupled-receptors required to respond to a variety of external cues (Dean *et al.,* 2005).

Heterotrimeric G proteins are composed of three bound sub-units α, β and γ, that dissociate into Gα and βγ subunits when bound to GTP in order to activate, or repress, the activity of effector proteins in the cytoplasm (Bolker, 1998). In *M. oryzae,* three α

subunit-encoding genes have been identified and named *MAGA, MAGB* and *MAGC* (Liu and Dean, 1997). Targeted gene deletion of *MAGA* has no effect on vegetative growth, conidiation or appressorium formation whereas deletion of *MAGC* causes defect in conidiation. However, deletion of *MAGB* significantly reduces conidiation, vegetative growth and appressorium formation (Liu and Dean, 1997). Two Gβ sub-units, Mgb1 and Mgb2, have also been identified as well as a Gγ sub-unit (Dean *et al.,* 2005; Nishimura *et al.,* 2003). Moreover, it was shown that dissociated Gβγ sub-units repress adenylate cyclase constitutively, resulting in impairment of appressorium formation (reviewed in (Talbot, 2003)).

Intracellular production of cAMP by adenylate cyclase results in the dissociation and activation of the regulatory subunit of Protein kinase A (PKA) (Lee *et al.,* 2003). Surprisingly, deletion of the PKA catalytic subunit (called CpkA) leads to formation of a small non-functional appressoria unable to cause any plant disease (Mitchell and Dean, 1995). Furthermore, *Δcpka* null mutants still respond to exogenous cAMP, suggesting that another catalytic subunit might be involved in early stages of appressorium formation (Talbot, 2003). It is also clear that cAMP signalling pathway is relevant not only for initiation of appressorium formation, but also for maturation of appressoria and generation of turgor (Thines *et al.,* 2000). Glycerol in appressoria of *M. oryzae* is thought to be synthesized from sources of glycogen, trehalose, mannitol, or other lipid storage products (Talbot, 2003). However, the precise mechanism leading to synthesis of glycerol in the appressorium of *M. oryzae* has not yet been resolved.

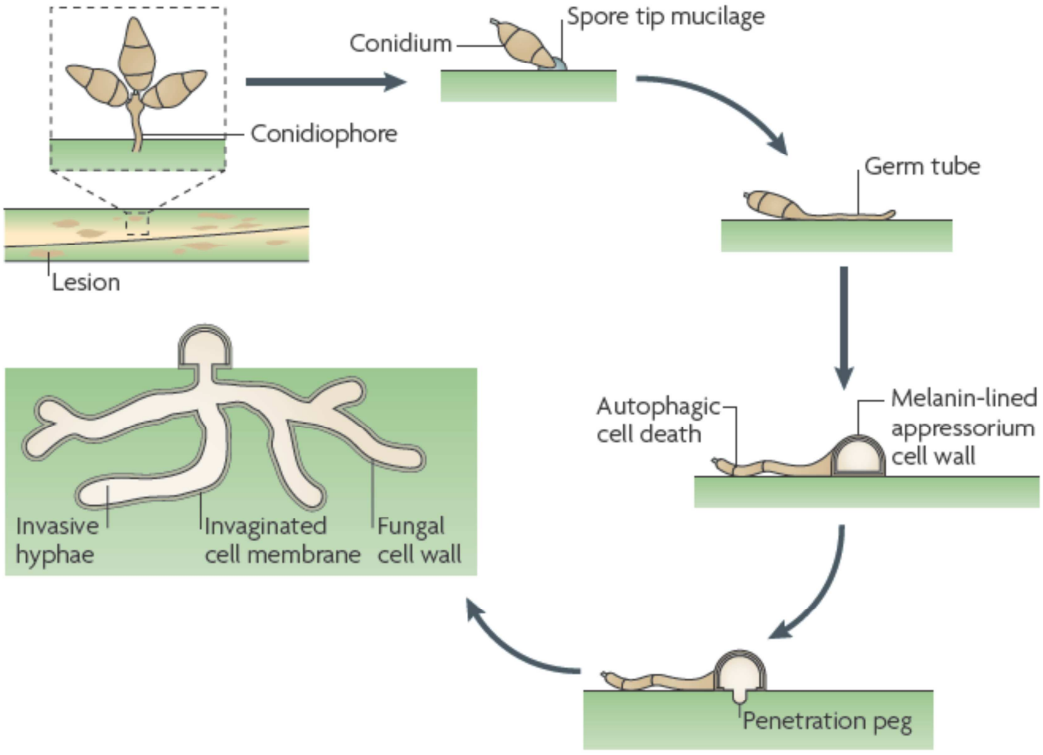

Figure 1.1 The life cycle of *Magnaporthe oryzae*. A three-cell conidium lands on the surface of a hydrophobic leaf and attaches by secreting spore tip mucilage. The spore germinates and forms a specialized-cell structure called the appressorium. The appressorium accumulates turgor pressure, which provides mechanical force required for formation of the penetration peg. Once inside the host, it forms primary invasive hyphae which later grow in a bulbous manner, colonizing the entire host cell. After four days, necrotic lesions become visible which generate conidia to continue life cycle (Wilson and Talbot, 2009).

1.3.2 The Pmk1 signalling pathway and its role in appressorium morphogenesis and plant infection in *M. oryzae*

Mitogen–activated protein kinase signalling pathways (MAPK pathways) are required for internalization of external stimuli to elicit a cellular response (Dickman and Yarden, 1999). MAPK signalling pathways are activated by receptors at the membrane, which activate downstream effectors leading to activation of the MAPK signalling module. The MAPK cascade is composed of a MAPKKK, MAPKK and MAPK which are phosphorylated in turn in order to activate downstream transcription factors leading to a re-programming of gene expression (Dickman and Yarden, 1999). In *M. oryzae,* three MAP kinase pathways have been described; the Osm1 MAPK pathway, the Mps1 MAPK pathway and the Pmk1 MAPK pathway (Bruno *et al.,* 2004; Dixon *et al.,* 1999; Xu *et al.,* 1998).

The Osm1 MAP kinase is a functional homologue of high-osmolarity-glycerol 1 Hog1 MAPK of *S. cerevisiae*, which regulates cellular turgor in yeast in response to hyperosmotic stress (Brewster *et al.,* 1993). Osm1 has been shown to regulate growth under hyperosmotic stress conditions in *M. oryzae* and this is independent of appressorial turgor generation (Dixon *et al.,* 1999). Therefore, turgor generation in appressoria of *M. oryzae* appears to be regulated in a different manner to the osmotic response of most eukaryotic organisms (Dixon *et al.,* 1999; Talbot, 2003).

The Mps1 MAP kinase of *M. oryzae* is a functional homologue of the Slt2 MAPK in *S. cerevisiae*, which regulates cell wall integrity under low osmotic conditions (Gustin *et al.,* 1998). Targeted deletion mutants of Mps1 in *M. oryzae* are hypersensitive to cell-

wall-digesting enzymes, show reduced conidiation, and are non-pathogenic because they are unable to form penetration pegs (Xu *et al.,* 1998). The main function of this pathway in *M. oryzae* is therefore to regulate cell wall biogenesis and facilitate turgor generation and thereby lead to development of a penetration peg and successful plant infection (Xu *et al.,* 1998).

The Pmk1 MAP kinase is a functional homologue of Fus3/Kss1 MAPK in *S. cerevisiae*, which is involved in the pheromone response pathway (Xu and Hamer, 1996). In *M. oryzae*, the Pmk1 MAP kinase regulates appressorium formation (Fig. 1.2). Null mutants of the Pmk1 kinase-encoding gene are unable to produce appressoria on inductive surfaces (Xu and Hamer, 1996). The Pmk1 MAPK cascade is thought to act downstream of cAMP signalling, because *Δpmk1* null mutants undergo hooking and terminal swelling of the germ tube in response to exogenous cAMP (Xu and Hamer, 1996), although they are unable to form appressoria under any conditions. In *S. cerevisiae*, following pheromone exposure and perception by the G-protein-coupled pheromone receptor, Gβ dissociation occurs and activates the scaffold protein Ste5 and a p21-activated kinase (PAK) Ste20 (Kusari *et al.,* 2004). Both in turn activate the Fus3 MAPK cascade through Ste11, Ste7 and, ultimately, Fus3 (Kusari *et al.,* 2004). The Pmk1 MAPK cascade is initiated through activation of Mst11 which phosphorylates Mst7 which in turn phosphorylates Pmk1 (Zhao *et al.,* 2005). Once activated, Pmk1 is translocated to the nucleus where it regulates a number of transcription factors (Bruno *et al.,* 2004). One of the most important targets is *Mst12,* the functional homologue of *Ste12* in *S. cerevisiae.* However, the interaction of Mst12 and Pmk1 has been only demonstrated by yeast two hybrid analysis (Y2H) and the identity of most of the

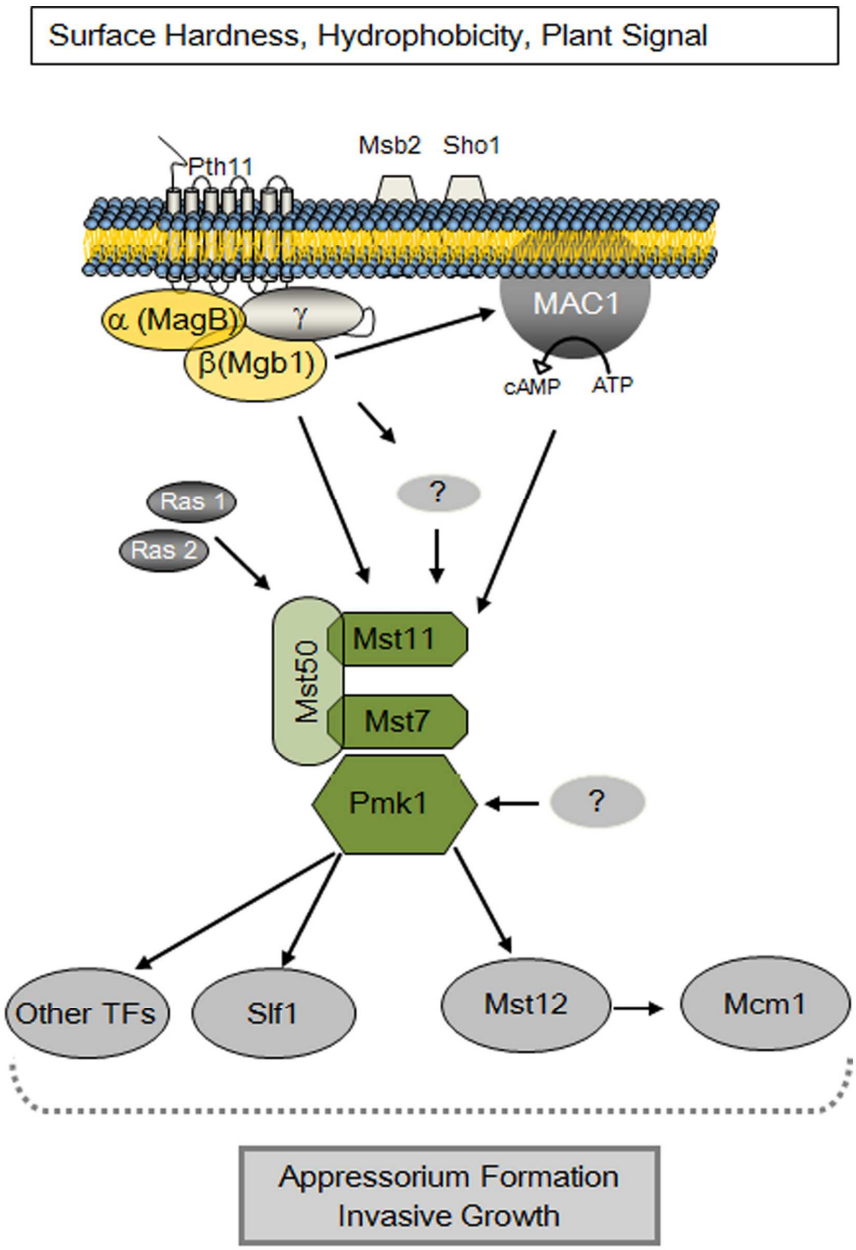

Figure 1.2 The Pmk1 MAP kinase signalling pathway in *Magnaporthe oryzae*. The Pmk1 MAP kinase pathway is activated by perception of the hydrophobic rice leaf surface. In this model, dissociation of Mgb1 causes activation of the Mst11 (MAPKKK), which activates Mst7 (MAPKK) and, ultimately, the Pmk1 (MAPK). Cross-talk with the cAMP response pathway may occur via Mgb1. The MAPK signalling complex is scaffolded by Mst50, which interacts with both Mst11 and Mst7. Pmk1 then activates a series of transcription factors, including Mst12 to regulate appressorium formation and invasive growth (adapted from R. Huguet, unpublished).

downstream targets of Pmk1 remains largely unknown (Park *et al.,* 2002). Mst12 is a C_2H_2 zinc finger and homeobox domain containing protein that regulates penetration peg formation (Kim *et al.,* 2009; Park *et al.,* 2002). Therefore although *Δmst12* null mutants are able to produce appressoria, they are unable to penetrate rice (Park *et al.,* 2002). Mst12 has also been shown to interact with the Mcm1 MADS-box transcription factor and regulate fertility and micro-conidia production (Zhou *et al.,* 2011). Therefore, the Pmk1 signalling pathway is involved in the regulation of both appressorium formation and invasive growth (Talbot, 2003). The Slf1 transcription factor has also been reported to be phosphorylated by Pmk1 to regulate infectious growth and may be involved in heat shock tolerance (Li *et al.,* 2011). Other Pmk1 interactors have also been described, including nine Pmk1-interacting clones (PICs) identified by Y2H analysis (Zhang *et al.,* 2011). However, only Pic5, a transmembrane protein containing two functionally unknown CTNS (cytosine/ERS1 repeat) motifs, has been shown to be required for virulence (Zhang *et al.,* 2011). Null mutants of *PIC5* form defective appressoria, show colony defects, and are reduced in pathogenicity (Zhang *et al.,* 2011). Downstream of Pmk1 there are also a number of appressorium-specific proteins, such as Gas1 and Gas2, which appear to depend on the presence of Pmk1 for their expression and which have been described as pathogenicity determinants (Xue *et al.,* 2002).

1.3.3 Cell cycle regulation in *M. oryzae*

Recent evidence suggests that appressorium morphogenesis is tightly linked to cell cycle control (Saunders *et al.,* 2010a). The cell division cycle in eukaryotes is divided into four phases, a gap (G1), in which the cell grows, a synthesis phase (S),

where cells replicate DNA, a second gap phase (G2), where the cell grows for second time, and mitosis (M), where sister chromatids are separated and distributed to new daughter cells. After mitosis, cytokinesis occurs forming the two daughter cells (reviewed in (Harashima *et al.,* 2013)). Progression through these phases is driven by activity of a serine/threonine protein kinase, called cyclin-dependent kinase (CDK) with associated conserved proteins called cyclins (Lew and Kornbluth, 1996). The activity of CDK depends on both association and concentration of cyclins, the inhibitory phosphorylations of CDK and changes in levels of inhibitors of CDK to regulate cell cycle, transcription of genes and cellular processes (Andrews and Measday, 1998). Moreover, the activity of CDK varies from low activity at G1 to maximum activity at M phase, after which CDK activity drastically decreases to re-start the cell cycle (Coudreuse and Nurse, 2010). Eukaryotic cells possess checkpoints that influence progression of the cell division cycle by modulating activity of CDK (Enoch and Nurse, 1990). For example, in *Schizosaccharomyces pombe*, during S phase and G2 phase, CDK (Cdc2) is phosphorylated at tyrosine-15 to block mitosis through the action of the kinases wee1 and Mik1 (reviewed in (Enoch and Nurse, 1990)). In *S. pombe,* it is the de-phosphorylation, mediated by the Cdc25 phosphatase, which determines the onset of mitosis ((Russell and Nurse, 1986)). Wee1 and Cdc25 therefore act in a dose-dependent manner to inhibit and activate CDK. In the case of Cdc25 accumulation will occur at G2 and above a certain threshold level, mitotic entry is induced (reviewed in (Enoch and Nurse, 1990)).

A number of cell cycle checkpoints have been identified in *M. oryzae* during appressorium formation. First, correct progression through DNA replication was found to

be required for formation of an incipient appressorium (Saunders *et al.,* 2010). When germinating conidia were treated with the DNA replication inhibitor hydroxyurea (HU) it resulted in impairment of appressorium formation. This was also the case when thermo-sensitive mutants of the regulatory subunit of the Dbf4-Cdc7 complex (encoded by Nim1), which was required for initiation of DNA replication, were incubated at a semi-restrictive temperature (Saunders *et al.,* 2010a). At the boundary of G2, a second checkpoint was also defined for appressorium development in *M. oryzae.* The protein kinase NimA has been previously reported to be necessary for mitosis in *Aspergillus nidulans* (Govindaraghavan *et al.,* 2014). In *M. oryzae*, generation of a thermo-sensitive *ΔnimA*^{ts} mutant causes G2 arrest during appressorium morphogenesis, which prevents maturation of the appressorium and subsequent plant infection (Saunders *et al.,* 2010a). Moreover, it was also shown that causing arrest of G2 in a *ΔnimA*^{ts} mutant, prevented collapse and cell death of the conidium (Veneault-Fourrey *et al.,* 2006). A third checkpoint at mitotic exit also appears to be significant for appressorium morphogenesis. Arrest of mitosis, either through the thermo sensitive mutant *ΔbimE*^{ts}, which prevents completion of anaphase, or by expression of a stabilised version of a b-type cyclin, Cyc1, resulted in a fully melanised appressorium that was not functional and therefore unable to cause plant infection (Saunders *et al.,* 2010a).

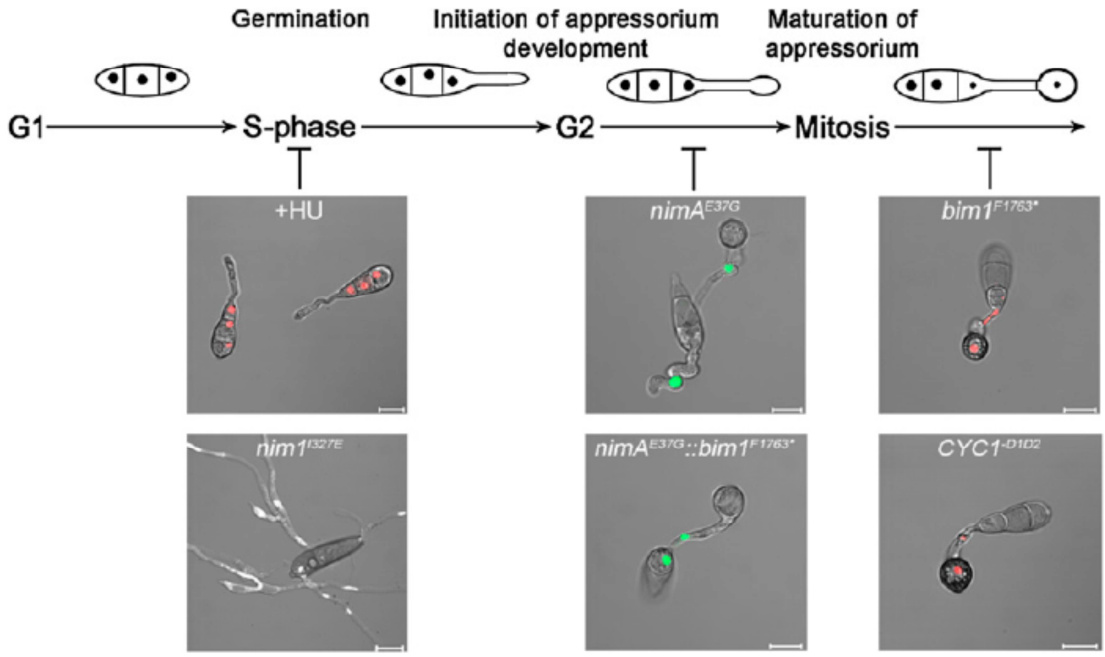

Figure 1.3 Cell cycle checkpoints during appressorium morphogenesis in *M. oryzae*. Initiation of appressorium formation depends on the completion of S-phase. The arrest of S-phase by HU treatment or in a *Δnim1*^{ts} mutant produces long germ tubes and prevents the formation of an incipient appressoria. The arrest of G2 in a *ΔnimA*^{ts} mutant is sufficient for appressorium formation but not maturation, preventing the conidium- collapse to occur. The arrest in mitosis by *ΔbimE*^{ts} or by a stable form of the b-type cyclin Cyc1 prevents plant infection. Scale bar =10 µm (taken from (Saunders *et al.,* 2010a)).

1.4 Introduction to the current study

The primary aim of the research project reported in this thesis was to define the transcriptional signature associated with appressorium development and maturation in the rice blast fungus *M. oryzae* and to use this information to gain insight into genes associated with appressorium morphogenesis and their biological functions. Secondly, the project also aimed to understand cell cycle regulation of appressorium-mediated plant infection in *M. oryzae* in more detail and to place this within the wider context of appressorium development.

The experimental approach carried out was first to perform a comparative transcriptomic analysis in which a *Δpmk1* null mutant, a *Δmst12* null mutant, and the isogenic wild type strain, Guy11, were compared under conditions which normally induce appressorium development. Transcriptional profiling was therefore routinely carried out by incubation of fungal spores on an inductive hydrophobic surface, and compared to conditions which do not elicit appressorium formation, namely a hydrophilic surface. The datasets generated in all of these analyses where then collated to allow comparison of how each physical and genetic background affected gene expression of the fungus. RNA-Seq analysis was carried out, because it is the most high-resolution method for analysing global patterns of gene expression using next generation sequencing technology. In order to investigate cell cycle regulation during appressorium-mediated plant infection I examined the effect of arresting the cell cycle at specific points through use of pharmacological inhibitors and generation of conditional thermo-sensitive mutants to study their effect on development of the appressorium and, in particular, its ability to elaborate a penetration peg and carry out plant infection.

The key research questions that were addressed in this thesis are:

1. What is the transcriptional signature associated with appressorium development in *M. oryzae*?
2. Can we define patterns of global gene expression specifically associated with appressorium function?
3. Which cell cycle checkpoints are necessary for regulation of appressorium-mediated plant infection?
4. What are the major genetic control points for development and action of *M. oryzae* appressoria?

The thesis is presented with a general methods chapter, followed by four results chapters, describing each of these experimental approaches and associated results obtained and specific conclusions. This is followed by a general discussion which attempts to synthesise general conclusions from the study.

2 General materials and methods

2.1 Growth and maintenance of fungal stocks

All isolates of *Magnaporthe oryzae* used and generated in this study are stored in the laboratory of N. J. Talbot (University of Exeter). For long term storage of *M. oryzae*, the fungus was grown on filter paper disks (2 mm, Whatman International), which were desiccated for two days and stored at -20 ℃. Fungal strains were routinely incubated at 26 ℃ with a 12 h photoperiod. Fungal strains were grown on complete medium (CM) (Talbot, 2003). CM is 10 g L^{-1} glucose, 2 g L^{-1} peptone, 1 g L^{-1} yeast extract (BD Biosciences), 1 g L^{-1} casamino acids, 0.1 % (v/v) trace elements (22 mg L^{-1} zinc sulphate heptahydrate, 11 mg L^{-1} boric acid, 5 mg L^{-1} manganese (II) chloride tetrahydrate, 5 mg L^{-1} iron (II) sulphate heptahydrate, 1.7 mg L^{-1} cobalt (II) chloride hexahydrate, 1.6 mg L^{-1} copper (II) sulphate pentahydrate, 1.5 mg L^{-1} sodium molybdate dehydrate, 50 mg L^{-1} ethylenediaminetraacetic acid), 0.1 % (v/v) vitamin supplement (0.001 g L^{-1} biotin, 0.001 g L^{-1} pyridoxine, 0.001 g L^{-1} thiamine, 0.001 g L^{-1} riboflavin, 0.001 g L^{-1}, 0.001 g L^{-1} nicotinic acid), 6 g L^{-1} NaNO3, 0.5 g L^{-1} KCl, 0.5 g L^{-1} $MgSO_4$, 1.5 g L^{-1} KH_2PO_4, [pH to 6.5 with NaOH], 15 g L^{-1} agar. When making liquid stocks, agar is omitted. All chemicals were obtained from Sigma unless otherwise stated.

2.2 Pathogenicity and infection related developmental assays

2.2.1 Plant infection assays

Rice infections were performed using a dwarf Indica rice (*Oryza sativa*) cultivar, CO-39, which is partially susceptible to *M. oryzae* (Valent and Chumley, 1991). From 10

to 12 day old *M. oryzae* cultures were grown in CM agar, and conidia were harvested using 5 mL of sterile de-ionized water. The conidial suspension was filtered through sterile Miracloth (Calbiochem) and centrifuged at 5,000 x g (Beckman, JA-17) for 10 min at room temperature. The pellet was resuspended in 0.2 % gelatine (BDH) to a final concentration of 5 $x10^4$ conidia mL^{-1}. This suspension was then used in spray inoculation infection by using an artist's airbrush (Badger Airbrush, Franklin Park, Illinois, USA) to disperse the suspension uniformly. Rice plants were grown in 9 cm diameter pots containing 9 plants per pot and three pots were inoculated when plants were at the 2-3 leaf stage. After spraying, plants were kept for 48 h covered with plastic bags and 5 days more in a controlled environment chamber (REFTECH, Holland) at 24 ℃ with a 12 h photoperiod and 90 % relative humidi ty, as described by Valent *et al.,* (1991). Lesion formation was monitored for 3 d post inoculation and lesion density recorded 5 d post inoculation.

2.2.2 *In vitro* appressoria germination and formation assay

Germination and formation of appressoria were generated *in vitro* using borosilicate 18X18 glass coverslips (Fisher Scientific UK Ltd). The method is adapted from Hamer *et al.* 1988. Conidia were harvested (as described in 2.1.1) and a suspension of 5 $x10^4$ conidia mL^{-1} was prepared in double distilled water. Fifty microliters of the conidial suspension were placed onto the coverslip surface and incubated in a controlled environment chamber at 24 ℃ for the period of time required for the specific experiment. Conidia were counted (n=300) and the percentage making appressoria was determined. The development of conidia was observed using the IX81 motorized inverted microscope (Olympus, Hamburg, Germany) and images were

captured using a Photometrics CoolSNAP HQ2 camera (Roper Scientific, Germany). The system was under the control of MetaMorph software package (MDS Analytical Technologies, Winnersh, UK).

2.2.3 Onion epidermis infection assay

Onion epidermis layers were separated, washed in chloroform for 15 minutes and then washed three times in water. The epidermis layers were cut into 1 cm^2 small squares and placed onto microscope slides. A conidial suspension of $5x10^4$ conidia mL^{-1} was prepared in double distilled water and a 50 µL drop was inoculated onto the onion epidermis layers. The inoculated slides were incubated in a controlled environment chamber at 24 ℃ and high relative humi dity for the period of time required for the specific experiment. The percentage of penetration events were monitored and examined by microscopy as described in section 2.1.2.

2.2.4 Rice leaf sheath infection assay

To observe the invasive hyphae inside the cells, the rice leaf sheath method adapted from Kankanala *et al.,* (2007) was used. Conidial suspension of $5x10^4$ conidia mL^{-1} prepared in sterile semi distilled water was inoculated in 3-4 week old plants. The inoculation was performed with a syringe on the leaf vein and incubated in a controlled environment chamber at 24 ℃ for the period of time required for the specific experiment. An epidermal leaf layer was dissected using a blade and mounted into a microscope slide for analysis as described in section 2.1.2.

2.3 Fungal DNA extraction

2.3.1 Fungal genomic DNA extraction

M. oryzae was inoculated into a CM agar plate containing a cellophane disc (Lakeland). The cultures were incubated at 24 ℃ for 10 days, until the mycelium had grown over the disc. The disc with the mycelia was collected and ground in a mortar with liquid nitrogen until a fine powder was produced. The fine powder was then transferred into a 1.5 mL microcentrifuge and 500 µL of 2X CTAB was added. The eppendorfs were incubated for 30 min at 65℃ with occasional shaking. An equal volume of chloroform:isoamyl:alcohol (24:1:1) was added and shaken for 30 min at room temperature. The samples were then centrifuged at 14000 x g for 10 min and the supernatant was collected into clean eppendorfs. This step was repeated once more. An equal volume of chilled isopropanol was added to the supernatant in order to precipitate nucleic acids and incubated on ice for 5 min. The DNA was recovered by centrifugation at 14000 x g for 10 min and the pellet was drained and resuspended in 500 µL in nuclease-free-water. The DNA was re-precipitated by adding 0.1 vol of sodium acetate, 3M (pH 5.2) and 2 vol of absolute ethanol and incubated for 10 min at 20 ℃. The purified nucleic acid was recovered by centrifugation at 14000 x g for 20 min and washed with 400 µL of ethanol, 70% (v/v). The pellet was dried for 5 min in a vacuum rotary desiccator and resuspended in 50 µL of nuclease-free water (Sigma) containing RNAse A, 10µg mL^{-1}. Nucleic acids were quantified using a NanoDrop spectrophotometer (Thermo Scientific). The samples were routinely stored at -20 ℃.

2.4 DNA manipulations

2.4.1 Digestion of genomic or plasmid DNA with restriction enzymes

Restriction enzymes were purchased from Promega UK Ltd. (Southampton, UK) or New England Biolabs (Hitchin, UK). The restriction digestion was performed according to manufacturer instructions. The digestions were routinely performed in a final volume of 30- 50 µL using 0.2 to 1 µg of DNA and 5 to 10 units of enzyme. For Southern blot analysis, 30 µg of DNA and 60 units of enzyme in a 50 µL total volume reaction were used.

2.4.2 The polymerase chain reaction (PCR)

Polymerase Chain Reaction (PCR) procedure was used for DNA fragment amplification using an Applied Biosystems GeneAmp® PCR System 2400 cycler. The reaction was carried out using either GoTaq ® Green Master Mix (Promega), Phusion High Fidelity DNA Polymerase (NEB) or Thermo Start (Thermo Scientific) and used according to manufacturer's instructions. Routinely, the GoTaq ® Green Master Mix or Phusion High Fidelity DNA Polymerase, 50- 100 ng of template DNA was used for amplification. For PCR amplification with GoTaq ® Green Master Mix, the PCR reaction contained: GoTaq Green Master Mix (2x), 10 µM of each primer and nuclease free water made up to a final volume of 50 µL. PCR cycling parameters were: 95 ℃ for 2 min, 95 ℃ for 30 s, 55- 62 ℃ for 30 s, 72 ℃ for 1 min/Kb target length for 25- 35 cycles, followed by a final extension of 10 min at 72 ℃. For PCR amplification with Phusion High Fidelity DNA Polymerase each reaction contained: Phusion HF buffer (5X), 10 mM dNTPs, 10 µM of each primer and nuclease free water made up to a final

volume of 50 µL. PCR cycling parameters were: 98 ℃ for 30 s, 98 ℃ for 5- 10 s, 45- 72 ℃ for 10- 30 s, 72 ℃ for 15- 30 s /Kb target leng th for 25- 35 cycles, followed by a final extension of 5- 10 min at 72 ℃. The Thermo Start r eaction was used for screening of recombinant bacterial or yeast cells. The reaction contained: Thermo- Start PCR master mix (2X), 10 µM of each primer and nuclease free water made up to a final volume of 25 µL. PCR cycling parameters were: 95 ℃ for 15 min, 9 5 ℃ for 20 s, 50- 65 ℃ for 30 s, 72 ℃ for 1 min/Kb target length for 25- 35 cycles, followed by a final extension of 5 min at 72 ℃.

2.4.3 DNA electrophoresis

Digested DNA was separated by electrophoresis in 0.8% (w/v) agarose gel matrices using a 1 X Tris- borate EDTA buffer (TBE) (0.09 M Tris- borate, 2 mM EDTA) with the addition of ethidium bromide 4 µL of a 0.5 µg mL^{-1} stock per 100 mL of agarose. Digested DNA was visualized under UV light transiluminator (image Master VDS) with a Fuji Thermal Imaging System, FTI-500 (Pharmacia Biotech). The length of the fragments was determined using the 1 Kb plus size marker (Invitrogen).

2.4.4 Gel purification of DNA fragments

DNA fragments were purified using a commercial kit, Wizard® SV Gel and PCR Clean-Up System kit (Promega), according to the manufacturer's instructions. Fragments were excised from the agarose gel using a razor blade and placed in a pre-weighed 1.5 mL microfuge tube. An equal volume of Membrane Binding Solution (4.5 M guanidine isothiocyanate, 0.5 M potassium acetate, pH 5.0) was added to dissolve the fragment at 65 ℃. Dissolved gel mixture was placed in a Wizard® SV Minicolumn held

in a 2 mL collection tube to centrifuge for 1 min at 13 000 x g and flow-through discarded. The column was washed with 700 µL of Membrane Wash Solution (potassium acetate, 10 mM (pH 5.0), ethanol, 80%, ethylenediaminetetraacetic acid, 16.7 µM (pH 8.0) and centrifuged for 1 min at 13 000 x g. The flow-through was discarded and the wash repeated with 500 µL of Membrane Wash Solution. Following centrifugation for 5 min at 13 000 x g, the flow-through was discarded and the column processed by centrifugation for an additional 1 min at 13 000 x g. The Wizard® SV Minicolumn was placed in a clean 1.5 mL microfuge tube, 30 µL of sterile nuclease-free water added and following incubation at room temperature for 1 min, the DNA was recovered by centrifugation for 1 min at 13 000 x g. The eluted DNA was stored at -20℃.

2.4.5 Southern Blotting

Southern blot analysis was performed according to Southern (1975) (Southern, 1975). Twenty micrograms of fungal genomic DNA was digested with the required restriction enzyme overnight for a complete fractionation. Digested fungal DNA samples were run on 0.8% TBE agarose gels at 30 V overnight for a good DNA separation. Each agarose gel was immersed for 15 min into 0.25M HCl for depurination, then for 30 min into denaturing solution (0.4 N NaOH, 0.6 M NaCl) and finally for 30 min in neutralisation solution (1.5 M NaCl, 0.5M Tris-HCl (pH 7.5)).

2.4.5.1 Blotting

Gel blots were performed by placing the gel onto a sheet of Whatmann 3 mm paper supported into a Perspex sheet with each end of the filter paper submerged in 20

X SSPE solutions (3.6 M NaCl, 0.2 M $NaH_2PO_4H_2O$, 0.02 M EDTA). Hybond N-membrane (Amersham Biosciences) was then placed onto the gel and overlaid with 5 layers of wet Whatmann 3 mm paper and 5 layers of dry Whatmann 3 mm paper onto which 10 cm high pile of paper towels (Kimberley Clark Corporation) was placed. Finally, a 500 g weight was placed on the stack and the blot was left at room temperature overnight for transference. The transferred DNA was UV-cross linked to the membrane using a BLX crosslinker (Bio-Link).

2.4.5.2 Synthesis of radiolabelled probe

DNA hybridisation probes were labelled according to Feinberg and Vogelstein (1983) (Feinberg and Vogelstein, 1983) using a Ready-to-go random primer kit (Amersham Biosciences) according to manufacturer's instructions 150 ng of DNA was made up to a final volume of 46 µL in water. The sample was boiled for 5 min to denature the DNA and incubated on ice for 2 min. The tube was centrifuged briefly and contents were added into a Ready-to-go reaction mix containing buffer, dATP, dTTP, dGTP, FPLC pure Klenow polymerase (7-12 units) and random oligonucleotides, primarily 9-mers. Reagents were mixed by gentle pipetting and 2 µL of [α-^{32}P]dCTP (3000 Ci/mmol) was added. The labelling reaction was incubated at 37 ℃ for 10 min before being stopped by adding 100 µL of labelling stop dye (0.1 % SDS, 60 mM EDTA, 0.5 % bromophenol blue, 1.5 % blue dextran). Un-incorporated isotopes were removed by passing the reaction mix through a Biogel P60 (Biorad) column and collecting the dextran blue labelled fraction. The probe was denatured by boiling at 100 ℃ for 5 min before being added to the hybridization mixture.

2.4.5.3 Hybridization conditions

DNA gel blot hybridizations were performed following standard procedures (Sambrook, 1989). Blots were incubated in hybridization bottles (Hybaid Ltd.) in a hybridization oven (Hybaid) for at least 4 h at 65 ℃ in 15- 20 mL of pre-hybridization solution (6 x SSPE [diluted from a Stock (6 x SSPE [diluted from a 20 x stock prepared by dissolving 175.3 g of NaCl, 27.6 g of NaH2PO4 and 7.4 g of EDTA in 800 mL of ddH_20, adjusting the pH to 7.5 with NaOH and making up to 1 L with ddH20], 5 x Denhardt's solution [diluted from a 50 x stock prepared with 5 g Ficoll (type 400, Pharmacia), 5 g polyvinylpyrrolidone in 500 mL ddH20), 0.5 % SDS], with 100 µL denatured herring sperm DNA (1 % [w/v] in 0.1 M NaCl). A denatured radio-labelled probe was then added and the mixture incubated for 18 h at 65 ℃. Following hybridization, the pre-hybridisation solution was removed along with any unbound probe and 25- 30 mL of 2 x SSPE wash (0.1 % SDS, 0.1 % Sodium Pyrophosphate [PPi], 2 x SSPE [diluted from the 20 x SSPE stock][pH 7.4]) was added. The mixture was incubated for 30 min at 65 ℃. The wash solution was removed and replaced with 25 - 30 mL of 0.2 x SSPE wash (0.1 % SDS, 0.1 % Sodium pyrophosphate [PPi], 0.2 x SSPE, [pH 7.4]) and the blot again incubated for 30 min at 65 ℃. The membrane was then dried for 10 min on paper towels and wrapped in cellophane and autoradiography was carried out by exposure of membranes to X-ray film (Fuji Medical X-ray film, Fuji Photo Film UK Ltd.) at -80 ℃ in the presence of an intensifying screen (Amersham). X-ray films were developed using Kodak chemicals.

2.4.6 Plasmid purification for fungal transformation

Positive single colonies were grown in 5 mL of LB media overnight at 37 ℃ with vigorous aeration (200 rpm) in an Innova 4000 rotary incubator (New Brunswick Scientific). High quality plasmid purification was performed using a commercial kit, Midi-Prep DNA purification system (Promega® Wizard Plus SV) according to manufacturer's instructions. Bacterial cultures were centrifuged at 10,000 x g, resuspended in 250 µL of cell resuspension solution (50 mM Tris [pH 7.5], 10 mM EDTA, and 100 µg mL^{-1} of RNase) and transferred to a microfuge tube. A 250 µL aliquot of cell lysis solution (0.2 M NaOH, 1 % SDS) was added and the contents mixed by gentle inversion. A 10 µL aliquot of alkaline protease solution was added and the tube inverted gently. After a 5 min incubation at room temperature, a 350 µL aliquot of neutralisation solution (4.09 M guanidine hydrochloride, 0.759 M potassium acetate, 2.12 M glacial acetic acid [final pH 4.2]) was added and the tube contents mixed by inversion. The samples were processed by centrifugation at 14,000 x g in a microfuge for 10 min. A spin column was then inserted into a collection tube and the cleared cell lysate poured into the top of the column. This was processed by centrifugation at 14,000 x g in a microfuge for 1 min. The flow-through was then discarded and the spin-column re-inserted into the collection tube and 750 µL wash solution (60 mM potassium acetate, 8.3 mM Tris-HCl [pH 7.5], 0.04 mM EDTA, 60 % ethanol) then pipetted into the spin column. The spin-column and collection tube were then centrifuged at 14,000 x g for 1 min at room temperature. This centrifugation step was repeated and the column washed again with 250 µL of wash solution for 5 min. The flow through was discarded and the column processed by centrifugation for an additional minute (14,000 x g). The spin column was transferred to

a fresh sterile microfuge tube and 50 µL of nuclease free water (Sigma) added to the column. One final centrifugation at 14,000 x g for 1 min was required to elute the DNA from the spin column into the microfuge tube. Plasmid DNA samples were routinely stored at -20 ℃.

2.4.7 DNA mediated transformation of *M. oryzae*

A 2.5 cm^2 section of mycelium from a *M. oryzae* plate culture was transferred to 150 mL complete medium liquid and blended until small fragments of mycelium were formed. The liquid culture was incubated at 24 ℃ with shaking at 125 rpm in an orbital incubator for 48 h. The mycelium was filtered through sterile Miracloth (Calbiochem) and washed twice with sterile distilled water. The mycelium was transferred to a Falcon tube (Becton Dickinson) containing 40 mL OM buffer (magnesium sulfate, 1.2 M, sodium phosphate, 10 mM (pH 5.8), Glucanex 5% (Novo Industries, Copenhagen)) and shaken at 75 rpm for 2-3 h at 30 ℃. The digested mycelium was transferred to sterile polycarbonate Oakridge tubes (Nalgene) and overlaid with an equal volume of cold ST buffer (sucrose, 0.6 M, Tris-HCl 0.1 M (pH 7)). Resulting protoplasts were recovered at the OM/ST interface by centrifugation at 5000 x g, for 15 min at 4 ℃ in a swinging bucket rotor (Beckman JS-13.1) in a Beckman J2.MC centrifuge. The recovered protoplasts were transferred to a sterile Oakridge tube, which was filled with cold STC buffer (sucrose, 1.2 M, Tris-HCl, 10 mM (pH7.5), calcium chloride, 10 mM). Protoplasts were pelleted at 3 000 x g for 10 min at 4 ℃, (Beckman JS-13.1 rotor) and washed twice more with 10 ml STC, with complete re-suspension each time. After re-suspending in 1 mL of STC, the concentration of protoplasts was determined by counting using a haemocytometer. DNA-mediated transformation was undertaken in 1.5

mL microfuge tubes by combining an aliquot of purified protoplasts (10^7 ml^{-1} with DNA (~6 µg) in a total volume of 150 µL. The mixture was incubated at room temperature for 25 min and then 1 mL of PTC (PEG 4000, 60%, Tris-HCl, 10 mM (pH 7.5), calcium chloride, 10 mM) was added in 2 aliquots and mixed by gentle inversion. The mixture was incubated at room temperature for 15-20 min then added to 150 mL molten (46 ℃) 1.5% agar/OCM (CM osmotically stabilised with sucrose, 0.8 M), mixed gently and poured into 5 sterile Petri dishes (25 mL $plate^{-1}$). For selection of transformants on hygromycin B (Calbiochem), plate cultures were incubated in the dark for at least 16 h at 24 ℃ and then overlaid with approximately 15 mL OCM/1% agar containing 600 µg mL^{-1} hygromycin B. For selection of bialophos (Basta) resistant transformants, OCM was replaced with BDCM (yeast nitrogen base without amino acids and ammonium sulfate, 1.7 g L^{-1} (Difco), ammonium nitrate, 2 gL^{-1}, asparagine, 1 gL^{-1}, glucose, 10 gL^{-1}, sucrose, 0.8 M, pH 6). In the overlay, CM was replaced with BDCM without sucrose and hygromycin B was replaced by glufosinate 30 µg mL^{-1}. For selection of sulfonylurea resistant transformants, OCM was replaced with BDCM and in the overlay, hygromycin B was replaced with chlorimuron ethyl, 50 µg mL^{-1} freshly diluted from a stock solution, 100 mg mL^{-1}.

2.5 RNA sequencing

2.5.1 Preparing appressorial assay for RNA extraction

Conidia were harvested from 12-day old CM agar plates using 5 mL of sterile de-ionized water. The conidial suspensions for several plates were filtered through sterile

Miracloth (Calbiochem) and centrifuged at 5,000 x g (Beckman, JA-17) for 25 min at room temperature. Conidia were quantified and then diluted in sterile water to 7.5×10^5 conidia mL^{-1} in the presence of 50 ng μL^{-1} 1,16-Hexadecanediol (Sigma SA). This solution was poured into square petri plates (Greiner Bio One) to which 10 glass cover slips (Cole-Parmer) had been attached by gluing. Appressorium formation was monitored under a Will-Wetzlar light inverted microscope (Wilovert®, Hund Wetzlar, Germany) for each of the timepoints ensuring a homogeneous and sincronize structure formation. Samples were collected at the desired time points by scraping the surface of the coverslips with a sterile razor blade (Fisher Scientific). Recovered samples were immediately frozen in liquid nitrogen, lyophilized and stored at −80 ℃ until required.

2.5.2 RNA extraction and processing

Lyophilized material was ground in a sterile mortal prior using of Qiagen RNeasy Plant Mini kit for Total RNA extraction. The RNA extraction was performed according to manufacturer's instructions. RNA was eluted in RNase-free water and store at −80 ℃ until needed.

2.5.3 RNA quantification

Total RNA samples were first quantified with the NanoDrop spectrophotometer (Thermo Scientific). Samples were aliquoted and diluted up to 500 ng μL^{-1} for Bioanalyzer analysis. RNA aliquots were checked for integrity and quantity on an Agilent 2100 Bioanalyzer using an RNA 6000 nano chip kit (Agilent). Total RNA with integrity number of at least 6 was used for library preparations.

2.5.4 RNA-Seq library preparation and Sequencing

RNA-Seq libraries were prepared using 5 µg of total RNA with True Seq RNA Sample Preparation kit from Illumina (Agilent) according to manufacturer's instructions. All the consumables were supplied in the True Seq RNA Sample Preparation kit unless otherwise stated.

2.5.5 Purification and fragmentation

In this step Poly-A containing mRNA was purified using poly-T oligo attached magnetic beads and was performed twice. Five µg of total RNA were dissolved to a final volume of 50 µL in RNAse free water. Fifty µL of RNA purification beads were added to the mixture and denatured for 5 min at 65 ℃. The r eaction was incubated for 5 min at room temperature and transferred to a magnetic stand for 5 min from which supernatant was separated from the beads. The beads were washed twice by adding 200 µL of bead washing buffer, incubating 5 min in the magnetic stand and removing the supernatant. The purified mRNA was eluted by adding 50 µL of Elution Buffer and incubated at 80 ℃ for 2 min. A final mRNA elution was performed by adding 19.5 µL of Elute, Prime and Fragment mix and incubated for 8 min at 94 ℃.

2.5.6 Synthesis of first strand cDNA

The primed mRNA bound beads were incubated in the stand for 5 min until 17 µL of supernatant were transferred into new tubes. The primed mRNA was used for cDNA synthesis using 8 µL of First Strand Master Mix with Superscript II reverse transcriptase and random primers. The PCR cycling parameters were 25 ℃ for 10 min, 42 ℃ for 50 min and 70 ℃ for 15 min.

2.5.7 Synthesis of second strand cDNA

Second strand cDNA was synthesized by adding 25 µL of Second Strand Master Mix and incubating for 1h at 16 ℃. The reaction was purified from the reaction mix by adding 90 µL of AMPure XP beads, incubated for 15 min at room temperature then left for 5 min on the magnetic stand, from which supernatant was removed. The beads were washed twice by incubating for 30 s with 200 µL of 80% ethanol without disturbing the beads. After the second 80 % ethanol wash, the beads were air dried for 15 min on the magnetic stand. The double-stranded (ds) cDNA was recovered from the beads by adding 52.5 µL of Resuspension Buffer, incubating for 2 min at room temperature, 5 min in the magnetic strand and rescuing 50 µL of the ds cDNA into fresh sterile tubes.

2.5.8 End Repair

The resulting ds cDNA was end repaired by removing 3' overhangs with an exonuclease and 5' overhangs by filling up with a polymerase activity to convert the fragments into blunt ends. Ten µL of Resuspension Buffer and 40 µL of End Repair Mix were added to the ds cDNA and incubated 30 min at 30 ℃. The reaction was transferred to a 1.5 mL microcentrifuge tube and 160 µL of AMPure XP beads were added. The mixture was incubated for 15 min at room temperature and transferred 5 min to the magnetic stand for 5 min, after which the supernatant was removed. The beads were washed twice by incubating for 30 s with 200 µL of 80% ethanol without disturbing the beads. After the second 80 % ethanol wash, the beads were air dried for 15 min on the magnetic stand. The ds end-repaired cDNA was recovered from the beads by adding of 17.5 µL of Resuspension Buffer, incubating 2 min at room temperature, 5 min in the magnetic strand and recovering 15 µL into fresh sterile tubes.

2.5.9 3’ end Adenylation

An A-tailing step was performed to prevent ligation to each other during the adapter ligation. The 15 µL of ds end-repaired cDNA was incubated at 37 ℃ for 30 min with 12.5 µL of A-tailing Mix and 2.5 µL of Resuspension Buffer to prepare it for the adaptor ligation step.

2.5.10 Adaptor ligation

Indexed Adapters were ligated to the ds cDNA by adding 2.5 µL of DNA Ligase Mix, 2.5 µL of Resuspension Buffer and 2.5 µL of the specific RNA Adapter Index. The mixture was incubated for 10 min at 30 ℃. The liga tion reaction was stopped by adding 5 µL of Stop Ligase Mix. A following purification step using 42 µL of AMPure XP beads and two washes were performed as described in section 2.4.4.4. The recovering of the ligated adaptor ds cDNA was performed by adding 52.5 µL of Resuspension Buffer, incubating 2 min at room temperature, 5 min in the magnetic strand and recovering 50 µL into fresh sterile tubes. A repeated AMPure XP purification step with two washes was performed yielding a final volume of 20 µL.

2.5.11 Enrichment of DNA fragments

An enrichment step is performed for those fragments ligated to the indexed adapters on both ends. The PCR reaction was performed using Phusion High Fidelity DNA Polymerase (NEB) as described in section 2.3.2. The reactions were purified with AMPure XP beads and washed as described in section 2.4.4.4. The libraries were quantified on an Agilent 2100 Bioanalyzer using a DNA 1000 chip kit. Libraries were

diluted to 10 nM in Elution Buffer (Qiagen) for sequencing in an Illumina HiSeq 2500 platform.

2.5.12 Bioinformatic analysis

The output short reads of the sequencing were aligned against version 8.0 of *M. oryzae* genome using Tophat software (Trapnell *et al.,* 2010). The analysis of the data was performed using DESeq which determines differential gene expression through the moderated log2 fold change value (mod_lfc) (Anders and Huber, 2010). Transcript abundances for each gene and adjusted P-values were generated as according to Soanes *et al.,* (2012). To determine the significant differences of the pair wise comparisons we adjusted the p-value <=0.01.The initial bioinformatics analysis involving the processing of the sequencing reads, alignment to the genome and use of DESeq software to determine significant differences was carried out by Dr. Darren Soanes.

3 Investigating the role of Pmk1 MAP kinase in appressorium morphogenesis by comparative transcriptional analysis

3.1 Introduction

Mitogen–activated protein kinases (MAP kinases) are a family of serine/ threonine protein kinases, which form part of a signalling cascade that internalizes external stimuli into the cell (Dickman and Yarden, 1999). This requires phosphorylation and de-phosphorylation of components of the MAP kinases cascade which, ultimately, will be transduced into re-programing of the transcriptional signature, resulting in adaptation to the external stimulus (Dickman and Yarden, 1999). The re-programming of transcription happens through activation of effectors downstream of MAPK cascades, leading to activation of biological processes, such as stress responses, reproduction, morphogenesis and cell cycle control (Merlini *et al.,* 2012). In the case of *M. oryzae*, although it possesses three MAP kinase pathways, the Osm1, Mps1 and Pmk1 pathways (Bruno *et al.,* 2004; Dixon *et al.,* 1999; Xu *et al.,* 1998), only the Pmk1 MAP kinase pathway has been shown to be a regulator of morphogenetic changes and cell cycle control (Xu *et al.,* 1998). Null mutants of the Pmk1 MAP kinase gene are unable to form appressoria and cannot invade the host (Xu and Hamer, 1996).

The *M. oryzae* Pmk1 MAP kinase pathway is activated when the spore lands on a hydrophobic surface, such as a rice leaf (Hamer, 1988). The activation happens through a plasma membrane receptor, Pth11 that is activated upon contact with an inductive hydrophobic surface (DeZwaan *et al.,* 1999). Germination and appressorium formation are therefore thigmotropic responses to the plant surface (Xu and Hamer,

1996). Such thigmotropic responses are important in a range of fungal species and a thigmotropic mechanism occurs, for example, in the human pathogen *Candida albicans*, which responds to surface characteristic such as pores or scratches (Watts *et al.,* 1998). In *M. oryzae,* appressorium formation is triggered by both nutrient deprivation and surface hydrophobicity, and these signals appear to be transduced through the Pmk1 pathway to induce appressorium formation (Wilson and Talbot, 2009). Moreover, nutrient deprivation triggers lipid and glycogen mobilization from conidia towards the incipient appressorium and this process is also Pmk1 dependent (Thines *et al.,* 2000). The β-oxidation and mobilization of fatty acids occurs in order to synthesize glycerol in the appressorium and to generate turgor pressure necessary for plant penetration (de Jong *et al.,* 1997; Dean *et al.,* 2005).

PMK1 encodes a functional homologue of the Fus3 MAP kinase of *S. cerevisiae* (Bruno *et al.,* 2004). In *S. cerevisiae*, Fus3 regulates the mating pathway by activating Far1, Ste12 and Sst2 (Elion *et al.,* 1993; Rispail *et al.,* 2009). Far1 is transcribed in a Ste12-dependent manner, leading to inactivation of the Cdc28-Cln complex, which causes a G1 cell cycle arrest (Chang and Herskowitz, 1990). In *M. oryzae,* Pmk1 phosphorylates the Ste12 homologue, Mst12, which might in turn activate a Far1 counterpart to cause a cell cycle arrest, however this is yet to be confirmed. During appressorium formation in *M. oryzae,* a single round of mitosis occurs which is required for formation of a functional appressorium. After mitosis, one of the daughter nuclei moves to the incipient appressorium and the other moves back to the conidium. Afterwards, the contents of conidia are degraded through non-selective autophagy (Kershaw and Talbot, 2009). At the specific moment at which *M. oryzae* starts

penetrating the host, only one nucleus in the appressorium remains intact and is the source of all genetic material, from which every subsequent nucleus is derived. This shows that there is tight temporal coordination of cell cycle events with appressorium morphogenesis. Consistent with this idea, *Δpmk1* mutants undergo multiple rounds of mitosis and form several septa along the germ tube, suggesting that impairment in cell cycle arrest may prevent normal morphogenesis. This suggests that cell cycle arrest is a pre-requisite for appressorium formation, and that this is mediated through the Pmk1 signalling pathway (Saunders *et al.,* 2010b).

Pmk1 has been shown to be translocated to the nucleus when activated and in turn activates transcription factors in response to external stimuli (Bruno *et al.,* 2004). These Pmk1-regulated transcription factors are possibly numerous, but until now only a small number have been identified and described. The most well-known Pmk1-activated transcription factor is Mst12 (Park *et al.,* 2002). The interaction between Pmk1 and Mst12 has been suggested by yeast two-hybrid analysis and Δ*mst12* null mutants form appressoria but are unable to penetrate rice leaves (Park *et al.,* 2002). In *S. cerevisiae,* Ste12 interacts with several accessory proteins, forming complexes to modify and regulate downstream targets. Ste12 forms a complex with Dig1 and Dig2 to regulate pheromone response elements and also forms a second complex with Dig1 and Tec1 to regulate filamentous responsive elements (Chou *et al.,* 2006). *M. oryzae*, however, does not have homologues of Dig1, Dig2, or Tec1. In *S. cerevisiae*, Ste12 also interacts with a Mcm1 MADS-box transcription factor to regulate pheromone response genes (Chou *et al.,* 2006). *M. oryzae* has a Mcm1 homologue, and *Δmcm1* mutants are defective in penetration (Zhou *et al.,* 2011). Interestingly, the double mutants

Δmst12/Δmcm1 are able to form appressoria on hydrophilic surfaces, suggesting an overlapping role for these two transcription factors to suppress appressorium formation on non- inductive surfaces (Zhou *et al.,* 2011).

In this chapter, through a comparative transcriptomics analysis, I set out to determine the identity of genes associated with appressorium morphogenesis. The experimental approach was carried out with both a *Δpmk1* mutant and an isogenic wild type strain, Guy11, over a time course of appressorium formation on a hydrophobic surface. Appressorium assays were set up and from these, total RNA was extracted from both a Δ*pmk1* mutant and Guy11 at 8 time points over a period corresponding to appressorium formation in the wild type. Libraries were then generated for RNA-Seq analysis. The data generated was used in a comparative analysis, to determine gene sets associated with early and late development of appressoria. I also set out to identify transcription factors that are likely to be Pmk1-regulated, to determine genes associated with appressorial morphogenesis, and to define the link between the Pmk1 pathway and pivotal processes associated with appressorium formation.

Moreover, a complementary transcriptomics comparative analysis was performed in which RNA-Seq libraries were also prepared from Guy11 on a hydrophilic surface. The aim of this analysis was to identify differential gene sets associated with the *PMK1*-dependent hydrophobic surface response associated with appressorium development, and compare this to the response to a hydrophilic, non-inductive surface. In this way I aimed to distinguish between genes associated specifically with appressorium development and those that may be differentially expressed solely as a consequence of the different environmental conditions.

3.2 Materials and methods

3.2.1 Standard materials and methods

For standard materials and methods see Chapter 2.

3.2.2 Preparing appressorium development assays for RNA extraction, RNA

Appressorial assays were conducted as described in General Materials and Methods section 2.4.1. Appressorial assays of Guy11 on non-inductive surface using Gelbond (hydrophilic surface) were prepared the same way as appressorial assays for inductive surfaces.

3.2.3 Analysis of the data

The output short reads of the Illumina HiSeq 2000 sequencer were aligned against version 8.0 of the *M. oryzae* genome sequence using Tophat software (Trapnell *et al.,* 2010). Analysis of the data was done using DE-Seq (Anders and Huber, 2010). Transcript abundances for each gene and adjusted P-values (P_{adj}) were generated as according to Soanes et al. (2012). To determine the significant differences of the pair wise comparisons we adjusted the p-value <=0.01. Data was analysed by using Microsoft Access. Heat-maps were generated using “gplots” package (http://cran.r-project.org/web/packages/gplots/gplots.pdf) from the free computing software platform R (http://www.r-project.org/).

3.3 Results

3.3.1 Conidium germination and appressorium development in Guy11 and the Δ*pmk1* mutant

Appressorium development assays were prepared with both the wild type Guy11 strain and the isogenic Δ*pmk1* mutant. Spores were inoculated onto glass cover-slips (hydrophobic) and incubated at 26℃. The development of infection structures was monitored every two hours over a 24 h period. Figure 3.1 shows a series of micrographs taken at different stages of development for each strain. At 2 h, Guy11 forms a polarized germ tube which by 4 h starts to swell and hook. By 6 h, the spores develop incipient appressoria. These appressoria became noticeably melanised at 8 h as the cells matured. At 24 h the appressoria were visible as typical dome shaped melanised structures, and the three cells of the conidia collapsed. The Δ*pmk1* mutant forms a polarized germ tube at 2 h, which elongates during the entire time course. Swelling and hooking of germ tubes is observed around 14 h, 16 h and 24 h, but no appressoria are formed and conidia do not collapse.

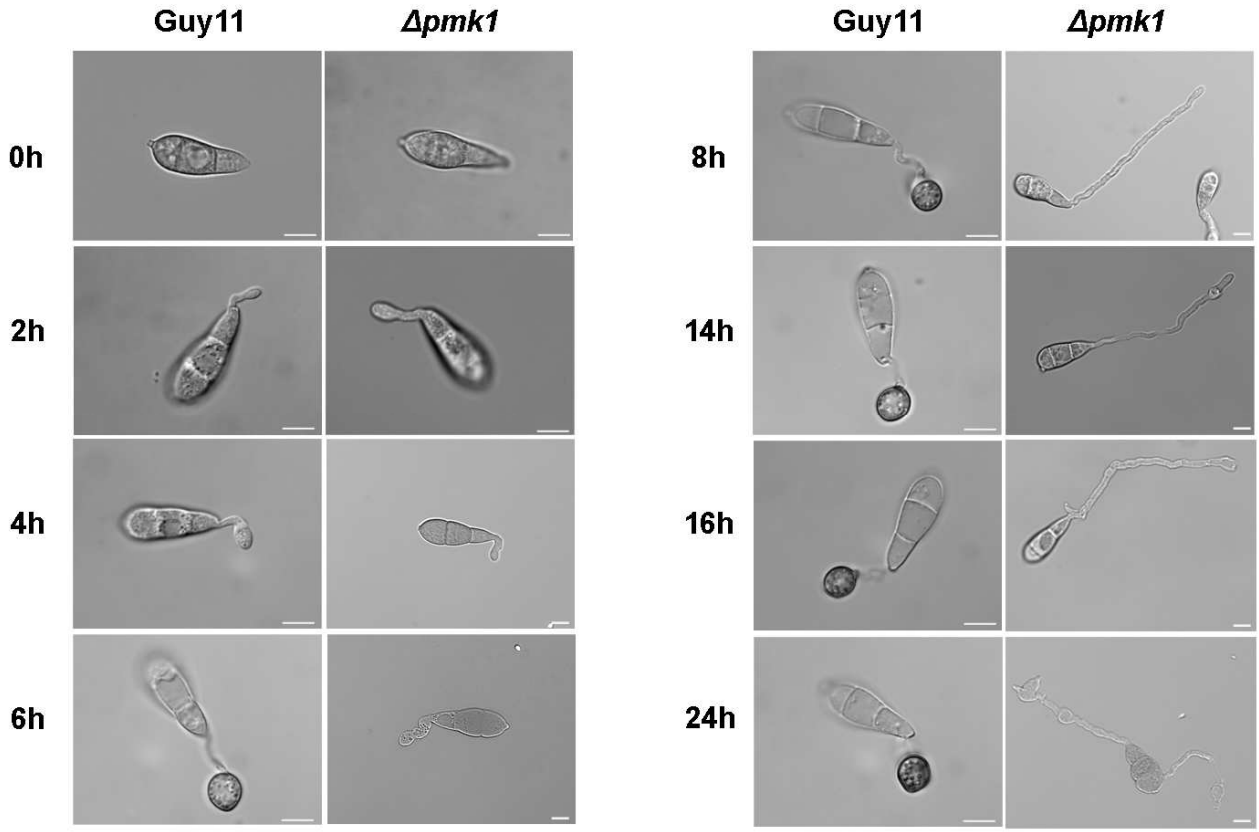

Figure 3.1 Micrographs showing appressorium development at time points used in this study from Guy11 and ∆*pmk1* mutant. Conidia were germinated on hydrophobic coverslips for a period of 24 hours. (bars = 10 µm in all panels)

3.3.2 Global changes in gene expression in the Δ*pmk1* mutant

To characterize the transcriptional profile associated with morphogenetic changes during appressorium formation, a comparative transcriptional analysis using RNA-Seq was performed between a strain impaired in appressorium formation, the Δ*pmk1* mutant, and wild type strain Guy11. For this, the appressorial time course described in section 3.3.1 was scaled up as described in section 2.5.1 to allow to generate enough material for the experiment. Conidia of both Δ*pmk1* mutants and Guy11 were incubated at 26 ℃ over a period of 24 h in the presence of the cutin monomer 1,16- hexadecanediol and distilled water, on glass cover- slips. The addition of 1,16-hexadecanediol acts as an inducer for appressorium development and helps sincronizing the formation of the structure {Gilbert, 1996 #1096}. Samples were collected every two hours by scraping the cover-slip surface with a razor blade and immediately snap freezing the material into liquid Nitrogen. Total RNA was then extracted and RNA-Seq libraries prepared. The libraries were sequenced using an Illumina HiSeq Sequencer 2500. Short sequencing reads were aligned against version 8.0 of the *M. oryzae* genome using Tophat software (Trapnell *et al.,* 2010). In total, in *M. oryzae* genome can be found 12828 genes, The analysis of the data was performed using DESeq which determines differential gene expression through the moderated log2 fold change value (mod_lfc) (Anders and Huber, 2010). Transcript abundances for each gene were obtained and adjusted p-values were generated according to Soanes *et al.,* (2012). The average number of reads obtained was 50 million reads.

To understand global transcriptional patterns of gene expression in a Δ*pmk1* mutant, Euclidean distances were determined between each sample of both Δ*pmk*1 and

Guy11 strains whereby the transcriptional abundance of every transcript was compared in a pair wise manner in all possible combinations. Similar patterns of gene expression were observed during early appressorium development (2 h to 4 h) in both Guy11 and the Δ*pmk1* mutant (Fig. 3.2). Specifically Euclidean distance analysis showed very similar patterns of transcript abundance at 2 h and 4 h. This indicates that early gene expression is largely common between both strains. However, there is also evidence that Δ*pmk1* mutants are delayed in gene expression associated with conidial germination and germ tube development. For example, gene expression patterns in Δ*pmk1* mutant at 6 h, and even 8 h, are more similar to those exhibited by Guy11 at 4 h and even 2 h, consistent with a pronounced delay caused by loss of Pmk1. Considerable divergence in gene expression occurs later, when Guy11 is elaborating an appressorium. For example, gene expression by 24 h is very distinct in Guy11 compared to the Δ*pmk1* mutant (Fig. 3.2) and this can be defined as different clades by Euclidean analysis.

To determine the subset of genes likely to be Pmk1-regulated, either directly or indirectly, and thereby define the transcriptional signature associated with appressorium development, the number of differentially expressed genes of the Δ*pmk1* mutant compared to Guy11 was determined for every time point during the time course of appressorium development. It was found that at early stages of development the number of differentially expressed genes was higher than at late stages of development, consistent with the increased phenotypic differences between the Δ*pmk1* mutant and Guy11. Furthermore, to distinguish between potential Pmk1-activation or repression roles, the number of genes up-regulated and down-regulated was determined (Fig.

3.3.). During the time course, the number of down-regulated genes in Δ*pmk1* in comparison to Guy11 was always greater than the number of up-regulated genes, consistent with the role that the Pmk1 MAPK possesses as an activator of numerous downstream targets.

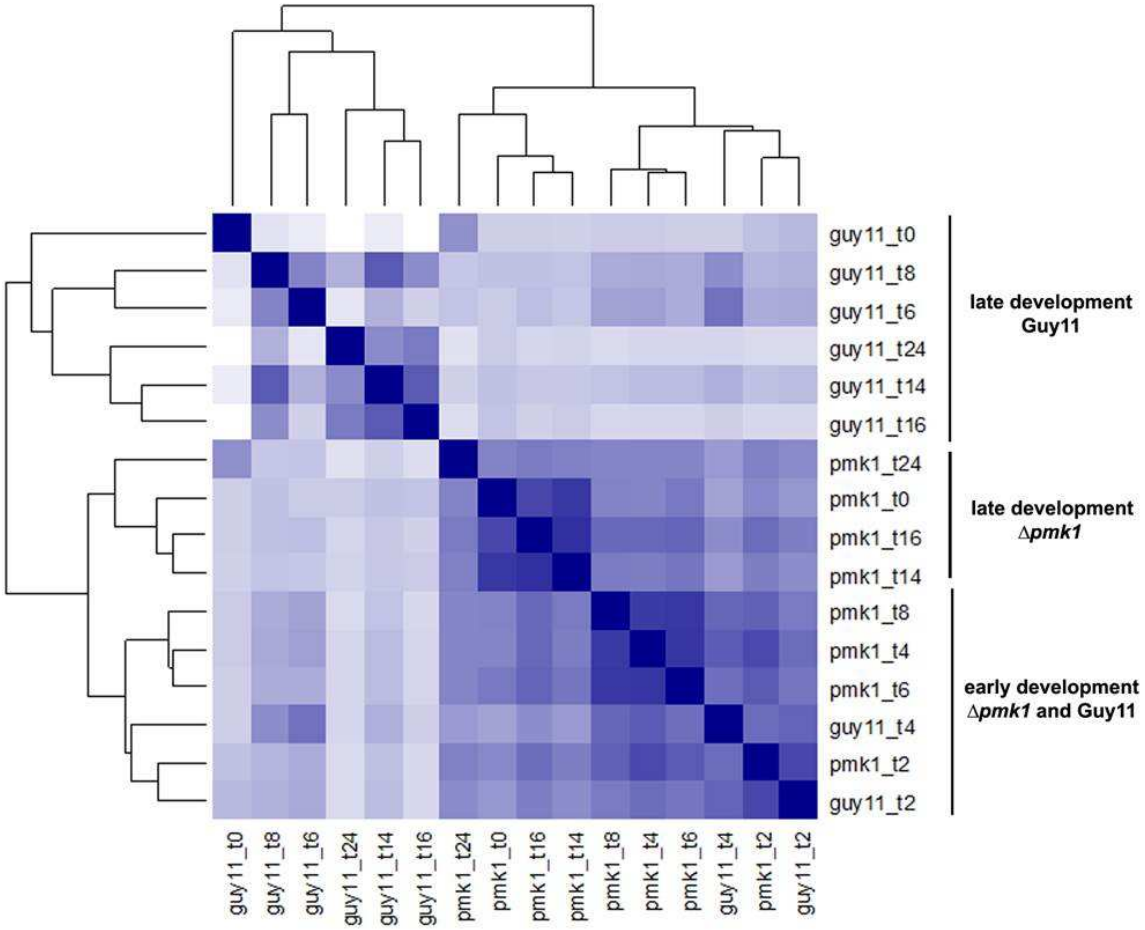

Figure 3.2 Heatmap showing the Euclidean distances between RNA-Seq samples from wild type Guy11 and the Δ*pmk1* mutant. Each label indicates the name of the strain and time point. Euclidean distance heatmap compared the entire time course of both Guy11 and the Δ*pmk1* mutant in a pair wise manner in all possible combinations. The heatmap shows higher similarity between samples as darker is the colour: white colour indicates high differences between the samples and dark blue colour indicates higher similarity between the samples. A dendrogram in parallel with the Euclidean heatmap was generated to determine sample clustering.

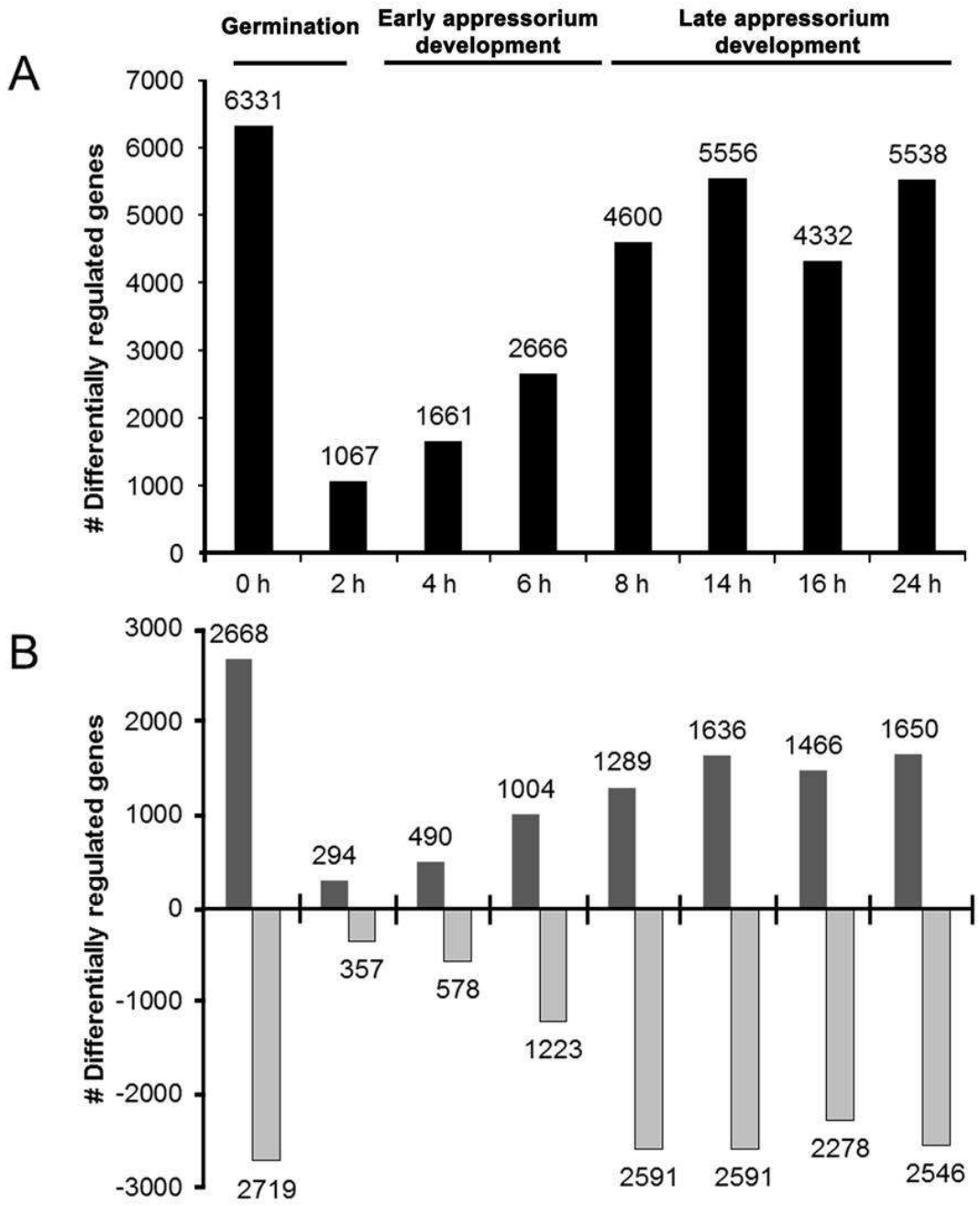

Figure 3.3 Bar charts to show the number of differentially regulated genes in the Δ*pmk1* mutant compared to Guy11. **A)** Bar chart to show total number of differentially regulated genes in the Δ*pmk1* mutant when compared with Guy11 (padj <0.01). **B)** Bar chart to show number of up-regulated (Dark gray) and down regulated genes in Δ*pmk1* when compared with Guy11 (padj <0.01; mod_lfc >1) (Light gray).

3.3.3 Global changes in gene expression during early and late stages of development of the Δ*pmk1* mutant

Previous data has shown that development of the Δ*pmk1* mutant can be divided between early stages of development and late stages of development (see section 3.3.2). These two stages showed increasing number of differences in gene expression, which were greater at late development than at early stage development in the Δ*pmk1* mutant compared to Guy11. Therefore, it was decided to investigate the nature of these differences by defining the associated biological processes. To do that, a FunCat analysis (Functional Catalogue), and complementary GO annotation, were used for functional classification of genes in terms of predicted biological processes in a hierarchical manner (Ruepp *et al.,* 2004). First, FunCat classifies each gene into different categories. Categories are organized hierarchically and they define a particular, predicted cellular pathway or process. Therefore, several categories can potentially be applied to the same gene because it may be involved in different cellular processes.

To initiate FunCat analysis, first it was necessary to define gene datasets corresponding to early development and late development in the Δ*pmk1* mutant. This was based in the findings of the Euclidean heatmap analysis, in which for the Δ*pmk1* mutant early development corresponded to 2 h, 4 h, 6 h and 8 h, and late development corresponded to 14 h, 16 h, and 24 h. and (because of the similarity in gene expression profile to late time points) the 0 h time point. The number of genes differentially regulated at 2 h, 4 h, 6 h and 8 h (Fig. 3.3 panel A) were used to create a Venn diagram, which defined 322 common genes strongly associated with early development

in the Δ*pmk1* mutant (Fig. 3.4 panel A). The number of genes differentially regulated at 14 h, 16 h, 24 h and 0 h (Fig. 3.3 panel A) were used to create a Venn diagram which defined 1551 common genes associated with late development that are likely to be under Pmk1-regulation. (Fig. 3.4 panel B).

Out of 322 genes associated with early development in the Δ*pmk1* mutant, 220 genes were non-classified and therefore considered as uncategorized gene functions. The 112 categorized genes represent 464 functional categories in total. From 1551 genes associated with late development, 977 genes were considered uncategorized. The 574 categorized genes represent 2608 functional categories in total. To analyse the importance of each identified biological process at early and late development in the Δ*pmk1* mutant, the percentage of genes in each functional group was calculated compared to the total, as shown in Figure 3.4 panel C. At early stages of development, the functional categorisation analysis revealed differences between Δ*pmk1* and Guy11 in metabolism (32.1%), proteins with a binding function (8%), regulation of metabolism and protein function (1.7%), cellular transport (18.1%), cellular communication and signal transduction (3.7%), cell rescue, defence and virulence (8.2%), environment interaction (5.4%) and development (0.4%). At late stages of development, however, differences were observed in gene products associated with energy (3.8%), cell cycle (5.4%), transcription (4.6%), in protein synthesis (2.5%), protein fate (7.2%), cell fate (1.4%), biogenesis of cellular components (4.8%) and cell type differentiation (3.5%).

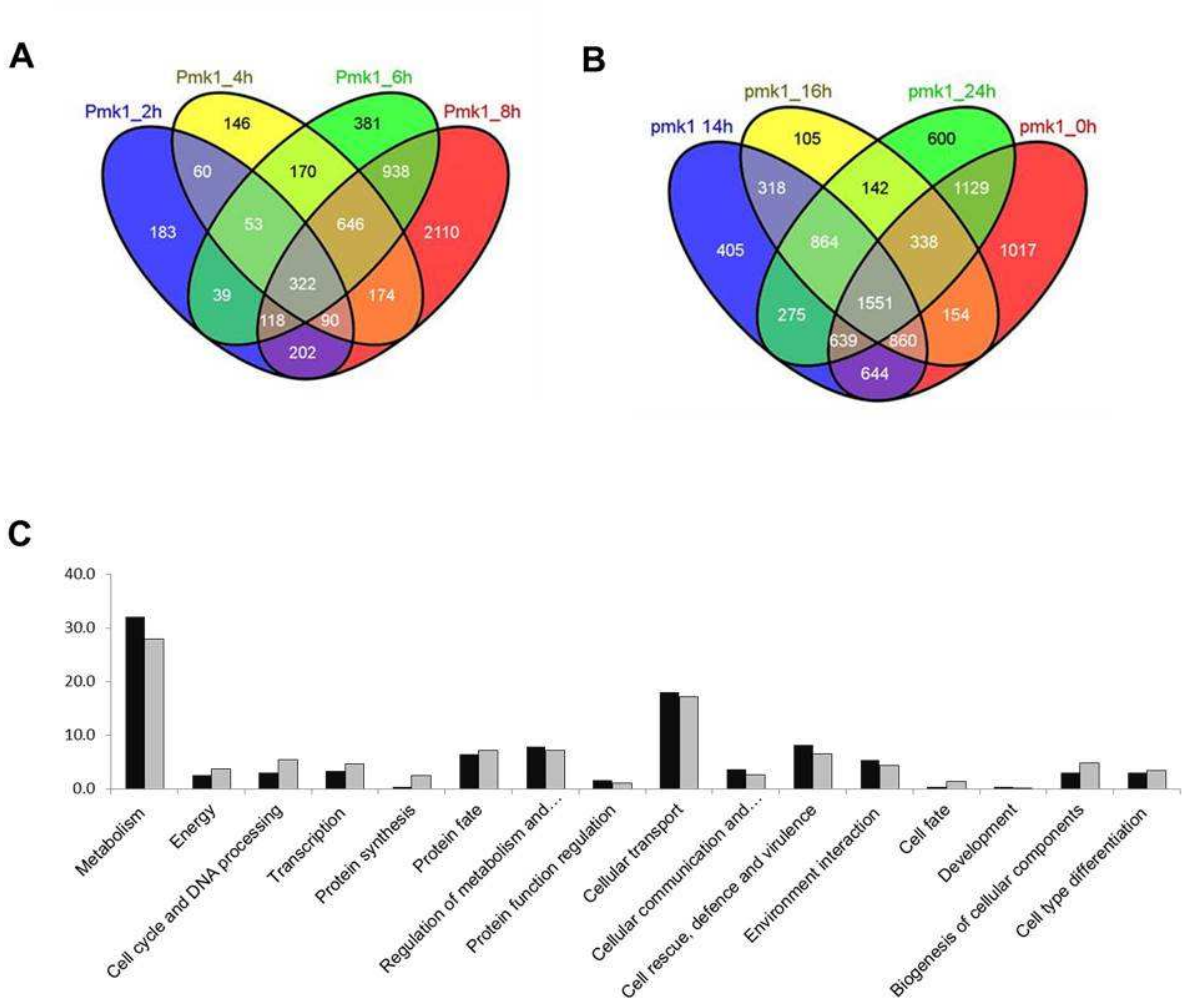

Figure 3.4 Global changes in gene expression at early and late development in the Δ*pmk1* mutant. Venn diagram illustrating overlaps between differentially regulated genes (padj< 0.01) of the *Δpmk1* mutant compared to Guy11. **A)** at early development (2 h, 4 h, 6 h and 8 h) **B)** and late development (14 h, 16 h, 24 h and 0 h). **C)** FunCat bar chart illustrating the percentage of genes in each predicted functional category relative to the total number in the early development dataset (Black bar) and late development dataset (Grey bar).

3.3.4 Determination of Pmk1-dependent hydrophobicity response genes

Appressorium formation in *M. oryzae* occurs under inductive conditions, which depend on certain surface characteristics such as hardness, hydrophobicity and the presence of plant waxes (Bourett, 1990). The Pmk1 MAP kinase signalling pathway has been reported to be responsible for transmitting signals associated with surface hydrophobicity because the null mutant Δ*pmk1,* is unable to form appressoria on hydrophobic surfaces (Xu and Hamer, 1996). For this reason, it was decided to identify genes responsible for the Pmk1-dependent hydrophobicity response using comparative transcriptomics. To do this, a transcriptional profile of genes regulated by Pmk1 were obtained by comparative transcriptomic analysis between a *Δpmk1* mutant compared to the isogenic wild type strain Guy11, both incubated on a hydrophobic surface, as shown in Figure 3.5. Transcriptional profiling of genes associated with perception of a hydrophobic response was obtained as a result of a comparative transcriptomics analysis of genes differentially regulated between the wild type Guy11 incubated on a hydrophobic surface (designated as $Guy1_{HPB}$) and Guy11 on a hydrophilic surface (designated as $Guy11_{HPL}$), as shown in Figure 3.5. After that, a third comparison was performed in which transcriptional profiling of genes regulated by Pmk1 was compared to the transcriptional profile of genes associated with a hydrophobicity response, resulting in the final Pmk1-dependent hydrophobicity response gene set, as shown in Figure 3.5. As a result, two further gene sets were obtained: genes that appear to be regulated by Pmk1 (independent of the hydrophobicity response) and genes that appear to be regulated by hydrophobicity (independent of Pmk1).

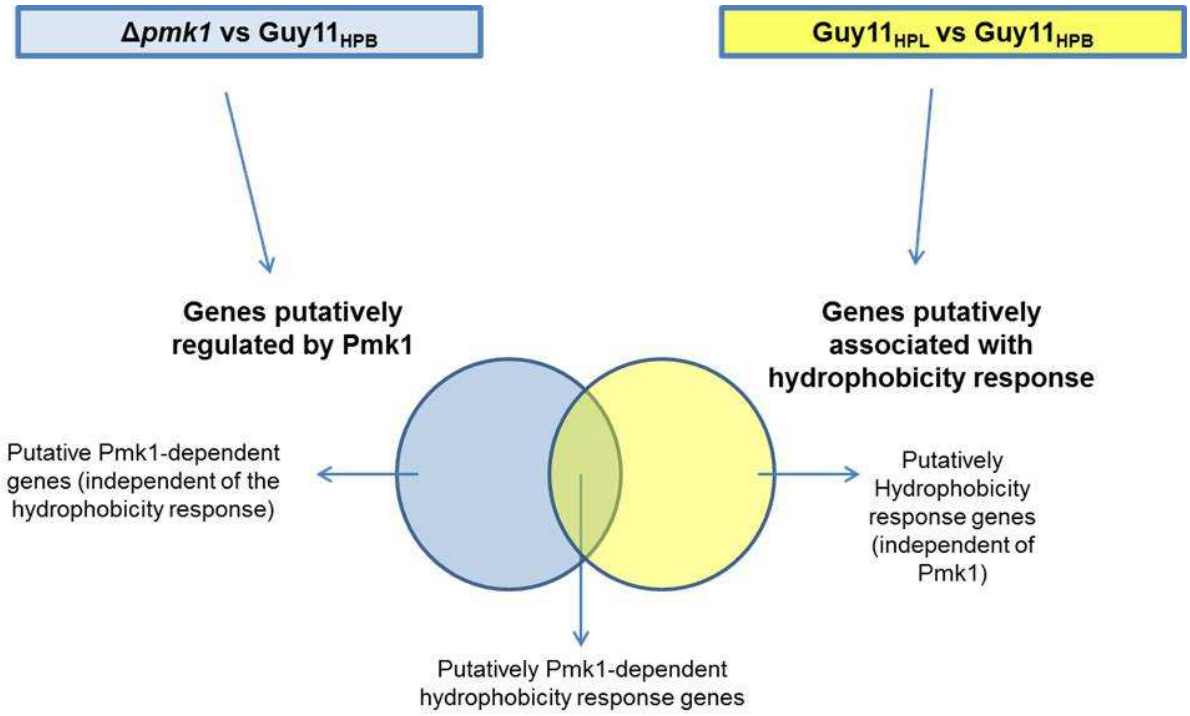

Figure 3.5 Diagram showing the strategy followed to identify Pmk1-dependent hydrophobicity response genes in *M. oryzae*. Differentially regulated gene set of the *Δpmk1* mutant compared with Guy11 $_{HPB}$ to determine genes putatively regulated by Pmk1. Differentially regulated gene set of Guy11 in hydrophobic surface ($Guy11_{HPB}$) compared with Guy11 in hydrophilic surface ($Guy11_{HPI}$) to determine genes putatively associated with hydrophobicity response. Venn diagram illustrating overlapping region between genes putatively regulated by Pmk1 and genes associated with hydrophobic response.

3.3.4.1 Determination of the transcriptional profile of genes regulated by Pmk1

The transcriptional profile of genes that are putatively regulated by Pmk1 was obtained previously in section 3.3.2 from comparative transcriptomic analysis that identified genes differentially regulated in the *Δpmk1* mutant compared to Guy11, following incubation of spores on a hydrophobic surface.

3.3.4.2 Determination of the transcriptional profile of genes associated with a hydrophobic response

The frequency of appressorium formation in Guy11 was first quantified in response to a number of different parameters such as, the degree of surface hydrophobicity, nutritional status and the presence or absence of cutin monomers. To test the effect of surface hydrophobicity, two different surfaces were used, glass cover-slips which provide an inductive hydrophobic surface, and Gelbond which has a non-inductive plastic surface (hydrophilic). To test the effect of nutritional status, two different incubation conditions were used: one in the presence of nutrients, with complete media (CM), and a second one in the presence of distilled water. The effect of cutin monomers was tested by two treatments; the first in the presence of cutin monomers and a second one in the absence. Spores of the wild type Guy11 were harvested and prepared at a concentration of 7.5×10^5 spores mL^{-1} and incubated for 24 h at which the phenotype was scored. As shown in Figure 3.5, in the presence of CM, appressorium formation did not occur on either hydrophobic or hydrophilic surfaces and this was not affected by addition of 1, 16-hexadecanediol. Secondly, we observed that appressorium formation did not occur on Gelbond even after addition of 1, 16-hexadecanediol. Therefore, these initial observations indicated that appressorium

formation was only found in the presence of distilled water, in the presence of 1,16-hexadecanediol, on a hydrophobic surface. As a consequence, it was decided to proceed with RNA-Seq experiment using the non- inductive surface, Gelbond, in the presence of 1, 16 hexadecandiol and distilled water.

To determine global changes in gene expression in Guy11 under non-inductive conditions, comparative transcriptomics approach was performed. Conidia of Guy11 were incubated in distilled water on the non-inductive hydrophilic surface (Gelbond; Guy11 $_{HPL}$) and on the inductive hydrophobic surface (glass cover-slips; Guy11$_{HPB}$), both in the presence of 1, 16- hexadecanediol. Conidia were incubated at 26 ℃ for 24 h and samples collected every two hours by scraping the cover-slip surface with a razor blade, the cells were then snap frozen, total RNA extracted, and RNA-Seq libraries prepared. Sequencing and analysis procedures were performed, as described in section 3.2.

The total number of differentially expressed genes in Guy11 $_{HPL}$, compared with Guy11$_{HPB}$ over the time course was determined for every time point (Fig. 3.6). The data revealed that the total number of differentially expressed genes was lower during the early developmental stages than during late developmental stages. Figure 3.6 shows two distinct patterns in the total number of differentially expressed genes. The first one includes the early time points at 2 h, 4 h and 6 h. The total number of differentially expressed genes within these samples varies from 1701 to 2257 genes. The second one includes later time points at 8 h, 14 h and 24 h and the total number of

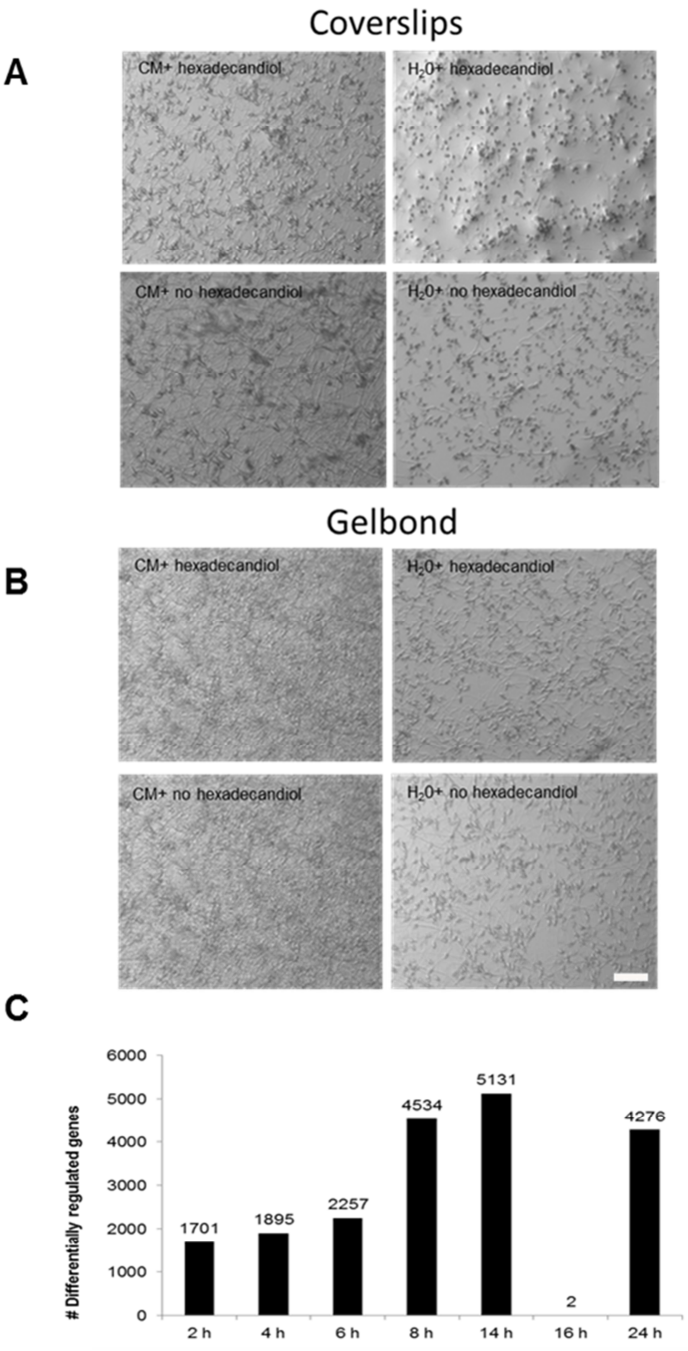

Figure 3.6 Determining the optimal conditions in which to carry out the experiments to generate Guy11 $_{HPL}$. Appressorium formation assay **A)** in a hydrophobic surface (glass cover-slips) or **B)** in a hydrophilic surface (Gelbond). **C)** Bar chart to show total number of differentially regulated genes in Guy11$_{HPL}$ compared to Guy11$_{HPB}$ (padj <0.01).

differentially expressed genes varies from 4276 to 5131. Surprisingly, the sample at 16 h only showed 2 genes differentially regulated so therefore it was therefore not considered for further analysis.

3.3.4.3 Determination of the transcriptional profile of genes associated with Pmk1-dependent hydrophobic response

To follow the analysis and define the transcriptional signature associated with the Pmk1-dependent hydrophobicity-response, genes differentially regulated in a *Δpmk1* mutant compared to Guy11, and genes differentially regulated in Guy11 $_{HPL}$ compared with Guy11$_{HPB}$, at 4 h were compared to each other and a Venn diagram generated, as shown in Figure 3.7. For this analysis, only the timepoint at 4h was considered. The reasoning underneath this decision is based on the fact that by 4h in a standard timecourse of Guy11 under an inductive surface, the development of an incipient appressorium occurs and therefore, it is considered that at 4h the appressoria-associated changes in gene expression occur. The number of differentially expressed genes in *Δpmk1* compared to Guy11 at 4 h is 1661 and for Guy11 $_{HPL}$ compared with Guy11$_{HPB}$ at 4 h is 1895. These differentially expressed genes are presented in Venn diagram (Fig. 3.7). To complete the analysis, all down-regulated genes (padj<1, mod_lfc<1) as well as up-regulated genes (padj<1, mod_lfc<1) were then included separately. This analysis identified 736 differentially-regulated genes, from which 285 were down-regulated and 62 up-regulated over 2-fold (Fig. 3.7). However, further analysis only took into account those genes that were either up-regulated or down-regulated.

In total, 18 genes were identified which were at least 25-fold down-regulated in both *Δpmk1* and Guy11$_{HPL}$ (Table 1). These included a phosphate repressible acid phosphatase (MGG_12020) a homologue of *A. nidulans PHOA,* a cell surface protein encoding gene *GAS2* (MGG_04202), an endochitinase (MGG_00086), a pectate lyase (MGG_17486), a Ubiquitin 3 binding protein But2 C-terminal domain (MGG_14179), two multi-copper oxidases (MGG_07220 and MGG_02876), a peroxidase (MGG_07790), a lysR family regulatory protein (MGG_09384) and a tat pathway signal containing protein (MGG_17053). Eight of those identified genes were hypothetical proteins and have no known homologue in Blast2go analysis or any pfam domain annotations.

Among genes identified in the down-regulated gene set were 3 chitin synthases, chitin binding or recognition related proteins (MGG_07676, MGG_05351, MGG_13275), 7 transcription factor-encoding genes: *STU1* (MGG_00692), *NIR1* (MGG_01518), *HOX7* (MGG_12865), *CMR1* (MGG_07215) and 5 hypothetical protein encoding genes (MGG_00587, MGG_01833, MGG_04758, MGG_09276 and MGG_09676). The analysis also revealed genes encoding cell cycle proteins, such as *FAR1* from *S. cerevisiae* (MGG_00134), a *S. pombe* homologue *CDC14* (MGG_00757) involved in septation and cytokinesis and a B-type cyclin *CYC2* (MGG_07065). The analysis also identified an acetyl CoA carboxylase (MGG_07613), *ALB1* (MGG_07219) and *RSY1* (MGG_05059), both encoding melanin biosynthetic enzymes. There were also two genes, *SPO12* (MGG_08639) involved in mitotic exit (Shah *et al.,* 2001) and *SPO7* (MGG_06158) involved in nuclear shape and morphogenesis (Santos-Rosa *et al.,* 2005; Siniossoglou *et al.,* 1998). Also an IQ calmodulin-binding domain containing protein (MGG_03743) was found in the analysis. Genes identified in the up-regulated gene set

included a C6 zinc finger domain-containing protein (MGG_01887) and a glucose-repressible protein (MGG_00715).

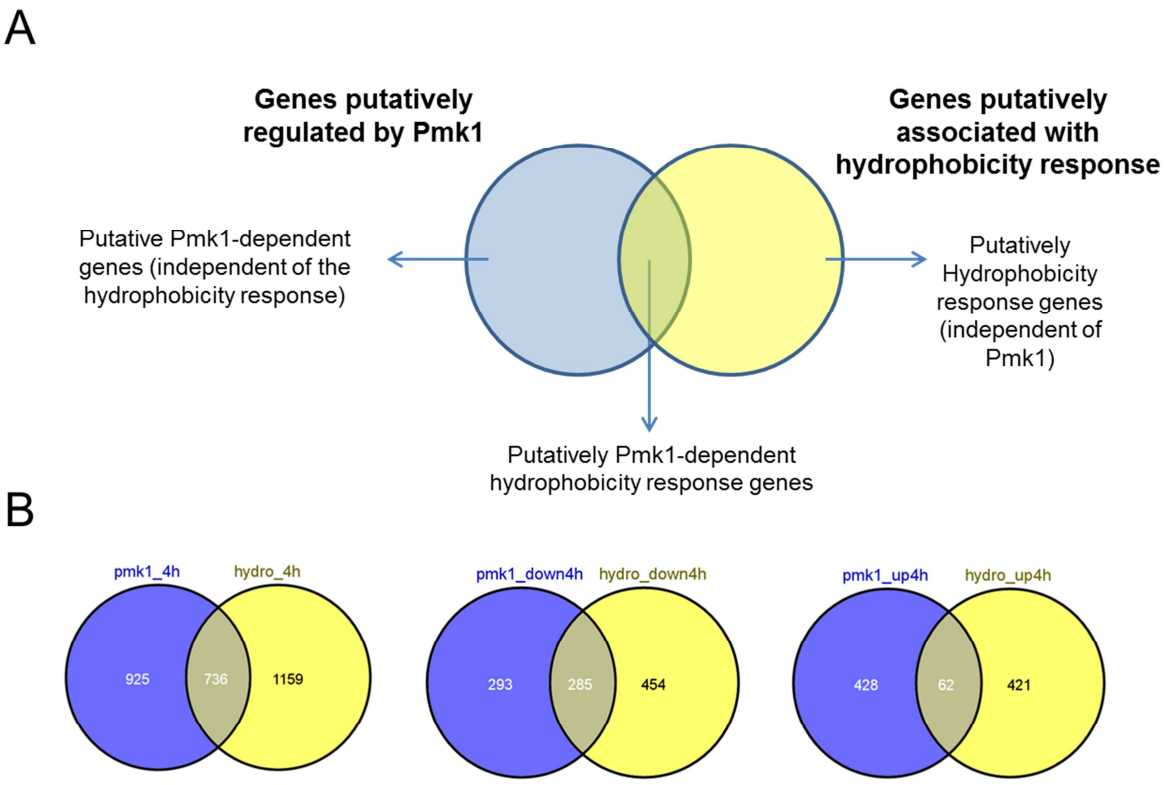

Figure 3.7 Identification of genes responsible for the response to surface hydrophobicity under Pmk1 regulation, appressorium impairment and hydrophilic response in *M. oryzae*. A) Venn diagram illustrating the strategy of the analysis showing overlaps between differentially regulated gene sets of *Δpmk1* compared with Guy11 and Guy11 on a hydrophilic surface compared with Guy11, to define the desired gene sets. **B)** Venn diagram illustrating overlaps between *Δpmk1* compared with Guy11 and Guy11 on a hydrophilic surface and Guy11 at 4 h for differentially regulated gene sets (padj< 0.01), down-regulated-gene sets (padj< 0.01; mod_lfc< 1) and up-regulated gene sets (padj< 0.01; mod_lfc> 1).

Table 3.1 List of genes whose gene expression was down-regulated at least 25-fold *Δpmk1* mutant and Guy11 $_{HPL}$ compared to Guy11 $_{HPB}$.

Gene	Broad Institute	BLAST2GO	Pfam	*Δpmk1*[1]	Guy11$_{HPL}$	Gene	Broad Institute	BLAST2GO
MGG_12020	phosphate-repressible acid phosphatase (534 aa)	acid phosphatase	Phosphoesterase family (PF04185) 107->281	-11.10	-10.81	MGG_12020	phosphate-repressible acid phosphatase (534 aa)	acid phosphatase
MGG_04202	GAS2 (291 aa)	cell surface protein	Protein of unknown function (DUF3129) (PF11327) 17->253	-7.11	-7.07	MGG_04202	GAS2 (291 aa)	cell surface protein
MGG_00086	endochitinase (425 aa)	endochitinase	Glycosyl hydrolases family 18 (PF00704) 39->382	-6.12	-8.02	MGG_00086	endochitinase (425 aa)	endochitinase
MGG_17486	HP[2](800 aa)	glycoside hydrolase family 55 protein	Pectate lyase superfamily protein (PF12708) 67->289, Pectate lyase superfamily protein (PF12708) 418->591	-5.49	-5.07	MGG_17486	HP(800 aa)	glycoside hydrolase family 55 protein
MGG_14179	HP(224 aa)	gpi anchored cell wall protein	Ubiquitin 3 binding protein But2 C-terminal domain (PF09792) 64->211	-11.26	-7.57	MGG_14179	HP(224 aa)	gpi anchored cell wall protein
MGG_02296	HP(165 aa)	HP		-11.22	-10.70	MGG_02296	HP(165 aa)	HP
MGG_02756	HP(276 aa)	HP		-6.73	-7.80	MGG_02756	HP(276 aa)	HP
MGG_04749	HP(407 aa)	HP		-7.79	-11.33	MGG_04749	HP(407 aa)	HP
MGG_04838	HP(1095 aa)	HP	Domain of unknown function (DUF4203) (PF13886) 103->309	-5.42	-5.40	MGG_04838	HP(1095 aa)	HP
MGG_05028	HP(189 aa)	HP		-8.95	-8.24	MGG_05028	HP(189 aa)	HP
MGG_07372	HP(143 aa)	HP		-7.04	-7.46	MGG_07372	HP(143 aa)	HP
MGG_12165	HP(530 aa)	HP		-5.39	-7.19	MGG_12165	HP(530 aa)	HP
MGG_16796	HP(97 aa)	HP		-8.48	-9.08	MGG_16796	HP(97 aa)	HP
MGG_07220	iron transport multicopper oxidase FET3 (543 aa)	iron transport multicopper oxidase fet3	Multicopper oxidase (PF07732) 30->144, Multicopper oxidase (PF00394) 154->281, Multicopper oxidase (PF07731) 364->493	-5.28	-5.28	MGG_07220	iron transport multicopper oxidase FET3 (543 aa)	iron transport multicopper oxidase fet3
MGG_02876	laccase-1 (596 aa)	laccase-1 precursor	Multicopper oxidase (PF07732) 84->199, Multicopper oxidase (PF00394) 211->371, Multicopper oxidase (PF07731) 450->561	-7.74	-6.05	MGG_02876	laccase-1 (596 aa)	laccase-1 precursor
MGG_07790	ligninase H2 (475 aa)	ligninase h2 precursor	Peroxidase (PF00141) 177->378	-5.81	-6.59	MGG_07790	ligninase H2 (475 aa)	ligninase h2 precursor
MGG_09384	HP(514 aa)	lysr family regulatory protein		-8.54	-9.56	MGG_09384	HP(514 aa)	lysr family regulatory protein
MGG_17053	HP(407 aa)	tat pathway		-5.82	-7.38	MGG_17053	HP(407 aa)	tat pathway

[1] The number indicates moderated log fold change (mod_lfc) for both *Δpmk1* and Guy11HPL
[2] HP stands for hypothetical protein

3.3.4.4 Determination of the transcriptional profile of Pmk1-dependent genes (independent on the hydrophobic response)

The analysis represented in Figure 3.7 also revealed genes that depend on Pmk1, but are independent of the hydrophobicity response. In total there were 925 differentially-regulated genes that are Pmk1-dependent, but independent of the hydrophobicity response, of which 293 were down-regulated and 428 up-regulated (Fig. 3.7). The analysis was carried out only with genes up-regulated or down- regulated and showed that the most down-regulated gene found in the analysis was the homologue of the cell-to–cell movement effector, *Bas2,* a biotrophy associated secreted protein 2 (MGG_07749), which was greater than 49 fold-down regulated in a *Δpmk1* mutant. Moreover, a second *Bas2* homologue, MGG_07969, was also found in this gene set, representing a 2.34 fold down-regulated expression. The analysis also identified a regulatory actin polymerization protein-encoding gene *BZZ1* (MGG_07332), an adhesion-encoding gene *MAD1* (MGG_12523), a hydrophobin (MGG_09460), a citrate synthase (MGG_07202), a serine threonine protein kinase involved in pheromone response in *S. cerevieiae STE20* (MGG_12118), a cyclin B1 type-encoding gene (MGG_03595), a Rho1 GTPase-encoding gene (MGG_12644) and Rho GTPase activator *RGA1* (MGG_04186). In total, six transcription factor encoding genes were found in this group, of which five contained a fungal Zn(2)-Cys(6) binuclear cluster domain (MGG_01833, MGG_05659, MGG_09273, MGG_09950, and MGG_11764) and also *STUA* (MGG_00692). The analysis also identified 11 glycosyl hydrolases and four glycosyl transferases, and six chitin syntheses, binding or recognition related proteins (MGG_01868, MGG_00245, MGG_04534, MGG_06771, MGG_09551, MGG_03609).

Moreover, nine major facilitator proteins (MGG_04850, MGG_04897, MGG_01516, MGG_03640, MGG_01485, MGG_09976, MGG_11713, MGG_07709, MGG_02840) were identified. The analysis also revealed two interesting genes MGG_06257 and MGG_00258, which are putative homologues of G protein-coupled glucose receptor related to Gpa2 of *S. cerevisiae*.

Analysis of the up-regulated gene set identified enzymes associated with quinate utilization, such as 3-dehydroshikimate dehydratase (MGG_07780), chorismate synthase (MGG_03281), QA-X (MGG_15250), quinate dehydrogenase (MGG_07781). Three transcription factor-encoding genes *ATF21* (MGG_02226), a C6 transcription factor-encoding gene (MGG_02226) and a bZIP transcription factor-encoding gene (MGG_04009), homologues of kinetochore protein-encoding gene *MIS14* and a AUR protein kinase-encoding gene (MGG_12408).

3.3.4.5 Determination of the transcriptional profile of genes associated with the hydrophobic response (independent of Pmk1)

The analysis represented in Figure 3.7 also revealed genes associated with the hydrophobicity response, but which are independent of Pmk1 regulation. In total there were 1159 genes associated with the hydrophobicity response, but independent of Pmk1, of which 454 were down-regulated and 421 up-regulated (Fig. 3.6). Among the down-regulated gene set were six transcription factor-encoding genes: four Fungal Zn(2)-Cys(6) binuclear cluster domain containing proteins (MGG_02226, MGG_05459, MGG_11119 and MGG_15139), the *A. nidulans* over-expressed fluffy transcription

factor C (Lee *et al.,* 2005) *OEFC* (MGG_10422),a homologue of the *Neurospora crassa* cross-pathway control protein 1 encoding gene, *CPC1* (MGG_00602), the transcription factor-encoding gene *ACLR* (MGG_02129) and MGG_04122 and MGG_04571 which were unknown. Interestingly, this analysis also identified eight NmrA-like family proteins (MGG_12714, MGG_12473, MGG_17002, MGG_05101, MGG_00156, MGG_02336, MGG_02860, MGG_09705), including the previously described *NMR1*, *NMR2* and *NMR3* genes which are important for fungal pathogenesis (Wilson *et al.,* 2010), four NADH:flavin oxidoreductase/NADH oxidase family (MGG_10583, MGG_08297, MGG_03823,MGG_04569), including *OYE1* (Wilson *et al.,* 2010), two NAD(P)-binding Rossmann-like domain (MGG_02320 and MGG_08880) a NADH(P)-binding domain containing protein (MGG_04736), NAD dependent epimerase (MGG_02304), and a NAD binding domain of 6-phosphogluconate dehydrogenase (MGG_01687). Also, five mitochondrial carrier proteins (MGG_04662, MGG_07616, MGG_00917, MGG_06821, MGG_01493), one mitochondrial import receptor subunit or translocase (MGG_03091), two mitochondrial proteins (MGG_17058 and MGG_05262), and a hexokinase (MGG_00623) were identified. Other genes identified included the protein kinase-encoding genes, *STE20* (MGG_08746) and *NIMA* (MGG_03026), cytoskeleton-associated encoding genes, such as the *PAX1* LIM protein-encoding gene (MGG_05738), a cell division control-encoding gene (MGG_11899) and a separin (MGG_06245). Moreover, autophagy-associated genes were also identified in this analysis, including, *ATG6* (MGG_03694) and *ATG9* (MGG_09559).

The set of genes up-regulated or only present in Guy11 upon incubation on a hydrophilic surface ($Guy11_{HPL}$), included 14 transcription factor-encoding genes (Table

3.2). One of these (MGG_06971), was identified as a putative flocculation suppressor protein encoding gene. DNA repair encoding genes, such as *RAD5* (MGG_06094), *SPA2* (MGG_03703), *MAD1* (MGG_12523), *BAS2* (MGG_07969 and MGG_7749) and *BAS3* (MGG_16415 and MGG_11610) were also identified as up-regulated.

Table 3.2 List of transcription factor-encoding genes found up-regulated in $Guy11_{HPL}$ compared to $Guy11_{HPB}$, that were identified in response to the presence of a hydrophobic surface (independently of Pmk1)

Gene	Broad Institute Annotation	BLAST2GO annotation
MGG_04024	HP (230 aa)	basic leucine zipper transcription factor domain-containing protein
MGG_04122	HP (336 aa)	HPMGG_04122
MGG_05016	HP (100 aa)	HPMGG_05016
MGG_02129	HP (887 aa)	regulatory protein alcr
MGG_05033	HP (743 aa)	c6 finger domain-containing protein
MGG_04665	HP (640 aa)	c6 finger domain
MGG_02377	HP (884 aa)	transcription factor
MGG_05659	HP (487 aa)	fungal zn binuclear cluster domain containing protein
MGG_03763	HP (731 aa)	c6 transcription
MGG_07368	HP (631 aa)	c6 finger domain protein acr-
MGG_07450	HP (907 aa)	fungal specific transcription factor domain-containing protein
MGG_04571	HP protein (853 aa)	c6 transcription
MGG_12339	HP protein (730 aa)	c6 finger domain-containing protein
MGG_06971	flocculation suppression protein (601 aa)	flocculation suppression protein

3.3.5 Transcription factor analysis: Identifying transcription factors likely to be Pmk1-regulated.

To identify transcription factor gene sets putatively co-regulated by Pmk1, genes encoding putative transcription factors were identified (Table 3.3). The number of differentially regulated genes was determined for every time point. They were then bulked together as 172 putative transcription factor-encoding genes differentially regulated in at least two time points. This putative transcription factor gene set is very likely to be Pmk1-regulated, and therefore more detailed analysis was performed.

Firstly, the putative Pmk1-regulated transcription factor gene set was classified according to Pfam analysis into 25 functional categories (Table 3.4). The most abundant category, with 37 transcription factors out of 56 present in the genome, corresponds to “no pfam associated” category (non-classified). The second and third most abundant categories correspond to “Fungal Zn(2)-Cys(6) binuclear cluster domain (PF00172)” and “Fungal Zn(2)-Cys(6) binuclear cluster domain (PF00172) and Fungal-specific transcription factor domain (PF04082)” containing 35 and 27 transcription factors ,out of 48 and 41 such proteins predicted in the genome, respectively. All putative transcription factors were classified in this way, including bZIP (PF00170)”, “GATA zinc finger (PF00320)”, “GATA zinc finger (PF00320)”, “Helix-loop-helix DNA-binding domain (PF00010)”, “HSF-type DNA-binding (PF00447)”, “NDT80 / PhoG like DNA-binding family (PF05224)”, “Copper fist DNA binding domain (PF00649)”, “PAS fold (PF08447)“, “GATA zinc finger (PF00320)“ , “Fungal specific transcription factor domain (PF04082)”, “Fungal Zn(2)-Cys(6) binuclear cluster domain (PF00172) and another domain”, “Homeobox domain (PF00046)”, “Basic region leucine zipper (PF07716)” and “Fork

head domain (PF00250)" classifications. Two putative transcription factors showed significant differentiall expression in the null mutant *Δpmk1* compared to the wild-type Guy11, during all the time points of appressorium development. The is MGG_00587, a *M. oryzae*-specific b-zip domain-containing transcription factor predicted to be 333 aa long whose expression was down-regulated. The second transcription factor corresponds to MGG_01518, a predicted nitrogen-assimilation transcription factor 4, whose expression was down-regulated. It contains one fungal Zn(2)-C(6) binuclear domain and is a fungal-specific transcription factor domain.

To establish co-regulation patterns within the set of 172 Pmk1-regulated, putative transcription factors, the levels of transcript abundance for every transcription factor gene was determined and a heatmap created (Fig. 3.8). A dendrogram was also created to identify different clades of co-regulated genes. The heatmap showed 5 different clades, containing differing numbers of putative transcription factor genes. The most abundant clade corresponded to Clade 4, containing 70 transcription factors. Clades 1, 2 and 3 contain 32, 26 and 35 putative transcription factor genes, respectively. The less abundant clade 5, contained only 9 transcription factor-encoding genes (Fig. 3.8). However, genes within clade 5 showed the greatest down-regulation in gene expression during the time course, especially from 4 h to 24 h. The heatmap also showed an interesting pattern of gene expression for each of the 5 different clades. Clade 1 and clade 5 were selected for further analysis, because the up-regulation and down-regulation of genes in these clades were the most dramatic.

Table 3.3 The number of transcription factor-encoding genes likely to be Pmk1 regulated during a time course of appressorium development.

Time point (h)[3]	Transcription factors n°[4]	MST12 present[5]
0	143	Yes
2	27	No
4	33	No
6	51	Yes
8	113	No
14	126	Yes
16	105	Yes
24	113	Yes

[3] Specific time point of the time course
[4] number of transcription factor encoding genes for every time point
[5] presence or absence of Mst12 transcription factor on the group

Table 3.4 Classification of transcription factor-encoding genes likely to be Pmk1-regulated during a time course of appressorium development.

Category[6]	#Tfs regulated by Pmk1[7]
No Pfam associated	37
Fungal Zn(2)-Cys(6) binuclear (PF00172)	35
Fungal Zn(2)-Cys(6) binuclear (PF00172) and Fungal specific (PF04082)	27
bZIP (PF00170)	14
Fungal specific transcription factor domain (PF04082)	13
Fungal Zn(2)-Cys(6) binuclear cluster domain (PF00172) and another domain	6
Homeobox domain (PF00046)	6
GATA zinc finger (PF00320) 114->145, GATA zinc finger (PF00320)	5
Basic region leucine zipper (PF07716)	3
Helix-loop-helix DNA-binding domain (PF00010)	3
HSF-type DNA-binding (PF00447)	3
NDT80 / PhoG like DNA-binding family (PF05224)	3
Copper fist DNA binding domain (PF00649)	2
Fork head domain (PF00250) 738->801	2
PAS fold (PF08447) 204->274, GATA zinc finger (PF00320)	2
Aflatoxin regulatory protein (PF08493)	1
Aft1 osmotic stress response (OSM) domain (PF11785)	1
BB1 family (PF08185)	1
Cgr1 family (PF03879)	1
KilA-N domain (PF04383) 37->102, Ankyrin repeat (PF00023)	1
Hap4 (PF10297)	1
Putative GTPase activating protein for Arf (PF01412)	1
SRF-type transcription factor (PF00319)	1
STE like transcription factor (PF02200)	1
Tuftelin interacting protein N terminal (PF12457)	1

[6] Family of transcription factors
[7] number of putative transcription factor-encoding genes belonging to a family regulated by Pmk1

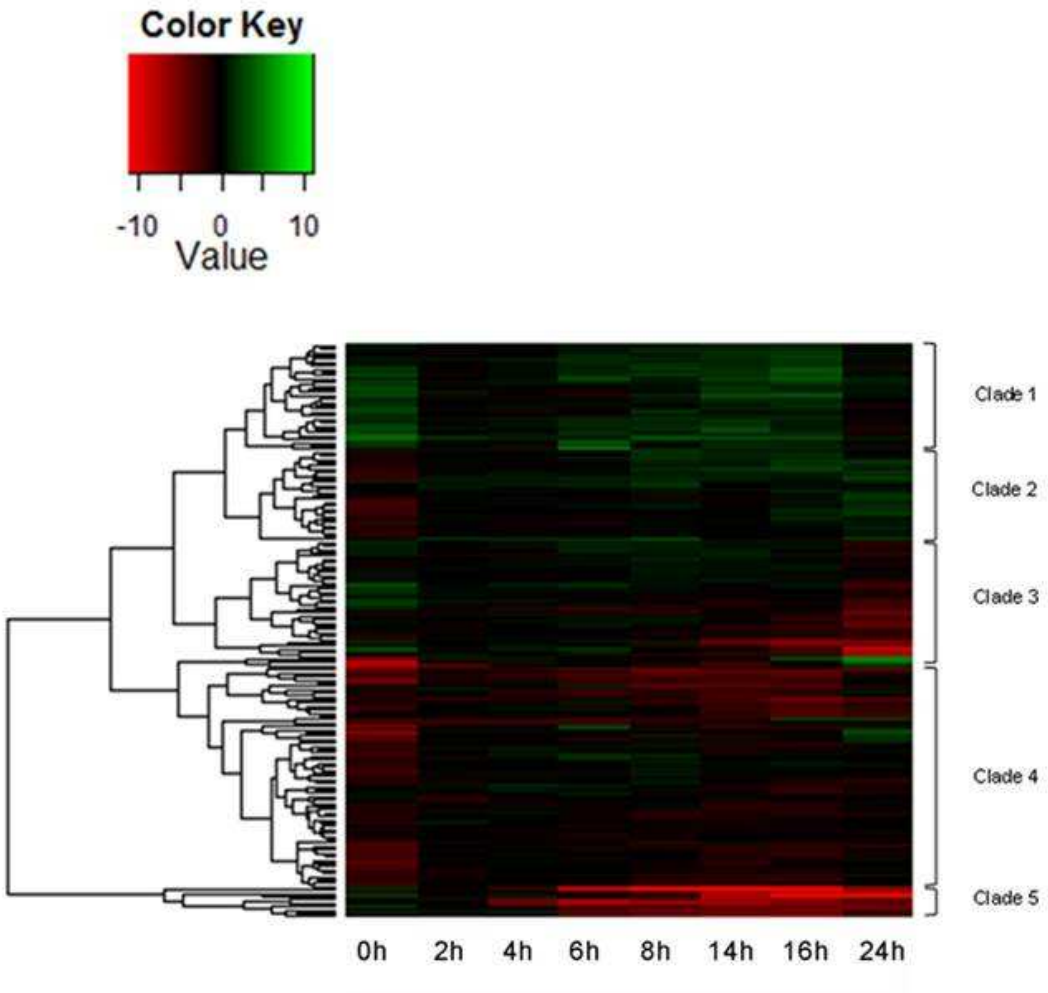

Figure 3.8 Heatmap showing relative levels of transcript abundance of transcription factor genes likely to be Pmk1 regulated during a time course of appressorium development. Transcription factor genes showing similar patterns of expression are clustered. A total of 172 transcription factor genes are shown. Levels of expression are represented as mod_lfc (moderated log fold change) of transcript abundance of the *Δpmk1* mutant compared to Guy11. (red= down-regulated in the *Δpmk1* mutant; green= up-regulated in the *Δpmk1* mutant).

3.3.5.1 Analysis of Clade 1

MAP kinases regulate transcription factors by a number of different mechanisms: phosphorylation can lead to alteration in interactions with associated regulatory proteins, binding to DNA, or alteration of intracellular location (Yang *et al.,* 2003). It has also been reported that MAP kinases may activate repressors and thereby down-regulate expression of downstream genes. For example, the mammalian MAP kinase, Erk1 is able to phosphorylate the repressor Hsf1 on serine residues, leading to transcriptional repression of the heat shock protein gene *HSP70B* (Chu *et al.,* 1996). In *M. oryzae* it is not known whether Pmk1 is able to directly de-activate transcription factors by phosphorylation.

Clade 1 contains 32 transcription factors (Fig. 3.9), which were classified into different families based on Pfam analysis. According to the Broad Institute (https://www.broadinstitute.org/) annotation of the 32 transcription factors, 31 of them were annotated as Hypothetical Proteins and one was annotated as *ACEII*, MGG_08058. AceII has been reported in *Trichoderma reesei* as a regulator of cellulase and xylanase-encoding genes (Aro *et al.,* 2001). Pfam analysis of the 31 proteins of unknown function revealed that 18 contained a fungal Zn(2)-Cys(6) binuclear cluster domain (PF00172), three contained a fungal specific transcription factor domain (PF04082), a BB1 domain containing protein (PF08185) and a fungal specific transcription factor domain (PF04082) and nine of them did not have any Pfam-associated domain.

3.3.5.2 Analysis of Clade 5

Clade 5 contained 9 transcription factors, summarized in Table 3.5, and a heatmap was created to be able to analyse their expression in more detail. MGG_09676 and MGG_10212 are two “Fungal Zn(2)-Cys(6) binuclear cluster domain (PF00172), Fungal specific transcription factor domain (PF04082)” containing transcription factors. Neither shows any similarity to known proteins. Clade 5 also contains four putative fungal Zn(2)-Cys(6) binuclear cluster domain (PF00172) containing transcription factors. From these, only one, MGG_07215, showed similarity with a known protein, the other three potential transcription factors only produced unknown hits when protein sequences were searched by blast against the NCBI database. The MGG_01887 transcription factor does not contain any Pfam associated domain, and when Blastp was performed, it did not give any known hit. MGG_07215 corresponds to the gene *CMR1* which was first identified in *M. oryzae* as *PIG1* by complementation of an unknown insertional mutant with a pigmentation-deficiency phenotype (Sweigard *et al.,* 1998) and it was subsequently shown to regulate melanin biosynthetic genes, similar to *Colletotrichum lageniarium CMR1* (Tsuji *et al.,* 2000). Disruption of *CMR1* in *M. oryzae* had no effect on pathogenicity (Sweigard *et al.,* 1998). A transcription factor-encoding gene, *ALCR*, (MGG_02129) is a homologue of the *Aspergillus nidulans ALCR* transcription factor-encoding gene, responsible for activation of the ethanol-utilization pathway through activation of *ALCA* and *ALDA* (Kulmburg *et al.,* 1992).

Another putative transcription factor identified was the homeobox transcription factor, *HOX7* MGG_12865. This transcription factor belongs to a family of 7 homeobox

transcription factors of *M. oryzae*. Disruption of *HOX7* impairs appressorium formation and therefore the ability of the fungus to cause disease in plants (Kim *et al.,* 2009).

To understand and define the hierarchy of Pmk1-activation and de-activation of putative transcription factors from Clade 5, an analysis of the expression in both Guy11 and *Δpmk1* was analysed for every transcription factor gene over time (Fig. 3.10). The bar charts showed that transcription factors in Guy11 showed a tightly regulated pattern of expression over the time course and the relative level of transcription was much higher in the wild type. Another major observation for all profiles was that in the *Δpmk1* mutant the expression of most transcription factor genes began very early during the time course, however the relative expression levels were much lower than in Guy11.

Putative transcription factor-encoding genes MGG_07215, MGG_9276 and MGG_12865 peak in expression at 6 h in Guy11, while MGG_07534 and MGG_01887 peak at 8 h in Guy11, MGG_09676 and MGG_07218 peak at 14 h in Guy11, and lastly MGG_02129 and MGG_10212 peak at 16 h. However, in a *Δpmk1* mutant the expression varied greatly during the time course. This analysis suggests that Pmk1-dependent activation of downstream transcription factors might happen before 6 h.

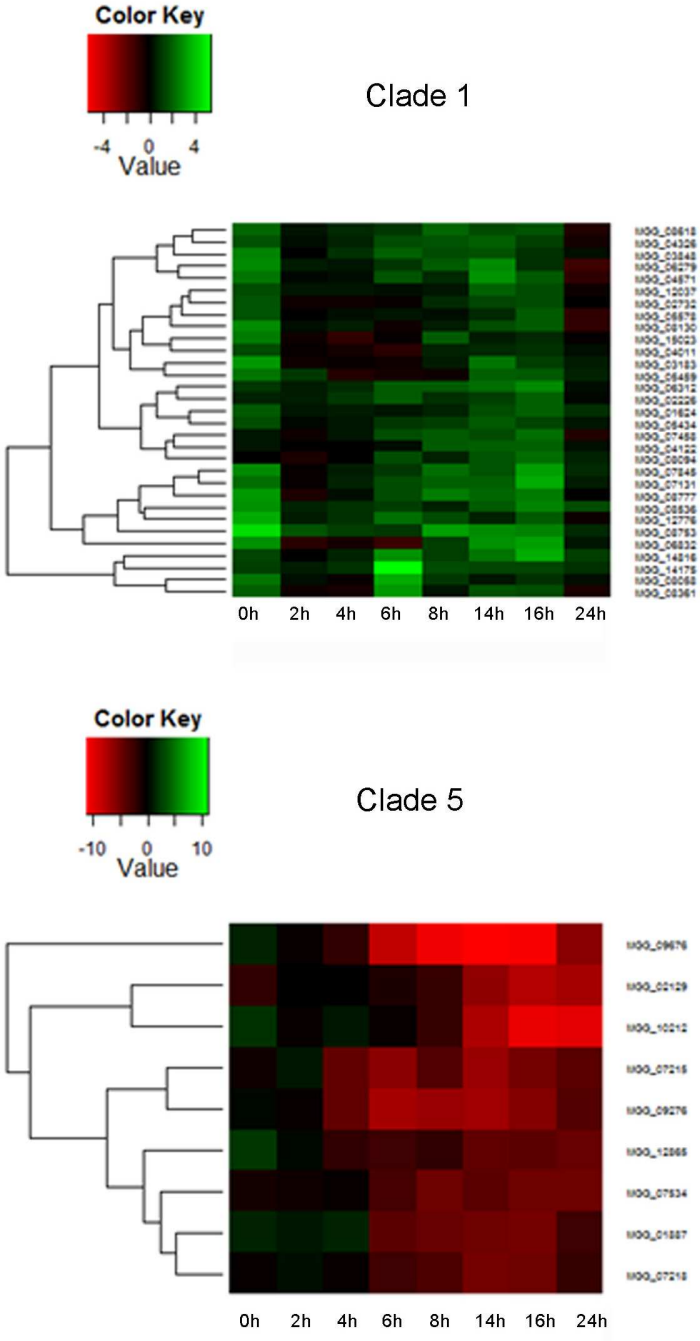

Figure 3.9 Heatmap showing levels of transcript abundance of putative transcription factor genes likely to be Pmk1-regulated A) from clade 1 **B)** from clade 5. Levels of expression are represented as mod_lfc of transcript abundance from *Δpmk1* mutant compared to Guy11 during a time course of appressorium development. (red= down-regulated in the *Δpmk1* mutant; green= up-regulated in the *Δpmk1* mutant).

Table 3.5 Table showing putative transcription factor encoding genes from clade 5 likely to be Pmk1-regulated.

Gene[8]	Annotation[9]	Pfam[10]
MGG_09676	HP[11]	Fungal Zn(2)-Cys(6) binuclear cluster domain (PF00172) 47->78, Fungal specific transcription factor domain (PF04082) 344->554
MGG_02129	AlcR	
MGG_10212	HP	Fungal Zn(2)-Cys(6) binuclear cluster domain (PF00172) 52->84, Fungal specific transcription factor domain (PF04082) 253->438
MGG_07215	Cmr1	Fungal Zn(2)-Cys(6) binuclear cluster domain (PF00172) 75->103
MGG_09276	HP	Fungal Zn(2)-Cys(6) binuclear cluster domain (PF00172) 97->141
MGG_12865	HP	Homeobox domain (PF00046) 320->377
MGG_07534	HP	Fungal Zn(2)-Cys(6) binuclear cluster domain (PF00172) 43->77
MGG_01887	HP	C6 zinc finger domain-containing protein (736 aa)
MGG_07218	HP	Fungal Zn(2)-Cys(6) binuclear cluster domain (PF00172) 15->50

[8] Accession number
[9] Annotation from Broad Institute (https://www.broadinstitute.org/)
[10] Indicates annotation from pfam containing domain (http://pfam.xfam.org/)
[11] HP= Hypothetical protein

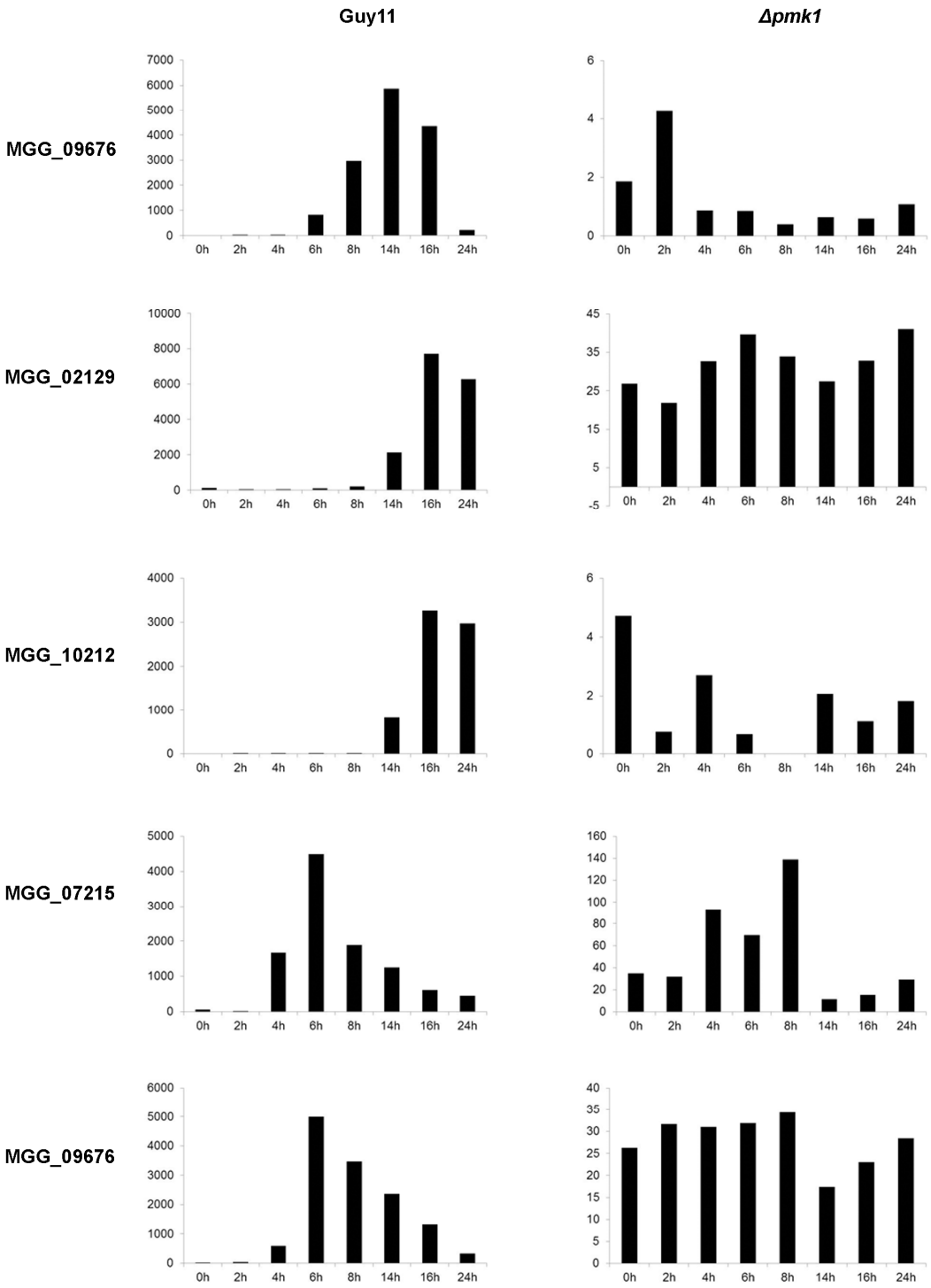
Guy11
Δpmk1
MGG_09676
MGG_02129
MGG_10212
MGG_07215
MGG_09676
0h
2h
4h
6h
8h
14h
16h
24h

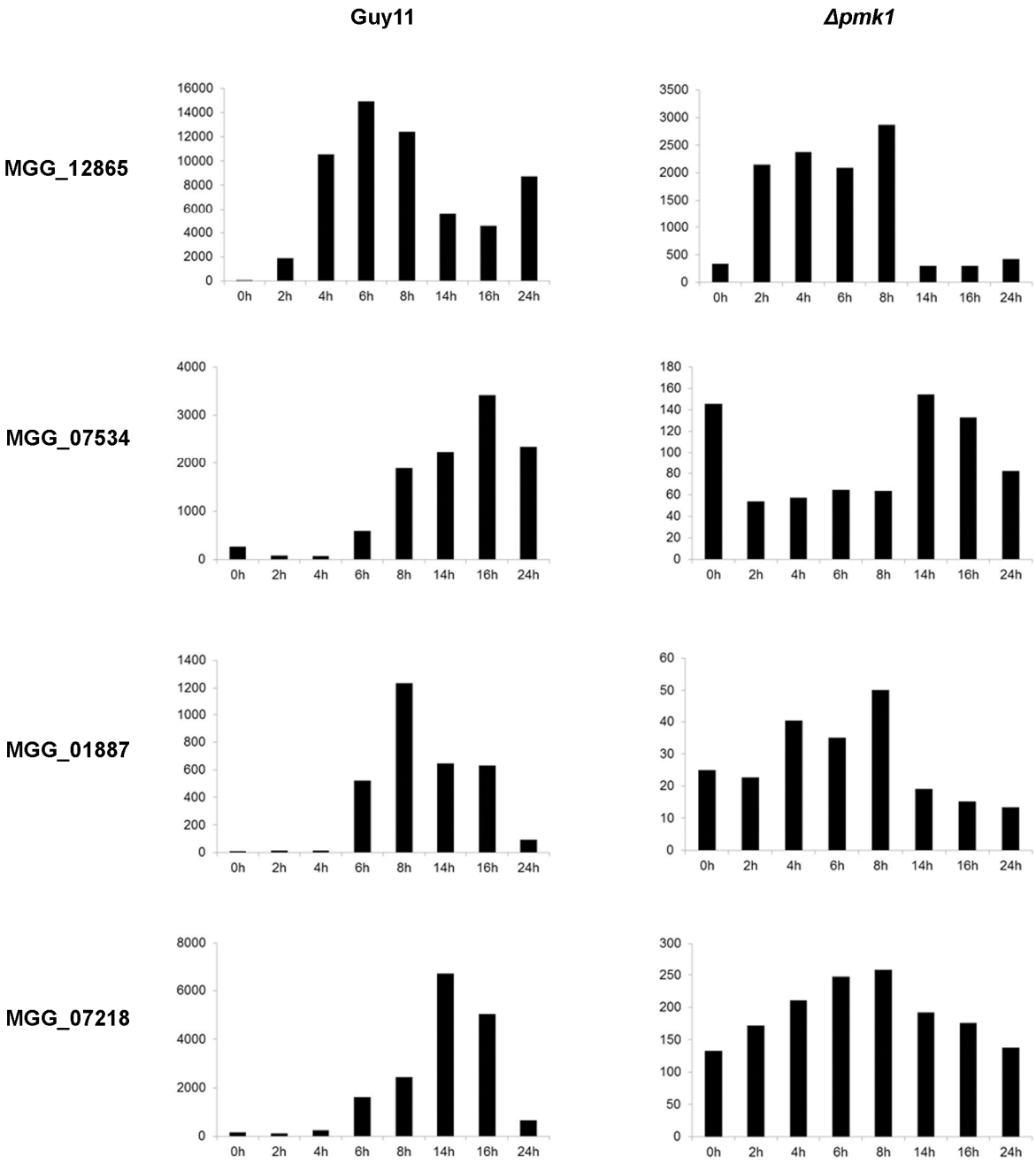

Figure 3.10 Bar charts showing levels of transcript abundance of putative transcription factor encoding genes in Guy11 and *Δpmk1* mutant from clade 5 that are likely to be Pmk1-regulated. Bar charts showing expression of each transcription factor gene from Clade 5 during a time course of appressorium development in Guy11 and the *Δpmk1* mutant. The vertical axes indicate the mean of normalized counts and the horizontal axes indicate time points.

3.3.6 Identifying genes specifically associated with appressorium morphogenesis

Appressorium formation in *M. oryzae* depends on large-scale changes in gene expression over time that lead to morphogenesis. In Guy11, when conidia are germinated *in vitro*, elongation of the germ tube occurs by 2 h, and by 4 h appressorium formation has begun. Therefore, between 2 h and 4 h, a large number of transcriptional changes associated with appressorium development must occur.

The Δ*pmk1* mutant is unable to form appressoria, even at 24 h, suggesting a global regulatory role for Pmk1 in governing the morphogenetic changes associated with appressorium formation (Xu and Hamer, 1996). Therefore, transcriptional profiling to identify a Pmk1-dependent gene set should provide significant candidate genes required for appressorium morphogenesis.

To identify this gene set Venn diagrams were generated to distinguish between genes down-regulated and up-regulated in the Δ*pmk1* mutant compared to Guy11 at 2 h and 4 h. We reasoned that those genes differentially regulated at 4 h in a *Δpmk1* would be putative candidate genes for those involved in appressorium morphogenesis. Genes differentially regulated at other times, in addition to the 4h time-point, clearly may affect appressorium morphogenesis as well, but to narrow the focus on specific gene function, I decided to investigate only those genes that differentially expressed specifically at 4 h.

In total, 357 and 578 genes were down-regulated at 2 h and 4 h respectively, and 294 and 490 genes were up-regulated at 2 h and 4 h respectively. Venn diagrams to

illustrate the overlaps of these gene sets were made (Fig. 3.11, panel A and B). Analysis of the Venn diagrams showed that in total, there were 436 down-regulated genes and 308 up-regulated genes, that were differentially expressed only at 4 h. An analysis was performed on these two gene sets to predict the functions of each gene using gene ontology (GO) categories by Blat2GO and Pfam domain prediction analysis.

Analysis of the down-regulated genes showed that the most repressed gene at 4 h is MGG_12020 (11 fold change), putatively encoding a phosphate-repressible acid phosphatase homologous to *PHOA* from *A. nidulans* (MacRae, 1988). The analysis revealed putative cell cycle-encoding genes, and especially those related to the Mitotic Exit Network, such as the homologues of *CDC15* (MGG_04100), *LTE1* (MGG_02419) and *SPO12* (MGG_08639) from *S. cerevisiae*. The analysis also identified a homologue of *CDC14* from *S. pombe* (MGG_00757), involved in septation and cytokinesis. Moreover, two cyclins, the B-type cyclin *CYC2* (MGG_07065) and G1-type cyclin *CLN3* (MGG_03595) were identified in this analysis. A collection of 10 putative transcription factor-encoding genes were identified in the down-regulated gene set. Three correspond to known homologues of *CMR1* from *Colletotrichum lagenarium* (MGG_07215), *HOX7* (MGG_12865), required for appressorium formation in *M. oryzae* (Kim *et al.,* 2009) and *STU1* (MGG_00692), previously described in *M. oryzae* as required for mobilization of lipids and turgor generation (Nishimura *et al.,* 2009). The other seven putative transcription factor-encoding genes were annotated as hypothetical proteins (MGG_00587, MGG_04758, MGG_11764, MGG_09950 and MGG_01833) two of which (MGG_09276 and MGG_09676) belong to clade 5.

The most up-regulated gene at 4 h was MGG_07733 (showing a 6-fold change in the Pmk1 mutant) which encodes a putative homologue of the pheromone precursor *CCG4* from *N. crassa.* The analysis also revealed genes encoding proteins related with quinate metabolism, such as chorismate synthase (MGG_03281), 3-dehydroshikimate dehydratase (MGG_07780), quinate dehydrogenase (MGG_07781) and QA-X (MGG_15250). Moreover, two proteins related to heterokaryon incompatibility (MGG_10558 and MGG_05881) two uncharacterized transcription factors (MGG_01887 and MGG_02226), and a kinetochore protein-encoding gene *MIS14* (MGG_00906) were identified.

To develop a global understanding of Pmk1 regulatory gene changes leading to appressorium morphogenesis, the Euclidean heatmap in Figure 3.2 (see section 3.2) was analysed in more detail. The Euclidean heatmap showed that transcriptomes from the Δ*pmk1* mutant cluster with samples of Guy11 at 2 h and 4 h, indicating that the main divergence between Guy11 and Δ*pmk1* gene expression happens at 6 h when appressoria are formed in the wild type. For this reason, a similar analysis to the previous one was performed using time points at 4 h and 6 h. Genes differentially regulated only at the 6h time-point were selected. A total of 578 up-regulated and 1223 down-regulated genes were identified at 4 h and 6 h, respectively. A Venn diagram to illustrate the overlaps of these gene sets was made (Fig. 3.10, panel C and D). Analysis of the Venn diagrams showed that in total, there were 747 down-regulated genes and 738 up-regulated genes that were differentially expressed only at 6 h. Functional analysis was performed on these gene sets using gene ontology (GO) categories using Blat2GO and Pfam domain prediction.

The analysis revealed that the most down-regulated gene at 6 h is MGG_07720 (showing a 9-fold change), encoding a hypothetical protein. The analysis also revealed proteins related to cell cycle control including homologues of *S. cerevisiae CDC7* (MGG_03488), *WEE1* (MGG_01816), *CYC1* (MGG_05646), *NIMA* (MGG_03026), *CDC25* (MGG_07734) and *CDC5* (MGG_09960). Two autophagy-related genes were also identified, *ATG9* (MGG_09559) and *ATG27* (MGG_02386), as well as three genes putatively encoding DNA mismatch repair-encoding genes, MGG_04627, MGG_07121 and MGG_09306. Other genes in this set included two fork-head domain containing kinases related to cell cycle checkpoints, *CDS1* (MGG_04790) and *DUN1* (MGG_01596), from *S. pombe.* Moreover, 11 putative transcription factor genes were identified, of which only MGG_08199, the cutinase transcription factor 1, is annotated. The identification of Rho GTPases in this gene set was also significant, *RHO3* and *RHO4* (MGG_10323, MGG_03901) and also the Arp2/3 complex protein-encoding gene, *LAS17* (MGG_02802) was identified.

The most up-regulated gene at 6 h was MGG_10531 (showing an 8-fold change), encoding a hypothetical protein. Another group of genes identified were linked with actin polymerization and de-polymerisation. These genes were MGG_17001 encoding an actin-like protein 2, MGG_05587, encoding actin-like protein 6, MGG_04352, encoding *arp2/3*, MGG_09902 and MGG_12818 encoding F-actin beta and alpha capping proteins respectively, and MGG_03164, encoding cofilin. Heterokaryon incompatibility proteins were also identified, MGG_05985, MGG_00569, MGG_08495 and MGG_15132, and also the homologue of the kinetochore protein-encoding gene *TINC* (MGG_15132). A total of 11 putative transcription factor genes

were also identified. Four showed similarity to acriflavine sensitivity control protein Acr2 (MGG_05434), a quinic acid utilization activator (MGG_07777), a transcriptional activator protein Acu15 (MGG_04108) and a white collar 2 (MGG_04521), respectively.

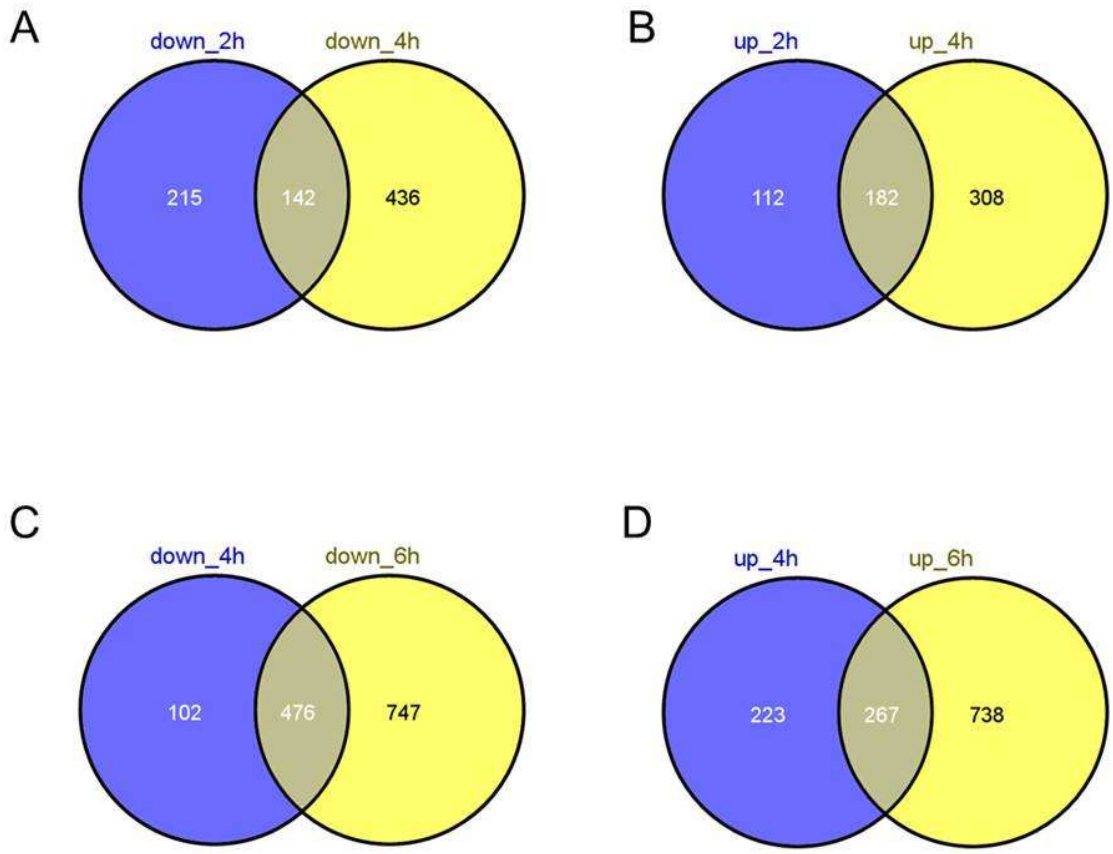

Figure 3.11 Identifying genes associated with appressorium morphogenesis in *M. oryzae* by transcriptional analysis. A) Venn diagram illustrating overlapping regions of genes down-regulated at 2 h and 4 h in a Δ*pmk1* mutant compared to Guy11 (padj<1, mod_lfc<1). **B)** Venn diagram illustrating overlapping regions of genes up-regulated at 2 h and 4 h in a Δ*pmk1* mutant compared to Guy11. **C)** Venn diagram illustrating overlapping regions of genes down-regulated at 4 h and 6 h in a Δ*pmk1* mutant compared to Guy11. **D)** Venn diagram illustrating overlapping regions of genes up-regulated at 4 h and 6 h in a Δ*pmk1* mutant compared with Guy11 (down-regulated (padj<1, mod_lfc<1) and up-regulated (padj<1, mod_lfc>1)).

3.3.7 Transcriptional analysis of different pathways

To follow the analysis, an overall overview of the transcriptional regulation of important cellular processes associated to appressorium development such as melanin production, autophagy, cutinase production, hydrophobin production and β-oxidation was analysed in $Guy11_{HPB}$, Δ*pmk1* and $Guy11_{HPL}$. To carry out the analysis, the total average of gene expression for each process was determined by using the transcript abundance of each gene involved in each process over the time course as shown in figure 3.12. The analysis revealed that in $Guy11_{HPB}$, most processes, such as melanin production, cutinase production, autophagy and β-oxidation, peak at 8 h, whereas in both Δ*pmk1* and $Guy11_{HPL}$, the expression of these processes over time is altered. In the case of hydrophobin production in $Guy11_{HPB}$, the induction happens mostly at 8 h and increases over time until reaching the maximum of expression at 24 h. However, in both Δ*pmk1* and $Guy11_{HPL}$, the expression of genes associated to this process remains invariable and constantly low over time. These observations indicate that these processes are tightly associated with the formation of appressorium

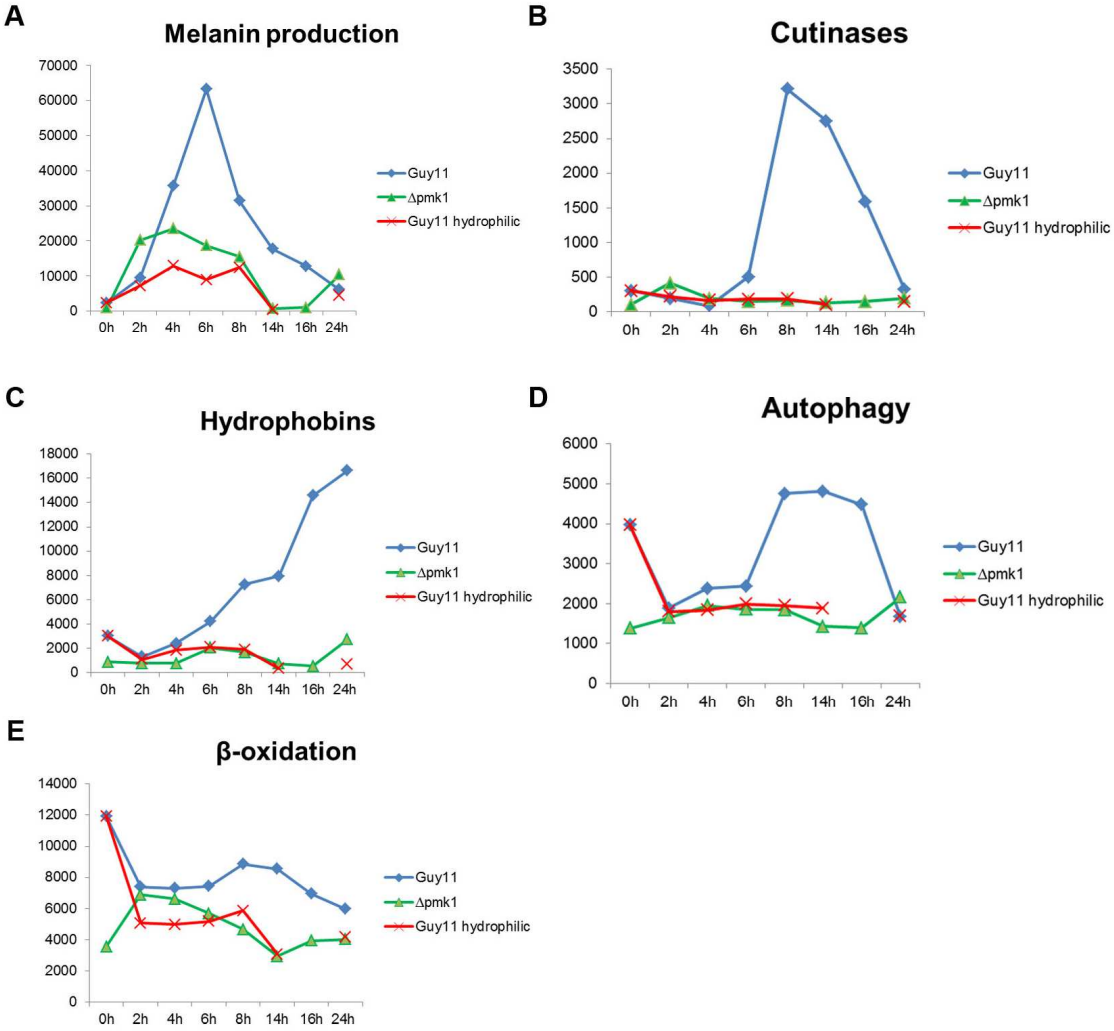

Figure 3.12 Overall analyses for cellular processes involved in appressorium development. **A)** Melanin production **B)** Cutinase production. **C)** Hydrophobin production. **D)** Autophagy. **E)** β-Oxidation. The overall average of gene expression was calculated for each time point of the time course for $Guy11_{HPB}$, $Guy11_{HPL}$ and Δ*pmk1* mutant.

3.3.7.1 Melanin biosynthesis pathway

A key process involved in appressorium maturation is the generation of the melanin layer around the appressorial dome (Valent and Chumley, 1991). The melanin layer is required to allow external water to enter the appressorium to allow generation of the high turgor pressure which is necessary for successful penetration into the host (Valent and Chumley, 1991). Melanin in *M. oryzae* is synthesized through 6 enzymatic reactions involving five different enzymes (Fig. 3.12). Melanin-deficient mutants, such as Δ*alb1,* Δ*buf1* or Δ*rsy1* are unable to synthesize melanin and are therefore impaired in turgor generation and plant infection (Chumley, 1990). However, the signals, whether external or internal, leading to the initiation of this pathway are not well understood.

Gene expression associated with melanin biosynthesis was compared under normal inductive conditions ($Guy11_{HPB}$), with non-inductive conditions ($Guy11_{HPL}$) and the *Δpmk1* mutant, as shown in Figure 3.13. Expression of all melanin biosynthetic genes was not induced in the *Δpmk1* mutant and $Guy11_{HPL}$, especially Rsy1 and Alb1. Furthermore, the individual expression profile of melanin biosynthesis enzymes was determined and the mean of normalized counts was represented as bar charts over the time course of appressorium formation (Fig. 3.13). The bar charts indicated that in $Guy11_{HPB}$, the peak expression in melanin biosynthesis genes occurs at 6 h, whereas in *Δpmk1* and $Guy11_{HPL}$ conditions, expression of melanin biosynthetic genes is dramatically decreased and a maximum peak of expression did not occur in a coordinated manner. Moreover, the levels of expression of the genes were highly reduced compared to the levels of expression in Guy11.

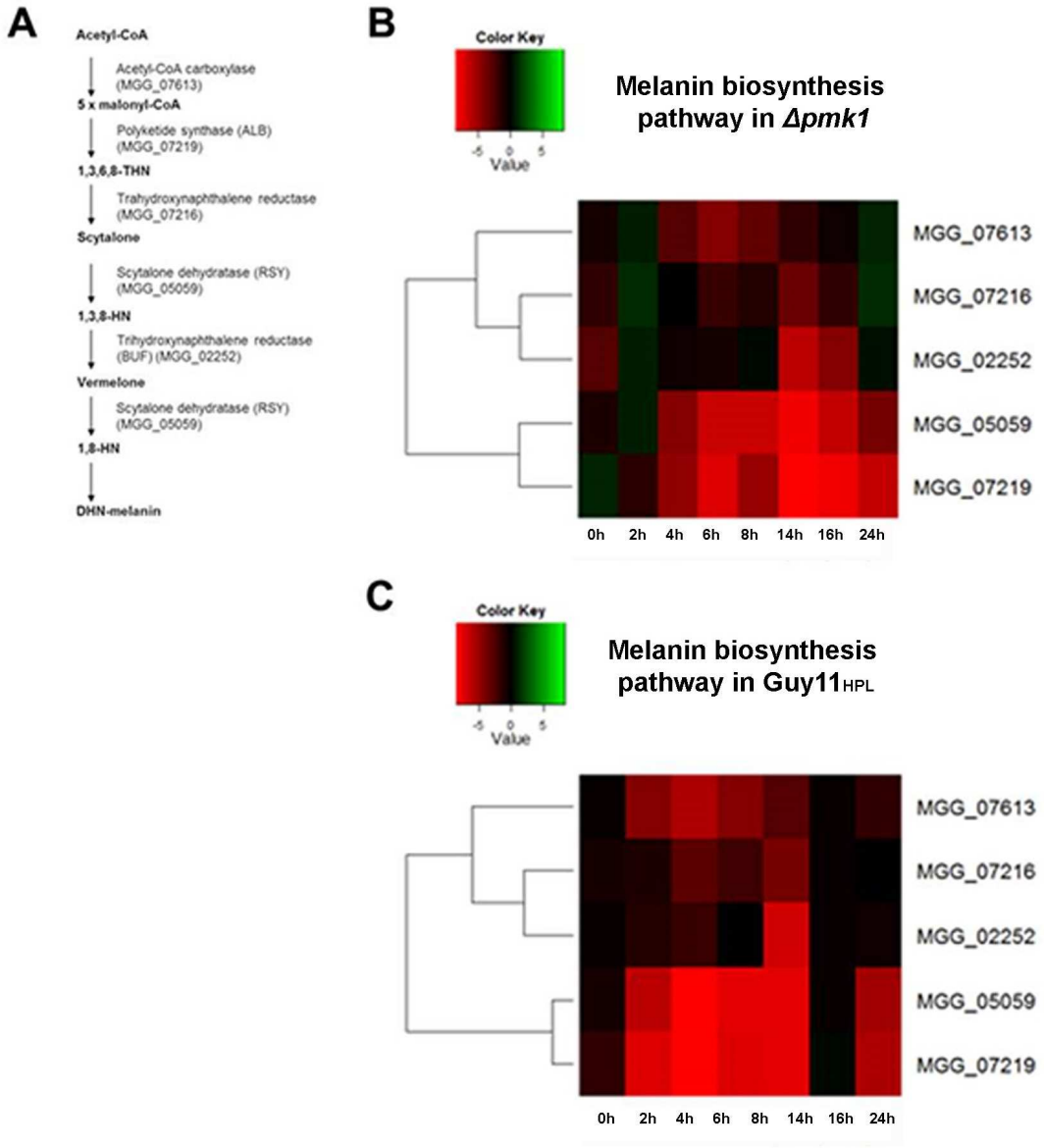

Figure 3.13 Analysis of melanin biosynthesis pathway. A) Diagram representing the melanin biosynthesis pathway and the enzymes involved on it. **B)** Heatmap showing levels of transcript abundance from genes involved in melanin biosynthesis in Δ*pmk1* mutant compared to Guy11. **C)** Heatmap showing levels of transcript abundance from genes involved in melanin biosynthesis in $Guy11_{HPL}$ surface compared to $Guy11_{HPB}$. Levels of expression are represented as moderated logarithmic fold change (mod_lfc) (red= down-regulated in the *Δpmk1* mutant; green= up-regulated in the *Δpmk1* mutant).

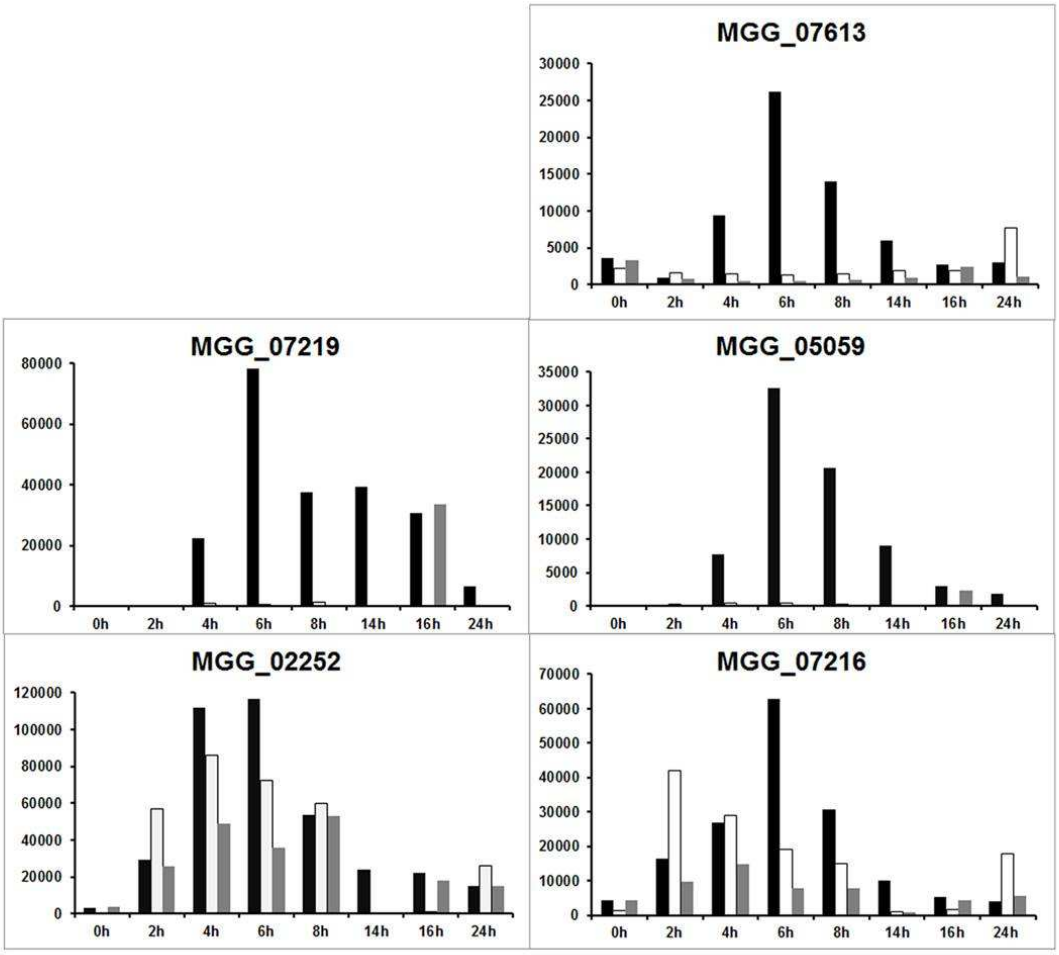

Figure 3.14 Analysis of melanin biosynthesis pathway in the Δ*pmk1* mutant, Guy11$_{HPL}$ and Guy11$_{HPB}$. Bar charts showing levels of transcript abundance for the enzymes involved in melanin biosynthesis. Vertical axes represents mean of normalized counts from genes involved in melanin biosynthesis in Guy11$_{HPB}$ (black), Δ*pmk1* (white) and in Guy11$_{HPL}$ (grey) and horizontal axes represent the time points during a time course of appressorium development.

3.3.7.2 Cutinase domain containing protein-encoding genes

The plant cuticle is the first barrier that a pathogen has to breach to be able to cause disease. Cutinases are methylesterase enzymes responsible for degrading the cuticle of a leaf and therefore facilitating penetration in many pathogenic fungi. A well-known example is the filamentous fungus, *Colletotrichum kahawae* which secretes cutinases at the pre-penetration stage to facilitate plant penetration (Chen, 2007). Despite using mechanical force to break through the plant cuticle and form the penetration peg (Howard and Valent, 1996), *M. oryzae* still possesses 18 cutinase genes in the genome. Two of these cutinases have been studied in the past, and *CUT2* was required for formation of functional appressoria and for full virulence in rice plants (Skamnioti and Gurr, 2007). Therefore, due to their potential role in plant penetration, the cutinase domain containing encoding genes were analysed for expression.

Cutinase gene expression was compared under normal inductive conditions ($Guy11_{HPB}$), with non-inductive conditions ($Guy11_{HPL}$) and in the *Δpmk1* mutant, as shown in Figure 3.14. Four cutinase genes, MGG_02393, MGG_03440 and MGG_14095 and MGG_09100 (*CUT2)*, were not induced from 6 h and clustered together. In the case of the *Δpmk1* mutant, another cutinase (MGG_03792) encoding gene also clustered with this group. An individual analysis for the cutinase-domain containing genes was done for *Δpmk1* mutant, as shown in Figure 3.15. The bar charts correlated with the previous data obtained in figure 3.14.

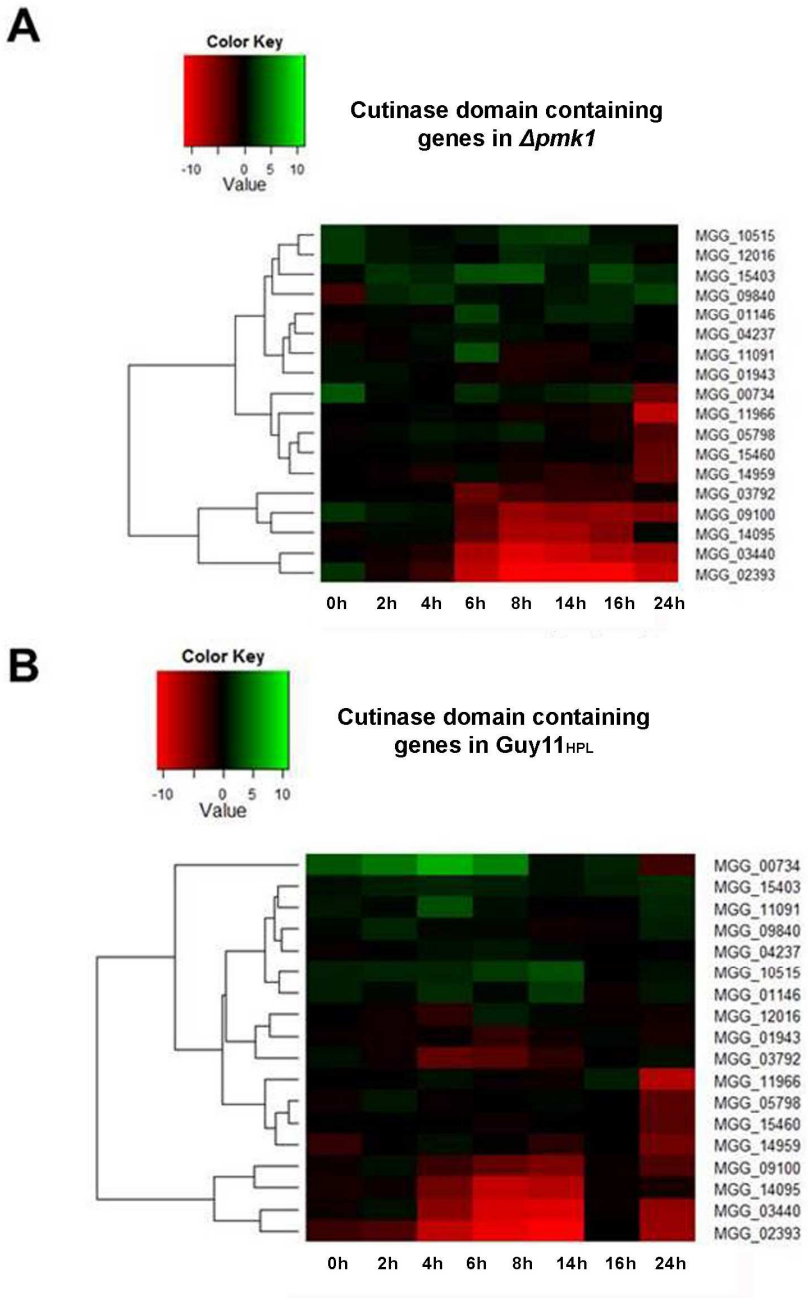

Figure 3.15 Levels of transcript abundance of cutinase domain containing genes in the Δ*pmk1* mutant of *M. oryzae*. A) Heatmap showing levels of transcript abundance during appressorium time course development. Levels of expression are represented as logarithmic fold change of the Δ*pmk1* mutant as compared to Guy11 during appressorium formation. **B)** Heatmap showing levels of transcript abundance during appressorium time course development. Levels of expression are represented as logarithmic fold change of $Guy11_{HPL}$ as compared with $Guy11_{HPB}$. (red= down-regulated in the *Δpmk1* mutant; green= up-regulated in the *Δpmk1* mutant).

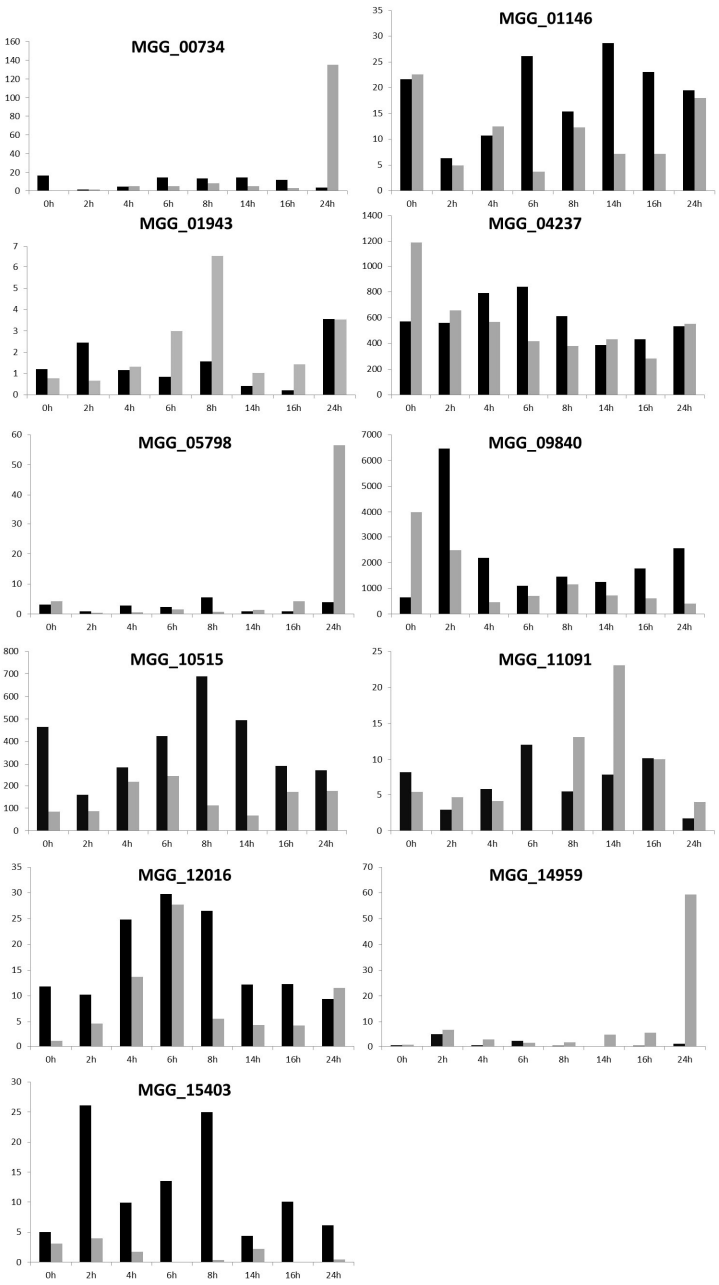
MGG_00734
MGG_01146
MGG_01943
MGG_04237
MGG_05798
MGG_09840
MGG_10515
MGG_11091
MGG_12016
MGG_14959
MGG_15403
0h
2h
4h
6h
8h
14h
16h
24h

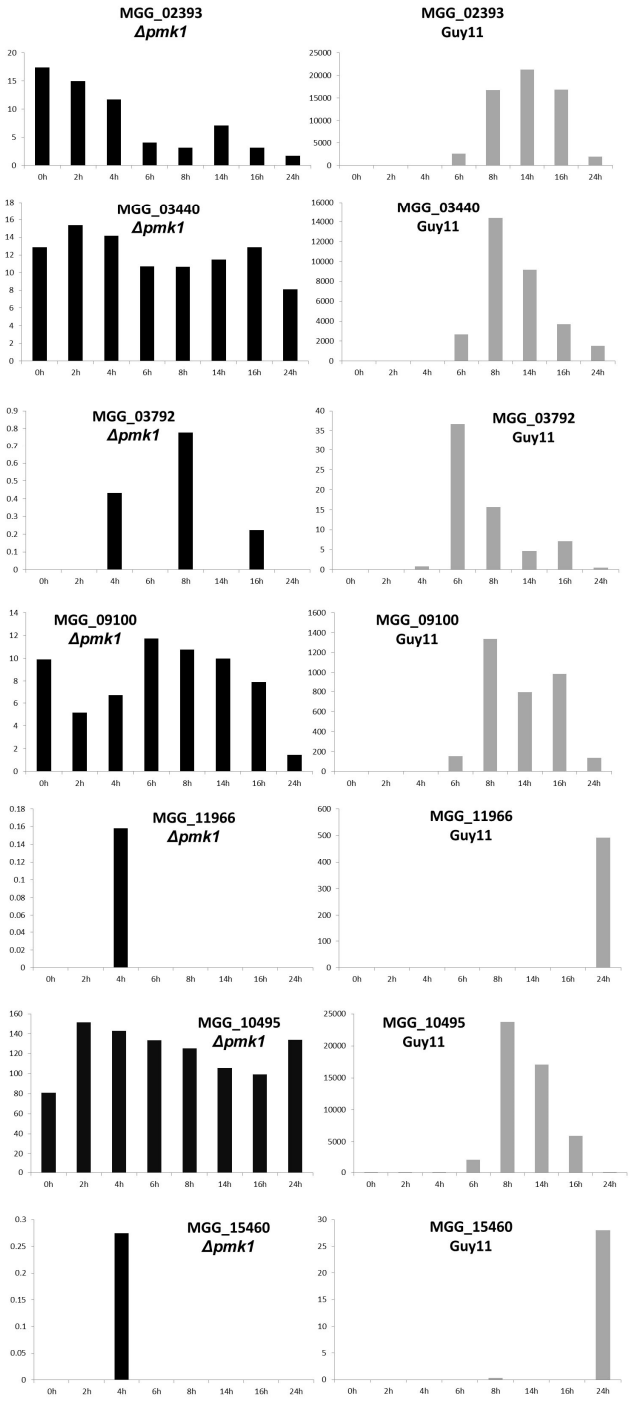

Figure 3.16: Analysis of individual gene expression of cutinase-domain containing genes in the Δ*pmk1* mutant and in wild-type Gu11 of *M. oryzae*. Bar charts showing levels of transcript abundance for cutinase-domain containing proteins. Vertical axes represents mean of normalized counts in Δ*pmk1* (black) and in Guy11 (grey) and horizontal axes represent the time points during a time course of appressorium development. Note that some of the graphs have been separated for Δ*pmk1* and in Guy11 to allow a better visualization of the data.

3.3.7.3 Regulation of hydrophobins by Pmk1 pathway

Hydrophobins are proteins required for both conidial attachment and appressorium formation in *M. oryzae* (Soanes *et al.,* 2012). Null mutants of the abundant *M. oryzae* hydrophobin *MPG1* produce predominantly undifferentiated germ tubes and are therefore reduced in virulence (Talbot *et al.,* 1993). In this analysis, hydrophobin-encoding genes were analysed in both *Δpmk1* and $Guy11_{HPL}$ compared to $Guy11_{HPB}$ and two separate heatmaps generated (Fig. 3.15). The analysis showed two separate clusters. In the *Δpmk1* mutant six hydrophobin genes clustered together, of which four showed a dramatic decrease in expression from 2 h onwards and two from 14 h. In the case of $Guy11_{HPL}$, a differentiated cluster of four hydrophobin genes showed a dramatic decrease in expression from 6 h onwards. These genes were the same as those not induced in the *Δpmk1* mutant. Moreover an individual analysis of every gene expression for every hydrophobin-domain containing protein gene was done for the *Δpmk1* mutant and Guy11 (Fig. 3.16). The graphs correlated with the conclusion observed in the figure 3.15 in which, overall, the expression of most of the hydrophobin genes was not induced in *Δpmk1* mutant compared to the wild-type.

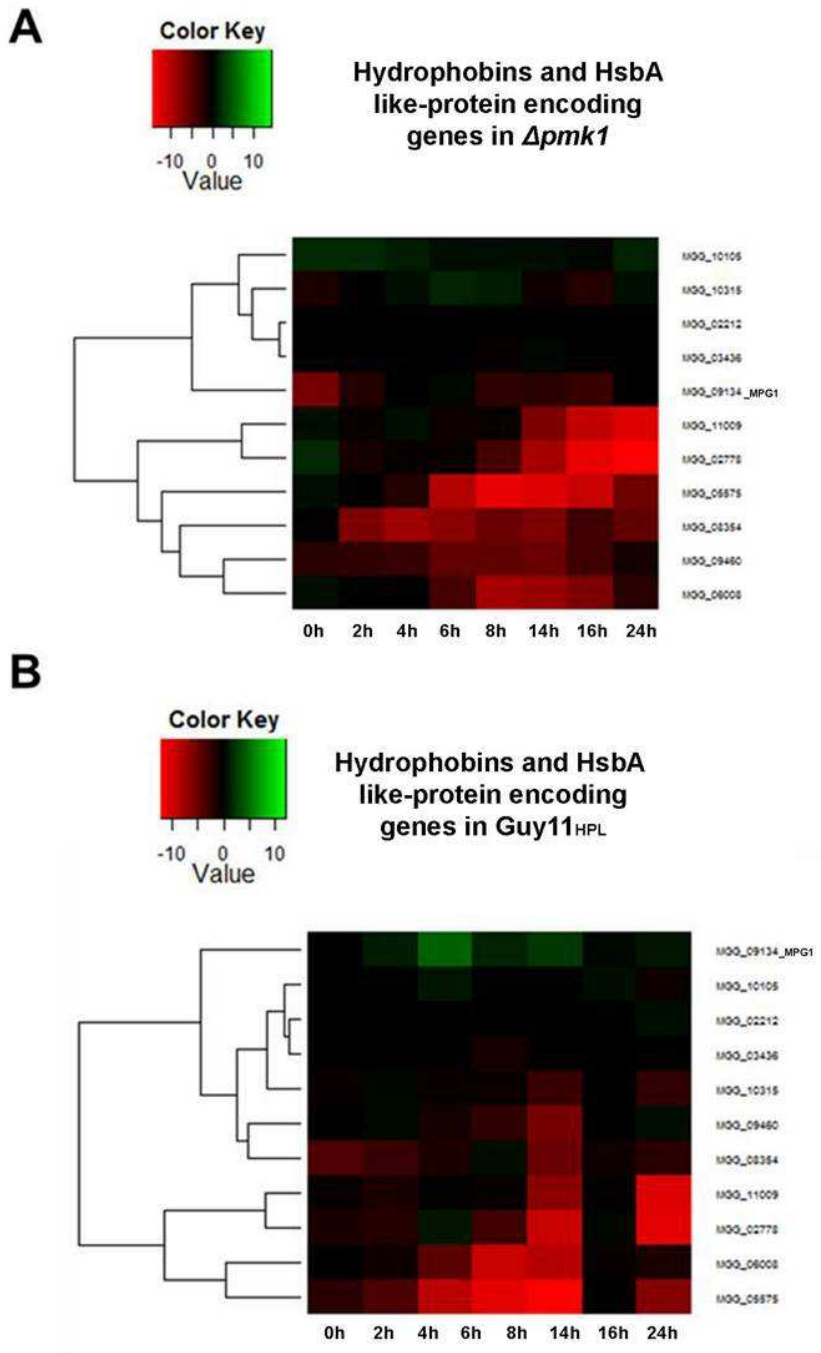

Figure 3.17 Heatmap showing transcript abundance differential expression of *M. oryzae* genes encoding hydrophobins and HsbA like-proteins during appressorium time course. A) Δ*pmk1* compared to Guy11. **B)** Guy11 $_{HPL}$ compared to Guy11$_{HPB}$. (red= down-regulated in the *Δpmk1* mutant; green= up-regulated in the *Δpmk1* mutant).

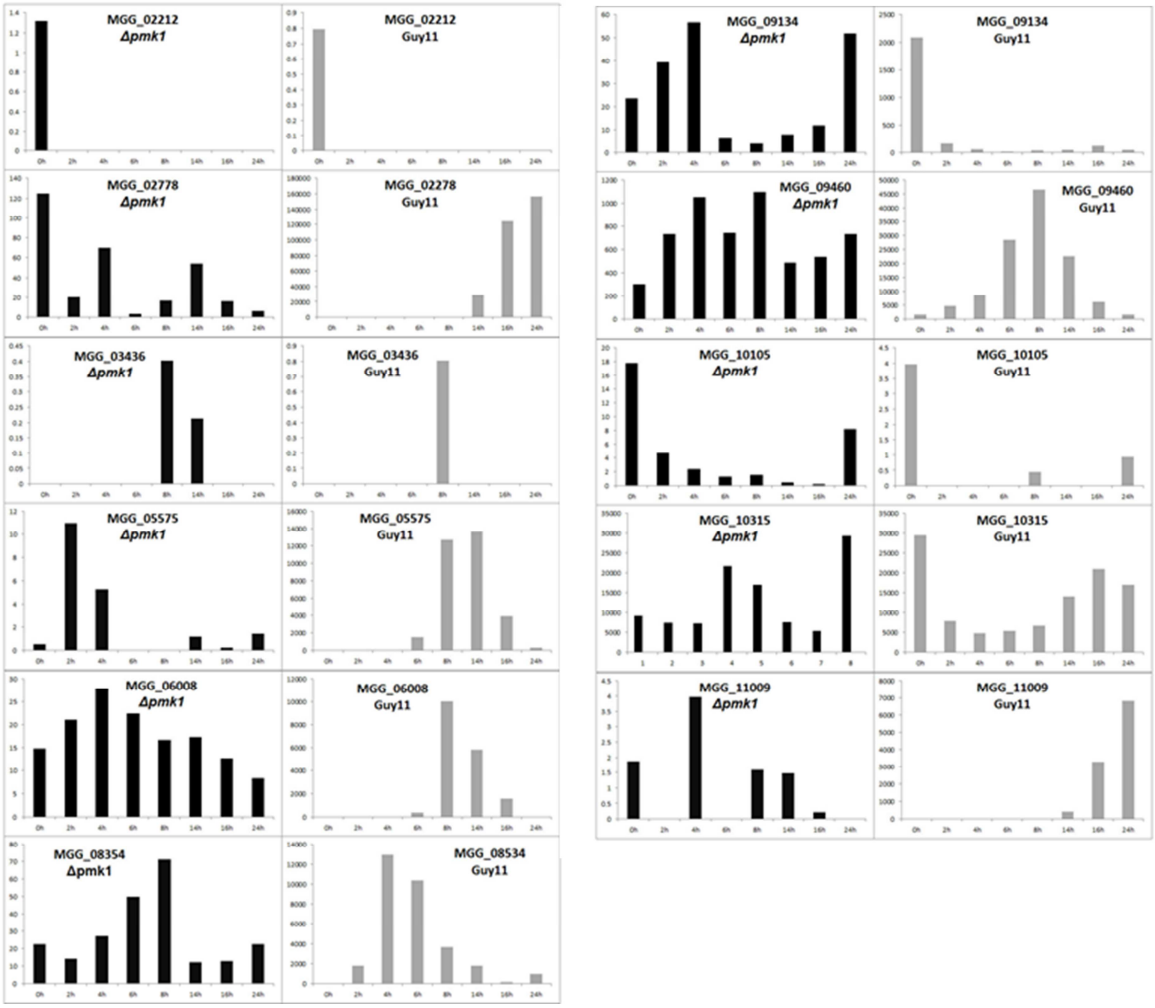

Figure 3.18: Analysis of gene expression of hydrophobin-domain containing genes in the Δ*pmk1* mutant and in wild-type Guy11 of *M. oryzae*. Bar charts showing levels of transcript abundance for cutinase-domain containing proteins. Vertical axes represents mean of normalized counts in Δ*pmk1* (black) and in Guy11 (grey) and horizontal axes represent the time points during a time course of appressorium development. Note that some of the graphs have been separated for Δ*pmk1* and in Guy11 to allow a better visualization of the data.

3.3.7.4 Autophagy

In *M. oryzae* autophagy-dependent, programmed cell death of the conidium is required for generation of a functional appressorium (Kershaw and Talbot, 2009). When *M. oryzae* genes encoding components involved in non-selective autophagy are disrupted, the resulting mutants are non-pathogenic (Kershaw and Talbot, 2009). In a ∆*pmk1* mutant the number of autophagosomes is reduced over a time course following spore germination and programmed cell death of the spore does not occur, suggesting involvement of the Pmk1 MAPK in regulation of autophagy (Kershaw and Talbot, 2009).

For this reason the expression of autophagy-related genes was analysed in both *Δpmk1* and $Guy11_{HPL}$ compared to $Guy11_{HPB}$ (Fig. 3.15). The heatmap in *Δpmk1* showed a cluster containing nine autophagy-related genes whose expression was not induced from 0 h to 16 h during appressorium formation and was up-regulated at 24 h. In the case of $Guy11_{HPL}$ compared to $Guy11_{HPB}$, a cluster containing 11 autophagy related proteins, the expression of these genes was not induced 4 h to 14 h, coincident with appressorium formation and, however, were highly expressed at 16 h and 24 h. Interestingly, *ATG7* shows a highly discrete down-regulation at both 8 h and 14 h.

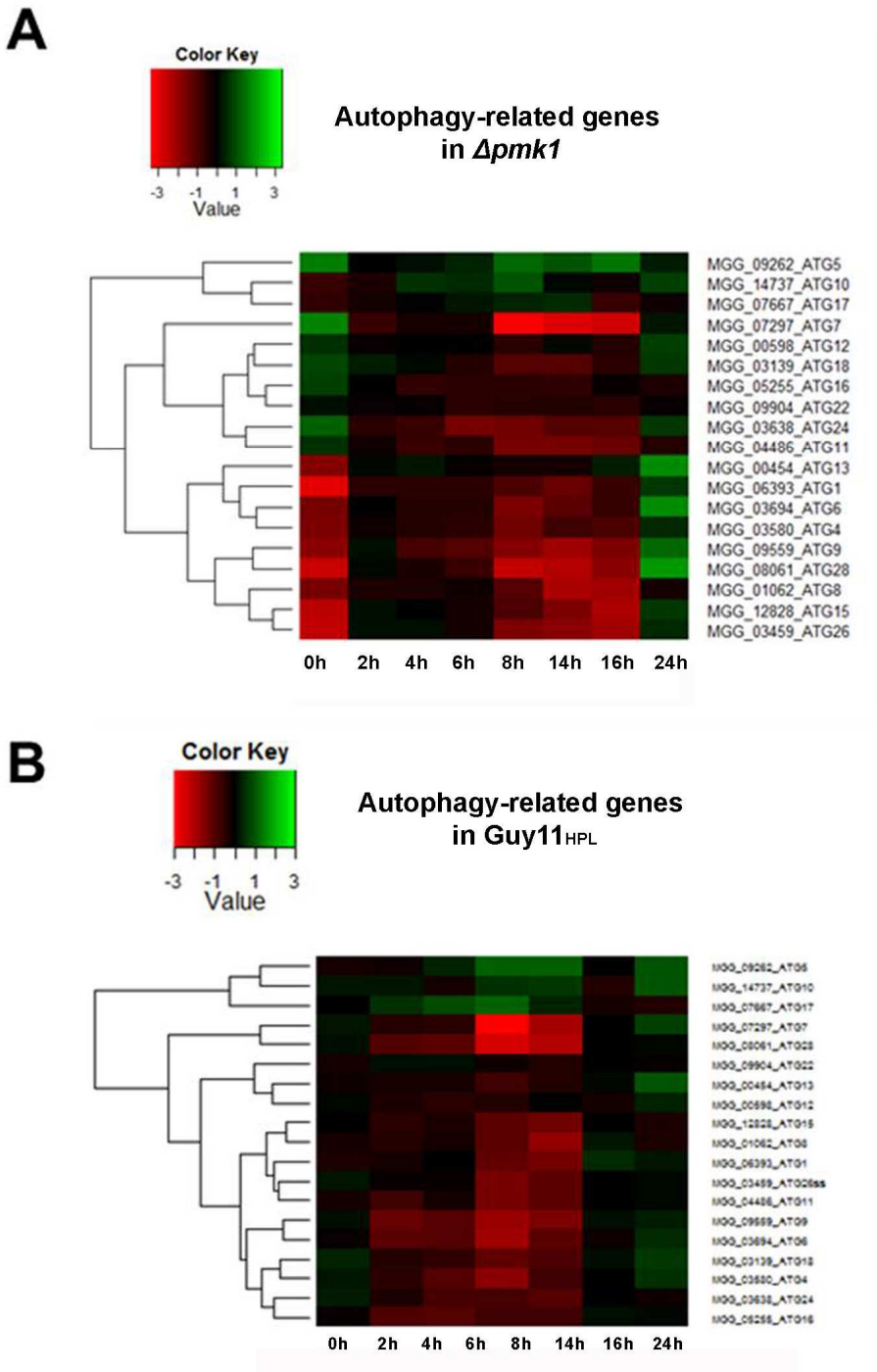

Figure 3.19 Heatmap showing transcript abundance differential expression of *M. oryzae* genes encoding autophagy-related proteins during an appressorium development time course. A) *Δpmk1* compared to Guy11. **B)** $Guy11_{HPL}$ compared to $Guy11_{HPB}$.

3.3.7.5 Beta-oxidation and glyoxylate cycle

During germination of *M. oryzae* conidia and formation of appressorium on a rice leaf, nutrients are not available. Therefore, mobilization of lipid droplets and storage compounds from the conidium to the appressorium is a pre-requisite for a functional appressorium (Thines *et al.,* 2000). This process has been shown to be Pmk1 dependent (Thines *et al.,* 2000). Moreover, an increase in lipase activity to liberate glycerol from lipids, and fatty acid beta-oxidation, are both important processes for appressorium development (Wang *et al.,* 2007). For this reason it is essential to analyse expression of enzymes involved in beta-oxidation and the glyoxylate cycle in both *Δpmk1* and $Guy11_{HPL}$ compared to $Guy11_{HPB}$ (Fig. 3.16).

The Heatmap of the *Δpmk1* mutant showed a cluster containing 10 gene encoding lipases or beta-oxidative enzymes whose expression was not induced from 0 h to 24 h during appressorium formation (Fig. 3.16). Moreover, another cluster containing seven enzymes was also highly down-regulated from 8 h to 24 h. In the case of $Guy11_{HPL}$ compared to $Guy11_{HPB}$, the general expression of these genes was higher than in the *Δpmk1* mutant. A cluster containing four enzymes was found, whose gene expression was not induced from 0 h to 24 h (MGG_13647, MGG_02613, MGG_15041 and MGG_04075) during appressorium formation.

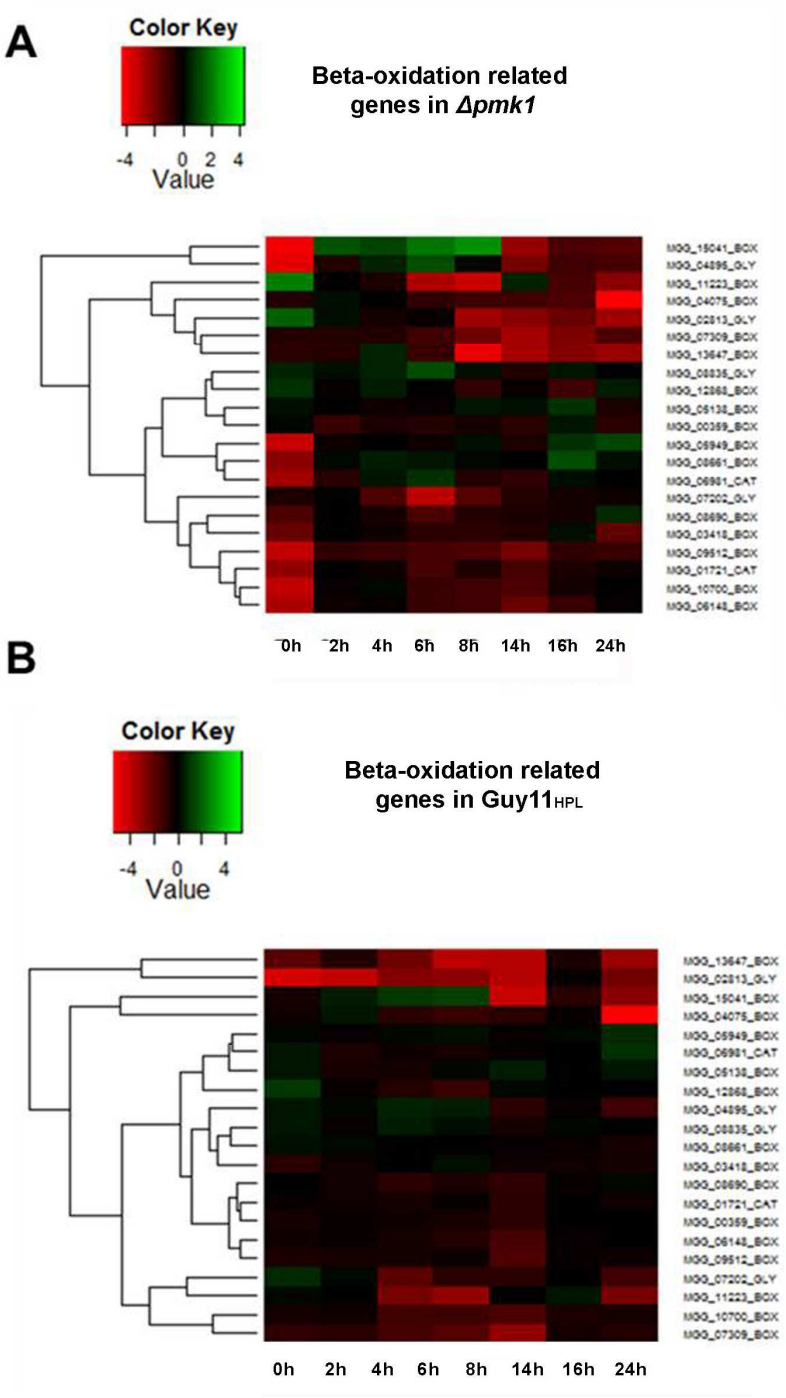

Figure 3.20 Heatmap showing transcript abundance differential expression of *M. oryzae* genes encoding enzymes related with β-oxidation and glyoxylate cycle during appressorium time course. A) Δ*pmk1* compared to Guy11. **B)** $Guy11_{HPL}$ compared to $Guy11_{HPB}$.

3.4 Discussion

Transcriptional re-programming downstream of a MAP kinase signalling pathway occurs through phosphorylation and de-phosphorylation of transcription factors in a hierarchical manner (Dickman and Yarden, 1999). The significance of defining the transcriptional signature associated with external stimuli and the resulting transcriptional hierarchy, is that it will allow us to understand the molecular mechanisms and regulation of morphogenetic changes in *M. oryzae*, associated with the ability of the fungus to cause disease and, in particular, to develop its specialised infection structure, the appressorium.

In this chapter, I set out to define the genes associated with appressorium morphogenesis in *M. oryzae*, as well as the regulatory transcriptional signature. I carried out a comparative transcriptomics analysis between a null mutant of the *PMK1* MAP kinase gene and the wild type strain Guy11 over a time course of appressorium formation. Also, to provide a more detailed analysis, a further comparative transcriptomic analysis was carried out on a non-inductive hydrophilic surface, resulting in failure to elaborate appressoria.

The global analysis of the transcriptomes based on Euclidean analysis was first used to compare the Δ*pmk1* mutant with Guy11 and showed that the Δ*pmk1* mutant globally shares transcriptional similarities to Guy11 at 2 h and 4 h. The entire Δ*pmk1* transcriptome time course forms a completely separate cluster from those of Guy11 subsequent from this time, from 6 h to 24 h. During early time points of appressorium formation in Guy11 at 2 h and 4 h, germination of the germ tube and hooking occurs.

Therefore, the similarities in gene expression patterns at these stages are consistent with the uniform development seen in both strains. However, as expected an increasing number of genes are differentially expressed at the onset of appressorium development, showing severe down-regulation in or when Guy11 is left to develop on a non-inductive hydrophilic surface on which it fails to form an appressorium. The divergence in gene expression therefore reflects the distinct developmental fates and can be used to define specific gene functions associated with appressorium formation.

To date, the only putative Pmk1-regulated transcription factor reported is the C_2/H_2-Zn^{+2} finger and homeobox domain-containing transcription factor, Mst12 (Park *et al.,* 2002). The Mst12 transcription factor regulates both appressorium penetration and invasive growth of *M. oryzae* (Park *et al.,* 2002). In the analysis of the transcriptomic data of the Δ*pmk1* mutant compared to Guy11, it was not found a statistical significant difference in Mst12 gene expression, suggesting that the regulation of Mst12 will probably occur by a post-translational mechanism. However, it is expected that other transcription factors also act downstream of Pmk1, regulating appressorium-related processes, such as, for example, melanin biosynthesis. We have defined nine putative transcription factors that might be regulated by Pmk1 in this study. Interestingly, a morphogenesis related homeobox transcription factor that plays a role in appressorium morphogenesis in *M. oryzae*, *HOX7,* was part of this group (Kim *et al.,* 2009). The role of Pmk1 in the downstream activation of *HOX7* needs to be determined, but it has already been shown that Pmk1 interacts with Mst12, which also possesses a homeobox domain (Kim *et al.,* 2009). The affinity of homeobox transcription factors for phosphorylation by MAP kinases has not been well defined. There are, however, a

number of examples of this type of interaction, such as in mammalian intestinal epithelial cells, where the p38 MAP kinase has been shown to regulate homeobox transcription factors to regulate cell differentiation (Houde *et al.,* 2001). Another example in fungi is in *Fusarium* species where the Htf1 transcription factor, a homologue of *M. oryzae HOX2,* is required for both morphogenesis of phialides and conidiogenesis (Zheng *et al.,* 2012).

Another putative Pmk1-regulated transcription factor identified here is Pig1. Pig1 has a fungal Zn(2)-Cys(6) binuclear cluster domain that has been reported to be a melanin biosynthesis regulator (Sweigard *et al.,* 1998). In fungi, melanin biosynthesis is coupled with development and regulated both transcriptionally and post-transcriptionally (Takano *et al.,* 1997). In the maize pathogen *Cochliobolus heterostrophus* melanin biosynthesis has been reported to be dependent on *CHK1* (*PMK1* homologue) and *MPS1* (*MPS1* homologue) dependent pathways, controlling the transcriptional level of *CMR1* (Eliahu *et al.,* 2007). Another example is in *Bipolaris oryzae*, which possesses a *CMR1* homologue involved in melanin biosynthesis (Moriwaki *et al.,* 2007). In *M. oryzae,* a *CMR1* homologue was found by insertional mutagenesis and named *PIG1* (Sweigard *et al.,* 1998). Null ∆*pig1* mutants are reduced in virulence and although they show albino non-pigmented mycelium, they still produce melanised appressoria, suggesting that there is an additional transcription factor that regulates melanin biosynthesis in the appressorium (Sweigard *et al.,* 1998). The Pig1 transcription factor contains a C_2H_2 type Zinc finger domain and a Fungal $Zn_{(2)}$-$Cys_{(6)}$ binuclear cluster domain. C_2H_2 Zinc finger domain regulators are able to form homo- and hetero-dimers (Todd and Andrianopoulos, 1997). The regulation of melanin might not therefore occur

only through Pig1. In this study, it was shown that clade 5 (a clade of nine transcription factor-encoding genes down-regulated in the Δ*pmk1* mutant), contained six Fungal Zn(2)-Cys(6) binuclear cluster domain containing proteins that might potentially interact with Pig1. Interestingly one of these, the putative transcription factor gene MGG_07218, forms a cluster with *PIG1* and four other genes in a contig on Chromosome II. The six genes in this putative cluster are *PIG1, THN,* a 940 nt hypothetical protein (MGG_07217), a 417 nt hypothetical protein (MGG_15881), the transcription factor MGG_07218 and *ALB,* encoding a melanin biosynthetic enzyme. The MGG_07218 transcription factor has been considered to be the main melanin biosynthesis regulator in appressoria. However, the corresponding null mutant was not affected in appressorium melanisation or pathogenicity (Valdovinos-Ponce, G. and Valent, B., unpublished). These results suggest that *PIG1* and MGG_07128 might putatively form heterodimers to co-ordinately regulate melanin biosynthesis in the appressorium. Another possible scenario is the existence of a compensatory mechanism carried out through other transcription factors, or the involvement of other unknown protein regulators of the melanin biosynthesis pathway. To elucidate this, a double null mutant for both *PIG1* and MGG_07218 should be generated to determine any possible cooperative role in appressorium melanisation for these two regulatory proteins.

Another putative transcription factor downstream of Pmk1 is homologous to *AlcR*, a positive regulator of ethanol utilization by *Aspergillus nidulans* (Felenbok *et al.,* 1988). *AclR* regulates *alcA* and *aldA,* an alcohol dehydrogenase and an aldehyde dehydrogenase, respectively (Felenbok *et al.,* 1988). *AclR* regulation is carbon catabolite repressed through the *creA* regulator (Bailey and Arst, 1975). The current

study suggests that *alcR* might be regulated by the Pmk1 kinase, although it is also possible that *alcR* down-regulation may be the result of *creA* (MGG_11201) up-regulation (Mathieu and Felenbok, 1994), although no differential expression of *creA* was observed in this analysis. Other sources of induction of *alcR* expression are induced by ethanol, threonine and ethylmethylketone (Creaser, 1984; Felenbok *et al.,* 1988). Further work would be required to determine the relationship between Pmk1 and the *ALCR* transcription factor by generation of an *ΔalcR* mutant.

The Pmk1 MAP kinase pathway is functionally related to the pheromone response pathway of *S. cerevisiae* and the Fus3 MAP kinase is the direct equivalent of Pmk1 (Elion *et al.,* 1993; Xu and Hamer, 1996). The Fus3 MAP kinase pathway is responsible for triggering cell cycle arrest, as well as polarized growth through actin remodelling, and cytoskeleton rearrangements that lead to morphogenesis of the 'shmoo' cell prior to cell fusion (Rispail *et al.,* 2009). Homologues of FUS3 have been identified in a number of many fungi and null mutants in *Colletotrichum lageniarium* or *Metarhizium acridum* are impaired in conidial germination or appressorium formation, respectively (Jin *et al.,* 2014; Takano *et al.,* 2000). In *M. oryzae*, the ∆*pmk1* null mutant, shows excessive polarized germ tube and several nuclear divisions occur, with the first nuclear division happening after 8 h (Salkukoo W., personal communication). This suggests that cell cycle arrest does not occur in Δ*pmk1*, and instead, uncontrolled rounds of nuclear division occur in during germ tube extension. Rho guanosine triphosphatases are a family of proteins involved in cell signalling that leads to actin cytoskeletal remodelling (Evangelista *et al.,* 1997). In yeast, the pheromone signal triggers activation of Cdc42 which interacts with the Bni1 formin and Rho1, leading to F-

actin remodelling (Evangelista *et al.,* 1997). In *M. oryzae,* Pmk1 activation leads to polarized growth, so it is therefore possible that Pmk1 regulates actin polymerization through Bzz1 and another SH3-domain containing protein MGG_03275, which has been related with the activation of Las17, a WASP (Wiskott–Aldrich syndrome) protein that promotes actin filament assembly (Kaksonen *et al.,* 2003). Las17 has been previously shown to localize to the appressorium pore in a septin-dependent mechanism in M. *oryzae* (Dagdas *et al.,* 2012). In this study, Bzz1 was shown be down-regulated in Δ*pmk1* mutants at 4 h post germination. However, later on at 6 h, many actin polymerisation and de-polymerisation genes start to be up-regulated in the mutant associated with hyphal growth.

In yeast, Far1 causes a G1 arrest of the cell cycle by inactivating the Cdc28-Cln complex (Chang and Herskowitz, 1990). It has been reported that a cell cycle arrest can only be triggered when “Start” of the cell cycle does not occur. In the case that “Start” does occur, triggered by Cdc28-Clns, a cell cycle arrest will not happen until the cell cycle has been completed (McKinney, 1993). In *M. oryzae,* Pmk1 phosphorylates a Ste12 homologue called Mst12 which might ultimately activate an equivalent of Far1 to cause cell cycle arrest at G1, although this is still to be experimentally tested. Consistent with this idea, however, is the fact that a putative *FAR1* homologue in *M. oryzae* (MGG_00134) is down-regulated from 4 h onwards in the Δ*pmk1* mutant. Therefore, it may be that, as a consequence of *FAR1*-mediated down-regulation of gene expression in the Δ*pmk1* mutant, the normal cell cycle arrest does not occur, resulting in numerous rounds of mitosis. This is consistent with the importance of the cell cycle

arrest that always occurs in *M. oryzae* after a single round of mitosis during appressorium formation.

Interestingly, analysis of genes related to the response to surface hydrophobicity and Pmk1-dependent regulation, revealed that the gene most down-regulated corresponded to the biotrophy-associated secreted protein 2 (*BAS2*) gene (MGG_07749). *M. oryzae* possess three biotrophy associated secreted protein 2: MGG_09693, MGG_07969, and the previously mentioned MGG_07749. These two proteins are homologues of the cell-to-cell movement effector, *Bas2* (MGG_09693). *M. oryzae* appears to move from cell-to-cell through plasmodesmata and Bas2 and Bas3 secreted proteins have been shown to be localised to plant cell crossing points during tissue invasion (Mosquera *et al.,* 2009). These observations, coordinated with evidence that Pmk1 is also required for plant penetration and cell-to-cell movement (Salkukoo. W. and Talbot. N. J. unpublished), suggest that Pmk1 might regulate the effectors, Bas2 and Bas3, probably through a specific transcription factor that binds to a regulatory DNA region to induce effector transcription. This transcription factor has yet to be identified. However, the analysis carried out here is consistent with the idea that appressorium formation and subsequent infection is a tightly co-ordinated process involving a large repertoire of enzymes and effectors, a great number of which are under control of the Pmk1 MAP kinase pathway, which is essential for the successful invasion of the plant.

4 Mst12 transcription factor is involved in cytoskeleton re-organization during plant infection

4.1 Introduction

MAP kinase pathways are responsible for internalizing external stimuli in eukaryotic cells in order to trigger an adaptive response (Rispail *et al.,* 2009). In *M. oryzae*, one of the most important MAP kinase pathways is the Pmk1 MAP kinase pathway because it controls formation of the appressorium (Zhao and Xu, 2007). Pmk1 is a MAP kinase that activates downstream effectors, including transcription factors. One of these effectors is the zinc finger and homeobox domain containing transcription factor, Mst12 (Kim *et al.,* 2009; Park *et al.,* 2002). The Δ*mst12* null mutant forms an appressorium but it does not have the ability to form a penetration peg and therefore cannot infect the host (Park *et al.,* 2002). However, Δ*mst12* mutants can generate normal levels of turgor pressure, suggesting that the emergence of the penetration peg is controlled separately from turgor generation (Park *et al.,* 2004).

The turgor inside the mature appressorium of *M. oryzae* is estimated to be as much as 8.0 MPa (Howard *et al.,* 1991), and is generated by diffusion of water through the cell wall into the cell, against a concentration gradient of glycerol in the appressorium (de Jong *et al.,* 1997). This is maintained by melanin in the cell wall that prevents efflux of glycerol, while allowing free diffusion of water (de Jong *et al.,* 1997; Talbot, 2003). However, both the melanin layer and the cell wall, are absent from the appressorium pore, which is an area at the base of the cell from which the penetration peg emerges to rupture the cuticle of the leaf (Howard and Valent, 1996). The pore is

therefore, initially, an exclusively plasma membrane-containing area at the base of the appressorium, which allows the fungus direct contact with the plant and to establish a communication point (Howard and Valent, 1996), from which effectors may be secreted prior to penetration (Giraldo *et al.,* 2013). *Colletotrichum higginsianum* secretes effectors from the appressorial penetration pore to counteract early plant defence responses (Kleemann *et al.,* 2012). There are some lines of evidence which suggest that turgor pressure is not the only mechanism responsible for plant penetration, but that the action of secreted extracellular enzymes at the appressorial pore is also required (Deising *et al.,* 2000). However, direct evidence for the importance of these enzymes in plant infection is lacking. Secretion of extracellular enzymes and effectors at the appressorium pore is supported by the fact that the exocyst complex and polarisome structures localize as a small ring-like structures around the pore in *M. oryzae* at the time of infection (Y. Gupta, personal communication).

Emergence of the penetration peg occurs through anisotropic (polarized) membrane biogenesis at the base of the appressorium, driven through actin-generated force (Howard and Valent, 1996). Anisotropic growth at the base of the appressorium requires a hetero-oligomeric septin complex which allows formation of a toroidal F-actin network at the base of the appressorium (Dagdas *et al.,* 2012). This provides rigidity to the cortex of the cell around the pore, and also acts as a diffusion barrier to direct proteins into the pore region required for membrane curvature (Dagdas *et al.,* 2012). In budding yeast, to establish polarity and bud formation, the activation of the master polarity regulator, Cdc42 must occur (Howell and Lew, 2012). Cdc42 is required for septin ring formation or F-actin polarization through PAK kinases and the formins, Bni

and Bnr (reviewed in Howell and Lew,2011). Null mutants of *Δcdc42* in *M. oryzae* are unable to assemble a septin ring (Dagdas *et al.,* 2012). At the same time, the septin mediated F-actin network is scaffolded at base of the appressorium though a PAK kinase called Chm1, which is required for septin ring formation (Dagdas *et al.,* 2012; Kadota *et al.,* 2004), and by the action of an ERM (Ezrin/ Radixin/ Moesin) protein Tea1 which links F-actin to the plasma membrane (Dagdas *et al.,* 2012) and is NADPH oxidase-dependent (Ryder *et al.,* 2013). Cytoskeleton rearrangements at the base of the appressorium are essential for successful appressorium mediated plant penetration. For instance, septin null mutants are unable to organize the cytoskeleton at the base of the appressorium and therefore cannot produce a penetration peg to start infecting rice plants (Dagdas *et al.,* 2012). Currently, it is still not known what triggers the recruitment and assembly of cytoskeleton components at the base of the appressorium. However, some preliminary research indicates that turgor generation might be the trigger (Dagdas *et al.,* unpublished). Therefore in order to understand the mechanistic basis of impairment of the null mutant Δ*mst12* to produce a penetration peg, I decided to investigate cytoskeletal rearrangements around the appressorial pore in a Δ*mst12* mutant.

4.2 Materials and Methods

4.2.1 Standard materials and methods

For general methods see chapter 2

4.2.2 *In vitro* appressorium germination and formation assay

Germination and formation of appressoria were assayed *in vitro* using borosilicate 18 x 18 mm glass coverslips (Fisher Scientific UK Ltd). The method is adapted from that of Hamer *et al.* 1988. Conidia were harvested (as described in 2.1.1) and a suspension of 5 $x10^4$ conidia mL^{-1} was prepared in double distilled water. Fifty microliters of the conidial suspension were placed onto the coverslip surface and incubated in a controlled environment chamber under humid conditions (> 80% relative humidity) at 24℃ for the period of time required f or each specific experiment.

4.2.3 Vectors used in this study

In order to further characterize Δ*mst12* phenotypically, the localization of various proteins was performed in this study by transformation into the mutant background of a series of vectors containing these genes fused to fluorescent markers. The plasmids used in this study are listed in Table 1.

Table 4.1 List of vectors used for localization of proteins in the Δ*mst12* mutant.

Name	Pattern of localization	Resistance	Reference
Sep3-GFP	Core septin	SUR[12]	(Dagdas *et al.,* 2012)
β-tubulin-GFP	Tubulin	SUR	(Saunders *et al.,* 2010a)
Lifeact-RFP	F- actin	BAR[13]	(Dagdas *et al.,* 2012)
Chm1-GFP	PAK kinase	SUR	(Dagdas *et al.,* 2012)
Tea1-GFP	ERM protein	SUR	(Dagdas *et al.,* 2012)
Rvs167-GFP	I-BAR protein	SUR	(Dagdas *et al.,* 2012)
Las17-GFP	WASP/Arp2/3 complex	SUR	(Dagdas *et al.,* 2012)
Stt4-GFP	PtdIns-4-kinase	SUR	(Dagdas *et al.,* 2012)
Mss4-GFP	PtdIns-4-phosphate-5-kinase	SUR	(Dagdas *et al.,* 2012)

[12] Sulfonylurea resistance due to ILV1 acetolactate synthase allele
[13] Bialaphos resistance due to phosphimothricin acetyltransferase

4.3 Results

4.3.1 Generation of GFP fusion protein recombinants in Δ*mst12* mutants of *M. oryzae*

The GFP and RFP fusion vectors listed in Table 4.1 were transformed into *Δmst12* using the fungal transformation protocol described in Chapter 2. The resulting transformants were screened first by selection on complete medium plates containing either sulfonylurea (50 µg mL^{-1}) or bialaphos (50 µg mL^{-1}). The resistant *M. oryzae* transformants for each construct were screened by microscopy fluorescence signals, and the positive transformants were selected for further analysis.

4.3.2 Conidium germination and appressorium differentiation in Δ*mst12* mutant of *M. oryzae*

To study the phenotype of Δ*mst12* mutant, conidia of both Guy11 and Δ*mst12* mutants were incubated on glass coverslips and appressorium formation was monitored every two hours for a total of 24 h (Fig. 4.1). Spores of Guy11 germinated and formed polarized germ tubes by 2 h post inoculation and by 4 h, an incipient appressorium was observed. By 6 h, hemi-spherical melanised appressoria were observed in Guy11. However by 6 h in Δ*mst12* mutants, only incipient appressoria were observed which after 8 h showed only partial melanisation. This observation indicated a delay in appressorium formation and maturation in Δ*mst12* mutants. At later time points, there were no obvious differences between appressoria of Guy11 and Δ*mst12*.

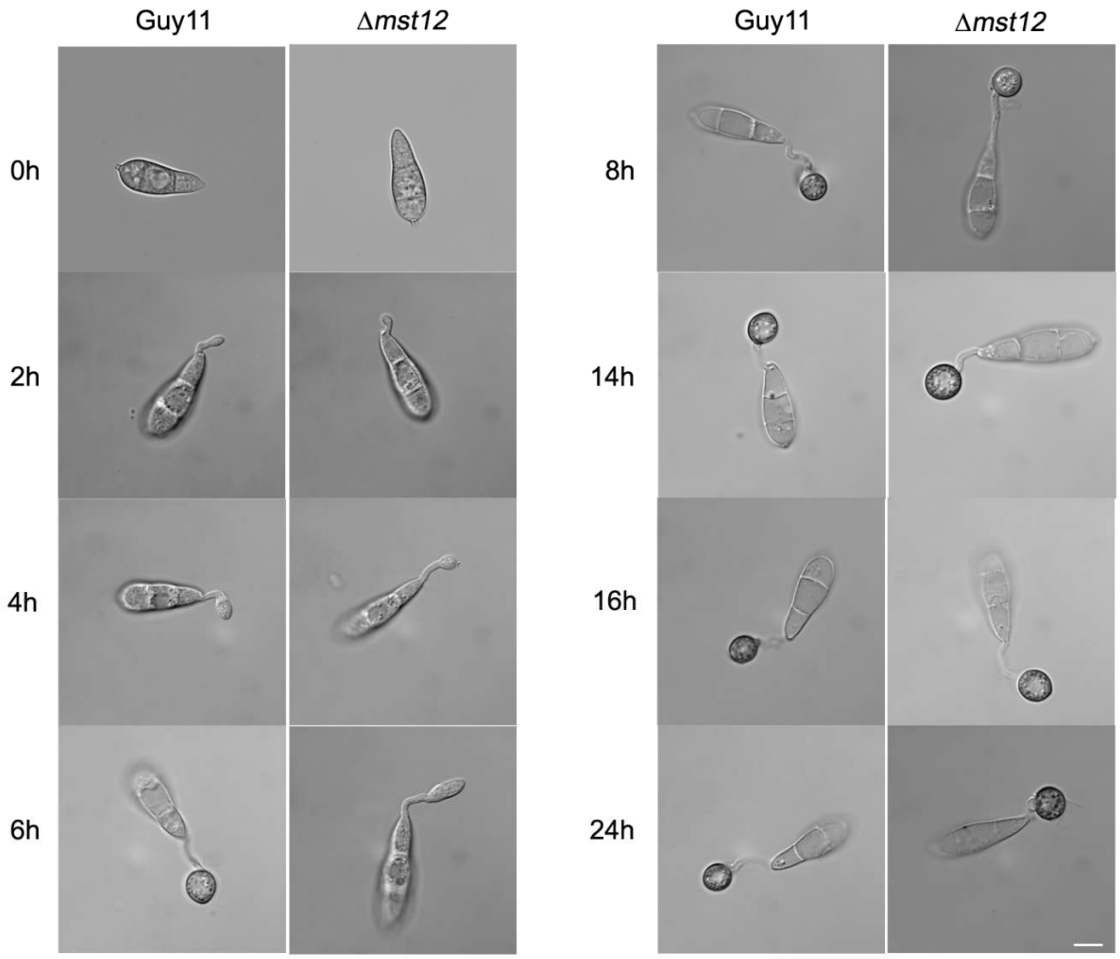

Figure 4.1 Micrographs showing appressorium development at time points used in this study from Guy11 and Δ*pmk1* on cover slips. (bar = 10µm)

4.3.3 F-actin, septin and microtubule dynamics in appressorium in Δ*mst12*

In *M. oryzae*, F-actin and septin localise as toroidal ring-like structures at the base of the appressorium and are both required for successful plant infection (Dagdas *et al.,* 2012; Ryder *et al.,* 2013). To understand the nature of these two components in a mechanistic model involving Mst12, their localization was studied. It is also known that microtubules fulfil a number of functions in filamentous fungi, including vesicle movement (Lee *et al.,* 2001) and polarity maintenance, in conjunction with actin (Steinberg, 1997; Takeshita *et al.,* 2014). Therefore, the involvement of microtubules in apical polarization of the penetration peg was also tested by localization of β-tubulin in the Δ*mst12* mutant.

To understand the localization of septins, actin and β-tubulin in Δ*mst12* mutants, conidia of Guy11 and Δ*mst12* both expressing Sep3-GFP, Lifeact-RFP and Tub1-GFP respectively, were germinated onto glass coverslips for 24 h and observed under the microscope (Figure 4.2). Lifeact-RFP showed an aberrant F-actin localization, forming a disorganized filamented structure outcentered from the appressorial pore in Δ*mst12,* as shown in Figure 4.2, whereas in the wild type Guy11, Lifeact-RFP localised as a toroidal ring structure at the base of the appressorium, as shown in Dagdas *et al.,* (2012) and Fig. 4.2.

Localisation of Sep3-GFP showed a small filamentous ring-like structure off-centred from the appressorial pore in a Δ*mst12,* as shown in Figure 4.2. However, in the wild type, Sep3-GFP localised as a toroidal ring structure to the base of the appressorium (Fig. 4.2). The β-tubulin-GFP shows mis-localised microtubules in Δ*mst12,* resembling those observed in immature radially expanding appressoria, as

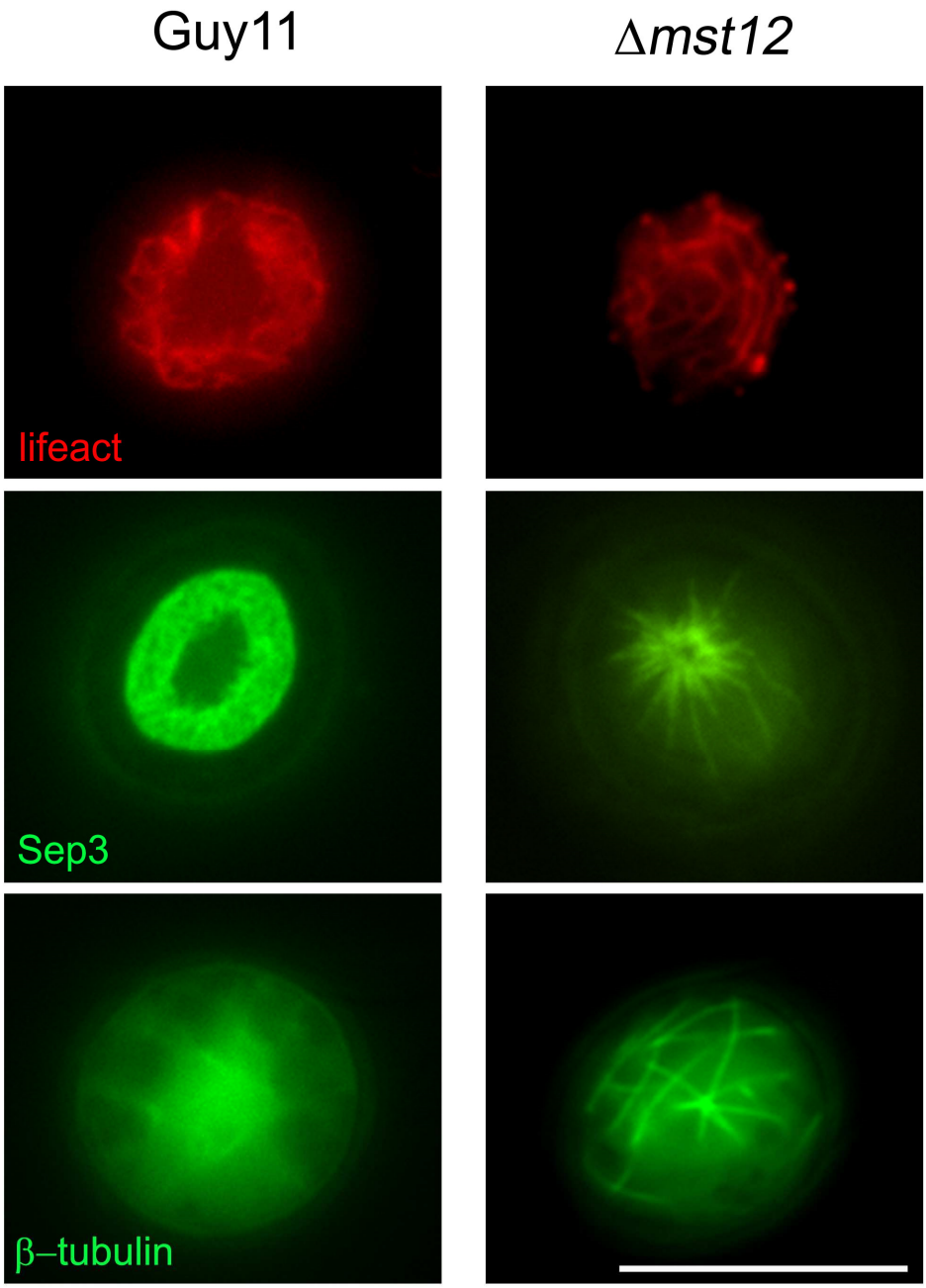

Figure 4.2 Micrographs to show cellular localization of lifeact-RFP, cdc3-GFP and β-tubulin-GFP in Guy11 and Δ*mst12* on cover slips at 24 h. (bar = 10µm).

shown in Figure 4.2. In the wild type, Guy11, microtubule filaments were no longer visible probably due to the compaction of the structure and instead, a compacted mass was observed at the appressorial pore (Fig. 4.2).

4.3.4 Localization of F-actin and septin interacting proteins in Δ*mst12* mutant of *M. oryzae*

Septin recruitment to the bud neck region in *Saccharomyces cerevisiae* is dependent on the small GTPase, Cdc42 and its two downstream effectors, the PAK kinases Ste20 and Cla4 (Kadota *et al.,* 2004). In *M. oryzae*, a Cla4 homologue, called Chm1, was identified and shown to form a ring-like structure at the base of the appressorium (Dagdas *et al.,* 2012). In the Δ*mst12* mutant, however, the localization Chm1 was observed as randomly distributed puncta within the appressorium (Fig. 4.3).

Tea1 is an Ezrin/ Radixin/Moesin protein which binds at its N-terminal domain to the plasma membrane and through its C-terminal domain to F-actin (Turunen *et al.,* 1994). In *M. oryzae,* Tea1 has been shown to co-localise as a toroidal ring-like structure with F-actin at the base of the appressorium (Dagdas *et al.,* 2012). In *Δmst12* mutants, F-actin was mis-localised (Fig. 4.2) and we reasoned that because localization of F-actin at the base of appressorium is Tea1 dependent, it would be of interest to determine Tea1 localisation in *Δmst12* (Fig. 4.4). Therefore, Tea1-GFP was transformed into the *Δmst12* mutant and examined over the course of appressorium formation. Fluorescent signal was observed at 16 h and later at 24 h, but mis-localised as randomly distributed puncta in the appressorium, suggesting that failure of the

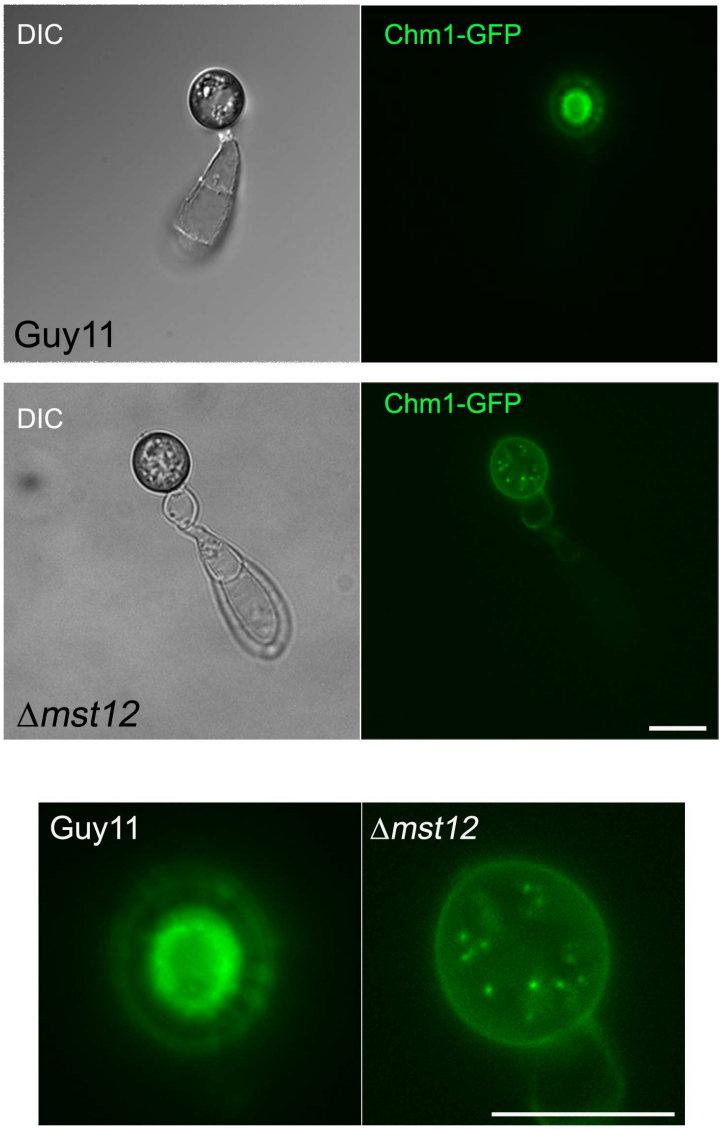

Figure 4.3 Micrographs to show cellular localization of Chm1-GFP in Guy11 and *Δmst12* on cover slips at 24 h. (bar = 10µm)

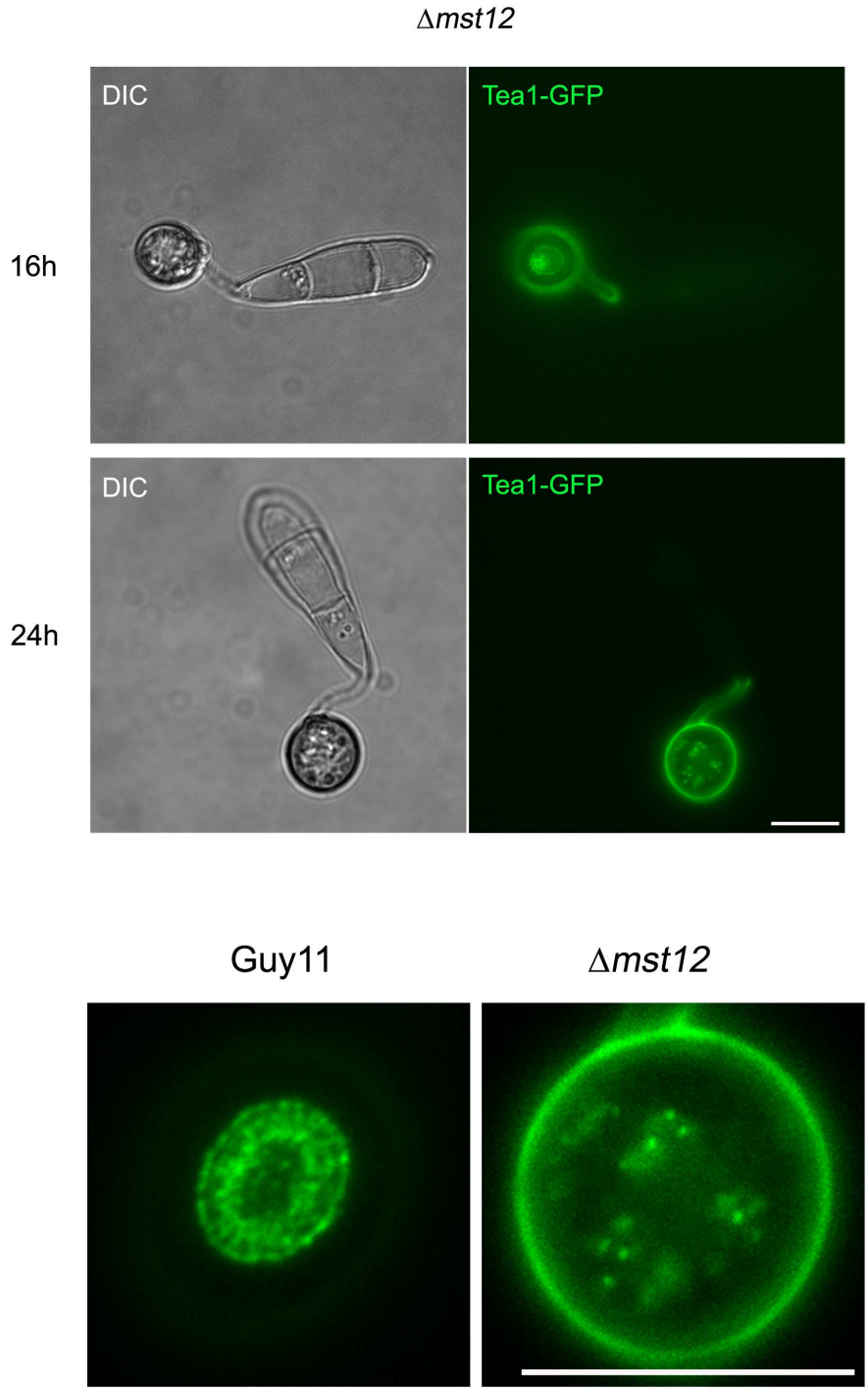

Figure 4.4 Micrographs to show cellular localization of Tea1-GFP in Δ*mst12* at 16h and 24h and Guy11 and Δ*mst12* on cover slips at 24 h. (bar = 10µm)

normal F-actin cytoskeleton re-modelling at the appressorium pore in *Δmst12* is in part due to impairment in the function of Tea1.

4.3.5 Localization Rvs167 and Las17 in Δ*mst12* mutant of *M. oryzae*

Bin-amphiphysin-Rvs (BAR) domain proteins have been shown to form oligomeric scaffolds involved in membrane curvature, and are involved in cellular invaginations (F-BAR) or protrusions (inverse or I-BAR proteins) (Dawson *et al.,* 2006). Bar proteins bind to actin and to PtdIns(4, 5)P_2 (Bompard *et al.,* 2005; Miki *et al.,* 2009). Localization of the I-BAR protein, Rvs167, in *M. oryzae* to the appressorium pore has been reported to be septin-dependent (Dagdas *et al.,* 2012). Therefore, we reasoned that the inability of Δ*mst12* to form a protrusion (penetration peg) might be due, in part, to impairment in the function of Rvs167 as a consequence of the failure of the Δ*mst12* mutant to direct formation of the septin ring to the appressorium pore. Rvs167-GFP was transformed into the Δ*mst12* mutant and its localization was observed on coverslips at 16 h and 24 h (Fig. 4.6). In Guy11 at 24 h, Rvs167-GFP localised to large punctate regions inside the appressorium pore. However, in the case of Δ*mst12* mutants the puncta were not present and instead a stronger signal was localized around the cell periphery.

Las17 is an actin activator and part of the actin-related protein 2/3 complex (Arp2/3) (Urbanek *et al.,* 2013). The Arp2/3 complex has been described to be required

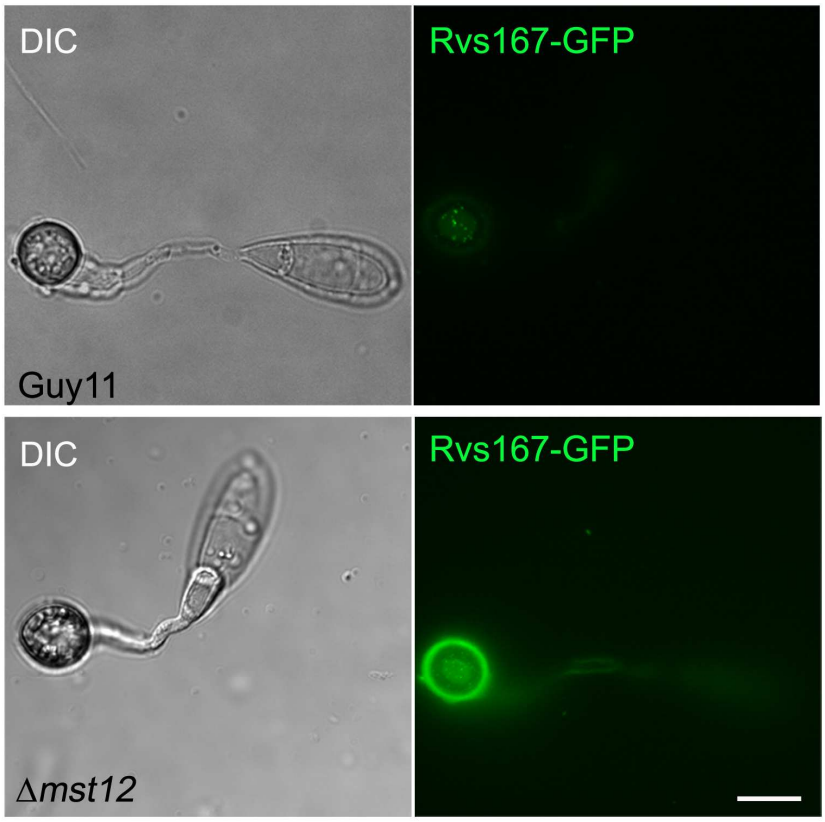

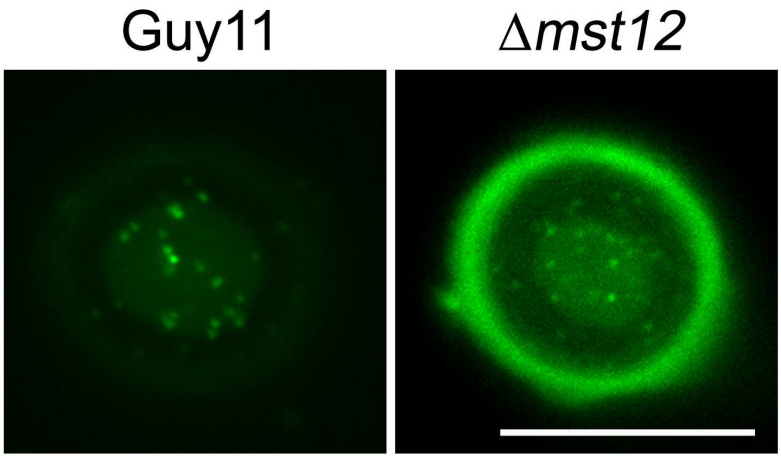

Figure 4.5 Micrographs to show cellular localization of Rvs167-GFP in Guy11 and Δ*mst12* on cover slips at 24 h. (bar = 10µm)

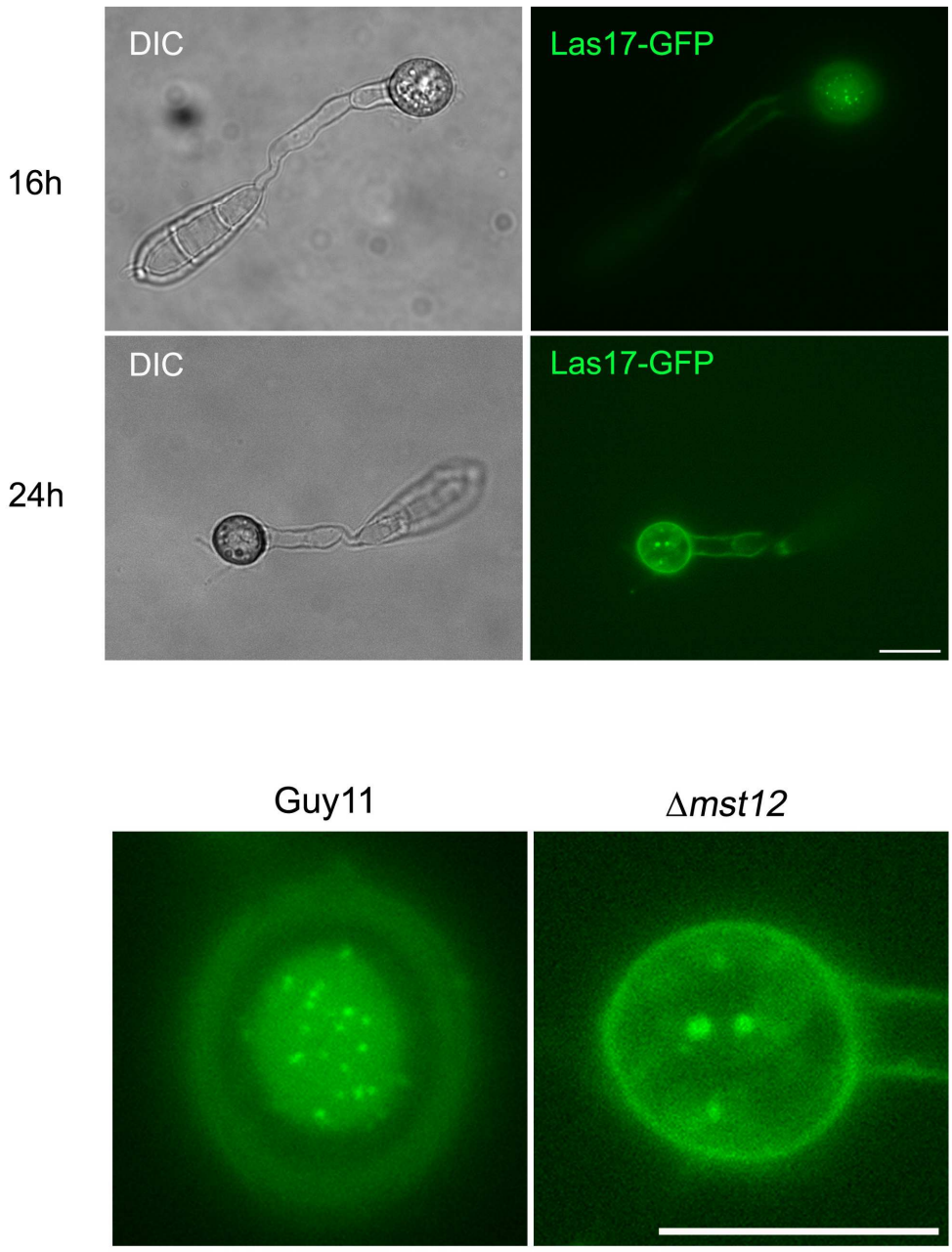

Figure 4.6 Micrographs to show cellular localization of Las17-GFP in Guy11 and Δ*mst12* on cover slips at 24 h. (bar = 10µm)

for F-actin polymerization, organization and recycling (Goley and Welch, 2006). In *M. oryzae* Las17-GFP was shown to be localised at the appressorial pore, in a septin-dependent manner (Dagdas *et al.,* 2012). As the septins are not correctly localised in Δ*mst12* mutant, the localization of Las17 was studied. Las17-GFP was transformed into the Δ*mst12* mutant and its localisation observed on coverslips at 16 h and 24 h (Fig. 4.7). In Guy11 at 24 h, Las17-GFP localised to puncta within the appressorium pore, consistent with Dagdas *et al.,* (2012). However, in the case of the Δ*mst12* mutant Las17-GFP was mis-localised with puncta no longer maintained in the pore, as shown in Figure 4.7.

4.3.6 Localization of Mss4 and Stt4 in Δ*mst12*

The phosphorylation and activation of ERM proteins is mediated by the PtdIns signalling pathway (Fievet *et al.,* 2004). Septins associate with PtdIns-4-phosphate and PtdIns(4,5)P_2 via their N- terminal polybasic domain (Casamayor and Snyder, 2003). Staurosporine and Temperature sensitive-4, Stt4, proteins as well as the Multicopy Suppressor of Stt4 (Mss4) are lipid kinases required for PtdIns(4,5)P_2 gradient formation at the plasma membrane and show a localised punctate distribution (Garrenton *et al.,* 2010). In *M. oryzae,* Mss4 and Stt4 are both localised as small puncta-like structures around the septin ring (Dagdas *et al.,* 2012). The localisation of these lipid kinases was therefore studied in Δ*mst12* mutants at 16 h and 24 h (Fig 4.7 and 4.8). At 16 h, Mss4 was mis-localised in the Δ*mst12* mutant, forming small puncta that were distributed randomly in the appressorium and, at 24 h, the puncta became larger, more clumped and disorganised. In the Δ*mst12* background Stt4 was also mis-localised at 16 h as

random puncta throughout the appressorium dome and by 24h, the puncta became larger and disorganised.

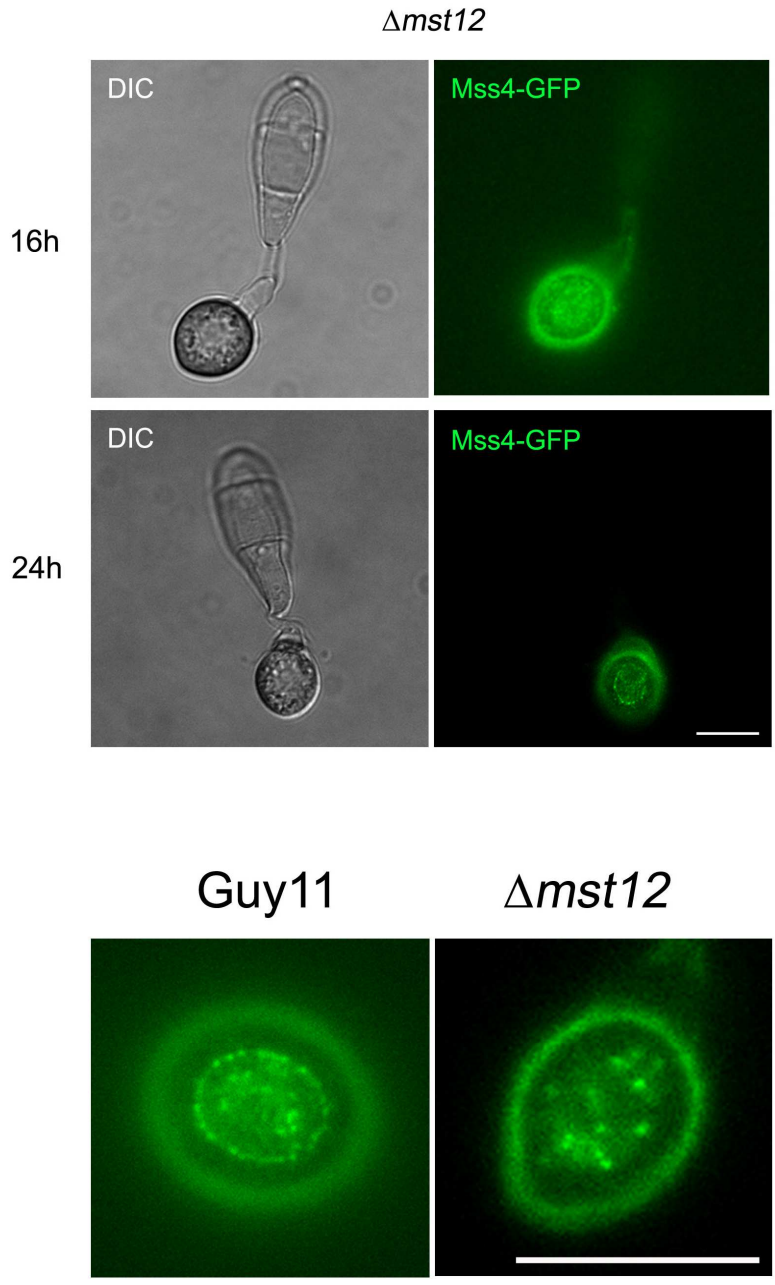

Figure 4.7 Micrographs to show cellular localization of Mss4-GFP in Guy11 and Δ*mst12* on cover slips at 16 h and 24 h. (bar = 10µm)

s

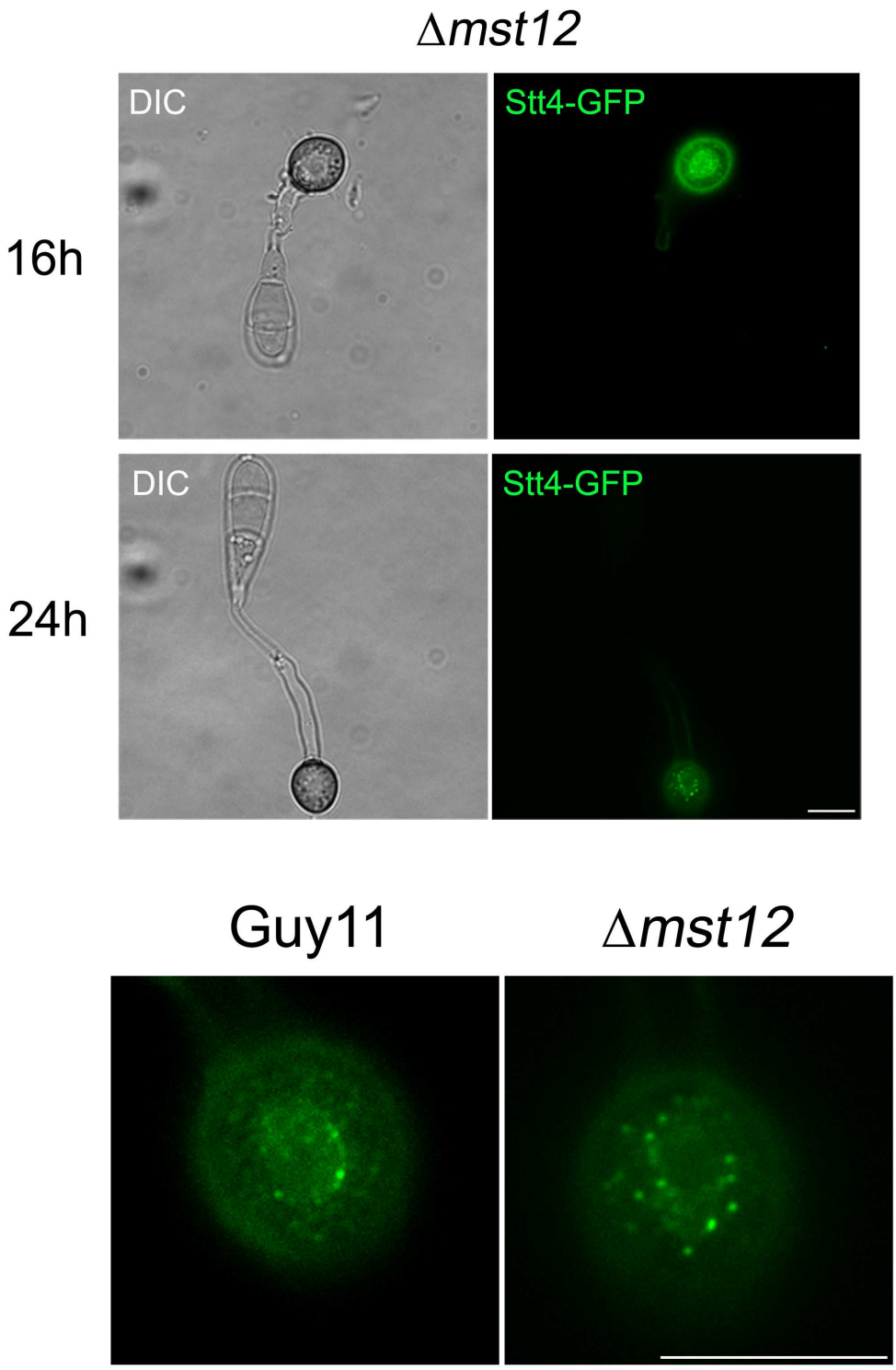

Figure 4.8 Micrographs to show cellular localization of Stt4-GFP in Guy11 and Δ*mst12* on cover slips at 16 h and 24 h. (bar = 10µm)

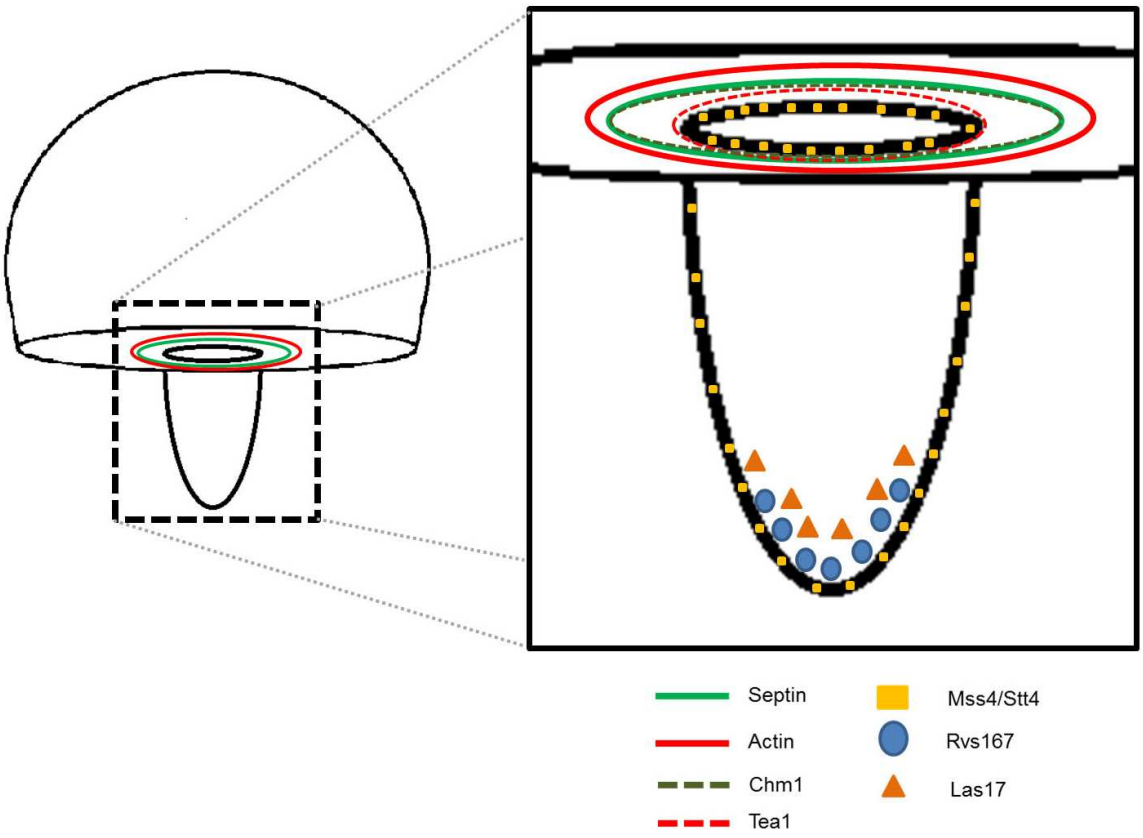

Figure 4.9 Model to represent septin-dependent proteins localized at the appressorium pore during penetration peg development.

4.4 Discussion

In this chapter I have presented evidence that the Mst12 transcription factor maybe involved in cytoskeleton re-organization at the base of the appressorium, which is necessary for a correct re-polarization and penetration peg formation. These observations are consistent with the inability of Δ*mst12* mutants to repolarize and form a penetration peg (Park *et al.,* 2002). It was shown that in a Δ*mst12* mutant, both septin and actin ring-like structures observed in the wild type are mis-localised in the Δ*mst12* mutant. In addition, the septin interacting protein Chm1 and actin interacting protein Tea1 were both mis-localised in Δ*mst12.* The mislocalization of these structures was consistent with the mislocalization of the lipase kinases Mss4 and Stt4 as well as the I-BAR protein Rvs167 and WASP protein Las17, outside of the appressorium pore region.

The null mutant of Δ*mst12* was reported to show turgor generation, but is impaired in the elicitation of localised host responses, suggesting that Mst12 might have a role in secretion and generation of mechanical force during cuticle rupture (Park *et al.,* 2002). For instance, in the human fungal pathogen *Candida albicans*, Ste12, seems to regulate virulence factors such as adhesins and proteases, which are required for biofilm establishment (reviewed in Won Sak Hoi *et al.,* 2007). In other filamentous fungi, such as, for example *C. lindemuthiamum,* the Ste12 equivalent has been reported to regulate pectinase genes as well as genes related to adhesion (Herbert *et al.,* 2002; Wong Sak Hoi *et al.,* 2007). Adhesion is an important step in pre-penetration stages of fungi, including *M. oryzae* (Tucker and Talbot, 2001). Some null mutants of *M. oryzae*,

for example, the cutinase 2 (Cut2), have been shown to be impaired in appressorium adhesion and therefore plant penetration (Skamnioti and Gurr, 2007).

In the wild type strain Guy11, formation of the septin ring occurs as early as 8 h during appressorium development on glass cover slips (Dagdas *et al.,* 2012). The septin ring has been reported to act as a diffusion barrier for proteins into the pore (Dagdas *et al.,* 2012) and therefore the defect in secretion of proteins in a Δ*mst12* mutant could be explained as being a consequence of the pore not being well defined and the turgor pressure not well focused in the pore region. This fact might also explain why Rvs167 and Las17, which are involved in formation of cellular protuberances and endocytosis patches, are also mislocalised in the Δ*mst12* mutant.

In this study, however, we did not determine whether, in a Δ*mst12* mutant, septin or actin rings are formed at earlier time points during appressorium development and simply not maintained, or whether their formation never occurs, at any stage of development. These experiments are required in future. In budding yeast, Ste20 and Cla4 are both required for the assembly of the septin ring and they are dependent on the Cdc42 (Kadota *et al.,* 2004). However, Cla4 and the two E2 ubiquitin ligases, Dma1 and Dma2, have been also described to contribute to septin ring recruitment and stabilization (Merlini *et al.,* 2012). In the case of the Δ*mst12* mutant, Chm1 was mislocalised suggesting that both assembly and maintenance of septins could be affected. Therefore, it would be interesting to investigate this further and determine whether Mst12 is involved in maintenance of the septin and actin ring or is just required for their formation. To investigate this, a more detailed appressorium development time course experiment, in which septin and actin are observed every two hours during

appressorium formation over a period of 24 h, would be needed. In this way, it would be possible to determine whether Mst12 could be involved in the maintenance or into the assembly of the ring-structures. Also, it will be necessary to determine whether Cdc42 localizes first at the appressorial pore, and thereby to determine whether the position of a new polarization site occurs in Δ*mst12* mutant. An essential part of the budding process in yeast, is the role of Rho1 in bud emergence, which works downstream of Cdc42 after septin ring is assembled (Chant and Stowers, 1995). It might therefore be the case that Mst12 is unable to activate Cdc42, which turn affects activation of the polarisome to direct polarized growth (Sheu *et al.,* 1998). In fact, in *M. oryzae*, null mutants of Δ*mst12*, and *Δcdc42* are both able to form appressorium, but are impaired in formation of the penetration peg and infectious growth, consistent with this idea (Zheng *et al.,* 2009).

Upstream of Cdc42, is the phosphatidylinositol 4-phosphate (PI4P). They have been shown to recruit Cla4 to the plasma membrane where it activates Cdc42 and triggers polarized growth (Wild *et al.,* 2004). Phospho-inositides are membrane-bound lipids involved in morphogenesis, polarization and cytoskeletal rearrangements on the plasma membrane (Strahl and Thorner, 2007). In budding yeast, septin ring assembly is dependent on PtdIns(4,5)P_2, as described in Bertin *et al.,* (2010). A gradient of PtdIns(4,5)P_2 is generated in the plasma membrane due to action of the lipase kinases Mss4 and Stt4 (Boronenkov and Anderson, 1995; Yoshida *et al.,* 2009). It has been hypothesised that anisotropic generation of PtdIns(4,5)P_2 occurs due to the septin ring which acts as a barrier against lipid phosphatases thereby preventing the degradation of Mss4 and Stt4 (Garrenton *et al.,* 2010). The anisotropic gradient of PtdIns(4,5)P_2 also

promotes the activation of the pheromone MAP kinase pathway MAPK Fus3 in yeast, through recruitment of the Ste5 scaffolding protein to the plasma membrane, defining a mechanistic model to link phosphoinositides with pheromone kinase signalling (Garrenton *et al.,* 2006). Phosphoinositides have also been linked to the Pkc1 and Slt2 cell wall integrity pathway through Stt4 (Audhya and Emr, 2002; Yoshida *et al.,* 1994). In the case of *M. oryzae,* septin null mutants are unable to form a penetration peg and re-polarize, possibly due to mis-localisation of Stt4 and Mss4. In Δ*mst12* mutants, septins are mis-localised and therefore Mss4 and Stt4 are probably de-activated, and as a consequence, the PtdIns(4,5)P_2 gradient is not generated, preventing repolarization and formation of the penetration peg. However de-activation of Mss4 and Stt4 has not been shown and more research will be required to test this idea. Another possibility is that Mst12 directly regulates the activation of Mss4 and Stt4. To study the mechanistic process of this model in *M. oryzae* and the involvement with Mst12*,* it will be necessary to generate null mutants involved in phosphoinositide signalling including, for example, temperature sensitive mutants of Stt4 and Mss4 in a wild type background, or lipid phosphatase mutants in an Δ*mst12* background to study their pathogenicity, and also the phosphorylation state of both the Fus3 homologue, Pmk1, and the Slt2 homologue, Mps1, in order to start defining the relationship of these signalling pathways and their relevance for penetration peg formation in *M. oryzae*.

5 Identification of genes regulated by Mst12 transcription factor required for appressorium-mediated plant penetration

5.1 Introduction

Mitogen Activated Protein (MAP) kinases are central regulators of signalling pathways that internalize external stimuli inside the cell. MAP kinases activate downstream effectors, including transcription factors, which regulate and re-programme gene expression to adapt to external stimuli (Zhao and Xu, 2007). This is the case for the PMK1 MAP kinase signalling pathway in *M. oryzae*, which is activated through surface hydrophobicity and other plant signals, and leads to the formation of an infection structure, called the appressorium (Xu and Hamer, 1996). Pmk1 has been shown to be translocated into the nucleus when activated, in order to stimulate downstream effectors, including transcription factors, in response to external stimuli, but until now, very few have been identified (Bruno *et al.,* 2004). Downstream of Pmk1 there are several putative interactors such as the cystinosin/ ERS1 repeat (CTNS) containing protein Pic5 which is required for pathogenicity (Zhang *et al.,* 2011). There is also a zinc finger and homeobox domain containing transcription factor, Mst12, which is the homologue of *S. cerevisiae* Ste12. In *M. oryzae,* null mutants of *MST12* make appressoria, but are unable to form a penetration peg and, therefore, to cause rice blast disease (Park *et al.,* 2002). In other filamentous fungi, such as the cucumber pathogen *Colletotrichum lageniarium*, the Δ*cst1* null mutant (a Ste12 homologue) is also unable to form primary invasive hyphae and to cause disease (Tsuji *et al.,* 2003). However, Mst12 is dispensable for mating in *M. oryzae*, suggesting a completely different function in

relation with its homologue in *S. cerevisiae* (Park *et al.,* 2002). Moreover, null mutants of Mst12 generate normal turgor pressure and contrary to Δ*pmk1*, null mutants of Mst12 show normal lipid and glycogen mobilization compared to the wild type, suggesting that both these processes are dependent on Pmk1, but independent of Mst12 (Park *et al.,* 2004)**.** Moreover, cytoskeleton components, such as septins, actin, tubulin and the cytoskeleton dependent proteins described in Chapter 4, were found to be mislocalised, indicating impairment of cytoskeletal rearrangements during appressorium maturation in the Δ*mst12* mutant. Therefore Mst12 might be involved in regulating genes that control the translation of turgor pressure into forces that lead to formation of the penetration peg (Park *et al.,* 2004).

In *S. cerevisiae,* the Mst12 homologue, Ste12, binds to and regulates genes via promoter elements. Ste12 binds to specific *cis*-acting sequences called pheromone response elements (PREs) and filament response elements (FREs) (Chou *et al.,* 2006) bind Ste12. The selective binding of Ste12 to these elements allows regulation of the expression of corresponding genes in response to the external conditions (Chou *et al.,* 2006). The identity of PREs and FREs has been well documented, and they have been found in the promoters of more than 800 genes (Lefrancois *et al.,* 2009). In the case of PREs, Ste12 probably regulates PREs expression through an interaction with other DNA regulators but the identity of these regulators is still unknown (Su *et al.,* 2010). In the case of Mst12, nothing is known about the downstream gene sets, the cognate binding motif or the interaction with other DNA regulators.

In this chapter, I set out to determine the identity of genes regulated by Mst12 and associated with appressorium-mediated plant penetration. To do this, a

comparative transcriptomics approach was carried out for both the Δ*mst12* mutant and Guy11, during a time course of appressorium formation on a hydrophobic surface. The data generated was used to determine the candidate genes regulated by Mst12 during appressorium formation. Candidate genes putatively regulated by Mst12 were identified through three different approaches. First, k-means cluster analysis was used to identify co-regulated patterns of gene expression in a time course of appressorium formation. Secondly, a direct comparison between genes differentially regulated in the Δ*pmk1* mutant (compared to Guy11) with genes differentially regulated genes in the Δ*mst12* mutant was carried out. Thirdly, the transcriptional hierarchy within the Pmk1 MAP kinase signalling pathway was analysed.

5.2 Materials and methods

5.2.1 Standard procedures

For standard procedures see Chapter 2 of this study

5.2.2 Appressorium development assays for RNA extraction and RNA-Seq library preparation

Appressorial assays were conducted, as described in General Materials and Methods section 2.4.1.

5.2.3 Analyzing the data

The output reads of next generation sequencing were aligned against version 8.0 of the *M. oryzae* genome using Tophat software (Trapnell *et al.,* 2010). The analysis of the data was performed using DE-Seq (Anders and Huber, 2010). Transcript abundances for each gene and adjusted P-values (P_{adj}) were generated according to Soanes et al. (2012). To determine significant differences in each pair wise comparison, we used the p-value (P_{adj}) to <=0.01. Data was analysed by using Microsoft Access. Heat-maps were generated using "gplots" package (http://cran.r-project.org/web/packages/gplots/gplots.pdf) from the free computing software platform R (http://www.r-project.org/).

5.2.4 K-means clustering analysis

K-means clustering was carried out using Multiple Array Viewer free-software (http://www.tm4.org/), using Euclidean Distance clustering with a maximum of 50 iterations. To calculate the number of clusters to use for K-means clustering analysis,

an R package called “Mclust” was used (http://www.stat.washington.edu/fraley/mclust/) which determines the optimal model and number of clusters according to the Bayesian Information Criterion for expectation-maximization, initialized by hierarchical clustering for parameterized Gaussian mixture models.

5.3 Results

5.3.1 Global changes in gene expression in Δ*mst12*

To determine genes putatively regulated by Mst12, a comparative transcriptomics approach was carried out using RNA-Seq for both the Δ*mst12* mutant and the isogenic wild type strain Guy11. Conidia of both the Δ*mst12* mutant and Guy11 were germinated on glass cover-slips at 26 ^{0}C for 24 h in the presence of the cutin monomer, 1,6-hexadecanediol in distilled water. Every two hours samples were collected by scraping the cover-slip surface with a razor blade and immediately snap frozen in liquid nitrogen. Total RNA was extracted and RNA-Seq libraries were prepared and sequenced using an Illumina Sequencer 2500. Short sequencing reads were aligned against version 8.0 of *M. oryzae* genome using Tophat software (Trapnell *et al.,* 2010). The analysis of the data was performed using DESeq, which determines differential gene expression through the moderated log2 fold change value (mod_lfc) (Anders and Huber, 2010). Transcript abundances for each gene and adjusted p-values were generated according to Soanes *et al.,* (2012). To determine the significant differences for pair-wise comparisons we used a p-value adjusted for false discovery rate (padj) < 0.01. The average number of reads obtained was 50 million reads.

To understand global transcriptional pattern of gene expression in the Δ*mst12* mutant, Euclidean distances were determined between each sample of both Δ*mst12* and Guy11 strains, whereby the transcriptional abundance of every transcript compared in a pair wise manner in all possible combinations. Similar patterns of gene expression were observed during early stages of appressorium development (from 2 h to 6 h) indicating that gene expression at early stages is largely common between the wild type

and the Δ*mst12* mutant. However, there is evidence suggesting a delay in appressorium formation in the Δ*mst12* mutant (see section 4.3.2) which is reflected in global gene expression which showed a distinct similarity between gene expression observed at 8 h in the Δ*mst12* mutant with gene expression patterns observed much earlier in the early development stages of Guy11, from 2 to 6 h, as shown in Figure 5.1. Consistent with a delay in development, distinct similarity in gene expression patterns also occurs later, during appressorium development. For example, gene expression patterns in the Δ*mst12* mutant at 16 h and up to 24 h, are similar to those exhibited by Guy11 at 16 h. This observation is based on the distinct clades identified by Euclidean analysis.

To determine the subset of genes potentially regulated by Mst12, the number of differentially expressed genes of Δ*mst12* compared to Guy11 was determined. The number of differentially regulated genes at 2 h, 4 h and 6 h varied between 753 and 1408 genes, whereas at later time points such as 8 h, 14 h, 16 h and 24 h, or in ungerminated conidia at 0 h, the number of differentially regulated genes varied between 1872 and 3523, as shown in Figure 5.2. These results indicated that there was a strong peak in the number of differentially expressed genes between Guy11 and the Δ*mst12* mutant at 8 h which was maintained at 14h, 16h and 24 h, probably due to the increasing phenotypic differences associated with penetration peg formation and cytoskeleton re-arrangements occurring in Guy11 but missing in Δ*mst12.* The number of genes up-regulated and down-regulated was also determined. This showed that the number of down-regulated genes in the Δ*mst12* mutant compared to Guy11 was always greater than the number of up-regulated genes, except at the 4 h time point. This result suggests that Mst12 is predominantly associated with transcriptional activation, or de-

repression, during appressorium development but also suggest that during early stages of development some genes are also repressed by its action, or the action of downstream regulators controlled by Mst12.

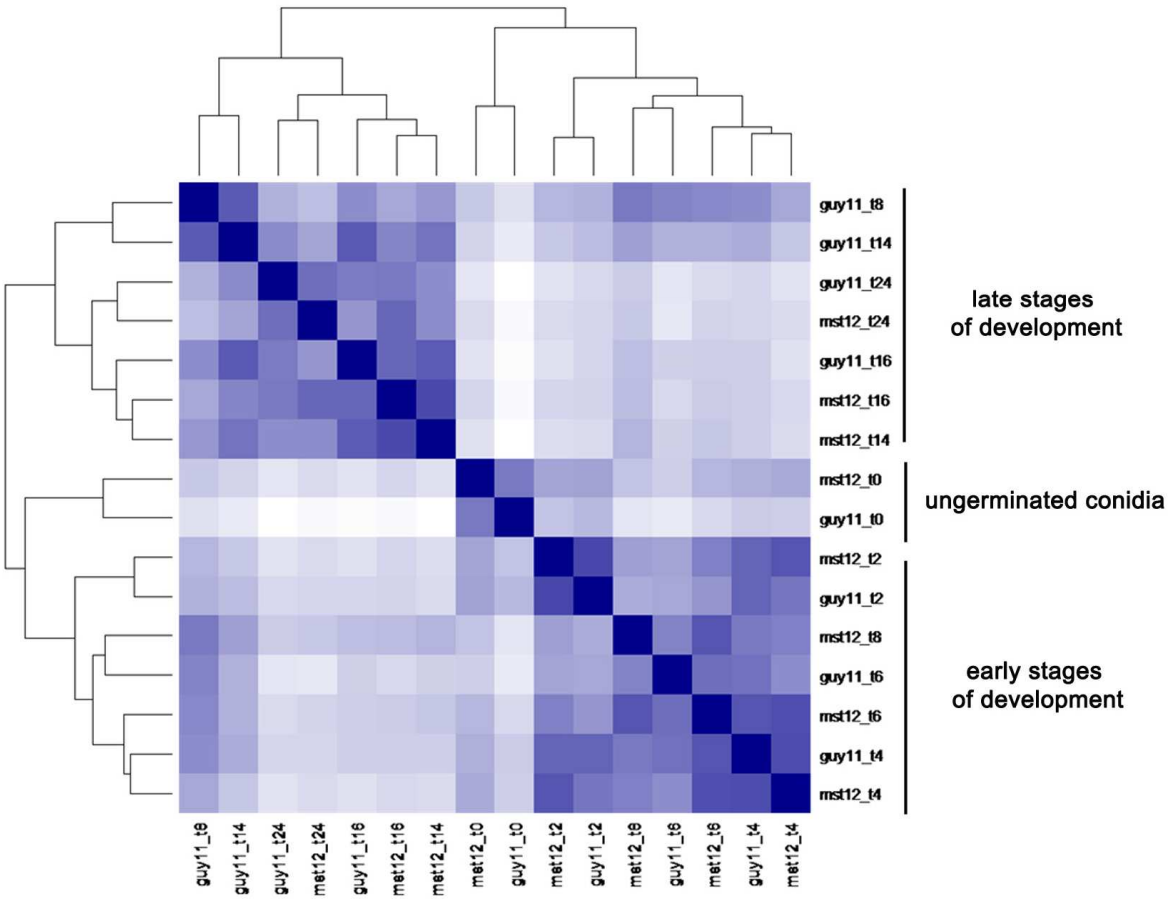

Figure 5.1 Heatmap showing the Euclidean distances between RNA-Seq samples from wild type Guy11 and the Δ*mst12* mutant. RNA samples were labelled with the name of the strain and specific timepoint within the time course experiment. Euclidean distance heatmap compared the entire time course of both Guy11 and the Δ*mst12* mutant in a pair wise manner in all possible combinations. A dendrogram was generated in parallel with the Euclidean heatmap to determine sample clustering.

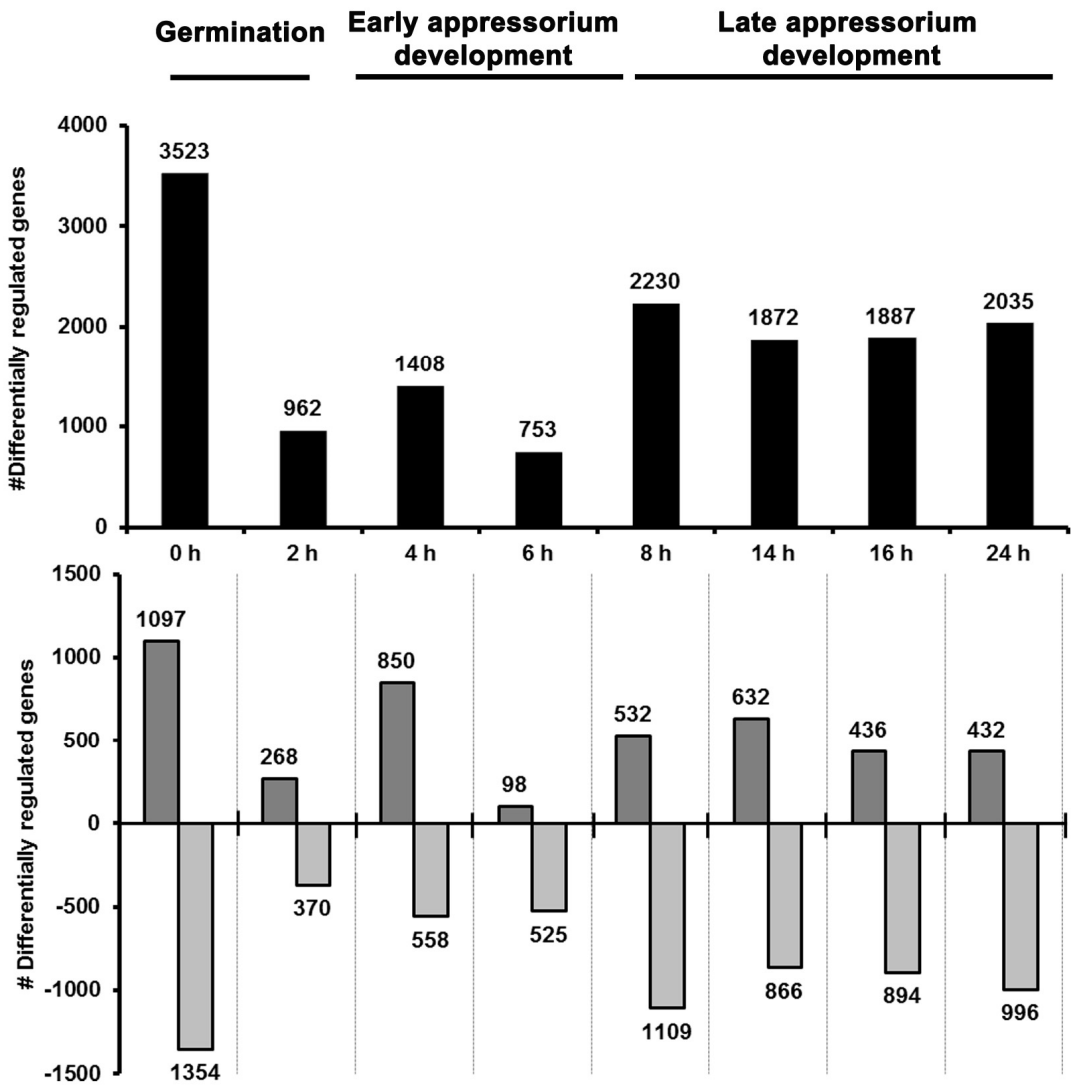

Figure 5.2 Bar charts to show the number of differentially regulated genes in the Δ*mst12* mutant when compared with Guy11 Bar charts to show total number of differentially regulated genes in the Δ*mst12* mutant when compared with Guy11 (padj< 0.01) (White), number of up regulated genes in the Δ*mst12* mutant when compared with Guy11 (padj< 0.01; logfold> 1) (Dark gray) and number of down regulated genes in Δ*mst12* when compared with Guy11 (padj < 0.01; mod_lfc < 1) (Light gray).

5.3.2 K-means Clustering

To investigate patterns of gene expression associated with appressorium formation and with pre-penetration stage development, K-means cluster analysis was carried out for the *Δmst12* mutant. K-means clustering is a centre-based cluster algorithm which in this case classifies a certain initial gene set based on their gene expression pattern over a time course of appressorium development. The initial gene was selected by picking genes that were differentially regulated by at least 4-fold at every time point in the *Δmst12* mutant, compared to the wild type Guy11. In this way the biggest changes in gene expression could be specifically analysed as a collective group. The number of genes that were down-regulated were 368, 94, 170, 214, 457, 297, 256 and 411, and those up-regulated were 290, 72, 68, 41, 128, 281, 151 and 173, at 0 h, 2 h, 4 h, 6 h, 8 h, 14 h, 16 h, and 24 h respectively. In total 3471 genes were selected which when bulked together, represented an initial gene set of 2006 genes. As the number of clusters for K-means analysis must be determined in advance (Jain, 2009), the “Mclust” R package was used (see section 5.2.3 in this chapter) to analyse the 2006 genes selected. The optimal number of clusters obtained was 6 and the number of genes for each cluster was variable and is represented in Table 5.1.

K-mean clustering analysis revealed the gene expression profile of the genes for each of the clusters, as shown in Figure 5.3. The centroid based graphs show the mean gene expression pattern for each cluster, based on the expression of each gene from the cluster. A heatmap of every cluster was also generated and showed two separate groups according to gene expression profiles (Fig. 5.4). Clusters k1 and k2, showed genes that were highly up-regulated at both early and late stages of appressorium

development. Clusters k3, k4, k5 and k6 conversely showed down-regulation of gene expression at various stages during the entire time course.

Table 5.1 Table showing an overview of K-means clustering results.

Cluster [14]	# of Genes in Cluster [15]	% of Genes in Cluster [16]
k1	370	18%
k2	327	16%
k3	384	19%
k4	333	17%
k5	159	8%
k6	433	22%

[14] Cluster identity
[15] Number of total genes for every cluster
[16] Percentage of genes for every cluster respective to the total (total= 2006)

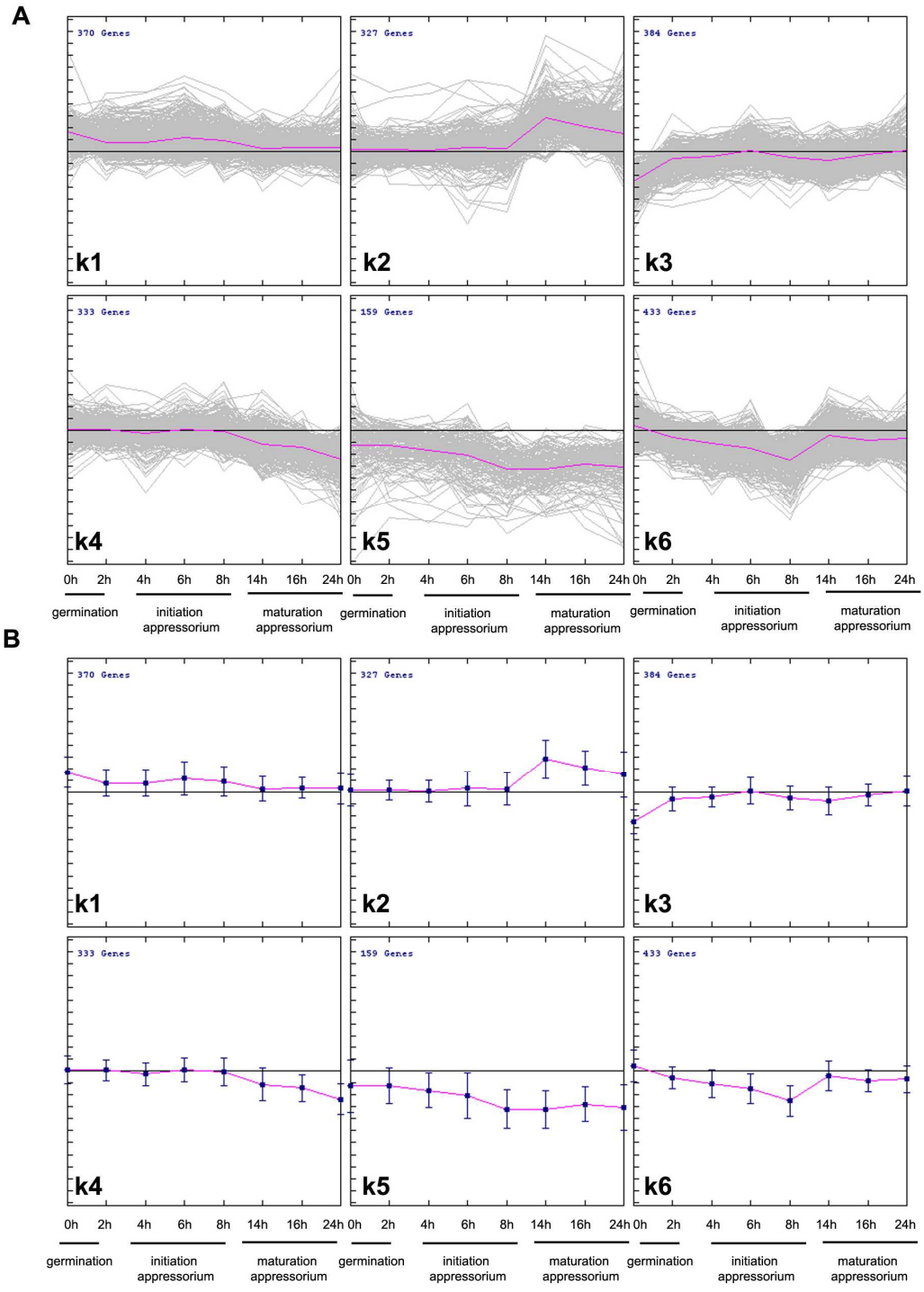

Figure 5.3 Expression pattern graphs for every cluster. A) Centroid graphs to show the mean expression pattern for every cluster. **B)** Expression graphs to show at the same time as centroid graphs, the expression level of each gene. For both panels cluster k1 corresponds to the upper left graph and cluster k6 corresponds to the bottom right graph.

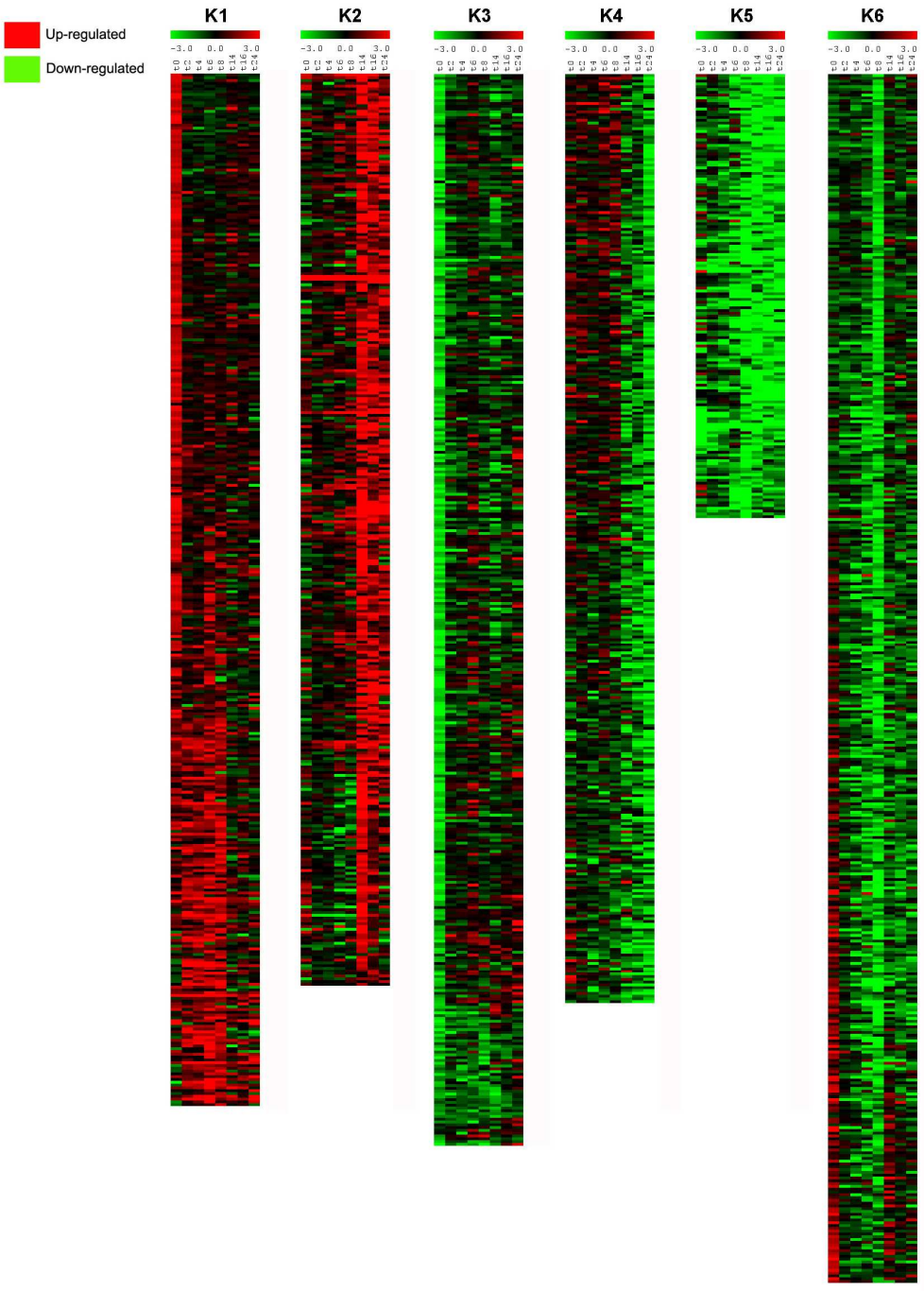

Figure 5.4 Heatmap showing levels of transcript abundance of clusters defined by K-means clustering method in the Δ*mst12* mutant when compared to Guy11 during the time course of appressorium development in those genes differentially regulated in at least 4-fold change. Levels of expression are represented as mod_lfc of transcript abundance. Note that down-regulation of gene expression appears in green and up-regulation of gene expression appears in red. (red= up-regulated in the *Δmst12* mutant; green= down-regulated in the *Δmst12* mutant).

To associate patterns of gene expression to putative biological functions and cellular processes, specific categories of gene product were selected for further analysis, including transcription factor encoding genes, signal peptide containing protein genes, transporters, known effectors, secondary metabolism enzymes, cysteine domain containing proteins (CFEM protein) and proteins of unknown function that were significantly differentially regulated. These gene sets were then analysed for each cluster (O'Connell *et al.,* 2012). The number of genes and their relative abundance corresponding to each putative pathogenicity-related gene function are summarized in Table 5.2.

a. Putative transcription factor-encoding genes

The relative abundance of putative transcription factor-encoding genes was more significant in cluster k3 than in the rest of the clusters. The gene expression pattern of cluster k3 shows strong down-regulation of gene expression especially at 0 h, as shown in Figure 5.4. Cluster k3 contains nine putative transcription factor-encoding genes including two fungal Zn(2)Cys(6) binuclear cluster domain containing proteins, the putative melanin regulator Pig1 (MGG_07215) a protein of unknown function MGG_03711, three proteins of unknown function (MGG_04933, MGG_13607 and MGG_13350), one helix-loop-helix domain containing protein (MGG_10575), two bZIP putative transcription factors (MGG_00587 and MGG_03288) and a fungal specific transcription factor (MGG_04571). The relative gene expression of these putative transcription factor genes is shown in Figure 5.5.

The relative abundance of putative transcription factor-encoding genes within cluster k6 was also high, containing a total of nine putative transcription factors. There

were four fungal Zn(2)Cys(6) binuclear cluster domain genes (MGG_08917, MGG_07534, MGG_09676, MGG_09276), two transcription factor encoding genes with no pfam associated domain (MGG_00342 and MGG_08536), one bZIP domain containing protein (MGG_07305), and the AclR regulatory protein (MGG_02129), which were down-regulated from 4 h to 24 h, within the cluster as shown in Figure 5.5.

Cluster k4 also contained a significant number of putative transcription factor encoding genes. Analysis of cluster k4 revealed 2 transcription factor-encoding genes containing fungal Zn(2)Cys(6) binuclear cluster domain (MGG_12339 and MGG_05659) down-regulated at 24 h (Fig. 5.5).

Analysis of cluster k1 revealed eight potential transcription factor-encoding genes that showed up-regulation in expression at 0 h (Fig. 5.5). In this cluster there were four proteins containing fungal Zn(2)Cys(6) binuclear cluster domains (MGG_10212, MGG_00320, MGG_08753, MGG_15023), one protein containing a bZIP domain (MGG_02006), a homologue of a transcriptional regulator of cellulase and xylanase genes in *Trichoderma reesei*, *ACEII* (MGG_08058) (Aro *et al.,* 2001) and *HOX7* (MGG_12865) (Kim *et al.,* 2009). Interestingly, two of these genes, *HOX7* (MGG_12865) and MGG_10212 were also differentially regulated in the Δ*pmk1* RNA-Seq experiments reported in Chapter 3 (Fig. 5.5). Analysis of cluster k2 revealed 6 putative transcription factor-encoding genes up-regulated at 14 h, 16 h and 24 h (Fig. 5.5). The transcription factors included in this cluster were three fungal Zn(2)Cys(6) binuclear cluster domain-containing proteins (MGG_05845, MGG_07386, MGG_07845), a basic leucine zipper domain containing protein (MGG_12560), an

aflatoxin regulatory protein (MGG_00417) and a protein of unknown function (MGG_01870). Cluster k5 did not include any transcription factor-encoding genes.

b. Putatively secreted protein-encoding genes

Genes that encoded products with a putative signal peptide were identified by SignalP analysis. These genes constituted the most abundant group of genes selected from each of the clusters. Clusters k4 and k5 showed the highest percentage of signal peptide-containing protein genes. The gene expression pattern of these two clusters showed strong down-regulation of expression at 14 h, 16 h and 24 h in the case of k4, and a strong down-regulation of expression during the entire time course in the case of k5. Therefore, this result suggests that the Δ*mst12* mutant might be impaired in producing certain secreted proteins, especially at later time points during appressorium formation.

Interestingly, it was found that cluster k4 contained a total of 13 chitin biosynthesis-related genes, compared to one chitin-related gene found in cluster k1 (agglutinin isolectin1 protein, MGG_15185), one found in cluster k3 (chitin binding protein MGG_07623), one found in cluster k5 (chitin binding protein MGG_00245), and two found in cluster k6 (chitin deacetylases MGG_08774 and MGG_01868). This result might indicate the impairment of the Δ*mst12* mutant in its ability to synthesize chitin-associated proteins at 14 h, 16 h and 24 h, as indicated by expression pattern of k4. Cluster k4 contained four chitin recognition proteins (PF00187) (MGG_06771, MGG_05351, MGG_13275 and MGG_05865), four polysaccharide deacetylases (PF01522) (MGG_09159, MGG_05023, MGG_12939 and MGG_14966), one chitosanase (PF07335) (MGG_07656) and four chitin-binding proteins (MGG_09717,

MGG_02142, MGG_12415 and MGG_05418). We conclude that cell-associated functions, such as chitin synthesis and re-modelling may be regulated via Mst12 during appressorium morphogenesis.

To degrade cellulose, lignin and hemicellulose and convert them into fermentable sugars, fungi produce a set of extracellular enzymes called glycoside hydrolases (Murphy *et al.,* 2011). In cluster k6 there were 10 putative glycoside hydrolases (MGG_10423, MGG_05599, MGG_00084, MGG_13622, MGG_09861, MGG_09733, MGG_00086, MGG_04732, MGG_1876, MGG_ 08938), whereas in cluster k4 there were only four (MGG_07631, MGG_01001, MGG_00374, MGG_09918), in cluster k3, five (MGG_08577, MGG_08577, MGG_06493, MGG_00592, MGG_17153), in cluster k2, four (MGG_07575, MGG_00296, MGG_06023, MGG_09988) and in cluster k1 only two (MGG_10431, MGG_02507). This is consistent with plant cell wall degrading ability, associated with plant tissue invasion being potentially regulated as a consequence of the action of Mst12.

Cutin is the first host barrier that the fungus has to breach in order to infect plants (Kolattukudy, 1985). Therefore, cutinases might play an important role especially when potentially co-regulated with similar temporal expression patterns. Putative cutinase encoding genes were found in cluster k6 (MGG_09100, MGG_10515, MGG_02393), cluster k5 (MGG_14095 and MGG_03440) and cluster k1 (MGG_12016). The expression pattern of genes in clusters k5 and k6 showed that genes were down-regulated during the entire time course.. Therefore, these results suggest that different cutinases may act downstream of Mst12, either regulated directly or indirectly, acting at

different time points during the entire course of appressorium development, and probably facilitating adherence to the surface or cuticle softening prior to penetration.

Interestingly, two proteins were identified in cluster k6, containing a fasciclin domain (PF02469), MGG_09372 and MGG_05483. In the *M. oryzae* genome there are in total 3 fasciclin domain containing proteins, two of them found in cluster k6 and the third one, Flp1 (MGG_02884), found in cluster k4. Flp1 is a beta ig –h3 fasciclin containing protein that in *M. oryzae* has been associated with conidial adhesion and sporulation. Null mutants in Flp1 were impaired in turgor generation and reduced in pathogenicity (Liu *et al.,* 2009). The authors proposed a possible role of appressorial attachment, consistent with the expression pattern observed here, although this has not yet been investigated.

Necrosis and ethylene-inducing proteins (MGG_08454, MGG_10532) were also found in cluster k1 and were, surprisingly, up-regulated in the Δ*mst12* mutant compared with the wild type.

c. Putative Transporter-encoding genes

Putative ABC transporters, sugar transporters and major facilitator superfamily-encoding genes were identified and found to be distributed within all the clusters, indicating complex co-ordination of expression. The multidrug and toxin extrusion (MATE) encoding genes (PF01554) were only found in cluster k1 (MGG_03123 and MGG_10534) and were up-regulated especially at 0 h. By contrast, the putative oligo-peptide transporter domain containing proteins (PF03169) (MGG_07228, MGG_10200, MGG_09354) were found in cluster k6 and strongly down-regulated at 8 h. Transporter-

encoding genes therefore show complex regulation, with both Mst12-dependent activation and repression observed during appressorium formation, consistent with their diverse, stage-specific roles.

d. Effectors

Known effector-encoding genes were identified by homology with published reports., *SLP1* (MGG_10097) (Mentlak *et al.,* 2012) was found in cluster k1 and up-regulated in the *Δmst12* mutant compared to Guy11, especially at 0 h. *BAS2* (MGG_09693) (Mosquera *et al.,* 2009) was present in cluster k4, and down-regulated in gene expression at 14h, 16h and 24 h. Moreover, *BAS3* (MGG_11610) and other two *BAS2* homologue-encoding genes (MGG_07749 and MGG_07969) (Mosquera *et al.,* 2009) were also found in cluster k5, indicating down-regulation of expression during the entire time course of appressorium development.

e. Secondary metabolism

In the case of secondary metabolism-related genes, analysis of the clusters indicated that cytochrome P450 (PF00067) domain containing proteins and multicopper oxidase (PF07732) domain containing proteins were distributed among all the clusters. A polyketide synthase/peptide synthetase (MGG_ 12447) and a lovastatin nonaketide synthase (MGG_ 05589) were both found in cluster k3, and up-regulated in expression in the *Δmst12* mutant, compared to Guy11, especially at 0 h. However, two other polyketide related proteins containing a beta-ketoacyl synthase, N-terminal domain (PF00109) and a beta-ketoacyl synthase, C-terminal domain (PF02801) (MGG_00806 and MGG_09236) were identified in cluster k4 and down-regulated in the *Δmst12* mutant at 14 h, 16 h and 24 h during the time course of appressorium development.

Secondary metabolism is therefore also stage-specific and clearly affected by the presence or absence of Mst12.

f. CFEM domain containing proteins

CFEM domain containing proteins are plasma membrane proteins of the G-protein coupled receptor family that are considered pathogenicity determinants for *M. oryzae* (Kulkarni and Dean, 2004). This analysis revealed CFEM domain-containing proteins in every cluster, with the exception of cluster k5.CFEM domain containing proteins therefore, show a complex regulation at various stages of development during appressorium formation that depends on the presence of Mst12.

Table 5.2 Table showing the total number of selected gene families in each cluster and their relative proportion (%) of the total.

Cluster	Transcription factors	Signal Peptide containing proteins	Transporters	Effectors	Secondary Metabolism	CFEM proteins	Proteins of unknown function	Uncharacterized genes	Total number of genes
K1	8	81	11	1	11	5	121	132	370
K2	6	51	22	0	12	1	100	135	327
K3	9	55	23	0	11	2	103	181	384
K4	2	98	20	1	13	4	98	97	333
K5	0	64	8	3	3	0	58	23	159
K6	9	90	36	0	11	5	122	160	433

Cluster	Transcription factors (%)	Signal Peptide containing proteins (%)	Transporters (%)	Effectors (%)	Secondary Metabolism (%)	CFEM proteins (%)	Proteins of unknown function (%)	Uncharacterized genes
K1	2.16	21.89	2.97	0.27	2.97	1.35	32.70	35.68
K2	1.83	15.60	6.73	0.00	3.67	0.31	30.58	41.28
K3	2.34	14.32	5.99	0.00	2.86	0.52	26.82	47.14
K4	0.60	29.43	6.01	0.30	3.90	1.20	29.43	29.13
K5	0.00	40.25	5.03	1.89	1.89	0.00	36.48	14.47
K6	2.08	20.79	8.31	0.00	2.54	1.15	28.18	36.95

*Grey colour indicates the most significant cluster for a selected gene family.

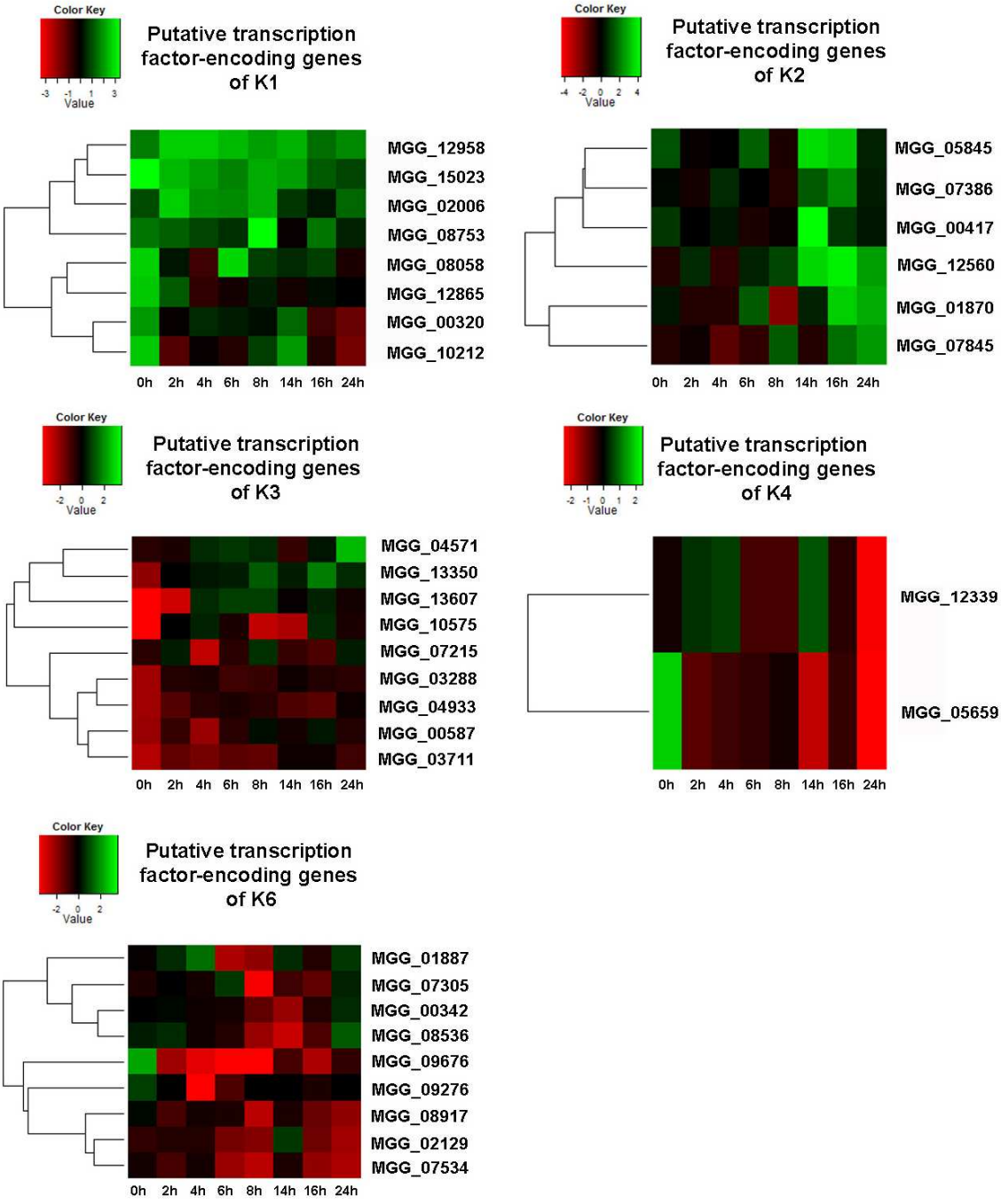

Figure 5.5 Heatmap showing levels of transcript abundance of putative transcription factor-encoding genes from each K-means cluster in the Δ*mst12* mutant when compared with Guy11 during a time course of appressorium development. Differentially expressed genes showed at least a 4-fold change in expression. Levels of expression are represented as mod_lfc of transcript abundance. (red= down-regulated in the *Δmst12* mutant; green= up-regulated in the *Δmst12* mutant).

5.3.3 Investigating the hierarchy of gene regulation by the Pmk1 MAP kinase pathway in *M. oryzae*

As reported previously in this chapter, Mst12 is a downstream transcription factor of the Pmk1 MAP kinase which regulates development of penetration pegs and invasive growth by *M. oryzae* (Park *et al.,* 2002). Therefore, to investigate hierarchical gene regulation within the Pmk1 MAPK pathway, putative Pmk1-regulated genes were directly compared to genes likely to be regulated by Mst12. As shown in Figure 5.6 panel A, Venn diagram analysis defined three sets of genes: genes likely to be regulated by Pmk1 (independently of Mst12), genes likely to be regulated by both Pmk1 and Mst12, and genes likely to be regulated by Mst12 (but independent of Pmk1). In this way, we set out to understand global regulation by the Pmk1 MAP kinase pathway in *M. oryzae* in a hierarchical manner.

The number of genes that were differentially expressed in the Δ*pmk1* and Δ*mst12* mutants compared to Guy11 was determined, and shown in Table 5.3. The total number of genes that were either down-regulated or up-regulated in the Δ*pmk1* mutant was 8085 and 4013, respectively. Both gene sets were combined and represented a total of 5474 genes (Table 5.3). The number was smaller than the total as it represents gene expression across the whole time course and some of the same genes are up-regulated and down-regulated at different stages of development, accounting for the redundancy. The total number of genes down-regulated and up-regulated in the Δ*mst12* mutant was 1949 and 1204, respectively. In the same way, both gene sets were combined and represented a total of 1962 genes (Table 5.3). Venn diagram analysis showed 3785 genes that are likely to be regulated by Pmk1, 1690 genes that are likely

Table 5.3 Table showing the total number of differentially regulated genes in the Δ*pmk1* and Δ*mst12* mutants compared to Guy11[17].

Time point	Δ*pmk1*		Δ*mst12*	
	Down	**Up**	**Down**	**Up**
0 h	1498	1452	368	290
2 h	77	103	94	72
4 h	224	154	170	68
6 h	579	281	214	41
8 h	1085	389	457	128
14 h	1571	534	297	281
16 h	1451	501	256	151
24 h	1599	619	93	72
Total	8085	4013	1949	1204
Bulked in at least 1 time point	5475		1962	

[17] The table indicates the number of genes down-regulated (mod_lfc<-2) and up-regulated (mod_lfc>2) in both Δ*pmk1* and Δ*mst12* mutants compared to Guy11. The Table also shows the total number of genes differentially regulated in at least one time point during the time course of appressorium development. The last row indicates the total number of genes combined in at least 1 time point.

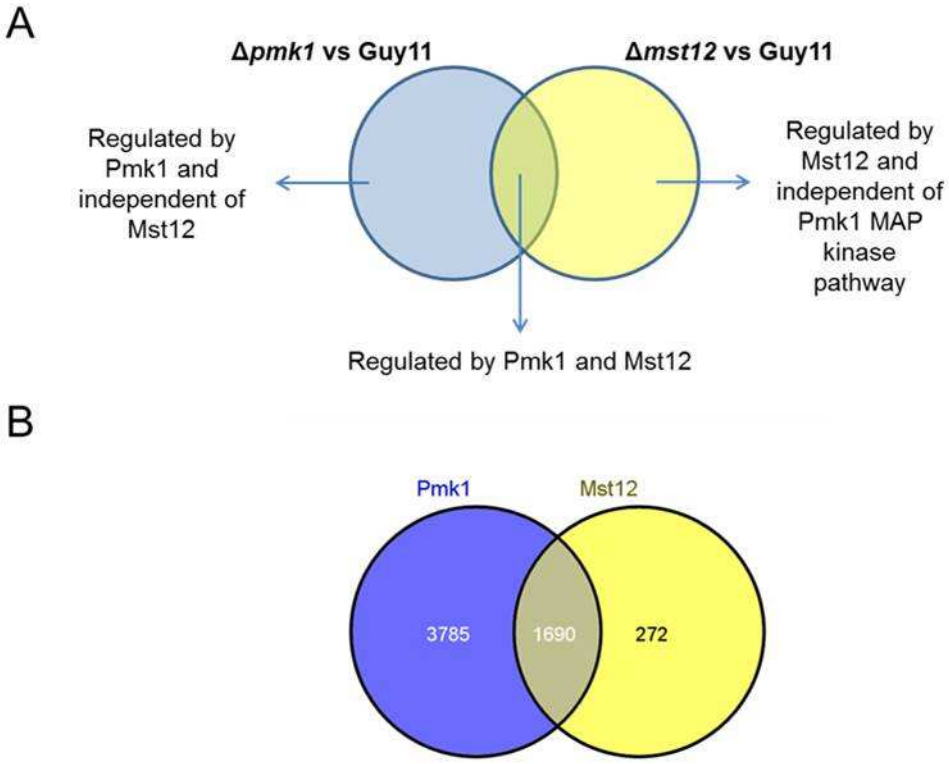

Figure 5.6 Investigating hierarchical gene regulation by the Pmk1 MAP kinase pathway in *M. oryzae.* A) Scheme illustrating the strategy followed for this analysis. The result shows 3 gene sets: genes likely to be regulated by Pmk1, genes likely to be regulated by both Pmk1 and Mst12 and genes likely to be regulated by Mst12. **B)** Venn diagram illustrating the overlapping number of genes resulting from the genes differentially regulated in the Δ*pmk1* mutant compared to Guy11 at least 4x fold (padj<0.01, mod_lfc>2 or mod_lfc<-2) were compared with genes differentially regulated in the Δ*mst12* mutant compared to Guy11 (padj<0.011, mod_lfc>2 or mod_lfc<-2).

to be regulated by both Pmk1 and Mst12, and 272 genes that are likely to regulated independently by Mst12. The significant overlap is consistent with Mst12 acting downstream of Pmk1 and the reported interaction between them (Park *et al.,* 2002).

5.3.3.1 Analysis of genes likely to be regulated by the Pmk1 MAP kinase

The analysis revealed that six autophagy-related genes, *ATG7* (MGG_07297), *ATG28* (MGG_08061), the vacuole flux protein *ATG22* (PF11700) (MGG_05505), *ATG9* (MGG_09559), *ATG8* (MGG_01062), and an autophagy-related protein with a 2-CAD motif (PF13329) (MGG_16734) were Pmk1-regulated. Expression of these genes was analysed and a heatmap was generated of the Δ*pmk1* mutant compared to Guy11 (Fig. 5.7, panel A). Genes expressed in the wild type but down-regulated in the Δ*pmk1* mutant are shown in red, and those up-regulated in the Δ*pmk1* mutant are shown in green. The heatmap showed that the gene expression of the vacuole flux protein *ATG22* (PF11700) (MGG_05505) was highly down-regulated at 24 h, while the other 5 autophagy-encoding genes down-regulated at 8 h, 14 h and 24 h in the Δ*pmk1* mutant compared to Guy11. This is consistent with reports that autophagy is always associated with appressorium morphogenesis in *M. oryzae* and is essential for plant infection (Veneault-Fourrey *et al.,* 2006).

A number of putative signalling protein-encoding genes were also found, including eight Ras family domain containing-proteins (PF00071) (MGG_06962, MGG_08144, MGG_04862, MGG_02457, MGG_07610, MGG_01179, MGG_01724, MGG_03901), two RasGEF N-terminal motif containing-proteins (PF00618), MGG_00199 and *LTE1* (MGG_02419), one rho-GTPase-activating

protein (MGG_09531), two RhoGEF domain (PF00621) (MGG_09954 and MGG_12644), a RHO protein GDP dissociation inhibitor (PF02115) (MGG_01689), a rho guanine nucleotide exchange factor *SCD1* (MGG_09697) and one Fes/CIP4, and EFC/F-BAR homology domain (PF00611) (MGG_03048). The expression of these was analysed and a heatmap was constructed (Fig. 5.7, panel B). A first cluster was observed which showed dramatic down-regulation of gene expression in the Δ*pmk1* mutant compared to Guy11, especially at 0 h. A second cluster which included Ras family domain containing-proteins (PF00071) (MGG_03901 and MGG_08144), RasGEF N-terminal motif (PF00618) (MGG_00199, MGG_06962, MGG_01724), the rho guanine nucleotide exchange factor *SCD1* (MGG_09697), *LTE1* (MGG_02419), RhoGEF domain (PF00621) (MGG_12644) showed down-regulation of expression in the Δ*pmk1* mutant compared to Guy11 at late time points.

The analysis also revealed the presence of several genes involved in DNA repair and DNA replication as part of this gene set. Amongst these, there were three GINS complex proteins (PF05916) (MGG_04434, MGG_01917, MGG_01611) required for establishment of replication forks (Kamada, 2012), the DNA damage checkpoint kinase *CDS1* (MGG_04790), *DUN1* (MGG_01596) a FHA-RING ubiquitin ligase *DMA1* (MGG_05257), DNA repair genes, *PSO2* (MGG_11590), *RAD14* (MGG_06208), *RAD16* (MGG_07014), *RAD26* (MGG_17795), *RAD5* (MGG_11047), DNA excision repair protein *RAD2* (MGG_00155), DNA repair and recombination protein *RAD54* (MGG_03549), pre-mRNA-splicing factor *SYF1* (MGG_07087), and a DNA damage response protein (MGG_05969). Gene expression in the Δ*pmk1* mutant compared to Guy11 showed that DNA damage checkpoint kinases *CDS1* (MGG_04790), *DUN1* (MGG_01596) and the FHA-RING ubiquitin ligase *DMA1*

(MGG_05257) and on GINS domain containing protein (MGG_01611) were highly down-regulated at 8 h, 14 h and 16 h. *RAD16* (MGG_07014), *RAD14* (MGG_06208), *PSO2* (MGG_11590), *RAD54* (MGG_03549) were down-regulated in the Δ*pmk1* mutant compared to Guy11 at 0 h (Fig. 5.8, panel A).

Other genes related to cell cycle control were found in this gene set, such as a WD repeat-containing protein-encoding gene *SRW1* (MGG_00682) which is involved in activating the APC/C (Anaphase Promoting complex/ cyclosome) (Blanco *et al.,* 2000), three cyclin domain containing protein-encoding genes (PF08613) (MGG_04929, MGG_15011, MGG_13439), the G2/mitotic-specific cyclin-B *CYC2* (MGG_07065), *CKS1* Cyclin-dependent kinase regulatory subunit (PF01111) (MGG_00682), two spindle pole body (SPB) components (MGG_07129 and MGG_17247), one spindle poison sensitivity protein-encoding gene (SPS) (MGG_03480), *SEP3* (MGG_01521), three cell division control protein-encoding genes (CDC) (MGG_01614, MGG_00371, MGG_01549), *CDC14* (MGG_00757), a cell-cycle control medial ring component (CDCMR) (PF12754) (MGG_036163), a Scd6-like Sm-domain containing protein (PF12701) (MGG_02405), *BUB2* (MGG_04676) and a HORMA domain containing protein (PF02301) (MGG_01694). The expression of these genes was analysed and a heatmap was generated for the cyclin domain-containing protein genes (Fig. 5.8, panel B). The heatmap revealed that only MGG_15011 showed strong down-regulation in Δ*pmk1* compared to Guy11 at 0 h. In the second heatmap in which the rest of cell cycle related proteins were represented, it was possible to observe two separate clusters (Fig 5.8). The first cluster showed strong up-regulation of gene expression at 0h. Scd6-like Sm domain (PF12701) (MGG_02405), spindle pole body component protein (MGG_07129),

HORMA domain containing protein (PF02301) (MGG_01694) and cell-cycle control medial ring component (PF12754) (MGG_036163) were part of this cluster.

Gene functions associated with polarization and cytoskeleton, such as Fes/CIP4 and EFC/F-BAR homology domain containing protein encoding gene (PF00611) (MGG_11899), two BAR domain-containing protein-encoding gene (PF03114) (MGG_05534 and MGG_05528), the *ABP1* cofilin/tropomyosin-type actin-binding protein encoding gene (PF00241) (MGG_06358), four dynamin family domain containing protein encoding gene (PF00350) (MGG_05937, MGG_05209, MGG_10656, MGG_10640), a polarized growth protein *BOI2* (MGG_07310), a cortical patch protein-encoding gene (MGG_10322), two actin cytoskeleton organization protein encoding genes *AAP1* (MGG_07714 and MGG_15175), an actin cytoskeleton protein-encoding gene with a RNA recognition motif (PF00076) (MGG_00444), an actin related protein 2/3 complex subunit encoding gene (PF00400) (MGG_04352) and an actin domain containing protein-encoding gene (PF00022) (MGG_01801) were also observed. The expression of these genes was analysed and a heatmap generated (Fig. 5.8, panel C). The heatmap revealed down-regulation of gene expression of the cluster which included the BAR domain containing proteins (PF03114) (MGG_05534 and MGG_05528), one dynamin domain containing protein (MGG_10640), the polarized growth protein *BOI2* (MGG_07310) and an actin filament organization protein *APP1* (MGG_15175) in the Δ*pmk1* mutant compared to Guy11 at 8 h, 14 h, 16 h and 24 h. These results are consistent with the major cytoskeletal rearrangements that accompany appressorium development in contrast to hyphal elongation in the Pmk1 mutant. BAR domain proteins, in particular, have been implicated in appressorium

cytoskeleton re-modelling and re-polarisation at the appressorium pore (Dagdas *et al.,* 2012).

The analysis also revealed proteins related to peroxisome biogenesis and activity, such as a peroxisomal membrane protein *PAS20* (MGG_00157), a peroxisomal biogenesis factor 3 (MGG_06424), a peroxin 14/17 peroxisomal membrane anchor protein (Pex14p) (PF04695) (MGG_01081), a further peroxisomal membrane anchor protein (Pex14p) (PF04695) (MGG_01028), a Pex2 / Pex12 amino terminal region containing protein (PF04757) (MGG_01771) and a peroxiredoxin type-2 protein (MGG_02710). The expression of these genes was analysed and a heatmap generated (Fig. 5.9, panel A). The heatmap revealed that all genes were down-regulated in the Δ*pmk1* mutant compared to Guy11 from 0 h to 24 h with the exception of MGG_02710, peroxiredoxin type-2, which was highly up-regulated in Δ*pmk1* compared to Guy11 at 0 h. Peroxisome function is associated with appressorium maturation and turgor generation in *M. oryzae* (Bhambra *et al.,* 2006).

Moreover there were also 10 fatty acid beta-oxidation and lipid metabolism-related protein genes: four fatty acid hydroxylase superfamily proteins (PF04116) (MGG_17103, MGG_06133, MGG_08832, MGG_06250), three lipases (class 3) (PF01764) (MGG_04555, MGG_12828, MGG_05340), one alpha/beta hydrolase (PF12695) (MGG_06610), one alpha/beta hydrolase (PF07859) (MGG_15936 and one lipase3-N-terminal region containing protein (PF03893) (MGG_07016). The expression of these genes was analysed and a heatmap is shown in Figure 5.9, panel B. The heatmap revealed that the lipase (class 3) (MGG_05340), the alpha/beta hydrolase (PF07859) (MGG_15936) and the lipase 3 (PF03893) (MGG_07016) formed an up-regulated cluster, whereas the 4 fatty acid hydroxylases

(PF04116) formed a separate cluster that showed down-regulation of gene expression in the Δ*pmk1* mutant compared to Guy11 at 0 h. A third cluster was also observed containing an alpha/beta hydrolase (PF12695) (MGG_06610) and two lipases (class 3) (PF01764) (MGG_04555 and MGG_12828) that were especially down-regulated in the Δ*pmk1* mutant compared to Guy11 at 8 h, 14 h and 16 h during the appressorium formation time course. These results suggest a complex pattern of expression, in which some lipases are associated with undifferentiated hyphal extension in the Δ*pmk1* mutant, while other specific lipases and beta-oxidation associated genes are specifically associated with appressorium morphogenesis as previously reported (Wang *et al.,* 2007).

Interestingly, we also found proteins involved in chromatin remodelling such as three chromatin organisation modifier (CHROMO) domain containing proteins (PF00385) (MGG_16490, MGG_17586, MGG_01080), a chromosome segregation protein Csm1/Pcs1 (PF12539) (MGG_01838), a chromatin remodelling complex Rsc7/Swp82 subunit (PF08624) (MGG_11643) and a chromatin associated protein *KTI12* (PF08433) (MGG_12920), which showed differential expression (Fig. 5.9, panel C). The heatmap revealed two separated clusters. One included the chromatin remodelling complex Rsc7/Swp82 subunit (PF08624) (MGG_11643) and two CHROMO-domain containing protein (PF00385) (MGG_16490 and MGG_17586) which were found to be highly down-regulated in the Δ*pmk1* mutant compared to Guy11 at 14 h, 16 h and 24 h. The second cluster showed strong up-regulation in Δ*pmk1* mutant compared to Guy11 at 0 h and contained a CHROMO-domain containing protein (PF00385) (MGG_01080), a chromosome segregation protein Csm1/Pcs1 (PF12539) (MGG_01838) and a chromatin associated protein *KTI12* (PF08433) (MGG_12920).

Of particular interest, transcriptomic analysis of the Pmk1 mutant revealed 96 putative transcription factor-encoding genes whose gene expression was analysed in detail, as shown in Fig. 5.10. Analysis of these putative transcription factor-encoding genes is reported in Chapter 3, but here a more stringent cut-off was used (4-fold regulation) to restrict the analysis to 96 highly differentially regulated genes. The data were also integrated with analysis of the Δ*mst12* mutant, in order to determine the hierarchy of transcriptional control in appressoria by the Pmk1 MAP kinase pathway (Fig. 5.10). The heatmap revealed that 5 putative transcription factor genes were highly down-regulated in the Δ*pmk1* mutant compared to Guy11, including *ALCR* (MGG_02129), MGG_07368, MGG_09273, MGG_07218 and MGG_07423. Both *ALCR* (MGG_02129) and MGG_07218 belonged to cluster 5 identified in Chapter 2, which suggests that these two transcription factors are dependent on Pmk1 MAPK regulation but are regulated independently of Mst12.

Within the 96 predicted transcription factors, it was possible to identify two homeobox domain-containing protein genes (PF00046) *HOX1* (MGG_ 04853) and *HOX2* (MGG_00184), the start control protein homologue *CDC10* from *S. pombe* or *SWI6* from *S. cerevisiae* (MGG_09869) which is required for regulation of gene expression at G1 to S phase during cell cycle in *S. pombe* (McInerny *et al.,* 1995), the transcription factor *IDI4* (MGG_01990) which has been described in *Podospora anserina* as a negative regulator of autophagy (Dementhon *et al.,* 2004), the *HAC1* transcription factor (MGG_09010), which is involved in the unfolded protein response in *S. cerevisiae* (Ogawa and Mori, 2004), the *MoAP1* (MGG_12814), *OEFC* (MGG_10422), *NIT4* (MGG_01518), the major nitrogen regulatory gene *NUT1* (MGG_02755) (Froeliger and Carpenter, 1996), the SRF-type transcription factors *MCM1* (02773) (Zhou *et al.,* 2011), *MIG1* (MGG_01204) (Mehrabi *et al.,* 2008), the

cell pattern formation-associated protein *STUA* (MGG_00692), a positive regulator of acetate induction *ACU15* (MGG_04108), the *XLNR* gene (MGG_02880), which regulates xylanases and endoglucanases in *A. niger* (Van Peij *et al.,* 1998) and the *A. fumigatus* homologue *HAPX* (MGG_05959) which is involved in iron starvation and virulence (Schrettl *et al.,* 2010). All these transcription factors have not been previously described to be downstream of Pmk1, but according to this analysis they all showed a Pmk1-dependent expression suggesting a possible regulation independent of Mst12, which also required Mst12.

Our analysis also revealed the presence of 14 heterokaryon incompatibility proteins (HET) (PF06985) (MGG_00082, MGG_00569, MGG_14884, MGG_10558, MGG_09224, MGG_15132, MGG_03082, MGG_08449, MGG_00820, MGG_02976, MGG_04176, MGG_06789, MGG_09096, MGG_16743, MGG_09383, MGG_01326) and 3 heterokaryon incompatibility Het-C proteins (PF07217), the *HETC* (MGG_03919) and two NIMA-interacting proteins *TINC* (MGG_09383 and MGG_01326). The expression of these genes was analysed and a heatmap generated (Fig. 5.14, panel A). The heatmap showed that most of the het proteins were up-regulated in the Δ*pmk1* mutant compared to Guy11, except 4 of them which formed a separate cluster and showed strong down-regulation in the mutant, coincident with the maturation stage of appressorium development. Genes associated with heterokaryon incompatibility, which involves cell fusion and control of cell death, appear therefore predominantly to be expressed within the un-differentiated germ tubes and hyphae of Δ*pmk1* mutants, but repressed during appressorium morphogenesis. A small sub-set, however, might be associated with the programmed cell death that accompanies appressorium maturation (Dagdas *et al.,* 2012; Veneault-Fourrey *et al.,* 2006).

5.3.3.2 Analysis of genes likely to be regulated by both the Pmk1 MAPK and Mst12 transcription factor

A total of 1690 genes appear to be differentially regulated in both the *Δpmk1* and *Δmst12* mutant with at least 4-fold differences observed at a given time-point. Analysis of this gene set revealed the presence of eight protein kinase domain-containing encoding genes of unknown function (PF00069) (MGG_10181, MGG_01393, MGG_08709, MGG_05086, MGG_09000, MGG_12513, MGG_08549, MGG_11636). Their expression was analysed and a heatmap generated for both the Δ*pmk1* mutant (Fig. 5.11, panel A) and for the Δ*mst12* mutant, compared to Guy11 (Fig. 5.11, panel B). The heatmaps showed that protein kinases MGG_08709 and MGG_12513 were both strongly down-regulated at 14 h, 16 h and 24 h in the Δ*pmk1* mutant compared to Guy11. Only MGG_12513, however, also showed significant down-regulation at 14 h in the Δ*mst12* mutant, compared to Guy11. Moreover, MGG_09000 and MGG_08549 were highly down-regulated at 14 h and 16 h in the Δ*mst12* mutant compared with Guy11. These two protein kinase domain-containing protein encoding genes were also less dramatically down-regulated in Δ*pmk1* compared to Guy11 at 14 h and 16 h.

The analysis revealed the presence of 21 chitin related proteins, including two chitin binding domain-containing protein (PF03067) (MGG_00245 and MGG_07676), four chitin recognition proteins (PF00187) (MGG_06771, MGG_05351, MGG_13275, MGG_05865), a chitin synthase (PF03142) (MGG_06064), two chitin synthesis regulators (PF12273) (MGG_01575 and MGG_03609), four chitin deacetylases (MGG_01868, MGG_05023, MGG_08774, MGG_09159) and seven chitin-binding proteins (MGG_09717, MGG_02142, MGG_05418, MGG_07623, MGG_12415, MGG_14966, MGG_15185). The expression of these chitin related protein-encoding

genes was analysed and a heatmap generated for both the Δ*pmk1* (Fig. 5.12, panel A) and Δ*mst12* mutant (Fig. 5.12, panel B). The heatmap for the Δ*pmk1* mutant revealed that both chitin binding domain-containing proteins (PF03067) (MGG_00245 and MGG_07676), a chitin synthesis regulator (MGG_03609) and 2 chitin deacetylases proteins (MGG_08774 and MGG_05023) were all highly down-regulated in the Δ*pmk1* mutant compared to Guy11 between 6 h and 24 h. In the case of the Δ*mst12* mutant all the chitin-related proteins were highly down-regulated at 14 h, 16 h and 24 h. This is consistent with chitin re-modelling during appressorium formation being a Pmk1-dependent process that also requires Mst12.

Hierarchical analysis revealed 30 transcription factor-encoding genes that were differentially regulated in both the *Δpmk1* and the *Δmst12* mutant, including four bZIP transcription factors (PF00170) (MGG_07305, MGG_02006, MGG_03288, MGG_00587), eight fungal Zn(2)-Cys(6) binuclear cluster domain containing proteins (PF00172) (MGG_15023, MGG_07845, MGG_07386, MGG_05845, MGG_08753, MGG_00320, MGG_08917, MGG_03711), one aflatoxin regulatory protein (PF08493) (MGG_00417), one helix-loop-helix DNA-binding domain-containing protein (PF00010) (MGG_10575), one basic region leucine zipper (PF07716) (MGG_12560), one fungal specific transcription factor domain (PF04082) (MGG_04571), six proteins of unknown function (MGG_04933, MGG_08536, MGG_00342, MGG_01870, MGG_13350, MGG_13607), and the *ACEII* transcription factor encoding gene (MGG_08058). Seven genes from this group were previously described in Chapter 2 as putatively regulated by Pmk1; MGG_01887, MGG_07534, MGG_09276, MGG_09676, MGG_10212, the melanin regulator *PIG1* (MGG_07215) and the homeobox transcription factor gene *HOX7* (MGG_12865). Expression of

these transcription factor- encoding genes was analysed and a heatmap constructed for both Δ*pmk1* (Fig. 5.13, panel A) and the Δ*mst12* mutant (Fig. 5.13, panel B).

The analysis revealed the presence of 7 heterokaryon incompatibility proteins (HET) (PF06985) out of 45 predicted such functions within the genome (MGG_05985, MGG_08495, MGG_15067, MGG_15242, MGG_05881, MGG_03415, MGG_07426). The expression of these genes was analysed and a heatmap generated for the Δ*pmk1* (Fig. 5.14, panel B) and the Δ*mst12* mutant (Fig. 5.14, panel C). The heatmap for Δ*pmk1* mutant showed that 3 of the het proteins (MGG_07426, MGG_15242 and MGG_15067) were highly down-regulated at 8 h, 14 h, 16 h, and 24 h, and the rest were up-regulated. However, in the case of the Δ*mst12* mutant compared to Guy11, only one het protein encoding gene, MGG_07426, was highly up-regulated at 14 h, 16 h and 24 h.

Moreover, the analysis also identified the homologues of the biotrophy associated protein *BAS2* (MGG_07749 and MGG_07969) and *BAS3* (MGG_11610), five cutinase domain-containing proteins (PF01083) (MGG_10515, MGG_14095, *CUT2* (MGG_09100), MGG_02393 and MGG_03440), a cutinase g-box binding protein *CGBP1* (MGG_00501), two dynamin domain-containing proteins (PF00350) (MGG_08732 and MGG_02049), nine NmrA-like domain containing proteins (PF05368) (MGG_12714, MGG_17002, MGG_09836, MGG_02095, MGG_05101, MGG_05022, MGG_10614, MGG_00156, MGG_09705), the putative *FAR1* homologue (MGG_00134) and the DNA repair protein *RAD7* (MGG_07015). In addition, three fasciclin domain containing proteins (PF02469) (MGG_09372, MGG_02884, MGG_05483) and two fatty acid desaturases (PF00487) (MGG_08474 and MGG_00392) were also identified.

Moreover, a number of genes encoding proteins related with peroxisomal function were identified, including two peroxisomal biogenesis factor 11 (PEX11) (MGG_08896 and MGG_00648) and the Pex2 / Pex12 amino terminal region (PF04757) (MGG_00145), peroxin 20 (MGG_00638), peroxin 26 (MGG_05171), peroxin 8 (MGG_05328), two mitochondrial carrier proteins (PF00153) (MGG_04662 and MGG_03247) and a peroxisomal hydratase-dehydrogenase-epimerase (MGG_06148). The expression of these was analysed and a heatmap was constructed for both the Δ*pmk1* mutant (Fig. 5.15, panel B) and the Δ*mst12* mutant compared to Guy11 (Fig. 5.15, panel C). The heatmaps in both cases indicated down-regulation of all the proteins at 0 h, except for a peroxisomal biogenesis factor 11 (PEX11) (MGG_00648), which clustered completely separated from the rest and showed down-regulation at 14 h, 16 h and 24 h.

5.3.3.3 Analysis of genes likely to be regulated by Mst12 independent of Pmk1

The analysis of genes likely to be regulated by Mst12 independently of Pmk1 showed that no big family of genes was represented in this gene set. However, several interesting genes were present. Some of these genes were the protein kinase *OSM1* (MGG_01822), the *STE20* (MGG_08746) protein kinase, two Ras-family domain containing proteins (PF00071) (MGG_15838 and MGG_02727), the LysM domain (PF01476) (MGG_10097) and autophagy-related protein 27 (PF09451) (MGG_02396). Strikingly, very few Mst12-regulated genes were identified that were independent of Pmk1 regulation, consistent with Mst12 acting downstream of the Pmk1 MAP kinase pathway.

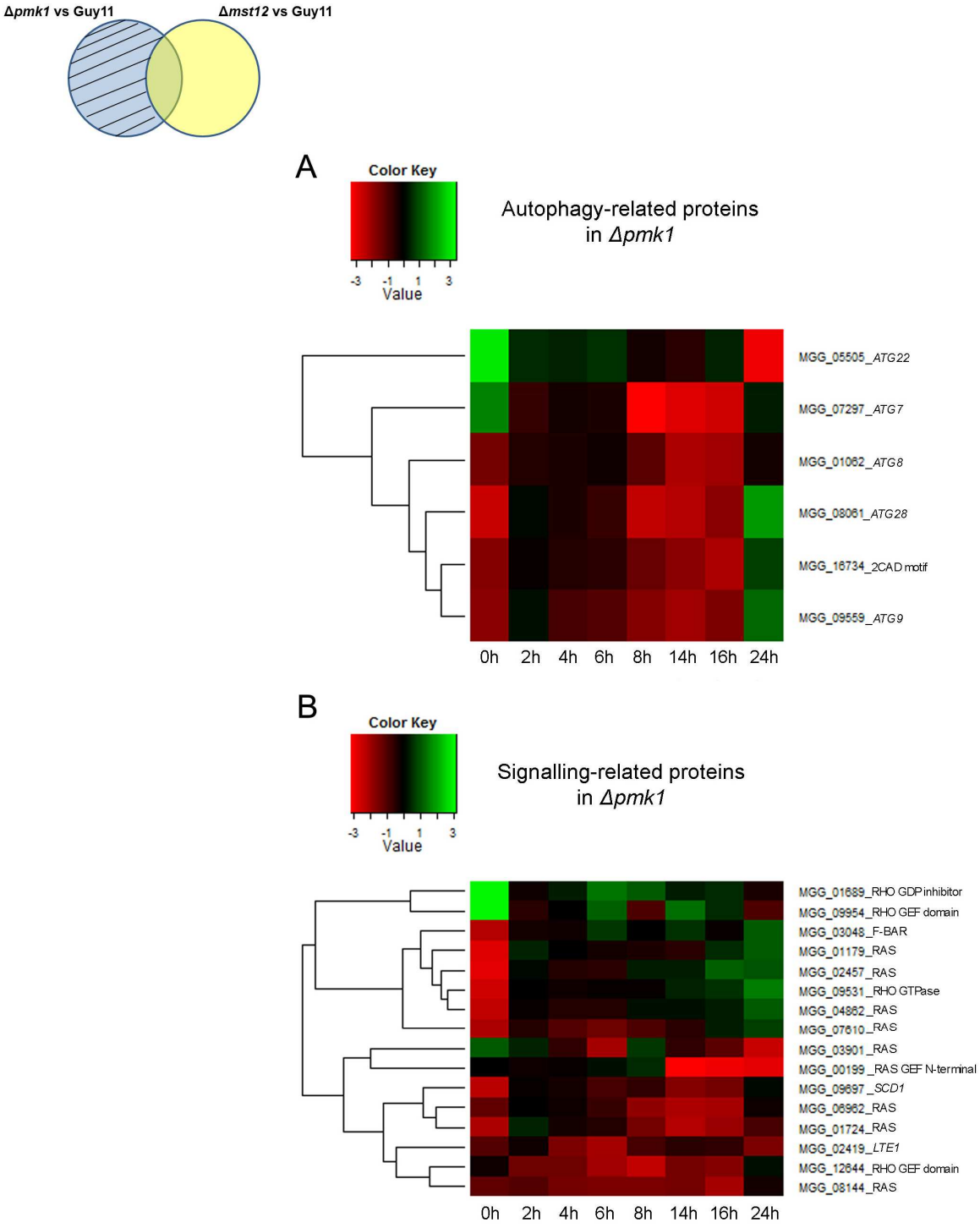

Figure 5.7 Heatmaps showing levels of transcript abundance of Pmk1-dependent genes. A) Heatmap in the Δ*pmk1* mutant compared to Guy11 for autophagy related proteins. **B)** Heatmap in the *Δpmk1* mutant compared to Guy11 for signalling related proteins. (red= down-regulated in the *Δpmk1* mutant; green= up-regulated in the *Δpmk1* mutant).

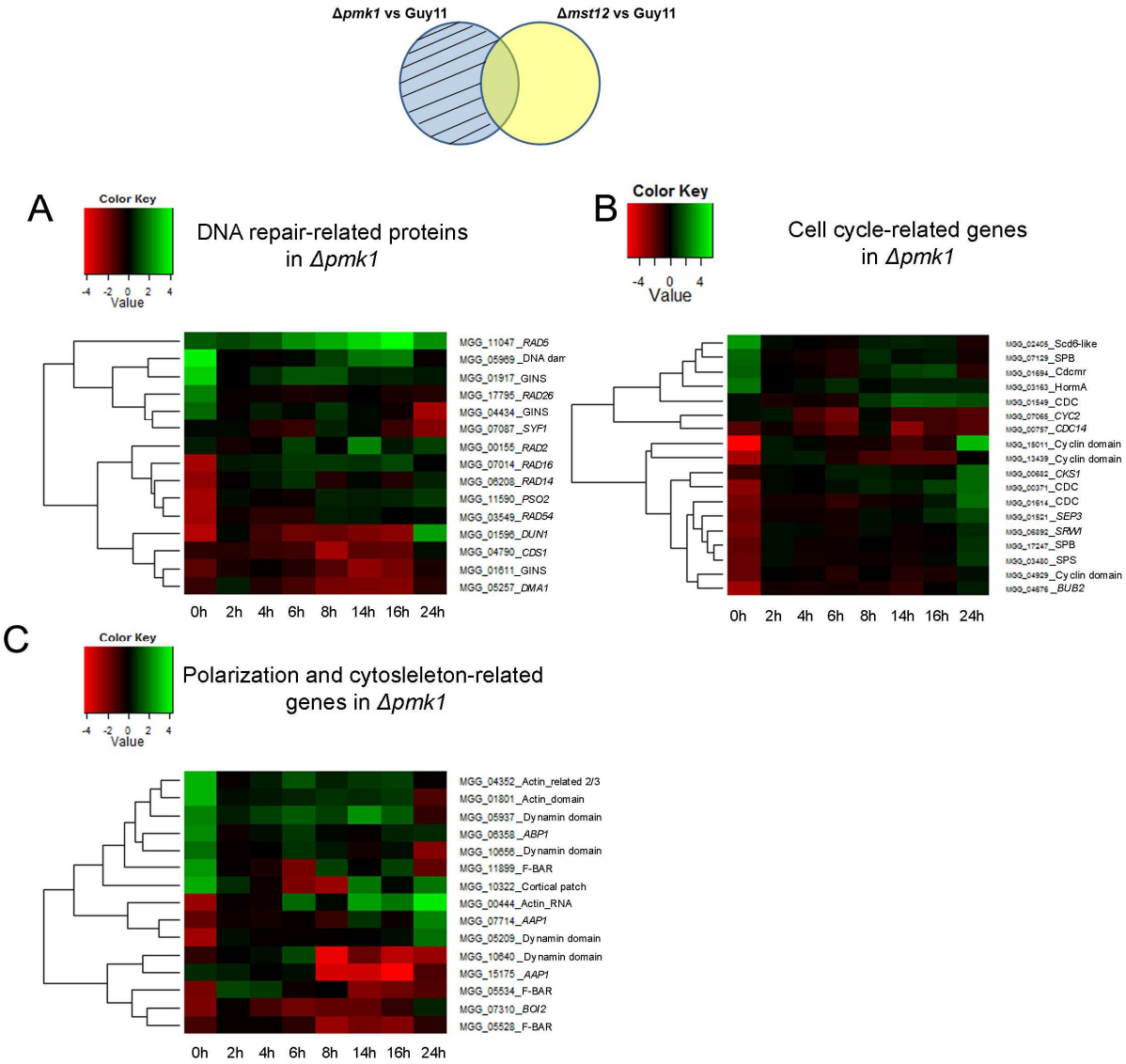

Figure 5.8 Heatmaps showing levels of transcript abundance of Pmk1-dependent genes A) Heatmap in the *Δpmk1* mutant compared to Guy11 for DNA repair related proteins. **B)** Heatmap in the Δ*pmk1* mutant compared to Guy11 for cell cycle related proteins. **C)** Heatmap in the Δ*pmk1* mutant compared to Guy11 for proteins related with polarization and cytoskeleton. (red= down-regulated in the *Δpmk1* mutant; green= up-regulated in the *Δpmk1* mutant).

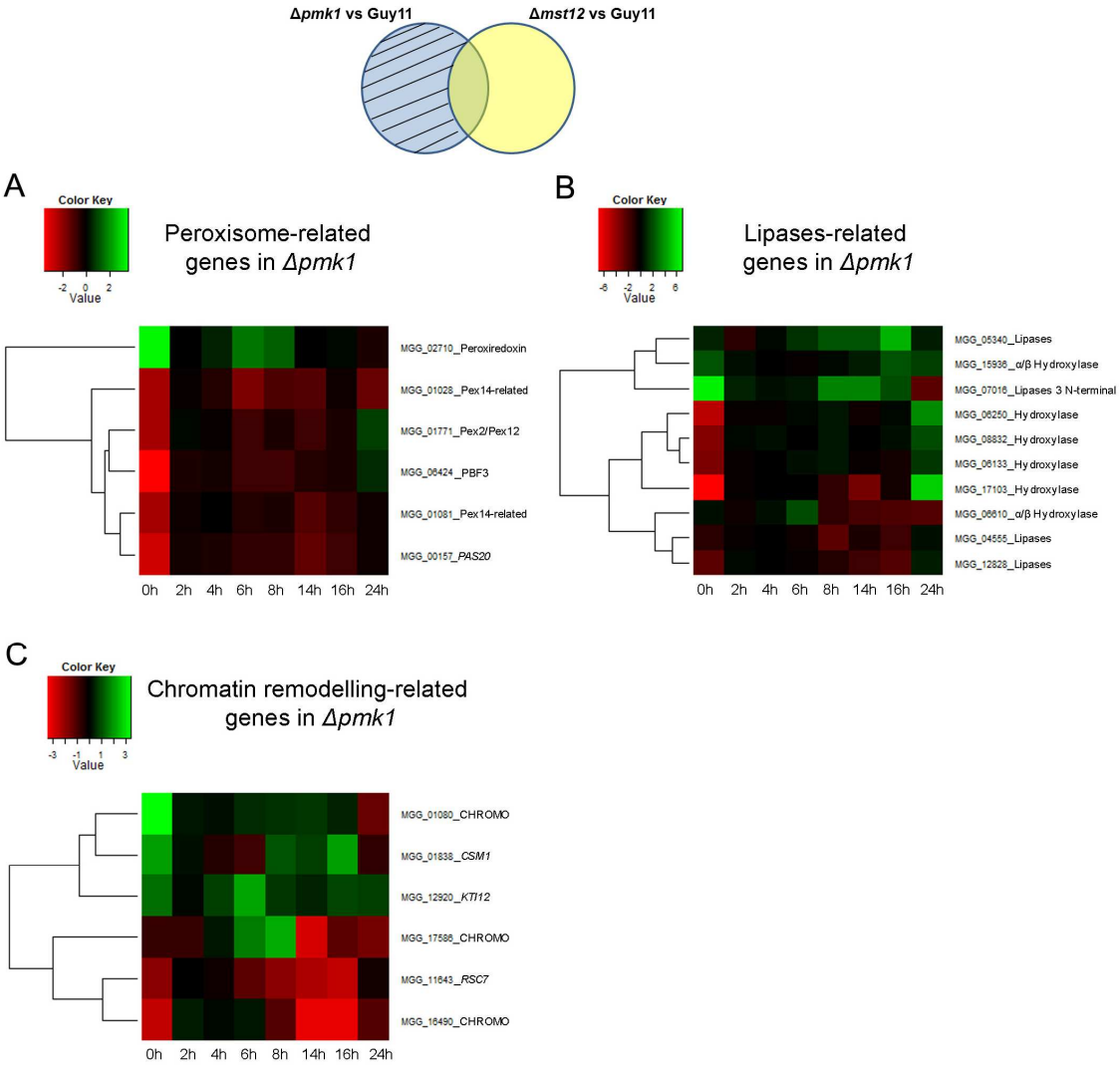

Figure 5.9 Heatmaps showing levels of transcript abundance of genes found in Pmk1-dependent and Mst12 independent gene set. A) Heatmap of the Δ*pmk1* mutant compared to Guy11 for peroxisome-related proteins. **B)** Heatmap of the Δ*pmk1* mutant compared to Guy11 for lipases-related proteins. **C)** Heatmap of the Δ*pmk1* mutant compared to Guy11 for gene set involved in chromatin remodelling. (red= down-regulated in the *Δpmk1* mutant; green= up-regulated in the *Δpmk1* mutant).

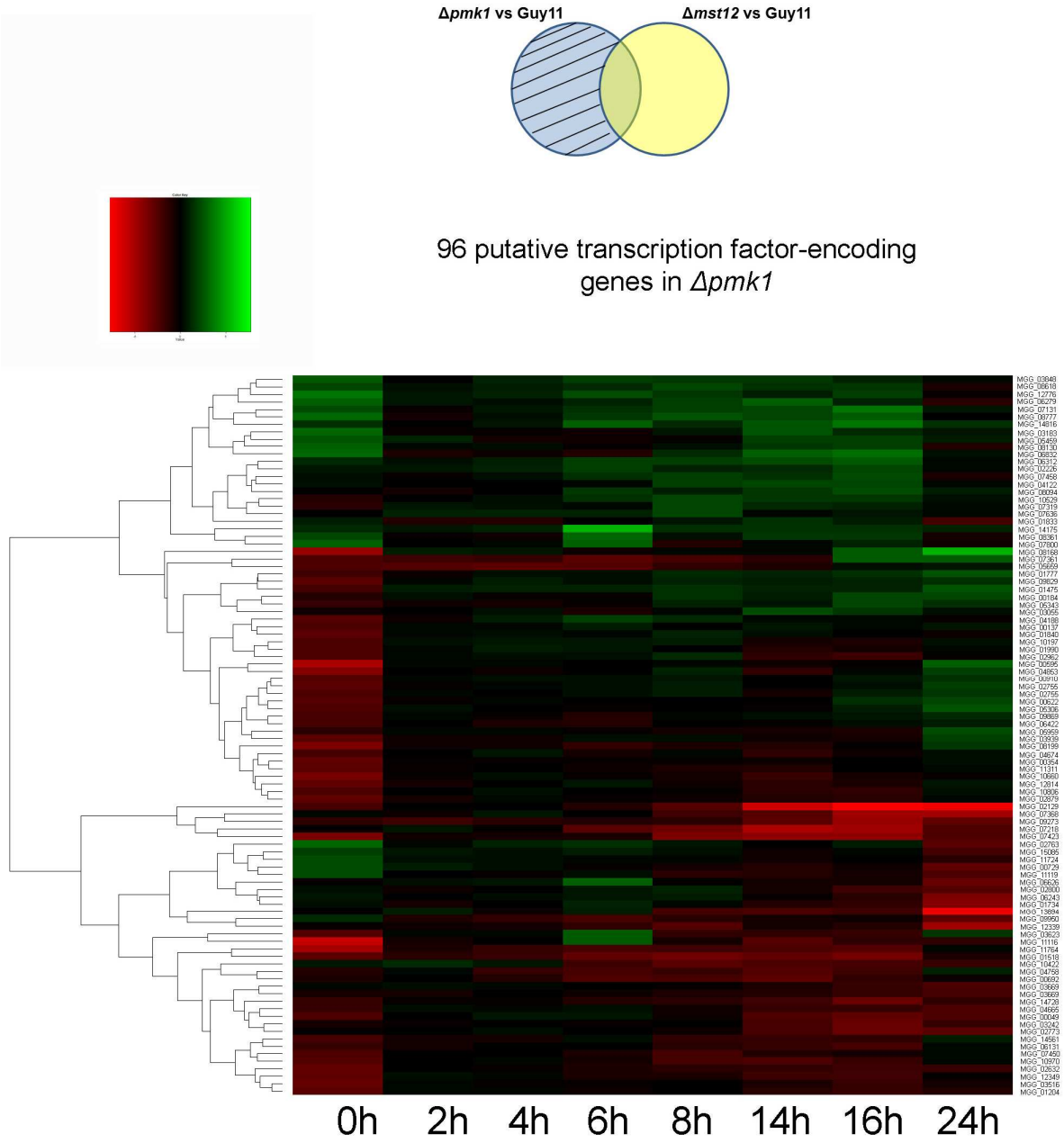

Figure 5.10 Heatmaps showing levels of transcript abundance of 96 transcription factor encoding genes in the *Δpmk1* mutant compared to Guy11 from genes Pmk1-dependent and Mst12- independent gene set. (red= down-regulated in the *Δpmk1* mutant; green= up-regulated in the *Δpmk1* mutant).

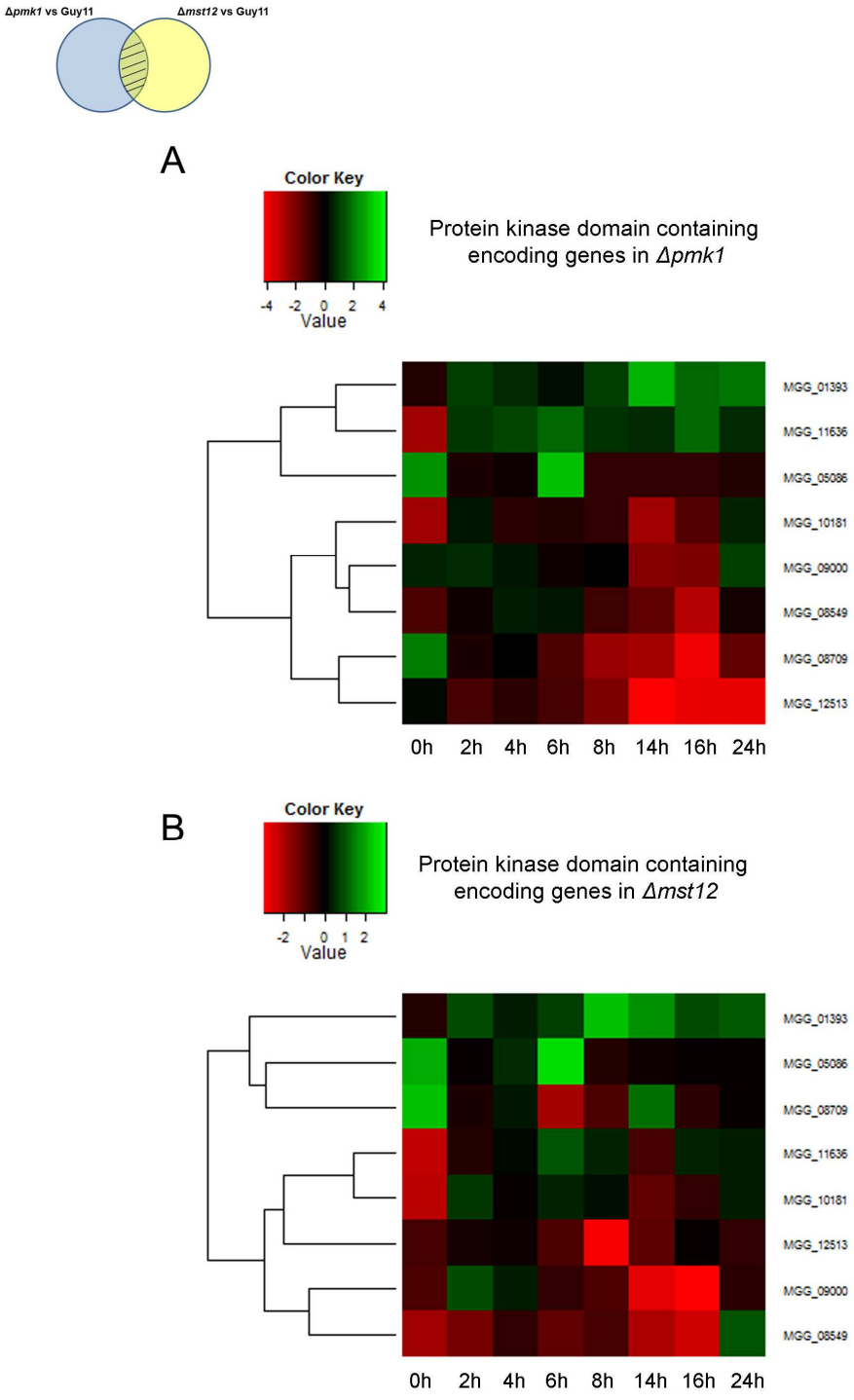

Figure 5.11 Heatmaps showing levels of transcript abundance of 8 unknown protein kinase domain containing encoding genes (PF00069) from genes Pmk1 and Mst12-dependent gene set. A) Heatmap of the Δ*pmk1* mutant compared to Guy11. **B)** Heatmap of the Δ*mst12* mutant compared to Guy11. (red= down-regulated gene expression in the mutants; green= up-regulated gene expression in the mutants).

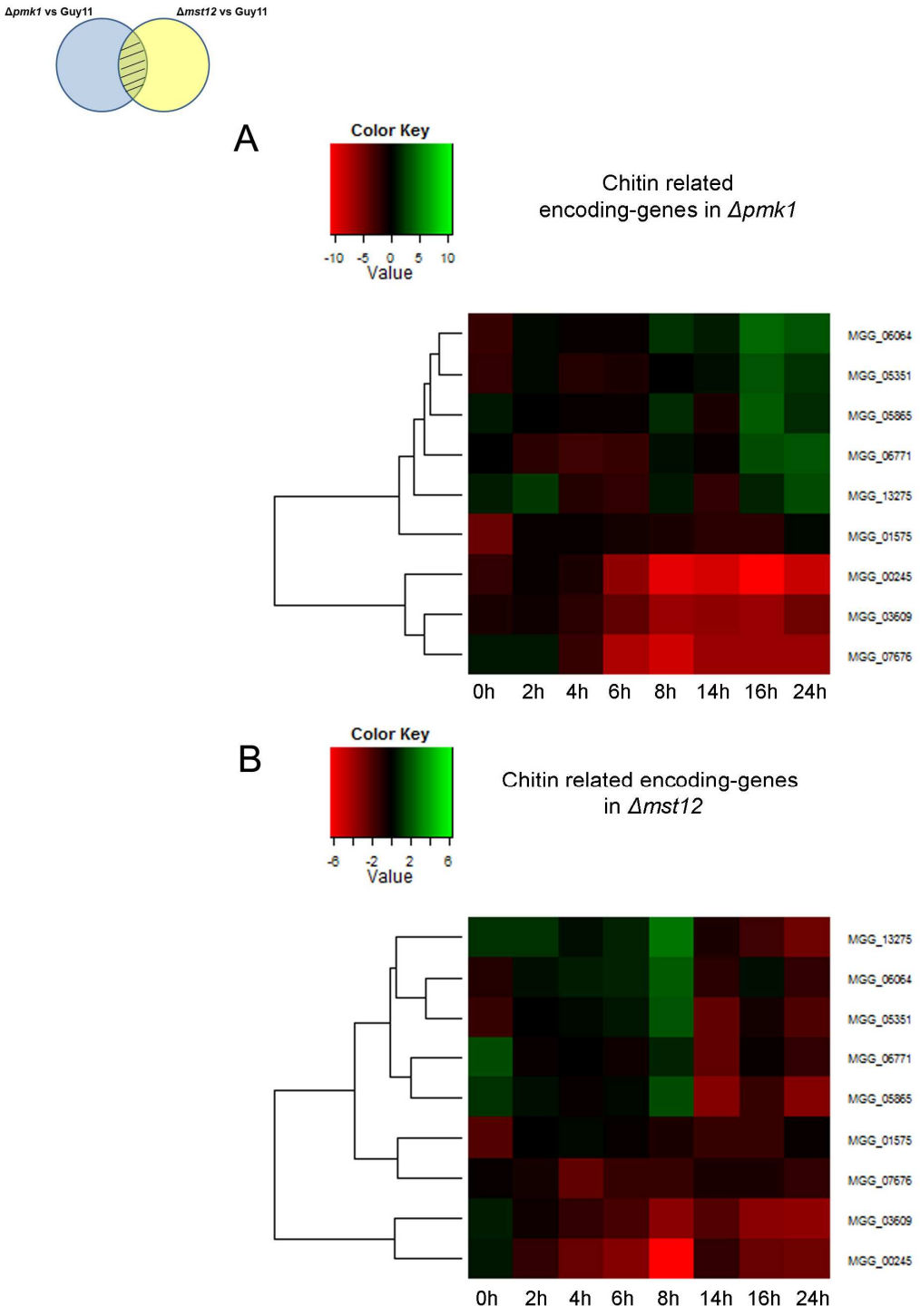

Figure 5.12 Heatmaps showing levels of transcript abundance of chitin related protein-encoding genes from genes Pmk1 and Mst12-dependent gene set. **A)** Heatmap of the Δ*pmk1* mutant compared to Guy11. **B)** Heatmap of the Δ*mst12* mutant compared to Guy11**.** (red= down-regulated gene expression in the mutants; green= up-regulated gene expression in the mutants).

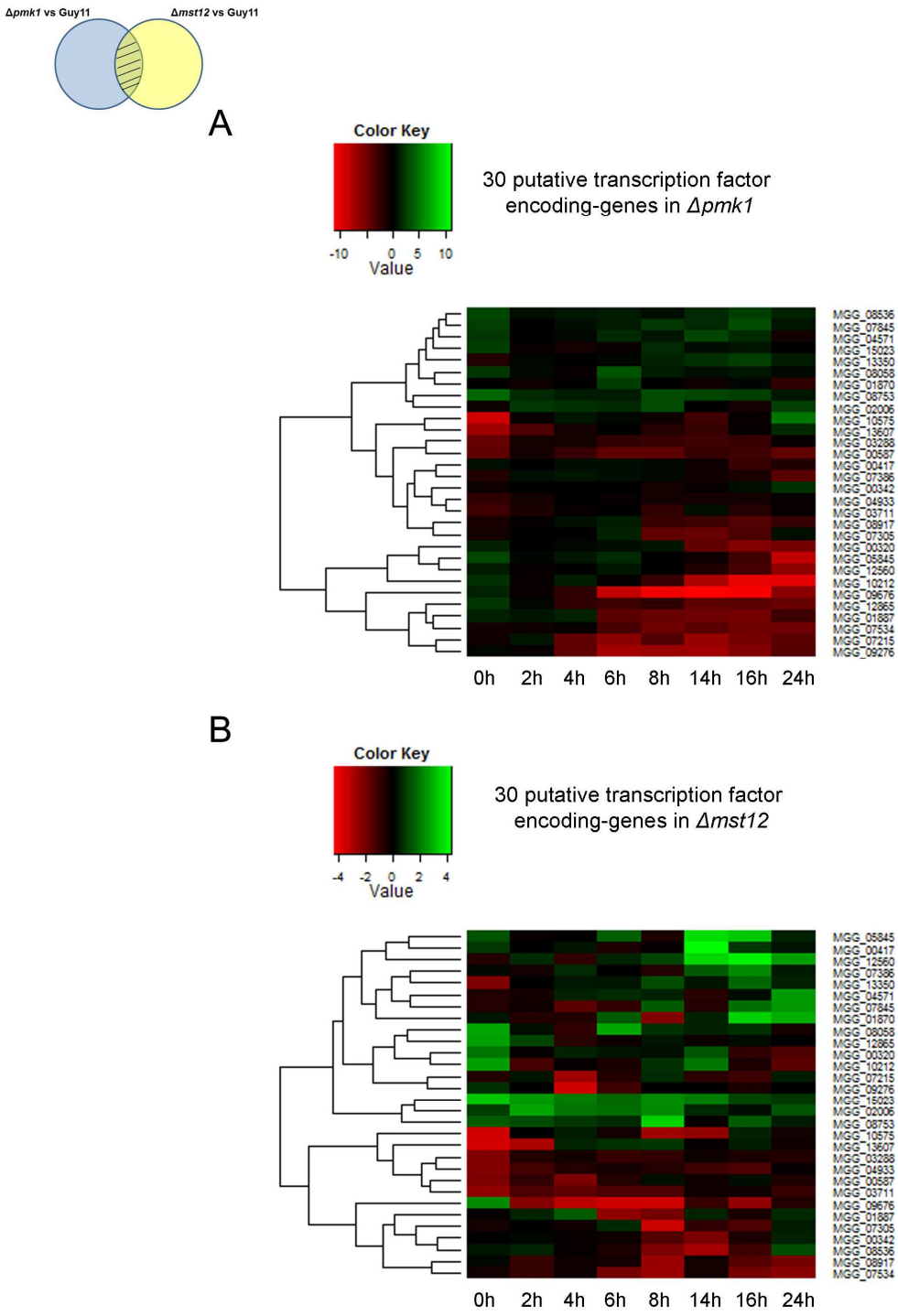

Figure 5.13 Heatmaps showing levels of transcript abundance of transcription factor-encoding genes from genes Pmk1 and Mst12-dependent gene set. **A)** Heatmap in the Δ*pmk1* mutant compared to Guy11. **B)** Heatmap of the Δ*mst12* mutant compared to Guy11. (red= down-regulated gene expression in the mutants; green= up-regulated gene expression in the mutants).

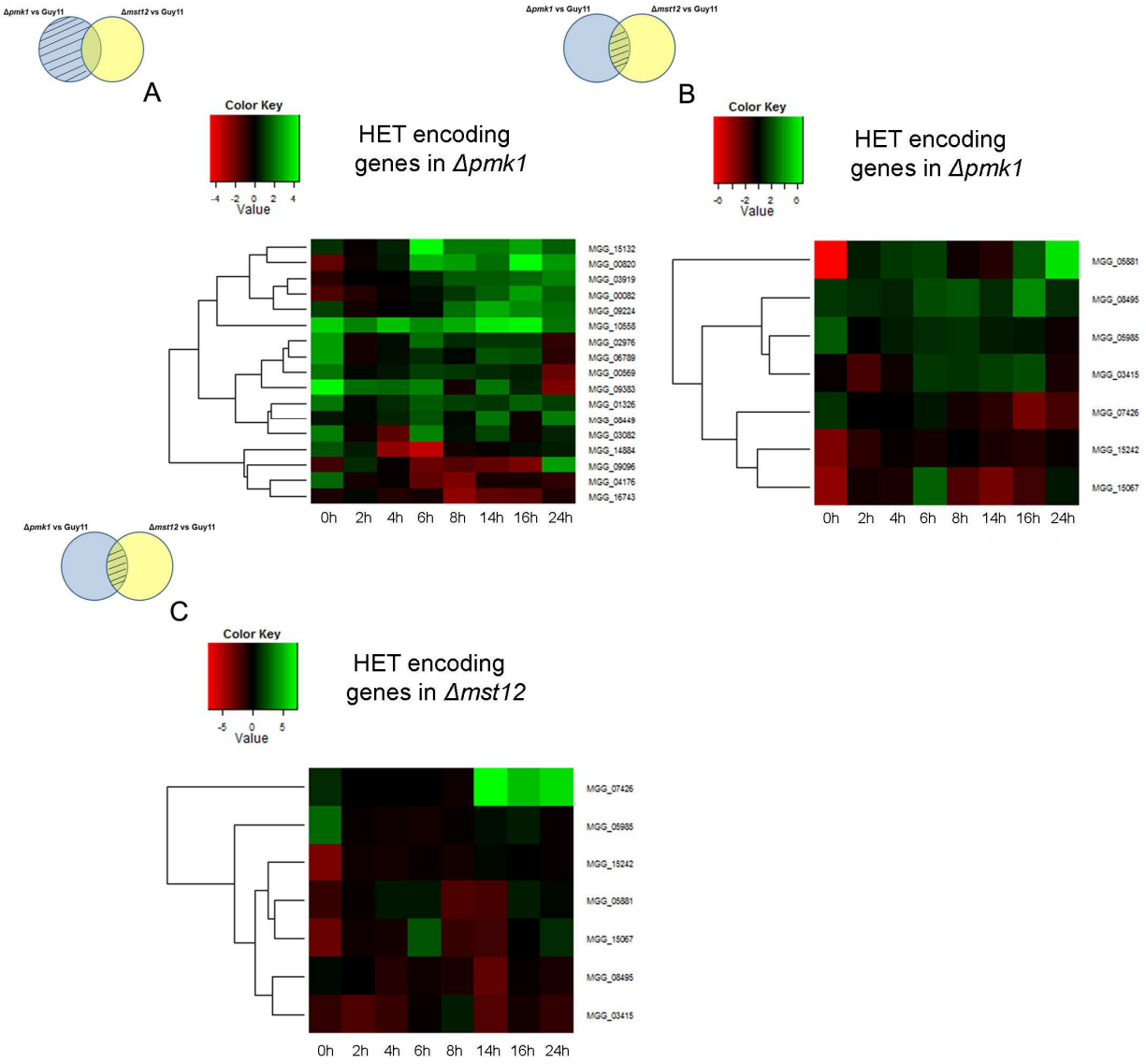

Figure 5.14 Heatmaps showing levels of transcript abundance of heterokaryon incompatibility protein (HET) (PF06985) regulated during the time course of appressorium development. **A)** Heatmap of the Δ*pmk1* mutant compared to Guy11 from genes Pmk1-dependent and independent of Mst12. **B)** Heatmap of the Δ*pmk1* mutant compared to Guy11 from genes Pmk1 and Mst12-dependent. **C)** Heatmap in Δ*mst12* compared to Guy11 from genes Pmk1 and Mst12-dependent. (red= down-regulated gene expression in the mutants; green= up-regulated gene expression in the mutants).

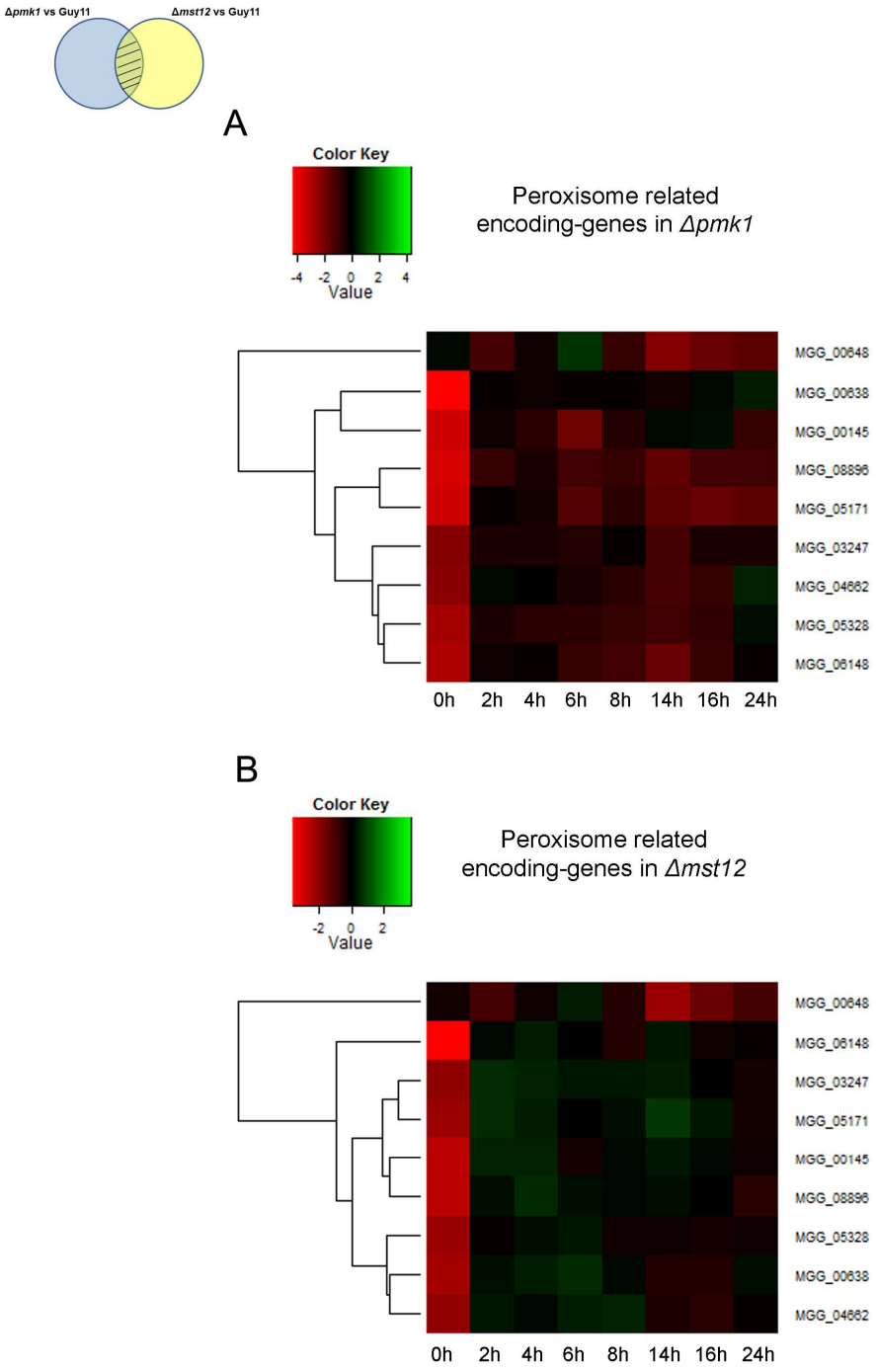

Figure 5.15 Heatmaps showing levels of transcript abundance of peroxisome-related proteins regulated during the time course of appressorium development from genes Pmk1 and Mst12-dependent gene set. **A)** Heatmap of the Δ*pmk1* mutant compared to Guy11. **B)** Heatmap of the Δ*mst12* mutant compared to Guy11. (red= down-regulated gene expression in the mutants; green= up-regulated gene expression in the mutants).

5.3.4 Transcription factor analysis: Identifying transcription factors that are likely to be regulated by Mst12.

Transcriptional regulation in organisms occurs in a hierarchical manner (Herskowitz, 1989). A global transcriptional regulator activates several downstream transcription factors, and those in turn activate other downstream transcription factors. I therefore set out to define the analysis of transcription factors for the entire Pmk1 MAP pathway, including transcription factors likely to be regulated by Mst12. To do this, it was necessary first to identify putative transcription factors likely to be downstream of Mst12, and second, to correlate these data with data obtained from analysis of Pmk1 transcriptional regulation presented in Chapter 3. Although analysis of transcription factor-encoding genes was presented in Section 5.3, here a separate and a more comprehensive analysis is presented. In order to identify transcription factor-encoding genes downstream of Mst12, I determined the number of putative transcription factors from the differentially regulated gene sets for every time point. The number of transcription factors differentially regulated at each time point was 81, 29, 32, 14, 46, 48, 42 and 42 for 0 h, 2 h, 4 h, 6 h, 8 h, 14 h, 16 h, and 24 h, respectively. These gene sets were combined and a total of 118 transcription factors identified as being differentially regulated in at least two time points during the time course.

To identify clusters of expression within the 118 transcription factor gene set, the levels of transcript abundance for every transcription factor were determined and a heatmap generated (Fig. 5.3.16). The heatmap showed 4 differential clusters. The most abundant cluster, 3, contained 44 transcription factors in total. Cluster 1, 2 and 4 contained 7, 29 and 38 number of transcription factors, respectively.

Cluster 1 contained a basic region leucine zipper (PF07716) domain containing protein (MGG_12560), one bZIP transcription factor (PF00170) (MGG_02006), three fungal Zn(2)-Cys(6) binuclear cluster domain containing proteins (PF00172) (MGG_15023, MGG_00417, MGG_05845), a protein of unknown function with no pfam associated domain (MGG_01870) and the Mst12 transcription factor, itself (MGG_12958). The expression of the Mst12 gene can be explained because the original null mutant was a disruption of the gene instead a of a complete deletion, therefore the initial portion of the gene can be transcribed. Moreover, it appears to be up-regulated because of a compensatory mechanism.

A heatmap showing their expression was constructed (Fig. 5.17). The heatmap showed that expression of the transcription factor encoding genes was highly up-regulated for the entire time course of appressorium development and especially at 14 h, 16 h, and 24 h.

Cluster 2 was formed of 16 fungal Zn(2)-Cys(6) binuclear cluster domain containing proteins (PF00172) (MGG_05578, MGG_14728, MGG_03848, MGG_06243, MGG_08130, MGG_03183, MGG_07368, MGG_06279, MGG_1172, MGG_02880, MGG_00320, MGG_00494, MGG_12776, MGG_09273, MGG_02408, MGG_08618, MGG_01414), two bZIP transcription factors (PF00170) (MGG_04009 and MGG_07925), *HOX7* (MGG_*12865*) and *HOX4* (MGG_06285) homeobox transcription factors, a fungal Zn(2)-Cys(6) binuclear cluster domain containing protein (PF00172) (MGG_10212), five proteins of unknown function with no pfam associated domain (MGG_02732, MGG_04011, MGG_05459, MGG_06832, MGG_04141) and the *ACEII* (MGG_08058) transcription factor. A heatmap showing their expression was constructed (Fig. 5.18). The heatmap showed that all the transcription factor encoding genes were up-regulated at 0 h during appressorium

development suggesting that they might be involved during the germination of the spore.

Cluster 3 contained the Aft1 osmotic stress response (OSM) domain containing protein (PF11785) (MGG_08212), *CDC10* or *SWI6* (MGG_09869) and the additional *MBP1* (MGG_08463), that both form a complex to regulate gene expression during the transition from G1 to S phase (Koch *et al.,* 1993), *HAC1* (MGG_09010), *IDI4* (MGG_01990), two transcription factors related with development of conidia in *M. oryzae COD1* (MGG_05343) and *COD2* (MGG_09263) (Chung *et al.,* 2013), four bZIP transcription factors (PF00170) (MGG_02632, MGG_04758, MGG_10660, MGG_05306), a CCAAT-binding transcription factor (CBF-B/NF-YA) subunit B (PF02045) (MGG_00354), a copper fist DNA binding domain-containing protein (PF00649) (MGG_07205), *NUT1* (MGG_02755), *DAL81* (MGG_ 06492) which regulates genes in multiple nitrogen degradation pathways in *S. cerevisiae* (Bricmont *et al.,* 1991), 16 fungal Zn(2)-Cys(6) binuclear cluster domain-containing proteins (PF00172) (MGG_04665, MGG_01777, MGG_10197, MGG_11764, MGG_02962, MGG_06954, MGG_04108, MGG_12349, MGG_13350, MGG_06355, MGG_07681, MGG_07386, MGG_07458, MGG_02226, MGG_01836, MGG_09002), a cutinase transcription factor beta (MGG_08199), two GATA zinc finger domain containing proteins (PF00320) (MGG_01840 and MGG_07319), a HSF-type DNA-binding domain containing protein (PF00447) (MGG_03516), a NDT80 / PhoG like DNA-binding family protein (PF05224) (MGG_00622), a NF-X1 type zinc finger domain-containing protein (PF01422) (MGG_00137), a putative GTPase activating protein for Arf (PF01412) (MGG_04954), a SNF5 / SMARCB1 / INI1 protein (PF04855) (MGG_10538), the *MIG1* MADS-box *MEF2* type transcription factor (MGG_01204) and four proteins of unknown function of unknown function with

no pfam associated domain (MGG_10562, MGG_01688, MGG_03413, MGG_01285). A heatmap showing their expression was generated (Fig. 5.19). The heatmap showed that most of the transcription factor encoding genes were highly down-regulated at 0 h with the exception of three fungal Zn(2)-Cys(6) binuclear cluster domain-containing proteins (MGG_10197, MGG_02226 and MGG_13350), and a protein of an unknown function with no pfam associated domain (MGG_10562) which all show a strong up-regulation of gene expression at later time points during appressorium morphogenesis.

Cluster 4 contained one basic region leucine zipper (PF07716) (MGG_14561), six bZIP transcription factors (PF00170) (MGG_06131, MGG_07305, MGG_12814, MGG_00602, MGG_03288, MGG_00587), two fungal specific transcription factors (PF04082) (MGG_00049 and MGG_10422), *NIT4* (MGG_01518), 13 fungal Zn(2)-Cys(6) binuclear cluster domain proteins (PF00172) (MGG_08536, MGG_02377, MGG_04933, MGG_05659, MGG_03763, MGG_15139, MGG_13994, MGG_11116, MGG_05939, MGG_08917, MGG_07450, MGG_03711 and MGG_11119), WC2 (MGG_10970), a helix-loop-helix DNA-binding domain containing protein (PF00010) (MGG_10575), a zinc finger, C_2H_2 type domain containing protein (PF00096) (MGG_09950), and four proteins of unknown function with no pfam associated domain (MGG_13607, MGG_07423, MGG_04024, MGG_00342). Six transcription factors were found in clade 5 during the analysis of transcription factors likely to be Pmk1-regulated: MGG_07218, MGG_01887, MGG_09676, MGG_07534, MGG_09276 MGG_02129 and *PIG1* (MGG_07215). A heatmap showing their gene expression in the *Δmst12* mutant compared to Guy11 was generated (Fig. 5.20). The heatmap showed 3 separate clusters. The first cluster showed strong down-regulation of gene expression from 2 h until 8 h. The

most dramatic gene expression profile within these groups corresponds to the gene MGG_09676, which was previously found in cluster 5 in the Pmk1-regulated dataset. This result suggests that MGG_09676 is also regulated by Mst12. The second cluster shows down-regulation in gene expression at 6 h, 8 h, 14 h and 16 h. In this cluster two genes previously identified in cluster 5 from the Pmk1-regulated dataset were found, namely MGG_01887 and *PIG1* (MGG_07218). Moreover other known transcription factors such as *IDI4* (MGG_01990), *MBP1* (MGG_08463) which in *S. cerevisiae* has been shown to be involved in the emergence of a bud (Bouquin *et al.,* 1999), *NUT1* (MGG_02755), and a cutinase transcription factor (MGG_01836), were also identified. The third cluster was the most numerous and the entire number of transcription factor encoding genes showed strong down-regulation in the *Δmst12* mutant compared to Guy1 over the entire time course. Two of these genes were previously identified in cluster 5 from the Pmk1-regulated dataset, namely *ACLR* (MGG_02129) and MGG_07534.

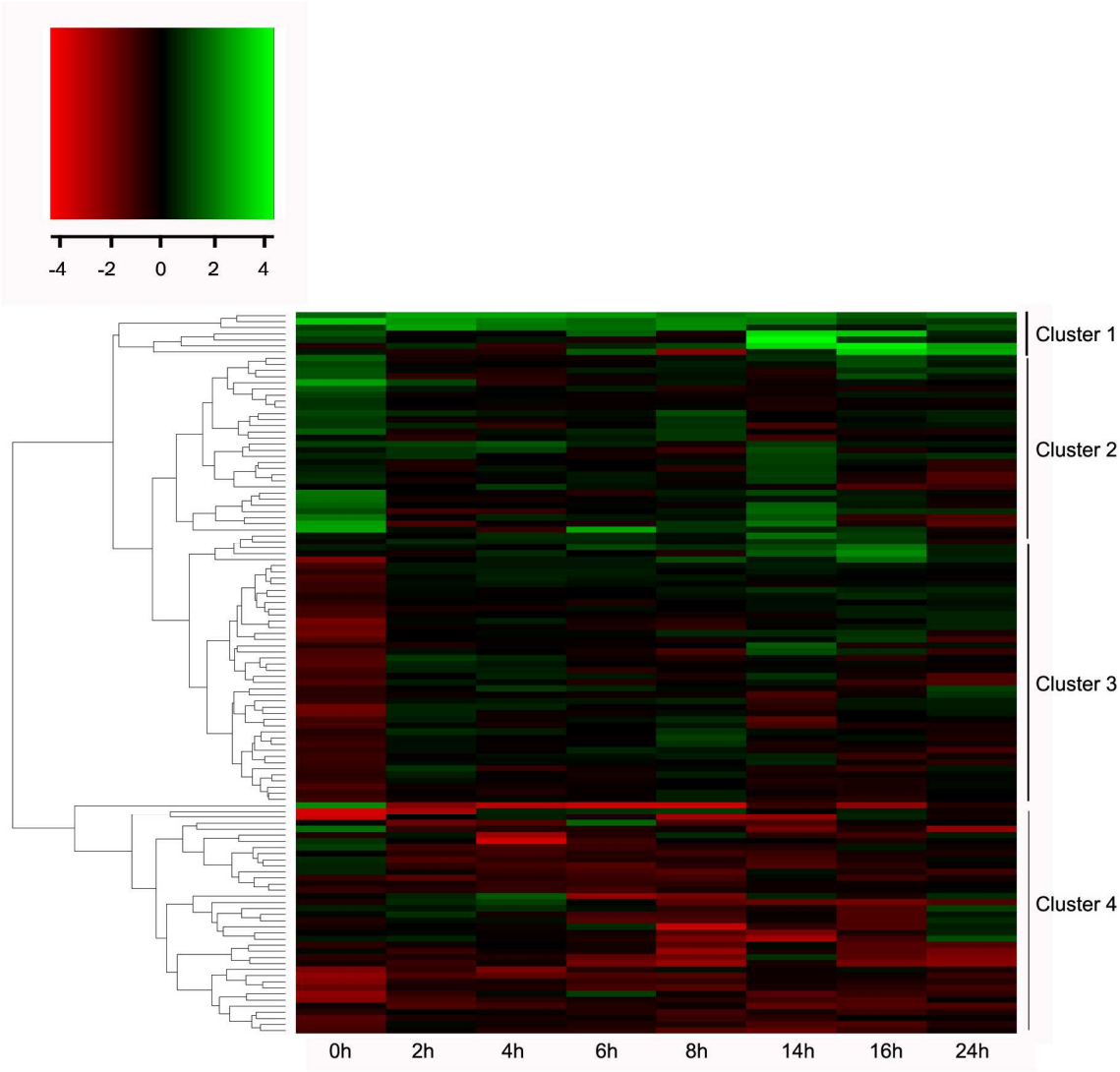

Figure 5.16 Heatmap showing levels of transcript abundance of transcription factors likely to be Mst12 regulated during the time course of appressorium development. Transcription factors showing similar patterns of expression are clustered. In total 118 transcription factors are shown. Levels of expression are represented as mod_lfc of transcript abundance from the *Δmst12* mutant compared to Guy11. (red= down-regulated in the *Δmst12* mutant; green= up-regulated in the *Δmst12* mutant).

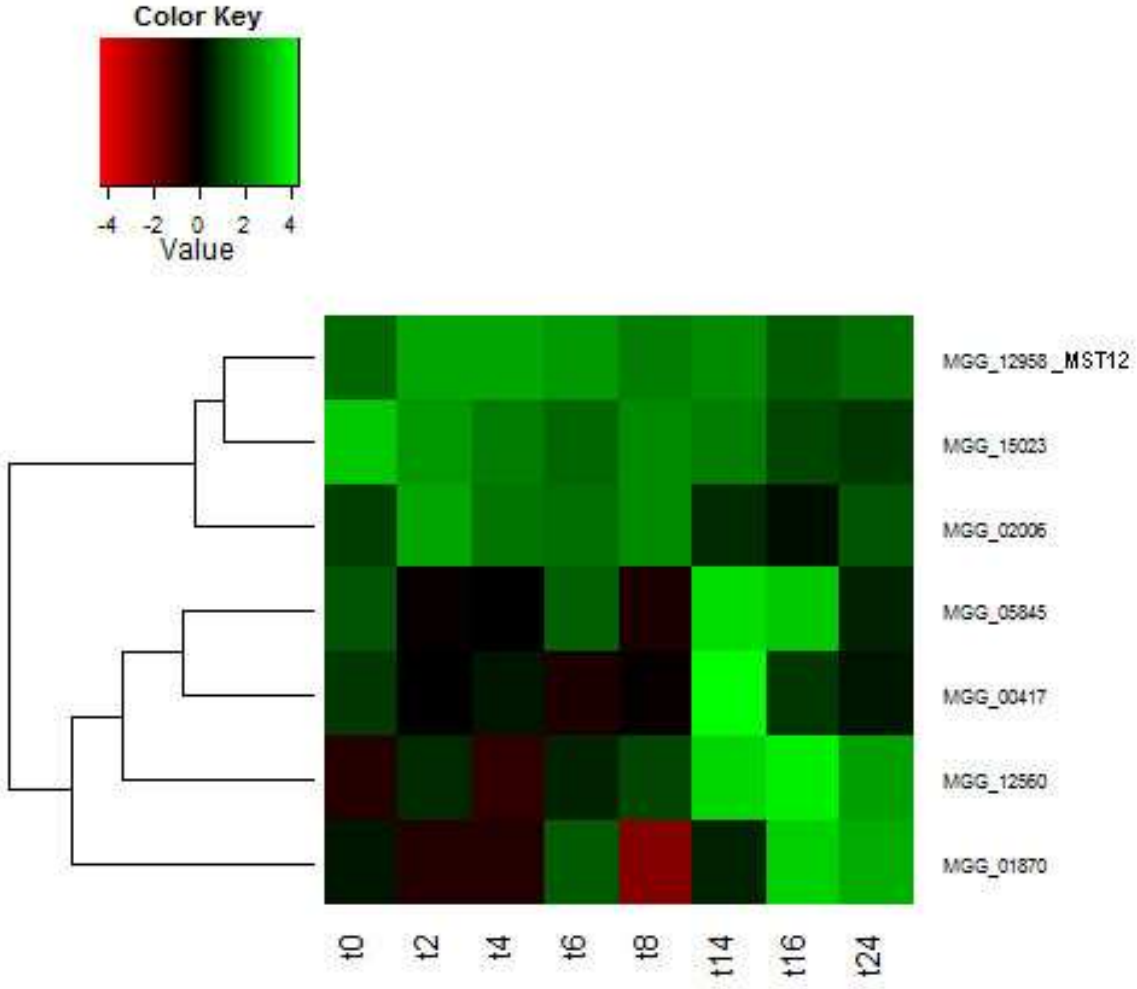

Figure 5.17 Heatmap showing levels of transcript abundance of transcription factors likely to be Mst12 regulated from cluster 1 during the time course of appressorium development. Transcription factors showing similar patterns of expression are clustered. In total seven transcription factors are shown. Levels of expression are represented as mod_lfc of transcript abundance from the *Δmst12* mutant *compared* to Guy11 (red= down-regulated in the *Δmst12* mutant; green= up-regulated in the *Δmst12* mutant).

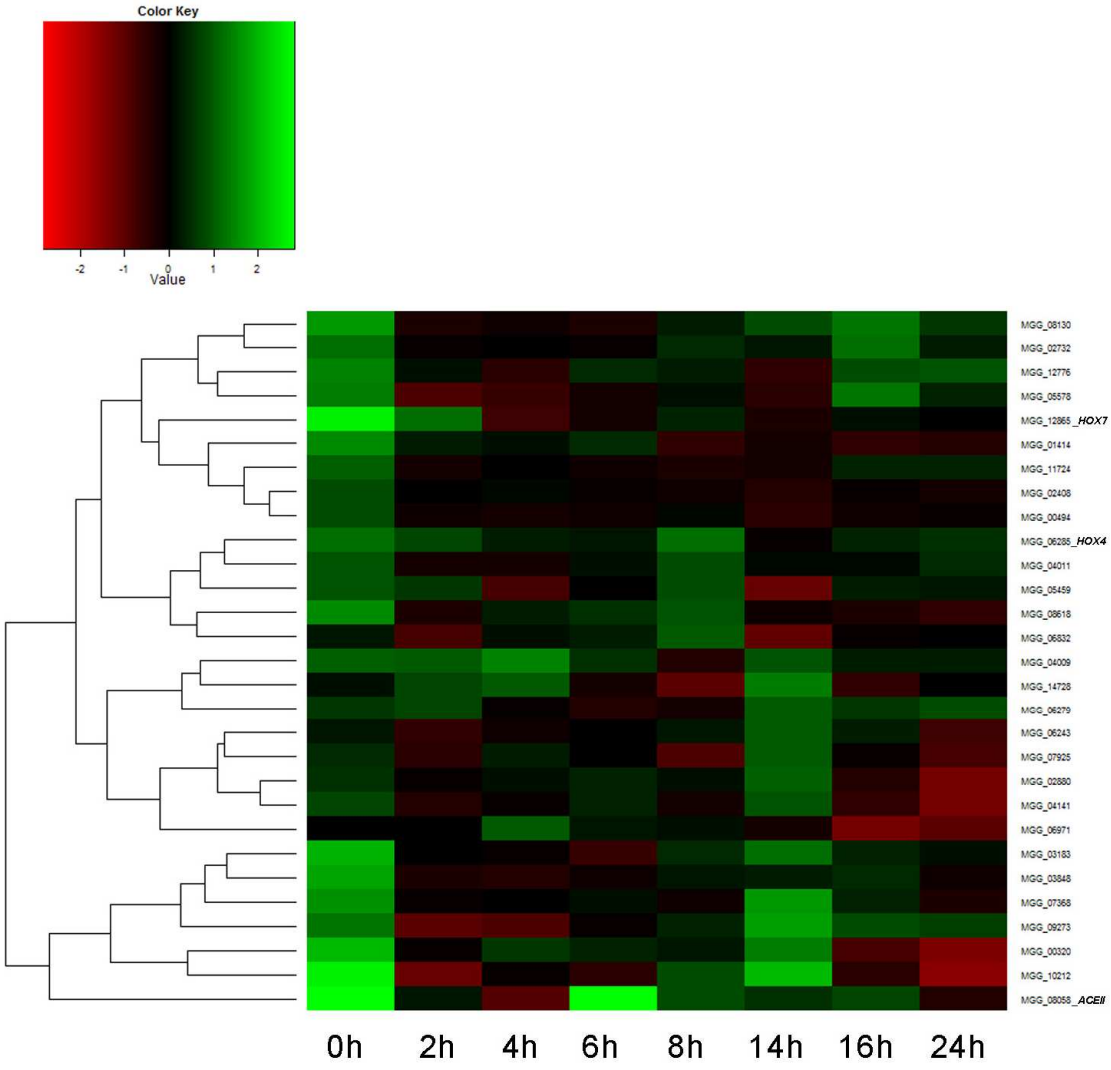

Figure 5.18 Heatmap showing levels of transcript abundance of transcription factors likely to be Mst12 regulated from cluster 2 during the time course of appressorium development. Transcription factors showing similar patterns of expression are clustered. In total 29 transcription factors are shown. Levels of expression are represented as mod_lfc of transcript abundance from the *Δmst12* mutant compared to Guy11. (red= down-regulated in the *Δmst12* mutant; green= up-regulated in the *Δmst12* mutant).

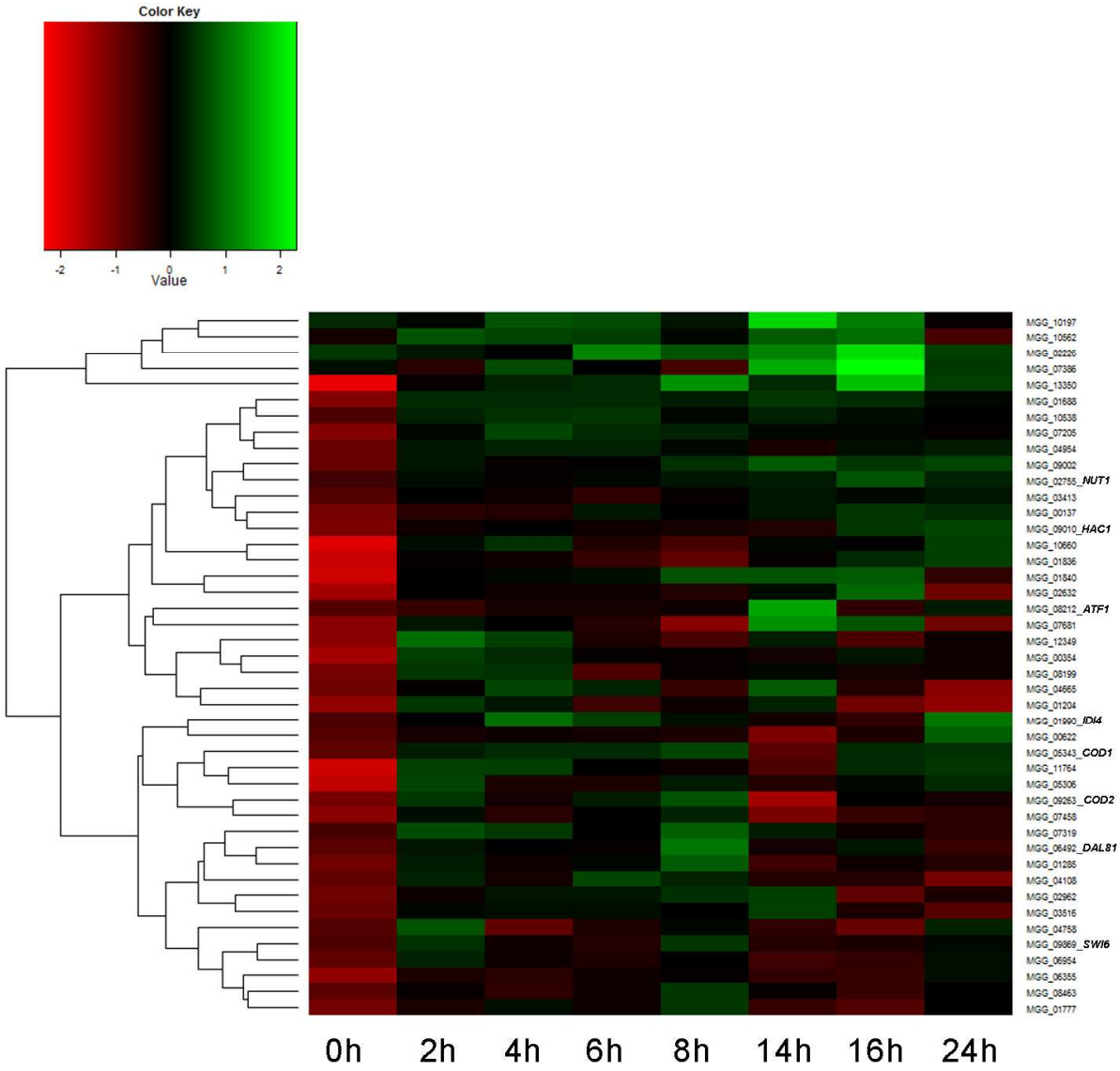

Figure 5.19 Heatmap showing levels of transcript abundance of transcription factors likely to be Mst12 regulated from cluster 3 during the time course of appressorium development. Transcription factors showing similar patterns of expression are clustered. In total 44 transcription factors are shown. Levels of expression are represented as mod_lfc of transcript abundance from the *Δmst12* mutant compared to Guy11 (red= down-regulated in the *Δmst12* mutant; green= up-regulated in the *Δmst12* mutant).

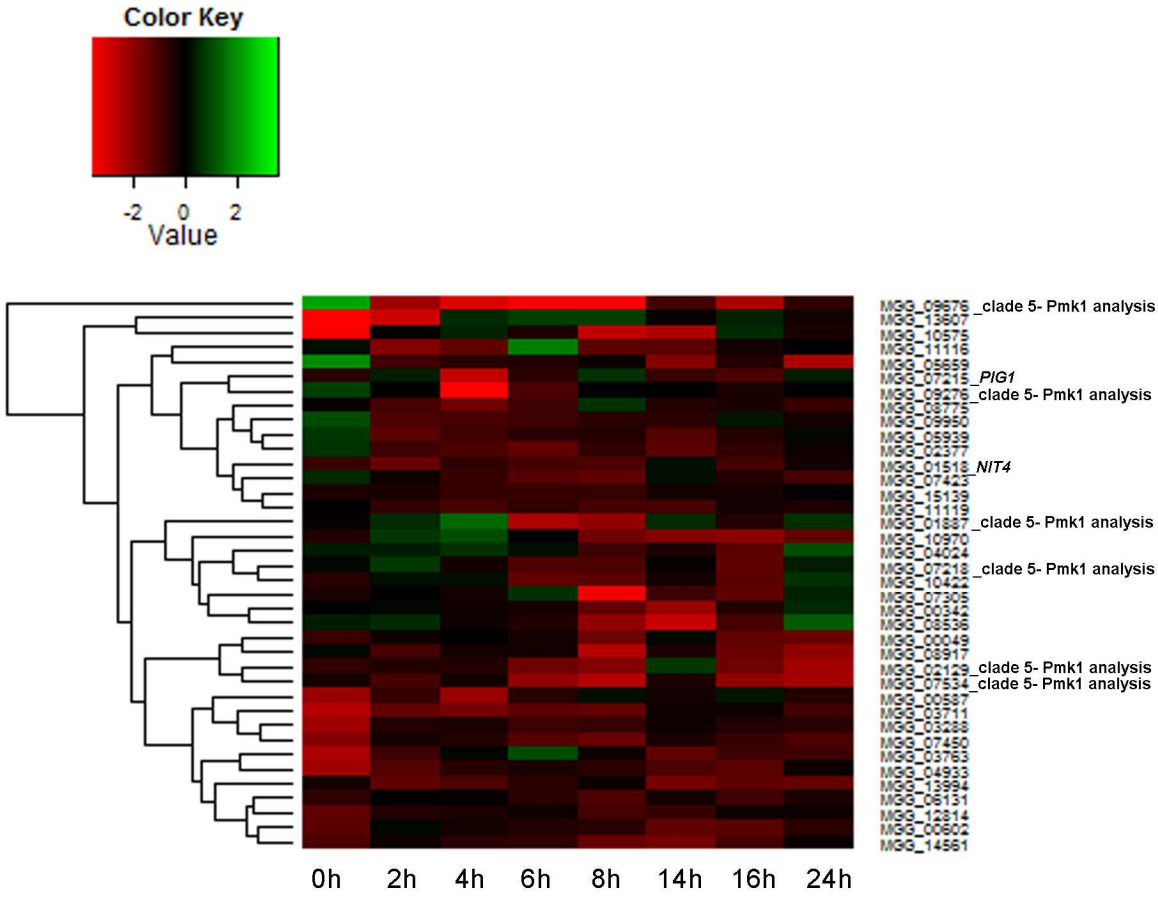

Figure 5.20 Heatmap showing levels of transcript abundance of transcription factors likely to be Mst12 regulated from cluster 4 during the time course of appressorium development. Transcription factors showing similar patterns of expression are clustered. In total 38 transcription factors are shown. Levels of expression are represented as mod_lfc of transcript abundance from the *Δmst12* mutant compared to Guy11 (red= down-regulated in the *Δmst12* mutant; green= up-regulated in the *Δmst12* mutant).

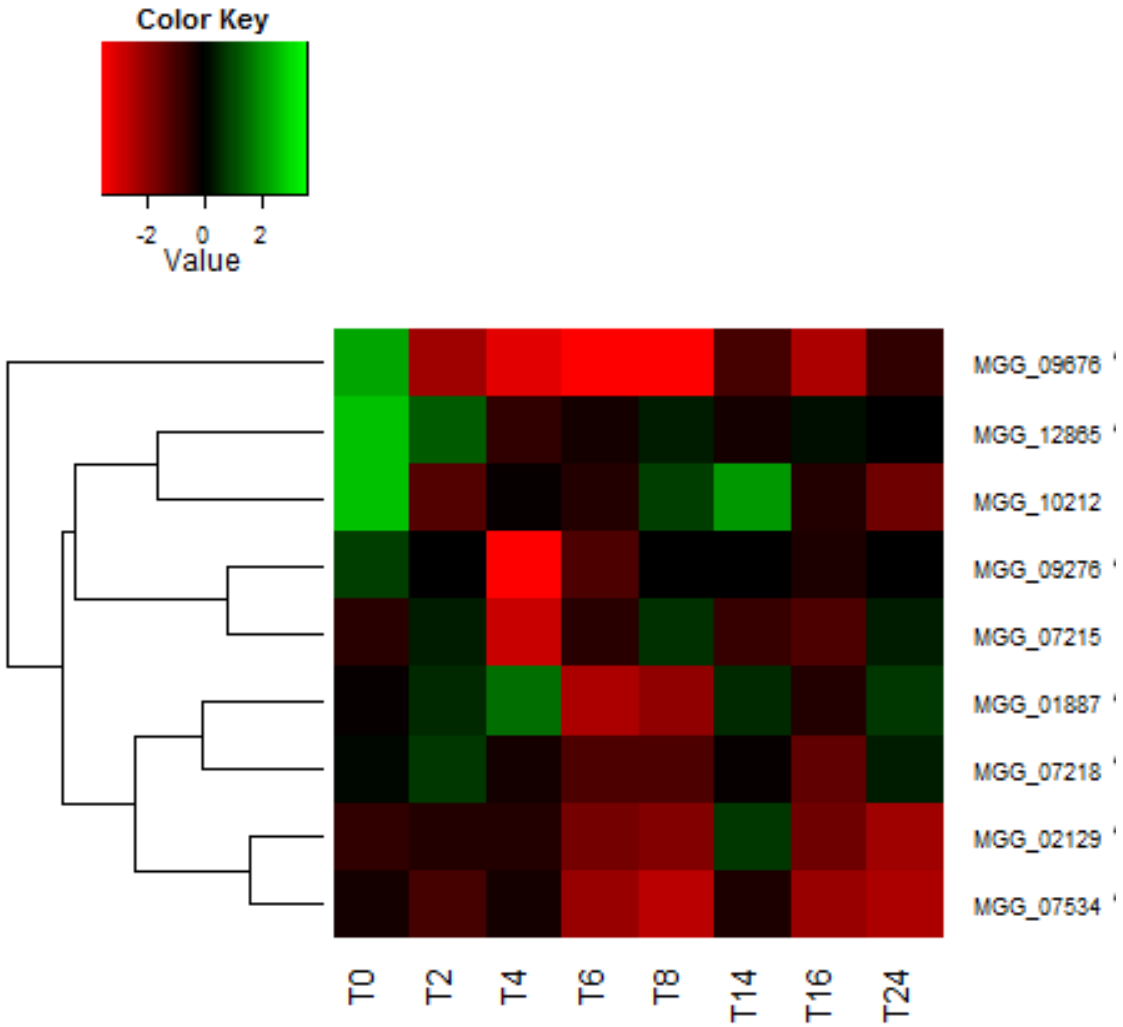

Figure 5.21 Heatmap showing levels of transcript abundance in *Δmst12* compared to Guy11 of transcription factors from cluster 5 defined in Chapter 2. Cluster 5 in Chapter 2 was found to have nine transcription factors that might be Pmk1 regulated. Levels of expression are represented as mod_lfc of transcript abundance from the *Δmst12* mutant compared to Guy11 (red= down-regulated in the *Δmst12* mutant; green= up-regulated in the *Δmst12* mutant).

5.3.5 Transcriptional analysis of different pathways

5.3.5.1 Melanin biosynthesis pathway

The high turgor pressure in the appressorium dome is generated by accumulation of water that diffuses inside the dome through the melanin layer (Valent and Chumley, 1991) against a concentration gradient. Melanin deficient mutants *alb1, buf1* or *rsy1* are unable to synthesize melanin and therefore are impaired in turgor generation and plant infection (Chumley, 1990). However, regulation of melanin biosynthesis is not well understood. The *Δmst12* null mutant is able to form appressoria, but does not cause rice blast disease because it is unable to develop a penetration peg (Park *et al.,* 2002). However, although appressoria of the null mutant *Δmst12* are melanised, it is not known whether the melanin content of the mutant is affected. Individual expression of melanin biosynthesis enzyme-encoding genes was analysed in Guy11 and *Δmst12* and bar charts plotted (Fig. 5.28). The bar charts indicated that in a wild type strain, Guy11, a peak of expression of melanin biosynthesis genes occurs at 6 h, whereas in the case of the *Δmst12* this happens at 8 h, indicating a delay in melanisation. Moreover, heatmaps showing the gene expression levels of melanin biosynthesis enzymes in Δmst12 compared to Guy11 were also plotted (Fig. 5.29). The heatmap showed strong down-regulation of *RSY* (MGG_05059), Acetyl Co-A carboxylase (MGG_07613) and *ALB1* (MGG_07219) genes at 4 h and down-regulation of the 5 enzymes at 14 h, 16 h, and 24 h, suggesting possible impairment, or delay in melanin biosynthesis in the *Δmst12* null mutant.

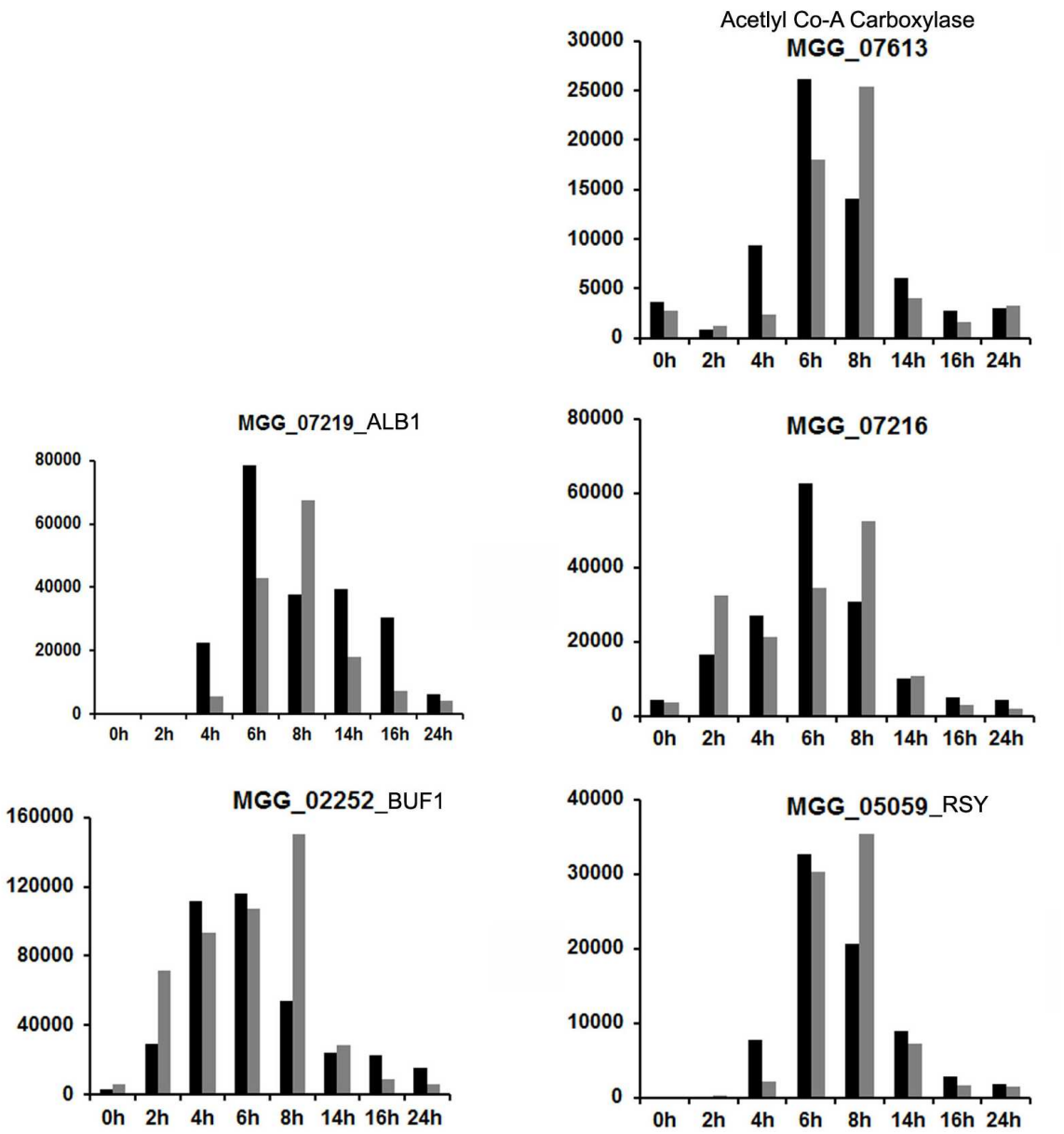

Figure 5.22 Analysis of melanin biosynthesis pathway genes in *M. oryzae*. Bar charts showing levels of transcript abundance from genes involved in melanin biosynthesis in Guy11 and the Δ*mst12* mutant. (Back= gene expression in Guy11; Grey= gene expression in Δ*mst12*). Vertical axes represents mean of normalized counts from genes involved in melanin biosynthesis.

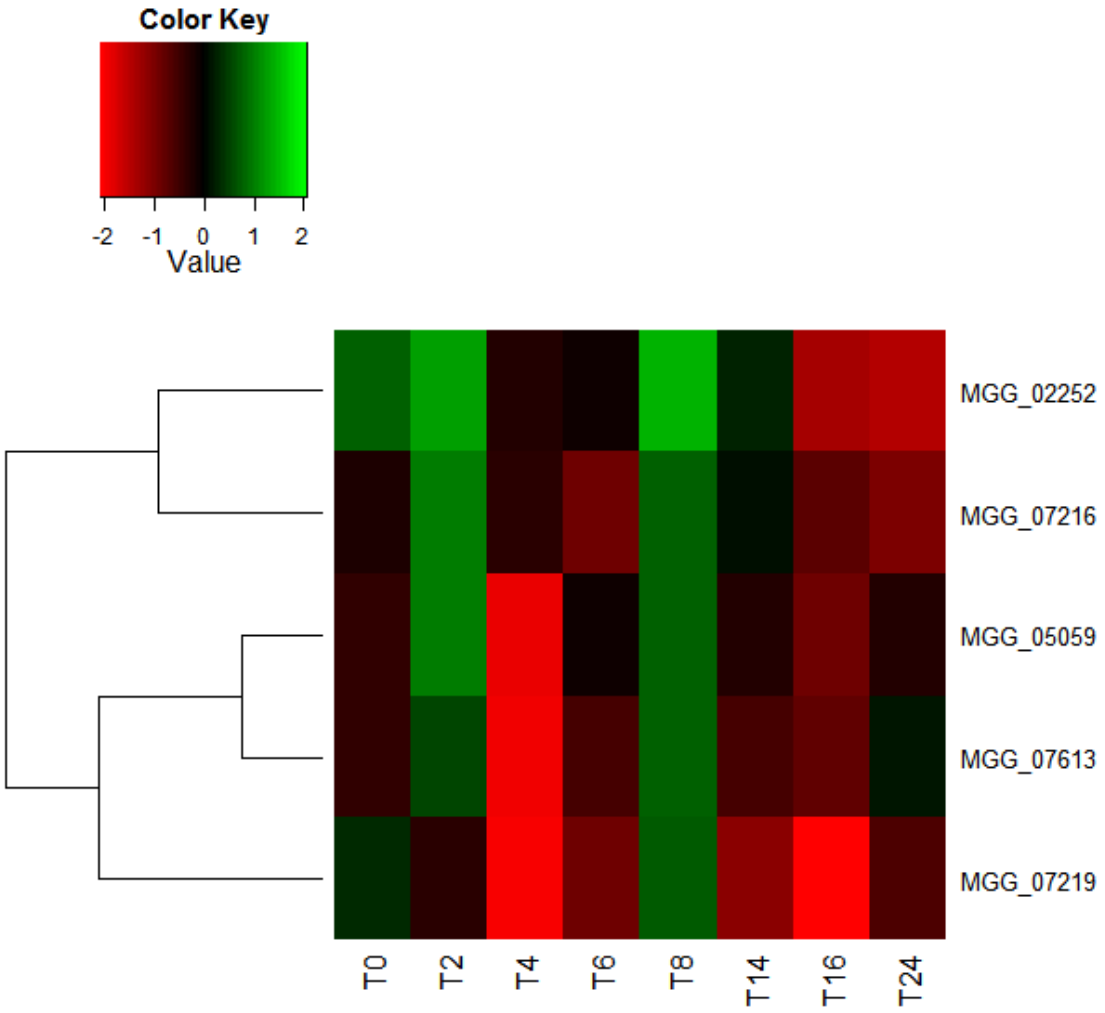

Figure 5.23 Heatmap showing levels of transcript abundance from genes involved in melanin biosynthesis in the Δ*mst12* mutant. Levels of expression are represented as modified logarithmic fold change (mod_lfc) (red= down-regulated in the *Δmst12* mutant; green= up-regulated in the *Δmst12* mutant).

5.3.5.2 Cutinase domain containing proteins

Cutinases are methyl esterases responsible for degrading the cuticle of a leaf and thereby facilitating entry of a fungus into host cells (Kolattukudy, 1985). This is the case for many pathogenic fungi, such as *Colletotrichum kahawae* which secretes cutinases in a pre-penetration stage to facilitate plant penetration (Chen, 2007). *M. oryzae* possesses 18 cutinase domain containing proteins in its genome. Two of these cutinases have been studied in the past, and *CUT2* is required for formation of a functional appressorium and for full virulence in rice plants (Skamnioti and Gurr, 2007). Therefore due to their potential role in plant penetration, the cutinase domain containing encoding genes were analysed in the Δ*mst12* mutant. The gene expression of cutinase domain containing proteins in the *Δmst12* mutant was analysed and a heatmap plotted (Fig. 5.29). The heatmaps showed that MGG_15015, MGG_09840, MGG_09100 (CUT2), MGG_02393, MGG_14095 and MGG_03440 were strongly down-regulated at 6 and 8 h, and in the case of MGG_09100 (CUT2), MGG_02393, MGG_14095 and MGG_03440, the down-regulation was prolonged during 14 h, 16 h and 24 h. This result suggested possible impairment in the synthesis of a group of cutinase domain containing proteins in the Δ*mst12* null mutant, consistent with its lack of penetration peg development.

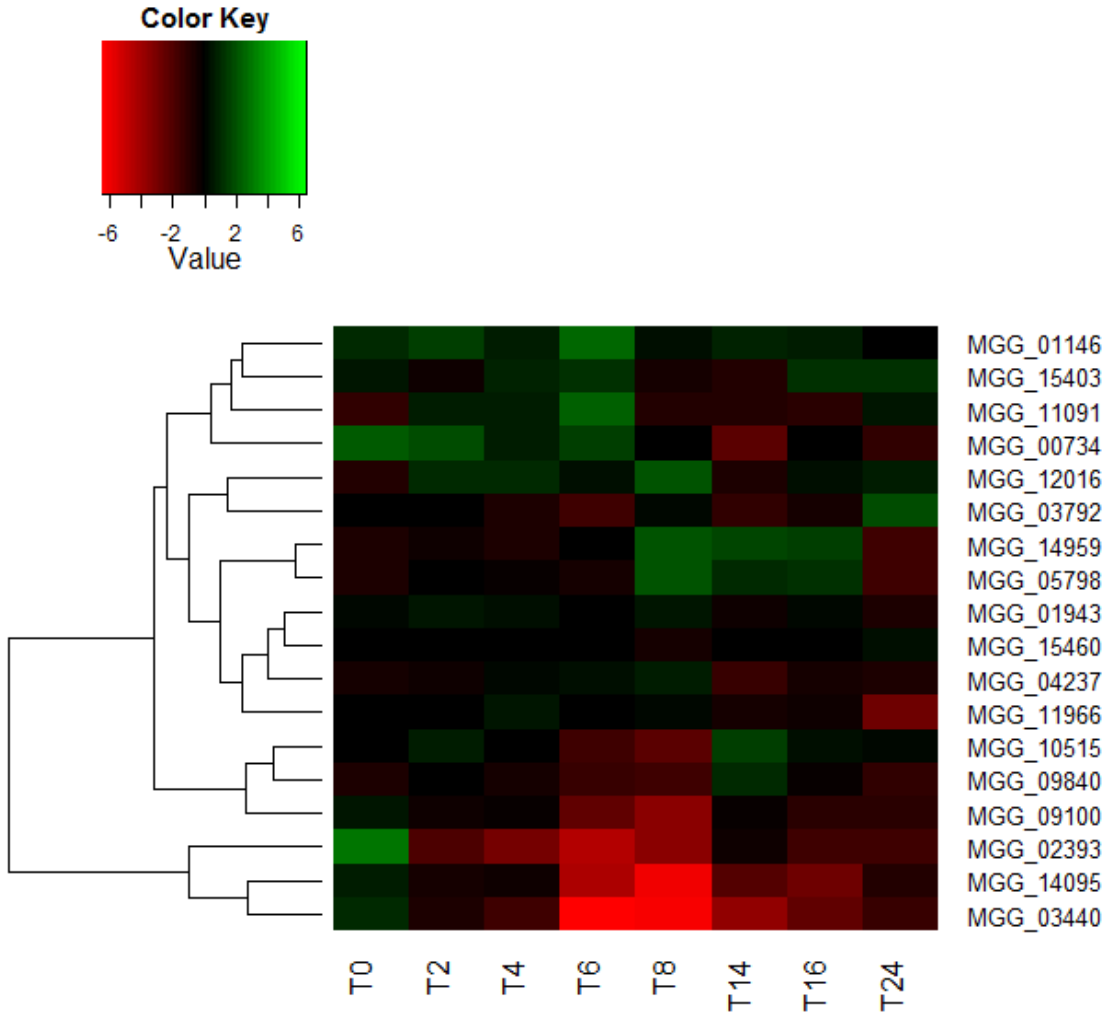

Figure 5.24 Heatmap showing levels of transcript abundance from cutinase domain containing protein encoding genes in the Δ*mst12* mutant compared to Guy11. Heatmap showing levels of transcript abundance during appressorium time course development. Levels of expression are represented as logarithmic fold change of the Δ*mst12* mutant compared to Guy11 during appressorium formation. (red= down-regulated in the *Δmst12* mutant; green= up-regulated in the *Δmst12* mutant).

5.4 Discussion

The response of an organism to a changing environment depends on the perception of external signals through receptors at the plasma membrane, the internalization of these receptor signals and transcriptional reprogramming (Rispail *et al.,* 2009). One mechanism by which signal transduction occurs in eukaryotic cells is by MAP kinase signalling pathways. These are controlled by receptors at the membrane for perception of a signal, by a MAP kinase cascade for internalization of the signal, and ultimately, by transcription factors that genetically re-programme the organism to respond appropriately. Activation of transcriptional re-programming downstream of a MAP kinase signalling pathway occurs through phosphorylation and de-phosphorylation of transcription factors in a hierarchical manner (Roman *et al.,* 2007). However, to establish the hierarchy, and understand it, is a complex process. In *M. oryzae,* the Pmk1 MAP kinase pathway is a global regulatory pathway essential for successful infection by *M. oryzae* (Bruno *et al.,* 2004). This is because Pmk1 controls formation of the infection structure, the appressorium (Bruno *et al.,* 2004). Null mutants of Pmk1 are unable to develop an appressorium and, therefore, to cause rice blast disease (Bruno *et al.,* 2004). Pmk1 is able to phosphorylate transcription factors and modulate their activity in order to promote morphogenetic changes leading to the formation of a functional appressorium. One of the transcription factors downstream of Pmk1 is the zinc finger- and homeobox- domain containing transcription factor, Mst12 (Park *et al.,* 2002). Mst12 is required for infection, controlling formation of the penetration peg and repolarization of the cytoskeleton, both processes required for plant penetration (Dagdas *et al.,* 2012; Park *et al.,* 2002). However, the downstream set of genes regulated by Mst12 is still unknown. For this reason, I set out in the experiments presented in this chapter to

define the downstream targets of Mst12 by carrying out comparative transcriptomics analysis between a null mutant of Mst12 and the isogenic wild type strain Guy11 during a time course of appressorium formation.

The global analysis carried out using Euclidean distance analysis revealed the clustering of the gene expression profile of the Δ*mst12* mutant at 8 h with expression profiles of Guy11 at 2h, 4h and 6 h, suggesting a delay in appressorium development in Δ*mst12*. This result was consistent with the data presented in Chapter 4, Figure 4.1, in which no appressorium was observed until 8 h in the Δ*mst12* mutant, whereas in the wild type strain, appressoria were already observed by 6 h, suggesting a delay in appressorium formation. Moreover, during the time course experiment, the number of down-regulated genes in Δ*mst12* in comparison to Guy11, was always greater than the number of up-regulated genes, except at 4 h. This result is consistent with the predicted role for Mst12 as a transcriptional activator during appressorium development, but also on that causes significant repression of gene expression at 4 h, perhaps normally associated with hyphal development.

In *S. cerevisiae*, the Fus3 MAP kinase phosphorylates the Ste12 transcription factor to regulate transcription of genes containing pheromone response element genes (PREs) in their promoters (Elion *et al.,* 1993). In Chapter 3, comparative transcriptome analysis performed between the Δ*pmk1* mutant and Guy11 revealed a large downstream regulated gene set of Pmk1 MAP kinase. In this chapter, by performing a comparison between the predicted Pmk1-regulated gene set and Mst12-regulated gene set, it was possible to begin to define the global regulatory signature associated with the Pmk1 MAP kinase pathway and one of its downstream

regulatory effectors, Mst12. The analysis revealed a total of 1690 genes that were differentially regulated in both in *Δpmk1* and *Δmst12* mutants compared to Guy11 by at least 4-fold. This gene set is likely to act downstream of the Pmk1 MAP kinase and be regulated by both Pmk1 and Mst12 in at least one time point during appressorium development. Analysis of this gene set revealed a number of predicted biological processes and gene functions that appear likely to be regulated by the Pmk1 MAP kinase pathway.

One surprising group of proteins that appear to be controlled by Pmk1 and Mst12, either directly or indirectly, are the heterokaryon incompatibility (Het) proteins involved in vegetative incompatibility between fungal isolates. Fourteen Het proteins were found to be regulated by Pmk1 and seven Het proteins were found to be regulated by both Pmk1 and Mst12. Het proteins are limited to filamentous ascomycetes and required for heterokaryon incompatibility (HI), which leads to programmed cell death (PCD) in incompatible strain interactions (Fedorova *et al.,* 2005; Glass *et al.,* 2004). HI requires het genes to act either as inducers or suppressors of cell death (Fedorova *et al.,* 2005). Moreover, other related genes such as het-C domain containing genes, were found to be regulated by Pmk1. The het-C domain is present in the protein TinC in *A. nidulans* which stabilizes the mitotic kinase NimA and when overexpressed, affects cell cycle control and growth (Davies *et al.,* 2004). *M. oryzae* contains a total of 42 Het domain containing proteins and their function is still unknown. In other fungal species Het proteins are associated with self/non-self-recognition as well as cellular differentiation and cell death (Fedorova *et al.,* 2005). Therefore, it could be hypothesized that Het proteins found downstream of Pmk1 MAP kinase pathway may be associated normally with hyphal propagation, in which heterokaryon incompatibility is manifested, and are therefore

repressed by the Pmk1 pathway during appressorium morphogenesis. Interestingly, Δ*pmk1* mutants are unable to undergo through autophagic cell death and potentially this is a process that may also be affected by Het proteins, although no experimental evidence has yet been generated to test this idea (Kershaw and Talbot, 2009).

Appressorium formation can be considered a result of an orchestrated set of processes beginning with germination of conidia, hooking, tip swelling, appressorium formation, melanisation, repolarization, penetration peg formation, cuticle penetration and primary invasive hypha development. By looking at appressorium formation in this chronological manner, it is worth predicting that discrete sets of genes may be temporally co-regulated and responsible for each discrete process leading to appressorium formation. This is the hypothesis that led me to perform K-means cluster analysis of gene expression patterns. K-means clustering is an algorithm that classifies genes according to their temporal expression profile (Jain, 2009). Comparative analysis of the Δ*mst12* mutant and Guy11 defined 6 co-regulated patterns of gene expression. Clusters k2, k4, k5 and k6 were interesting in defining clear co-regulated sets of genes. In the case of k2 and k4, differential gene regulation patterns were defined at 14 h, 16 h and 24 h, concomitant with penetration peg emergence and maturation of the appressorium. This is K5 cluster defined an expression profile showing significant down-regulation from 6 h onwards, while cluster k6 showed strong down-regulation at 8 h. Clusters k4 and k5 showed the highest percentage of predicted secreted protein-encoding genes, indicating that Δ*mst12* may be severely impaired in secretion of a large group of proteins during appressorium development. Among these functions were genes associated with cell wall biogenesis, cell wall re-modelling, and extra-cellular depolymerising enzymes. Among these, there was evidence that the cutinase gene family is regulated by the

Pmk1 MAPK pathway. Cutinases are secreted methyl esterases that degrade cutin and facilitate penetration of several phytopathogenic fungal species (Fan and Köller, 1998). Cutinases were first discovered in *Fusarium solani* and found to be involved in pathogenicity (Koller, 1991; Purdy and Kolattukudy, 1975). In certain *Fusarium* and *Colletotrichum* species, cutinases are secreted at the infection site and when chemically or immunologically inhibited, plant penetration is prevented (Koller, 1991). A model explaining the mechanism by which cutinase expression is induced was first described by Kolattukudy in 1985. In this model, basal activity of cutinase genes in the fungal spore generates cutin monomers that in turn, induce the expression of cutinase activity required for plant penetration (Kolattukudy, 1985). In *M. oryzae* there are 18 cutinase domain-containing proteins and up to now, only two cutinase genes, *CUT1* (Sweigard *et al.,* 1992) and *CUT2* (Skamnioti and Gurr, 2007) have been characterized. The Δ*cut2* null mutants formed abnormal appressoria and were reduced in pathogenicity (Skamnioti and Gurr, 2007), while Cut1 was dispensable for infection (Sweigard *et al.,* 1992). Chemical inhibition of cutinases in *M. oryzae* has no effect in plant penetration (Woloshuk *et al.,* 1983). It has been suggested that hydrophobins and cutinases may operate at the leaf surface in a co-ordinated manner (Skamnioti *et al.,* 2008). It is known, for instance, that *A. oryzae* uses RolA or HsbA hydrophobins to recruit cutinases to the leaf surface to degrade cutin (Maeda H, 2005; Ohtaki S, 2006; Takahashi T, 2005). It is not known whether this interplay occurs in the same way in *M. oryzae*, but one of the reasons for the inability of *Δmst12* to cause disease may be that both cutinases and hydrophobins are down-regulated, as suggested by the transcriptional profile analysis presented here. A good approach to test this idea would be first to carry out targeted deletion of the whole cutinase family as predicted in this analysis, starting with those showing the

greatest suppression of gene expression in the Pmk1 and Mst12 mutants. It may also be informative to carrying out RNAi-dependent silencing of all the cutinase genes to determine the precise role in appressorium-mediated infection.

This analysis also demonstrated differential regulation of putative effector-encoding genes of *M. oryzae*. These proteins are likely to play important roles in suppression of plant immunity and proliferation of the fungus in plant tissue. Several biotrophy-associated protein homologues of the *BAS2* family (MGG_07749 and MGG_07969) and *BAS3* (MGG_11610) appear likely to regulated by both Pmk1 and Mst12, showing severe down-regulation in each mutant, compared to Guy11. These effectors are associated with epidermal cell colonisation and spread of *M. oryzae* invasive hyphae (Mosquera *et al.,* 2009), and consistent with this they localize at the periphery of invasive hyphae (Giraldo, M. and Valent, B., personal communication). The localization of these effectors in the *Δmst12* mutant has not been studied yet by live cell imaging, and would be revealing in determining the extent of regulation of these functions by Mst12.

One of the most interesting findings within gene families regulated by both Pmk1 and Mst12, was the identification of fasciclin-domain containing genes. *M. oryzae* possesses three fasciclin domain-containing proteins and two of them were found in clusters k4 and k6 showing down-regulation in gene expression in the Δ*mst12* mutant specially at 8 h, 14 h, 16 h and 24 h, at which time repolarization of the penetration peg begins (Dagdas *et al.,* 2012). Fasciclins are membrane-associated glycoproteins involved in cell adhesion in both plants and animals (Elkins *et al.,* 1990; Huber and Sumper, 1994). The fasciclin domain contains 110-150 amino acids, and the domains show only limited sequence similarity (Johnson *et al.,* 2003). Fasciclins contain a putative GPI anchor region that connects them to lipid

microdomains or lipid rafts (Johnson *et al.,* 2003; Seifert and Roberts, 2007). The first fasciclin protein was described in the fruit fly *Drosophila melanogaster*, Fas1, and was reported to promote cell adhesion (Elkins *et al.,* 1990). In *Arabidopsis thaliana*, fasciclins are a subclass of arabinogalactan proteins (AGPs) and there are several that have been studied as plasma membrane associated signalling molecules (Johnson *et al.,* 2003). For example, in tobacco suspension cultures AGPs link the plasma membrane to the cytoskeleton (Sardar and Showalter, 2007). In the fission yeast, *S. pombe*, Fsc1, contains 5 fasciclin domains, and was shown to localize to the membrane of vacuoles and play a role in fusion of autophagosomes with vacuoles (Sun *et al.,* 2013). In *M. oryzae*, the fasciclin domain containing protein Flp1 (MGG_02884) was identified as differentially regulated by both Pmk1 and Mst12. Flp1 has been previously reported as associated with conidial adhesion and sporulation, with null mutants impaired in turgor generation and pathogenicity (Liu *et al.,* 2009). The role of the other two fasciclin domain containing proteins in *M. oryzae* has not yet been studied yet, but they are also down-regulated in Δ*mst12.* It is possible that these proteins are required for appressorium adhesion to the surface, prior to penetration and functional analysis of the whole family will be required to clarify their function further.

To analyse the hierarchical regulation of transcriptional control by the Pmk1 MAP kinase pathway, an analysis was performed using two different approaches. First, all differentially regulated putative transcription factor-encoding genes were identified during the time course of appressorium development. Second, those transcription factor genes that were highly differentially regulated (4-fold) were selected. This identified a group of 9 predicted transcription factors that were regulated by Pmk1 and Mst12. Among these were members of the Hox family of

transcriptional regulators. *HOX7* was found to be up-regulated in the *Δmst12* mutant at 0 h, suggesting possible regulation of Hox7 by Mst12 perhaps repressing its activity during spore germination. Hox7 is a homeobox transcription factor and null mutants are unable to form appressoria (Kim *et al.,* 2009). In *M. oryzae* a total of eight homeobox transcription factors have been identified, including Mst12. Global analysis indicates that *HOX5* (MGG_07437), *HOX6* (MGG_11712), *HOX1* (MGG_04853), *HOX2* (MGG_00184) are all regulated by Pmk1, and *HOX7* by both Pmk1 and Mst12. The homeobox transcription factors contain a DNA binding domain called the homeodomain, which was first discovered in *Drosophila melanogaster* and involved in body segmentation and patterning, including the well known *Ultrabithorax* and *Antennapodia* mutations (Burglin, 1994; McGinnis and Krumlauf, 1992). The importance of this family of transcription factors has been also shown in fungi. In the basidiomycetes *Ustilago maydis*, the transcription of homeobox genes increases dramatically following pheromone treatment and formation of the dikaryotic filament itself requires genes directly regulated by homeobox transcription factors (Casselton and Olesnicky, 1998; Urban *et al.,* 1996) and the well-known bE/bW mating system involves dimerization of two homeodomain transcription factors (Kamper *et al.,* 1995). Among transcription factors, homo- and hetero- dimerization is a common regulatory mechanism of transcription. As a consequence, it may be that homeobox transcription factors might interact with one another to regulate genes downstream of the Pmk1 MAP kinase signalling pathway, providing more permutations and potential plasticity to the transcriptional response. Moreover, the Mst12 transcription factor (also called *HOX8* in Kim *et al.,* 2011) is potentially phosphorylated by Pmk1 to regulate gene expression and this might, for example, affect its propensity to dimerize with other Hox proteins, such as Hox7, given the similarity in their mutant

phenotypes. In future it will be necessary to investigate the interactions between these transcription factors by, for example, bimolecular fluorescence complementation systems (BiFC) (Papadopoulos *et al.,* 2012). Moreover, comparative transcriptome analysis of a Δ*hox7* mutant during a time course of appressorium development would be revealing when compared to the expression data of *Δmst12* and *Δpmk1* mutants in order to define more closely the precise hierarchy of transcriptional regulation of appressorium formation.

In summary, the transcriptional profiling analysis reported here has allowed definition of gene sets regulated by Pmk1 and Mst12, and established that co-regulation of groups of genes such as chitinases, BAS effectors, cutinases, secreted proteins and fasciclins occurs during appressorium development. Moreover, the analysis provided evidence that Mst12 also specifically regulates a sub-set of gene functions, independently of Pmk1. These results are discussed in the context of the role of the cell cycle in regulating appressorium morphogenesis in the General Discussion section presented in Chapter 7.

6 An S-phase checkpoint is necessary for appressorium-mediated plant infection in the rice blast fungus *Magnaporthe oryzae*

6.1 Introduction

In all eukaryotic organisms, cell cycle progression must occur in a uni-directional order, to ensure that late events of the cell cycle do not occur before completion of earlier events (Elledge, 1996; Murray, 1992; Russell and Nurse, 1986). In order to ensure this correct ordering, cells possess cell cycle checkpoints to control each stage of the cell cycle (Hartwell and Weinert, 1989). When a problem occurs in DNA replication, for example, or when DNA damage is encountered, cell cycle checkpoints are activated to cause an arrest in the cell cycle and allow DNA repair to occur (Murray, 1992; Russell*, 1998). However, it is not known whether the replication checkpoint is constitutively active or only becomes activated when a problem with DNA replication is detected (Elledge, 1996). Eukaryotic cells possess three DNA damage checkpoints operating at G1 phase, S-phase and G2-phase (Rhind and Russell, 1998). When DNA damage occurs at G1-phase, cells arrest before committing to a new cell cycle, in order to repair DNA before proceeding. When DNA damage occurs at S-phase, cells delay progression of DNA replication in order to allow the cell to repair the problem. When DNA damage occurs at G2-phase, cells prevent progression of the cycle into mitosis to allow DNA repair (Elledge, 1996; Kastan and Bartek, 2004). DNA damage checkpoints have increasingly being studied in the medical field because mutations in DNA repair genes increase genetic instability, therefore predisposing cells to develop cancer (Kastan and Bartek, 2004; Parsons *et al.,* 1995).

The model organisms for cell cycle studies over the past decades have been the fission yeast *Schizosaccharomyes pombe* and the budding yeast *Saccharomyces cerevisiae*, and although they share some similarities in the function of DNA damage and replication checkpoints, the way that cell cycle progression is regulated is different and therefore the molecular mechanism associated with the checkpoints also differs.

Cell cycle progression is driven by the binding of cyclin-dependent kinases (Cdc28 in *S. cerevisiae*, CDK1 in Mammals and Cdc2 in *S. pombe*) to specific cyclins of each phase of the cell cycle (Coudreuse and Nurse, 2010). The activation of CDK depends on the cyclins. and the specific cyclin to which the CDK binds determines the activation of downstream processes (Coudreuse and Nurse, 2010). The activity of CDK increases with cell cycle progression, reaching a maximum during mitosis and a dramatic decrease afterwards (Coudreuse and Nurse, 2010). In *S. pombe* and higher eukaryotes, DNA damage causes a cell cycle arrest as a result of the inhibitory phosphorylation of the main cyclin-dependent kinase, Cdc2, at the tyrosine-15 residue (Rhind and Russell, 1998). The inhibitory phosphorylation of Cdc2 is carried out by the kinases Wee1 and Mik1 (Lundgren *et al.,* 1991) and maintained through inhibition of the activator phosphatase Cdc25 (Millar *et al.,* 1991; Russell and Nurse, 1986). Inhibition of Cdc25 is caused by the DNA damage-checkpoint kinases, Cds1 and Chk1, via phosphorylation at serine residues 99, 192 and 359, allowing the 14-3-3 proteins to bind and inhibit it (Furnari *et al.,* 1999; Zeng *et al.,* 1998). The DNA damage checkpoint pathway consists of several sensors on DNA that immediately send signals to downstream kinases that ultimately, inhibit the entry into mitosis and induce DNA repair genes (reviewed in Elledge, 1996). Cds1 and Chk1 are effector kinases in the DNA damage checkpoint pathway (Murakami

and Okayama, 1995; Walworth *et al.,* 1993). Both Cds1 and Chk1 are activated through Rad3 which, by forming a complex with Rad26, senses the stalled replication forks in DNA and transmits the signal (Noguchi *et al.,* 2003).

In *S. cerevisiae*, the DNA replication checkpoint acts in a different way and seems to be separated into a Chk1-response and a Rad53-mediated response. DNA replication stress and DNA damage activate the phosphoinositide 3-kinases, Tel1 and Mec1, the homologues of ataxia telangiectasia mutated (ATM) and ataxia telangiectasia (ATR) in humans (Sun and Fasullo, 2007). Tel1 and Mec1 transduce the signal through phosphorylation of the effector kinases Chk1 and Rad53 to arrest the cell cycle (Sanchez *et al.,* 1996). Activated Chk1 phosphorylates the anaphase inhibitor Pds1, preventing its degradation (Sun and Fasullo, 2007; Wang *et al.,* 2001). Pds1 inhibits sister chromatid separation by inhibiting the protease Esp1 and therefore arresting the cell cycle prior to anaphase (Ciosk *et al.,* 1998). Activated Rad53 phosphorylates the transcription factor Swi6, blocking its activity, to regulate transcription of G1 cyclins, Cln1 and Cln2, required for G1 to S phase transition (Sidorova and Breeden, 1997). The activated Rad53 also interacts with the replication complex Cdc7-Dbf4 that is essential for initiation of DNA replication in eukaryotes (Ogi *et al.,* 2008). In the presence of hydroxyurea (HU), which inhibits DNA replication, Rad53 phosphorylates Dbf4 causing its removal from chromatin and stalling the initiation of replication. Therefore, it has been proposed that Cdc7-Dbf4 plays a role in the full activation of Rad53 (Ogi *et al.,* 2008; Pasero *et al.,* 1999). Another target of Rad53 is a fork head domain-containing protein kinase called Dun1 (Bashkirov *et al.,* 2003). Dun1 is the downstream target of Rad53 that regulates the ribonucleotide reductase (RNR) regulon and genes required for DNA repair (Zhou and Elledge, 2000). Via Rad53 and Dun1, arrest of the cell cycle occurs by inhibiting

the polo kinase Cdc5, which is required for mitotic-cyclin degradation, preventing cells from exiting mitosis (Sanchez *et al.,* 1999). Therefore arrest of the cell cycle following DNA damage in *S. cerevisiae* does not depend on inhibitory phosphorylation of Cdc28, but on the inhibition of origin firing and chromosome segregation (Amon *et al.,* 1992; Sanchez *et al.,* 1999; Santocanale and Diffley, 1998; Sorger and Murray, 1992). Indeed, the inhibitory phosphorylation of Cdc28 in *S. cerevisiae* does not occur at the tyr-15 residue of Cdc2 as in *S. pombe* (Gould and Nurse, 1989) or in the thre-14 and tyr-15 residues, as in mammals (Liu *et al.,* 1997; Parker *et al.,* 1992), but rather in the tyr-19 of Cdc28, via the inhibitory kinase Swe1 (Booher and W.Kirschner, 1993; Sorger and Murray, 1992). Swe1 is a protein kinase related to the morphogenetic checkpoint of *S. cerevisiae* (Lew, 2003). Over the course of the cell cycle, the timely degradation of Swe1 in *S. cerevisiae* is required for the switch from apical growth to isotropic growth during budding (Pruyne and Bretscher, 2000). Swe1 degradation depends on Nim1-kinases, septins, and also the ubiquitin ligases Dma1 and Dma2 (McMillan *et al.,* 2002; Raspelli *et al.,* 2011). However, Swe1 degradation also depends on Rad53 (Smolka *et al.,* 2006). Null mutants of Rad53 show abnormal hyperpolarized buds as a result of accumulation of Swe1 (Smolka *et al.,* 2006). Moreover, Rad53 interacts with septins in a FHA-dependent manner in the bud neck, and it has been suggested that the septin Shs1 may play a role in the DNA replication checkpoint, but this has still not been well defined (Enserink *et al.,* 2006).

The role of the morphogenetic checkpoint and DNA damage checkpoint has been also studied in other fungi, such as *A. nidulans* (Malavazi *et al.,* 2006) and *N. crassa* (Wakabayashi *et al.,* 2008). However, the best example of detailed analysis is

in the basidiomycete corn smut fungus *Ustilago maydis*, whose dikaryotic filament requires a G2 cell cycle arrest for plant infection, which is dependent on the DNA damage kinase Chk1. This supports the idea that DNA damage kinases serve other distinct roles in addition to DNA damage response (Malavazi *et al.,* 2006; Mielnichuk *et al.,* 2009; Perez-Martin, 2009). Therefore the targets of these kinases have evolved differently in different organisms (Rhind and Russell, 1998).

In *M. oryzae*, the ability of the fungus to infect and form appressoria is tightly dependent on cell cycle checkpoints (Saunders *et al.,* 2010a; Veneault-Fourrey *et al.,* 2006). However, little is known about the cellular mechanisms and proteins involved in these cell cycle checkpoints. The first checkpoint occurs at S-phase and is required for appressorium formation by *M. oryzae*. This checkpoint coincides with the early stages of conidial development with the switch from apical to isotropic growth in the germ tube, which is required for formation of an incipient appressorium (Saunders *et al.,* 2010a). When germinating conidia are treated with hydroxyurea, the fungus is unable to develop incipient appressorium and instead, a long germling is formed (Saunders *et al.,* 2010a). Moreover the temperature sensitive mutant in the regulatory subunit of the Dbf4-Cdc7 kinase complex, *Δnim1*^{ts} when incubated at restrictive temperature, arrests at S-phase and therefore is unable to form incipient appressoria (Saunders *et al.,* 2010a). Maturation of the appressorium and the ability to penetrate plant cells are also cell cycle-regulated processes. At a restrictive temperature the temperature sensitive mutant *ΔnimA*^{ts} develops non-melanised appressorium that are unable to cause disease (Saunders *et al.,* 2010a). Moreover, when mitosis exit is inhibited by the Δ*bimE*^{ts} mutant at restrictive temperature, the mutants are unable to cause plant disease suggesting that the completion of mitosis is a pre-requisite for appressorium-mediated plant infection (Saunders *et al.,* 2010a).

In fact, after mitosis and degeneration of the conidium in an autophagy-dependent programme, a single nucleus-containing appressorium is left at the time of penetration (Kershaw and Talbot, 2009; Veneault-Fourrey *et al.,* 2006). However, it is not known whether further phases of the cell cycle are required for appressorium repolarization and penetration peg formation.

In this chapter I describe work carried out to investigate cell cycle regulation associated with re-polarization of the mature appressorium and the formation of the penetration peg required for plant infection by the rice blast fungus *M. oryzae*. I set out to determine whether cell cycle control is necessary for the appressorium to be able to re-polarise and elaborate a penetration hypha for plant infection.

6.2 Materials and methods

6.2.1 Standard procedures

For standard procedures see Chapter 2 of this study.

6.2.2 *In vitro* appressoria germination and formation assay with HU treatment

Germination and formation of appressoria was carried out *in vitro* using borosilicate 18 x 18 glass coverslips (Fisher Scientific UK Ltd). The method was adapted from Hamer *et al.* 1988. Conidia were harvested (as described in 2.1.1) and a suspension of 5 x 10^4 conidia mL^{-1} prepared in double distilled water and incubated in a controlled environment chamber at 24℃. Fifty microliters of the conidial suspension were placed onto the coverslip surface. When required, the DNA-replication inhibitor hydroxyurea (HU) was used at 200 mM (Saunders *et al.,* 2010) by removing the water from the germinating spores and replacing with HU. Coverslips were then incubated in a controlled environment chamber at 24℃ for the period of time required for the specific experiment.

6.2.3 Onion epidermis infection assay in HU treatment

Onion epidermis layers were separated, washed in chloroform for 15 minutes and then washed several times in water. The epidermis layers were cut into small squares and placed onto microscope slides. A conidial suspension of 5 x 10^4 conidia mL^{-1} was prepared in double distilled water and a 50 µL drop was inoculated onto the onion epidermis layers. When HU was needed in the experiment the water was removed from the onion surface and replaced with 50 µL of 200 mM HU. The inoculated slides were incubated in a controlled environment chamber at 24℃ and

high relative humidity for the period of time required for the specific experiment. The percentage of penetration events were monitored and examined by microscopy.

6.2.4 Rice leaf sheath infection assay in: HU experiments, Benomyl experiments or block and release experiments with HU

To observe the invasive hyphae inside the cells, the rice leaf sheath method, adapted from Kankanala *et al.,* (2007), was used. A conidial suspension of 5 x 10^4 conidia mL^{-1} was prepared in sterile double distilled water and inoculated onto leaves of 3- 4 week old rice seedlings. The inoculation was performed with a syringe on the leaf vein and incubated in a controlled environment chamber at 24 ℃ for the period of time required for the specific experiment. In an HU experiment, at the desired time, 1 M of HU was added into the leaf sheath with a syringe after removal of the internal water from the sheath from the initial inoculation. In the case of benomyl experiments, the same procedure was followed but instead, 50 µg mL^{-1} were added (Veneault-Fourrey *et al.,* 2006). After the addition of either HU or benomyl, the samples were incubated in a controlled environment chamber at 24 ℃ for the period of time required for the specific experiment. Afterwards, an epidermal leaf layer was dissected using a blade and mounted into a microscope slide for analysis.

6.2.2 Multiple amino acid sequence alignment

Public available databases were searched using protein sequences based on homology to *M. oryzae* as the query. Sequences were aligned using CLUSTALW (Thompson *et al.,* 1994) and using BOXSHADE (http://www.ch.embnet.org/software/BOX_form.html) which depicts identical amino acids in black, similar amino acids in grey and non-identical residues are unshaded.

6.3 Results

6.3.1 Cell cycle progression during plant penetration

The cell cycle of *M. oryzae* starts when a three-cell conidium lands on the surface of a leaf. Leaf characteristics, such as hydrophobicity or hardness, trigger germination of the spore. In the apical cell of the conidium a single round of mitosis occurs and one of the daughter nuclei moves towards the developing appressoria whereas the other returns back to the apical cell of the conidia. Appressorium formation is a cell cycle coupled process, and DNA replication is also required. As the appressorium matures, the conidium will go through an autophagy-dependent process in which the three nuclei of the conidia will be degraded. At the moment at which the penetration peg starts to form there is only one nucleus inside the appressorial dome (Fig. 6.1, panel A). The penetration peg elongates further inside the cell and the nucleus migrates (Fig. 6.1, panel B) to be able to divide and form the primary invasive hyphae containing two nuclei (Fig. 6.1, panel C).

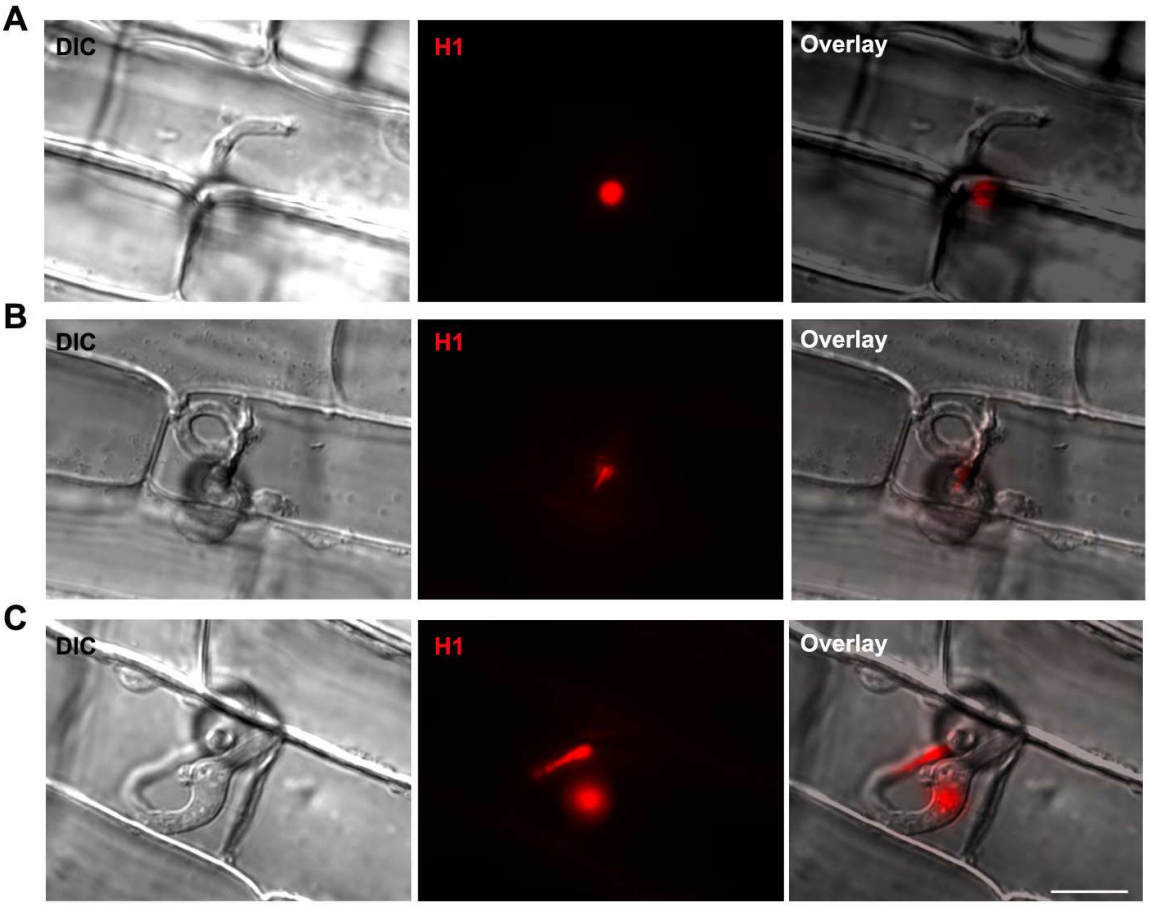

Figure 6.1 *M. oryzae* nuclear progression during plant penetration. Live cell imaging of CO-39 rice leaf sheath infections of *M. oryzae* Guy11 strain expressing H1-RFP. **A)** Micrograph of a penetration peg emerging from an appressorium containing a single nucleus. **B)** Micrograph showing a nucleus migrating through the peg **C)** Micrograph of primary invasive hyphae containing two nuclei. (bar= 10 µm).

6.3.2 HU blocks plant penetration by *M. oryzae* in rice leaf sheath and in onion epidermis

In *M. oryzae,* when germinating conidia are treated with HU, the formation of appressoria is inhibited, supporting the finding that appressorium initiation and formation is S-phase regulated (Saunders *et al.,* 2010a). Hydroxyurea is a DNA replication inhibitor which inhibits ribonucleotide reductase, preventing the DNA polymerase from obtaining nucleotides (Yarbro, 1992). In order to determine the cell cycle checkpoints during plant penetration, we first decided to evaluate the effect of hydroxyurea (HU) in plant penetration.

To optimize the concentration of HU to use, a leaf sheath experiment and leaf drop experiment in which 200 mM, 500 mM, 800 mM and 1 M HU were used, was carried out (Fig. 6.2). In the leaf sheath experiment, the different HU concentrations were inoculated at 10 h, and the results were scored at 30 h (Fig. 6.2, panel A). The results indicated that in the control experiment, where no HU was added, the penetration frequency was 93.2%. With the addition of 200 mM HU, the penetration frequency was 85.8%, at 500 mM it was 51.4%, at 800 mM it was 25.3%, and at 1 M it was 11.5%. For the leaf drop experiment the different HU concentrations were inoculated at 10 h and results were scored at 5 dpi. The leaf spot assay showed a normal infection lesion when no HU was added. Following addition of 200 mM lesions were still visible showing a high degree of necrotic area, whereas at 500 mM HU the symptoms on the leaf are less dramatic, and at 800 mM HU and 1 M HU symptoms were not perceptible (Fig. 6.2, panel B). This result indicated that HU blocks plant penetration in a dose-dependent manner.

To observe the effect of HU on nuclear division and plant penetration, a Guy11 strain expressing H1-RFP was inoculated into 28 day-old rice leaf sheath of cultivar CO-39 and incubated at 25 ℃ for 10 h when 1 M HU was added. At 30 h, non-HU treated leaf sheath, showed formation of the primary invasive hyphae with multiple nuclei (Fig. 6.3). However, under 1 M HU treatment, appressoria were unable to form a penetration peg and form invasive hyphae and only contained one nucleus, suggesting that completion of S-phase is necessary for penetration peg formation (Fig. 6.3, panel A). To quantify the result, percentage penetration into the leaf sheath was determined for 100 appressoria, and the experiment repeated three times. The control showed 80% penetration, whereas in the HU-treatment this decreased to 15% penetration (Fig. 6.3. panel B). The same experiment was performed in onion epidermis (Fig. 6.3. panel C). A Guy11 strain expressing H1-RFP was inoculated onto onion epidermis and incubated at 25 ℃ for 14 h, after which 200 mM HU was added. At 48 h, the non-HU treated sample showed formation of primary invasive hyphae containing multiple nuclei. However, in the HU treated sample, no primary invasive hyphae were found, suggesting that the completion of DNA synthesis is required for the formation of the penetration peg and primary invasive hyphae in onion epidermis.

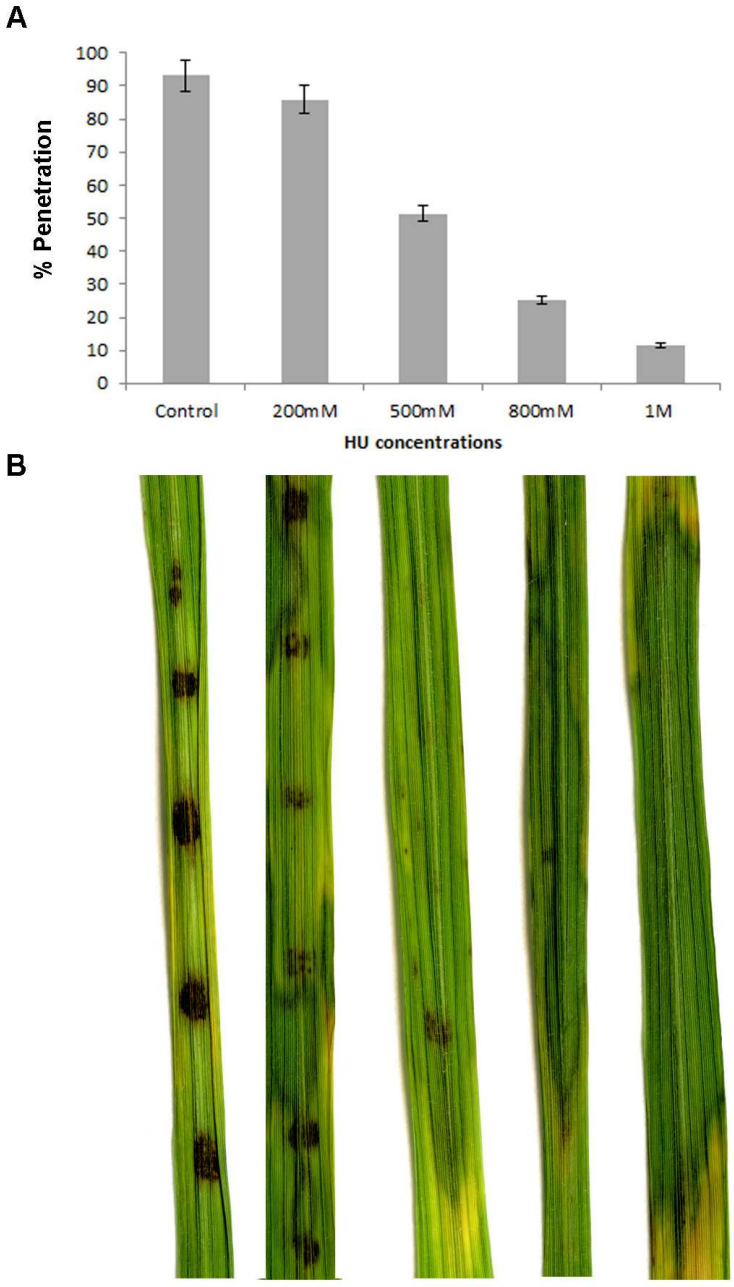

Figure 6.2 Determining the significance of S-phase control for plant penetration by *M. oryzae*. **A)** Bar chart showing the effect of 200 mM, 500 mM, 800 mM and 1M HU concentrations on rice leaf sheath into 28 day-old CO-39 rice plants. HU was added at 10 hpi and results were scored at 30 h in 3 biological replicates (n=50) (* denotes $p<0.05$; two-tailed t-test, $p=0.047$). **B)** Effect of 200 mM, 500 mM, 800 mM and 1 M HU concentrations on a leaf spot assay of wild-type Guy11 into 28 day-old CO-39 rice plants. HU was added at 10 h and leafs were harvested at 5 dpi.

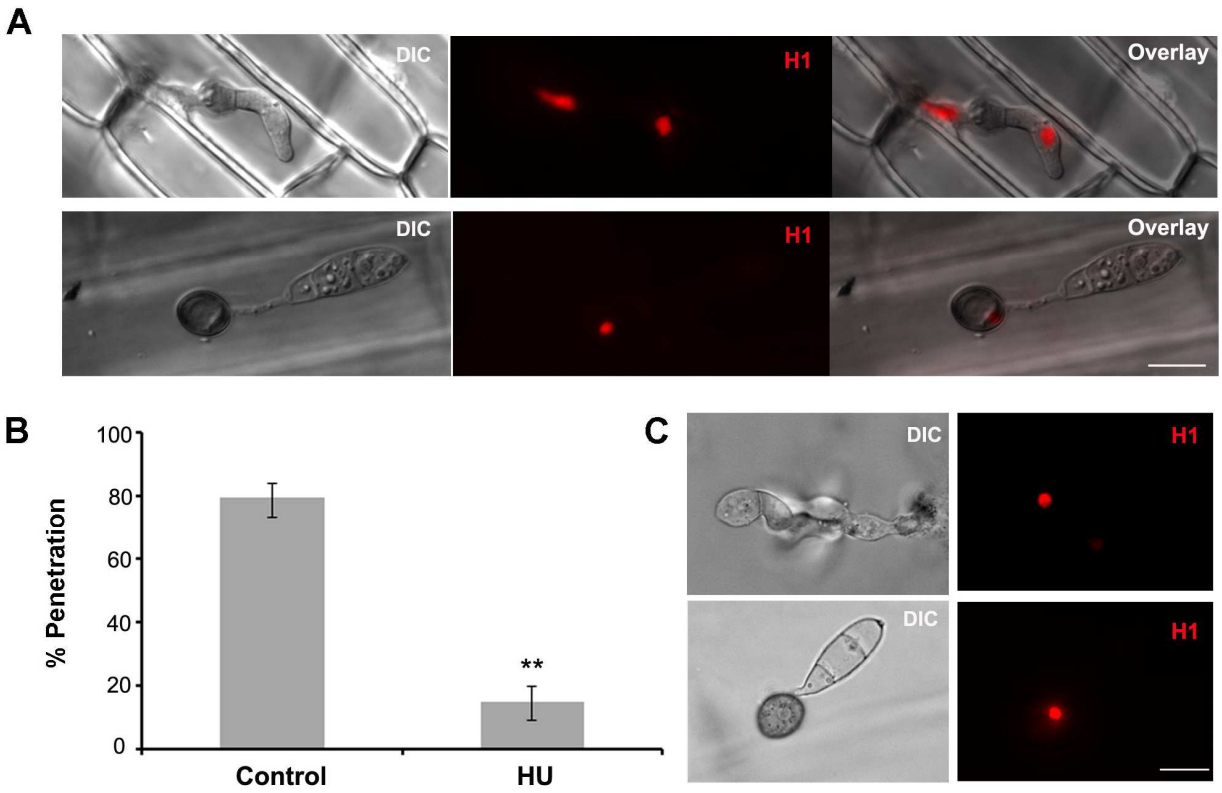

Figure 6.3 *M. oryzae* penetration peg formation is regulated at S-phase. *M. oryzae* is unable to penetrate when S-phase is blocked. **A)** CO-39 rice leaf sheath of wild-type Guy11 H1-RFP infection at 30 h (upper panel) and 30 h when HU treated at 10 h (bottom panel). **B)** Bar chart showing the relative abundance of appressoria forming penetration peg in wild-type Guy11 H1-RFP non- treated and HU treated. The graph represents three biological with two technical replicates observation of 100 appressoria. **C)** Onion epidermis wild-type Guy11 H1-RFP assay at 40 h. (bar= 10 µm).

6.3.3 S-phase occurs before 16 hpi during plant infection

To determine the exact time at which DNA replication occurs prior to plant penetration, a leaf sheath experiment and a leaf spot experiment were performed in which 1 M HU was added at 14 h, 16 h, 18 h and 20 hpi. In the leaf sheath experiment, the HU was added at different time points and the results were scored at 45 h (Fig. 6.4, panel A). The results indicated that in the control, where no HU was added, the percentage of appressorium-mediated penetration was 89.8%; however when HU was added at 14 h the percentage of penetration was 34.4%, at 16 h was 64.2%, at 18 h was 76.2% and at 20 h was 92%. For the leaf drop experiment the HU was inoculated at different time points and the results were scored at 5 dpi (Fig. 6.4, panel B). The leaf spot assay showed a normal infection lesion when no HU was added. When HU was added at 14 h only a faint small halo of lesions was visible, however, at 16 h, 18 h and 20 h lesions showed a high degree of necrosis (Fig. 6.4, panel B). These results showed that HU was only able to block plant penetration significantly when it was applied before 16 h, suggesting that DNA replication or S-phase happens before 16 hpi during appressorium formation.

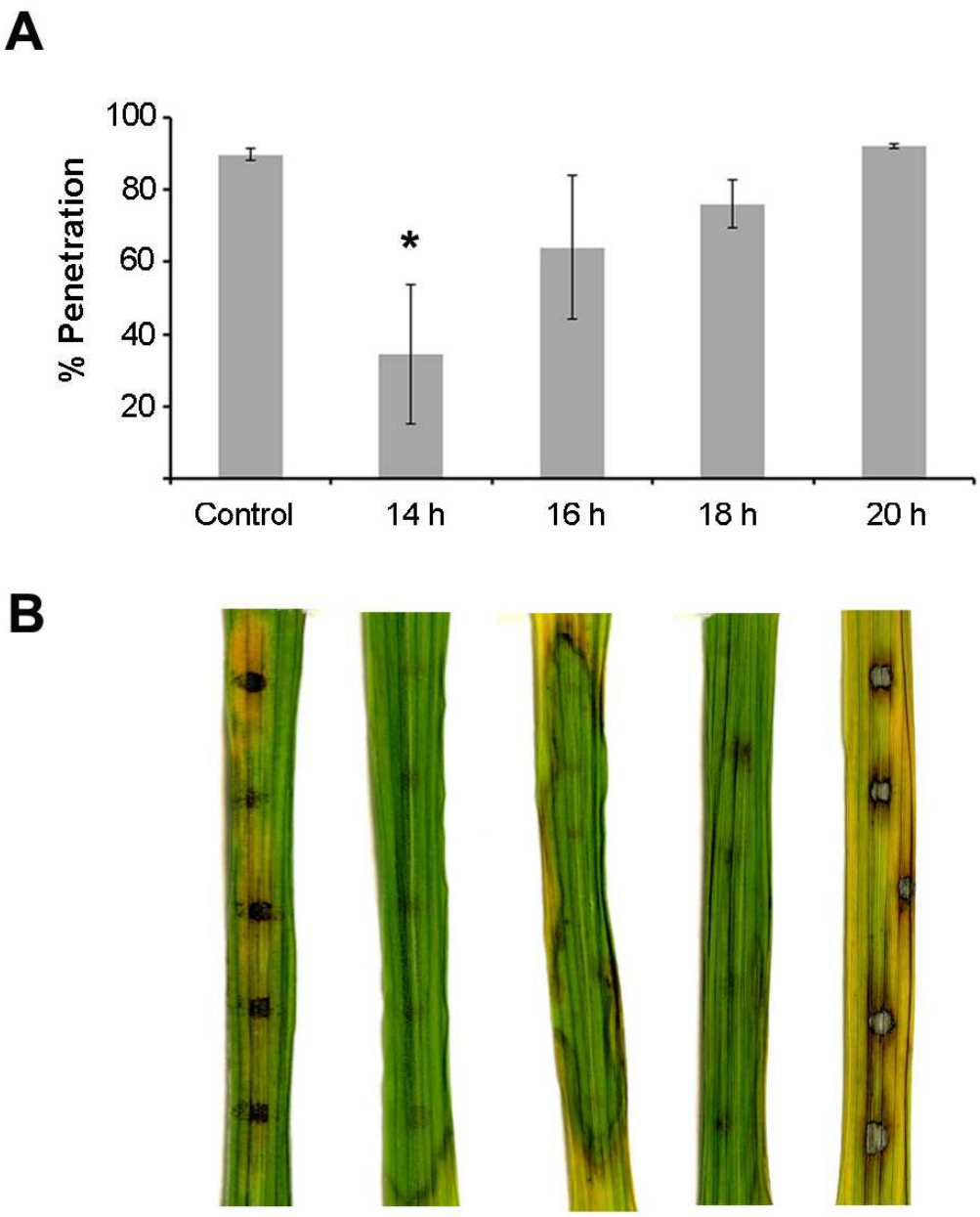

Figure 6.4 HU blocks *M. oryzae* plant penetration in a time-dependent manner. A) Bar chart showing the effect of 1 M HU at 14 h, 16 h, 18 h, 20 h on rice leaf sheath 28 day-old CO-39 rice plants. HU was applied at 10 h and disease symptoms quantified at 30 h. The result represents 3 biological replicates (n=50). **B)** Effect of 1 M HU at 14 h, 16 h, 18 h, 20 h on a leaf spot assay of wild-type Guy11 into 28 day-old CO-39 rice plants. HU was inoculated at 10 h and leaves were harvested at 5 dpi.

6.3.4 Block and release experiment of plant penetration of *M. oryzae* in rice leaf sheath

Having shown that HU blocks plant penetration, it was necessary to demonstrate that addition of HU did not cause appressoria to be non-functional and therefore, unable to form a penetration peg due to a toxic effect. To investigate this, a block and release experiment in a rice leaf sheath was performed. The experiment consisted of using 1 M of HU at 14 h to block plant penetration, at 20 h, to wash away the HU, and at 45 h to score the result in order to observe whether appressorium-mediated penetration is restored (Fig. 6.5). The results indicated that in the control experiment, in which no HU was added, at 45 h it was possible to observe a 97% (SE ± 0.52) of penetration and the presence of bulbous hyphae within the host cells containing multiple nuclei. On the other hand, in the blocked treatment in which 1 M of HU was added at 14 h, the results at 45 h showed a 31% (SE ± 4.34) penetration frequency and the presence of single nuclei-containing appressoria with no penetration pegs. In the released treatment, in which HU was washed away with sterile water at 20 h, the results at 45 h showed significant differences with the blocked treatment. The frequency of penetration was 81% (SE ± 11.52), which accounts for a 50% recovery in plant penetration compared to the HU-block experiment. These results showed that plant penetration can be restored after HU treatment, therefore demonstrating the viability of appressoria after HU treatment.

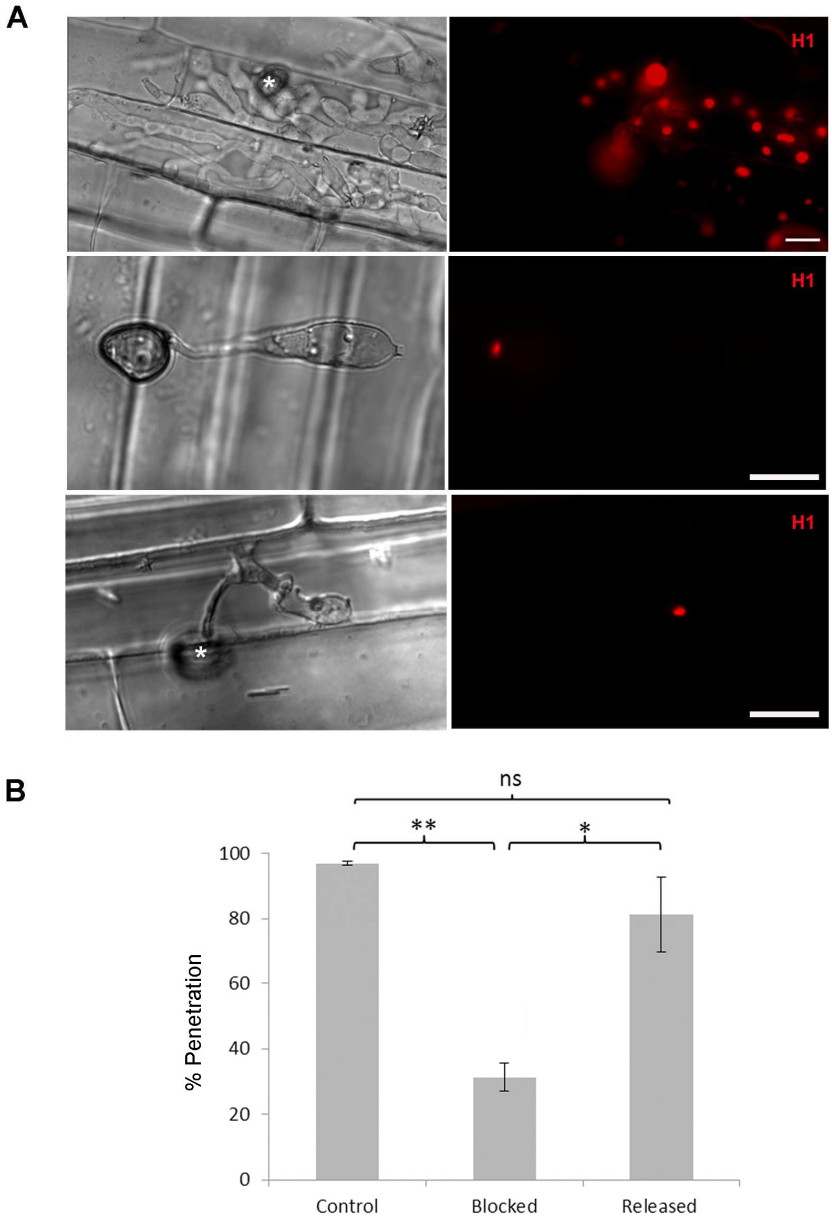

Figure 6.5 HU block and release experiment of *M. oryzae* in rice leaf sheath. A) Micrographs showing the block and release experiment of *M. oryzae* in rice leaf sheath. Upper panel shows the control in which no HU was added. Middle panel shows the block treatment in which 1 M of HU was added at 10 h. Bottom panel shows the release treatment in which HU was washed away at 20 h with sterile water. All the micrographs were taken at 45 h (* denotes the site of the appressorium; bar= 10µm). **B)** Bar chart showing the restoration of penetration when HU was washed away (Released) compared to the treatment of 1M HU (Blocked) in which penetration was prevented. on a leaf sheath assay of wild-type Guy11 on 28 day-old CO-39 rice plants. HU was inoculated at 10 h and was washed away at 20 h (* denotes $p<0.05$; ** denotes $p<0.01$).

6.3.5 Arrest at G2/M does not prevent plant penetration of *M. oryzae* in rice leaf sheath

Having shown that plant penetration is dependent upon successful DNA synthesis phase (or S-phase), it was still unclear whether transition to later phases of the cell cycle, such as G2 or M, is also required for plant penetration. To investigate this, the microtubule destabilizing agent benomyl was used to arrest the cell cycle in G2/M and then observe the effect on plant penetration (Veneault-Fourrey *et al.,* 2006). A leaf sheath experiment was set up in which 50 µg mL^{-1} of benomyl (Giraldo *et al.,* 2013) was added at 10 h and the results scored at 30 h (Fig. 6.6, panel A). The results in the control experiment, in which no benomyl was added, indicated that the frequency of appressorium-mediated penetration was 71.9% (SE ± 9.71) and primary invasive hyphae were observed containing multiple nuclei. Benomyl treatment showed no significant differences to the control and the percentage of penetration was 61.5% (SE ± 5.58). Moreover, the number of nuclei was quantified in the presence and absence of benomyl (Fig. 6.6, panel C). The results indicated that the number of appressoria that had penetrated containing one nucleus was higher in the presence of benomyl when compared to the control in which no benomyl was added. This correlates with the fact that the nucleus in the appressoria, when treated with benomyl, arrests in G2/M, preventing a further mitosis to occur and producing two nuclei in the primary invasive hyphae.

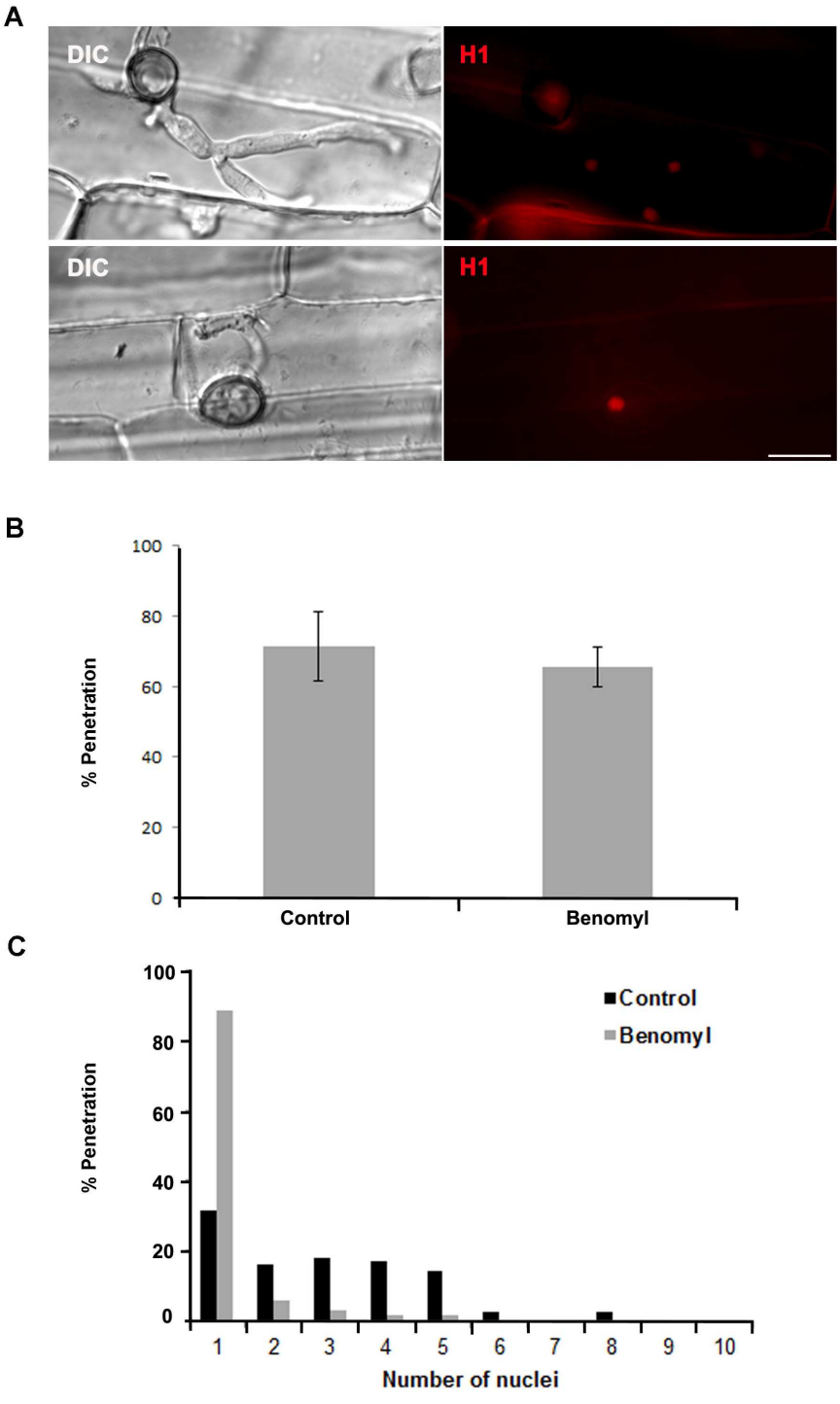

Figure 6.6 Benomyl treatment does not prevent plant penetration in *M. oryzae*. A) Micrographs at 30 h of Guy11 expressing H1-RFP inoculated on a rice leaf sheath showing the control at 30 h in which no benomyl was added (upper panel) and the benomyl treated at 10 h (bottom panel). **B)** Bar chart showing the effect of benomyl on the percentage appressorium mediated penetration. C) Bar chart to show the effect of benomyl treatment in the number of nuclei during penetration. (bar= 10 µm).

6.3.6 Using a genetic approach to investigate cell cycle progression in *M. oryzae* during plant penetration

6.3.6.1 Investigating the effect of S-phase arrest on plant penetration using the Δ*nim1*^{ts} mutant

Appressorium morphogenesis in *M. oryzae* is regulated through checkpoints of the cell cycle (Saunders *et al.,* 2010a). The first checkpoint controlling appressorium morphogenesis is the S-phase. Nim1 is the functional homologue of Dbf4 in *S. cerevisiae* and it has been shown to form a complex with Cdc7 kinase required for S-phase initiation (Jackson *et al.,* 1993). In *M. oryzae, a* Δ*nim1*^{ts} mutant is unable to replicate DNA and cannot develop incipient appressoria, demonstrating that successful completion of DNA replication is a pre-requisite for appressorium initiation (Saunders *et al.,* 2010a). Appressorium initiation and plant penetration are also inhibited when conidia are treated chemically with the DNA replication inhibitor HU. We decided to use the Δ*nim1*^{ts} strain to test genetically the effect of S-phase arrest in plant penetration and confirm the findings of chemical inhibition described above.

To test whether successful DNA replication is necessary for plant penetration, a leaf sheath experiment was prepared using the wild-type strain Guy11 and Δ*nim1*^{ts} mutant strain, which were incubated under standard conditions at 24 ℃ and then shifted to a semi-permissive temperature of 29 ℃ at 10 h. After 30 h post inoculation, rice leaf tissue was dissected and observed microscopically (Fig. 6.7). The results indicated that at both 24 ℃ and 29 ℃ Guy11 showed normal rates of appressorium-mediated penetration, 83% (SE±5.93) and 87% (SE±1.16) respectively. Moreover, the Δ*nim1*^{ts} mutant at 24 ℃ showed normal rates of

penetration, 62% (SE±5.93), when compared to Guy11 at 24 ℃ (n=100, two-tailed t-test, p=0.069). However, the percentage penetration of Δ*nim1*^{ts} at 29 ℃ was significantly reduced (16%; SE±9.52) compared to Guy11 at 29 ℃ (n=100, two-tailed t-test, p=0.0017) and to Δ*nim1*^{ts} at 24 ℃ (n=100, two-tailed t-test, p=0.014). This result indicates that successful DNA replication is required for appressorium initiation and also for penetration peg formation and plant penetration.

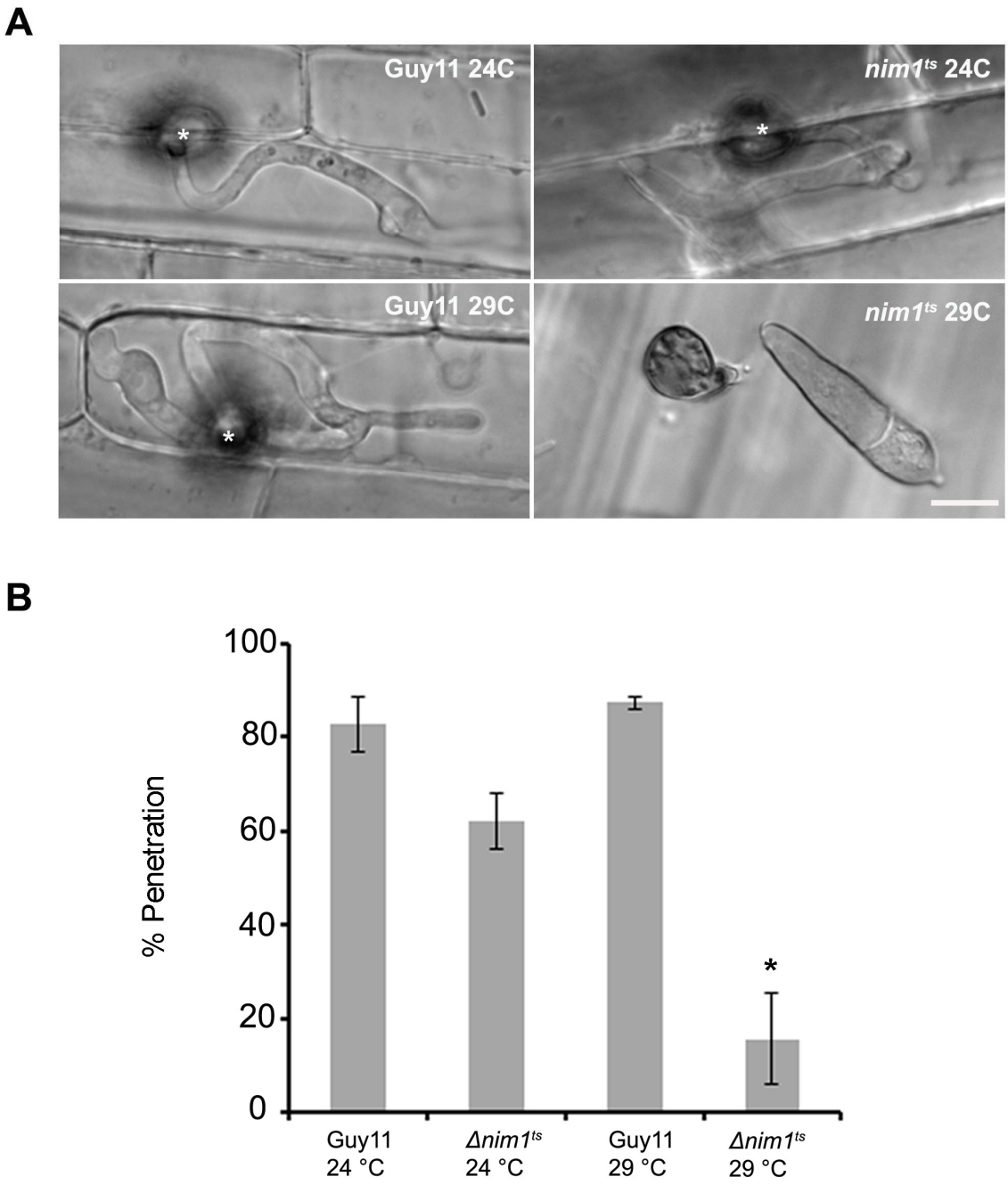

Figure 6.7 An S-phase arrest through Nim1 prevents plant penetration by *M. oryzae*. A) Micrographs at 30 h of rice leaf sheath of Guy11 and *Δnim1*^{ts} at 24℃ and 29℃. **B)** Bar chart to show the percentage penetration in Guy11 and *Δnim1*^{ts} at 24℃ and 29℃. The percentage penetration of *Δnim1*^{ts} at 29℃ was significantly lower than *Δnim1*^{ts} at 24℃ (n=100, two-tailed t-test, p=0.014) and Guy11 at 29℃ (n=100, two-tailed t-test, p=0.0017). (bar= 10 µm).

6.3.6.2 Genetic approach to study the effect of G2 arrest on plant penetration using the Δ*nimA*^{ts} mutant

One of the cell cycle checkpoints that regulates appressorium morphogenesis, blocks mitotic entry at G2/M and inhibits appressorium maturation (Veneault-Fourrey *et al.,* 2006). To investigate whether a block in mitotic entry affects plant penetration, the Δ*nimA*^{ts} mutant was used. NimA was identified as a homologue of the mitotic kinase NimA from *A. nidulans* (Veneault-Fourrey *et al.,* 2006). The thermo-sensitive mutant Δ*nimA*^{ts} does not form mature appressoria at restrictive temperature and prevents mitosis (Veneault-Fourrey *et al.,* 2006). To test whether entry into mitosis is a pre-requisite for penetration peg formation and plant penetration, a leaf sheath experiment was prepared using the wild-type strain Guy11 and the Δ*nimA*^{ts} mutant, which were incubated at standard conditions at 24 ℃ and then shifted at 10 h to a semi-permissive temperature of 29 ℃. At 30 h post inoculation, rice leaf tissue was dissected and observed microscopically (Fig. 6.8). The results indicated that at both 24 ℃ and 29 ℃ Guy11 showed normal frequency of penetration of 84.07% (SE± 3.91) and 82.6% (SE± 6.72), respectively. However at 24 ℃ Δ*nimA*^{ts} showed a decrease in penetration efficiency to 29.9% (SE± 10.15), significantly different to the frequency of appressorial penetration by Guy11 at 24 ℃ (n=100, two-tailed t-test, p=0.0012). Moreover, at 29 ℃ Δ*nimA*^{ts} showed 35.3% (SE± 4.57) penetration, which was not statistically significant with Δ*nimA*^{ts} at 24 ℃ (n=100, two-tailed t-test, p=0.59), but it was significant compared to Guy11 at 29 ℃ (n=100, two-tailed t-test, p=0.0005).

As the frequency of penetration in the Δ*nimA*^{ts} mutant was very low, even at the permissive temperature, a second leaf sheath experiment was set up to evaluate the results at 48 h (Fig. 6.8, panel A and C). The results indicated that Guy11 at both

24 ℃ and 29 ℃ showed 93.7% (SE±3.28) and 77.2% (S E±12.9) penetration, respectively. Similarly, at 24 ℃ and 29 ℃, the Δ*nimA*^{ts} mutant showed a frequency of penetration of 70.9% (SE±15.4) and 62.9% (SE±2.86). Therefore at 29 ℃ Δ*nimA*^{ts} showed no statistical significant differences to Δ*nimA*^{ts} at 24 ℃ (n=100, two-tailed t-test, p=0.62) or Guy11 at 29 ℃ (n=100, two-tailed t-test, p=0.33). Therefore, the results showed that the Δ*nimA*^{ts} mutant was still able to form penetration pegs at a frequency of 29.9% (SE±10.15) at 30 h and 70.9% (SE±15.4) at 48 h, indicating that the mutation causes a delay in plant penetration, but that a block in mitotic entry does not affect plant penetration and the fundamental ability to elaborate a penetration peg.

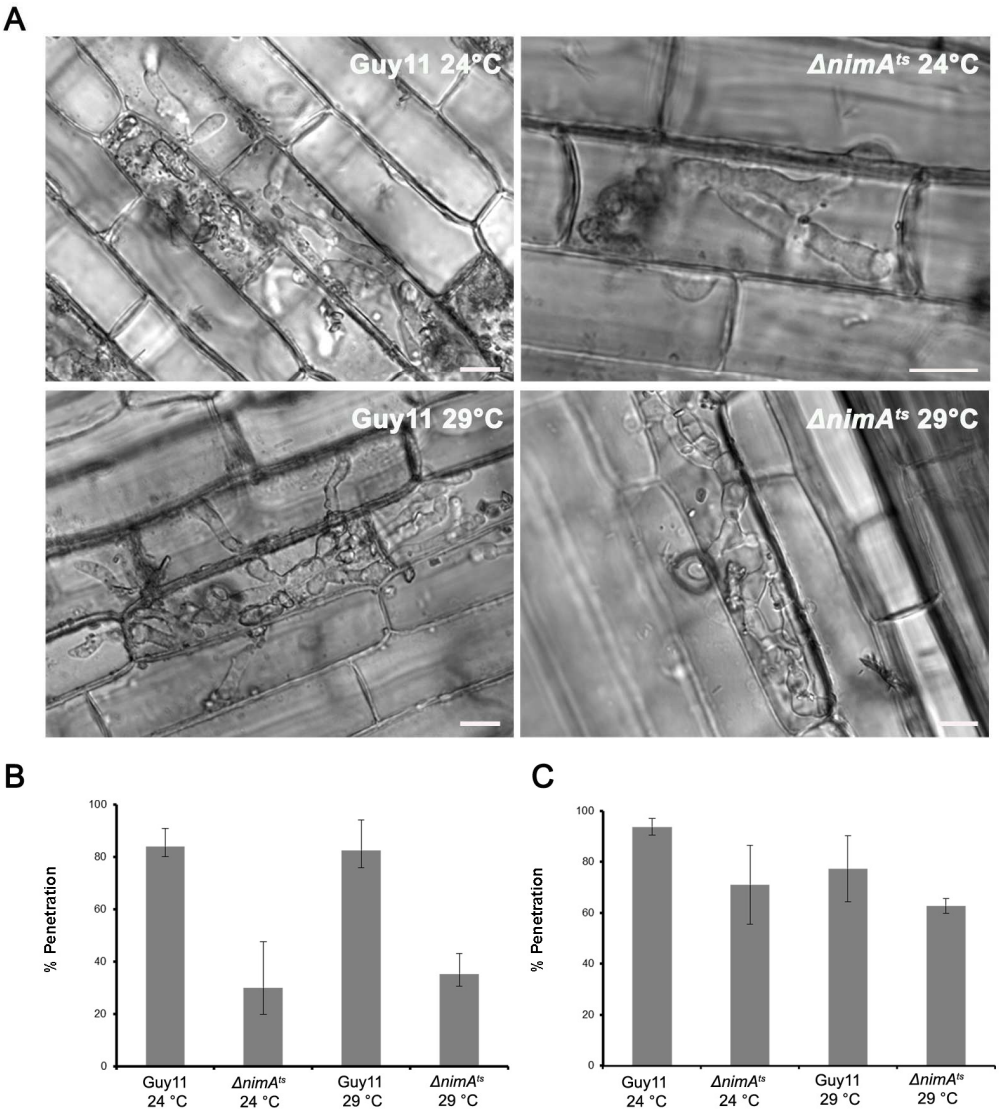

Figure 6.8 Entry into mitosis is not required for penetration peg formation. A) Micrographs at 48 h of Guy11 and Δ*nimA*^{ts} inoculated on a rice leaf sheath at 24 ℃ and 29 ° C. **B)** Bar chart showing the frequency of penetration for Guy11 and Δ*nimA*^{ts} inoculated on a rice leaf sheath at 24 ℃ and 29 ° C at 30 hpi. The percentage penetration of Δ*nimA*^{ts} at 29 ℃ was not statistically significant with Δ*nimA*^{ts} at 24 ℃ (n=100, two-tailed t-test, p=0.59), but was s ignificant from Guy11 at 29 ℃ (n=100, two-tailed t - test, p=0.0005). **C)** Bar chart showing the percentage penetration for Guy11 and Δ*nimA*^{ts} inoculated on a rice leaf sheath at 24 ℃ and 29 ℃ at 48 hpi. The frequency of penetration of Δ*nimA*^{ts} at 29 ℃ showed no statistical significant differences with Δ*nimA*^{ts} at 24 ℃ (n=100, two-tailed t-test, p=0.62) or Guy11 at 29 ℃ (n=100, two-tailed t-test, p=0.33). (bar= 10 µm).

6.3.6.3 Genetic approach to study the effect of M arrest on plant penetration using the Δ*bimE*^{ts} mutant

The thermo-sensitive *ΔbimE*^{ts} mutant of *A. nidulans* arrests cells in mitosis, and more specifically in anaphase preventing exit from mitosis (Osmani *et al.,* 1988). In *M. oryzae* BimE is an activator of mitotic progression (Saunders *et al.,* 2010). The thermo sensitive *ΔbimE*^{ts} mutant is able to form appressoria at the restrictive temperature but unable to cause disease suggesting that completion of mitosis is a pre-requisite for plant penetration (Saunders *et al.,* 2010a). To test genetically whether completion of mitosis was a pre-requisite for penetration peg formation and plant penetration, a leaf sheath experiment was performed using a wild-type strain Guy11 and Δ*bimE*^{ts} mutant which were incubated in standard conditions at 24 ℃ and then shifted to a semi-permissive temperature of 29 ℃ at 10 h. After 30 h post inoculation, rice leaf tissue was dissected and observed microscopically and the penetration frequency, quantified, (Fig. 6.9). Guy11 showed a standard penetration frequency of 85% (SE±4.8) and 87% (SE±12.3) at both 24 ℃ and 29 ℃, respectively. The thermo-sensitive mutant Δ*bimE*^{ts} mutant showed a significant decrease in appressorium-mediated penetration of 42% (SE±5.09) (n=100, two-tailed t-test, p=0.005) and 41% (SE±10.6) (n=100, two-tailed t-test, p=0.0013) compared to Guy11 at both 24 ℃ and 29 ℃, respecti vely. As the percentage penetration in Δ*bimE*^{ts} was found to be low under standard conditions, a second leaf sheath experiment was set out to evaluate the results at 48 h (Fig 6.9, panel A and C). The results indicated that Guy11 at both 24 ℃ and 29 ℃, showed a standard percentage penetration of 76% (SE±9.22) and 88% (SE±3.25), respectively. The results indicated that at 24 ℃ and 29 ℃ the Δ*bimE*^{ts} mutant showed 66% (SE±6.06) and 47% (SE±17.3), penetration. Therefore Δ*bimE*^{ts} at 29 ℃ showed no statistically

significant differences with Δ*bimE*^{ts} at 24 ℃ (n=100, two-tailed t-test, p=0.053) or Guy11 at 29 ℃ after 48 h (n=100, two-tailed t-test , p=0.079). Therefore, the results suggest that the Δ*bimE*^{ts} mutant showed a delay in plant infection, with a penetration frequency of 41% (SE±10.6) at 30 h and 47% (SE±17.3). Moreover, Δ*bimE*^{ts} showed no significant difference to Guy11 at the restrictive temperature confirming that mitotic exit was not required for penetration peg formation.

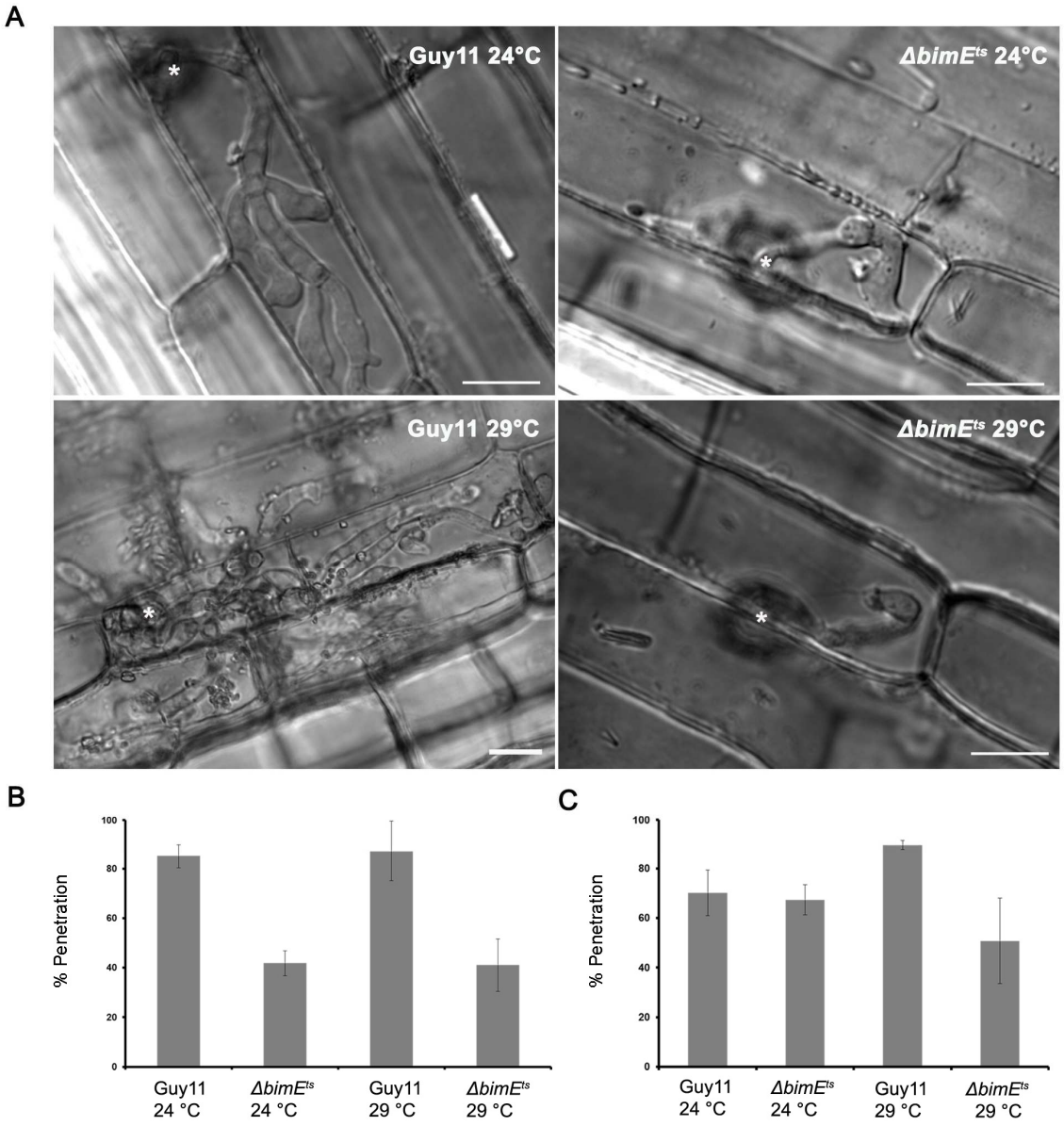

Figure 6.9 Completion of mitosis is not required for penetration peg formation. A) Micrographs at 48 h of Guy11 and Δ*bimE*^{ts} inoculated on a rice leaf sheath at 24 ℃ and 29 ° C. (bar= 10 µm). **B)** Bar chart showing the percentage penetration at 30 h for Guy11 and Δ*bimE*^{ts} inoculated on a rice leaf sheath at 24 ℃ and 29 ℃. The percentage penetrati on of Δ*bimE*^{ts} at 29 ℃ which was not statistically significant with Δ*bimE*^{ts} at 24 ℃ (n=100, two-tailed t-test, p=0.95), but w as significantly reduced when compared to Guy11 at 29 ℃ (n=100, two-tailed t-tes t, p=0.0013). **C)** Bar chart showing the percentage penetration at 48 h for Guy11 and Δ*bimE*^{ts} inoculated on a rice leaf sheath at 24 ℃ and 29 ℃. The percentage penetration of Δ*bimE*^{ts} at 29 ℃ which showed no significant differences w ith Δ*bimE*^{ts} at 24 ℃ (n=100, two-tailed t-test, p=0.053) or Gu y11 at 29 ℃ (n=100, two-tailed t-test, p=0.079).

6.3.7 Cytoskeleton rearrangement at the base of the appressorium are dependent on cell cycle S-phase in *M. oryzae*

As penetration peg formation appears to be an S-phase regulated process, it was our aim to understand whether the re-organisation and maintenance of the cytoskeleton at the base of the appressorium was also regulated by S-phase entry. To investigate this, an *in vitro* appressorial assay was prepared using a wild-type Guy11 strain expressing LifeAct-RFP and Gelsolin-GFP to observe F-actin, and Cdc11-GFP to observe septins. Conidia were harvested and inoculated onto hydrophobic glass coverslips and incubated for 10 h at 24 ℃ when 200mM HU was added. After 24 hpi, the coverslips were observed microscopically (Fig. 6.10).

The results indicated that at 10 h F-actin, as observed with both LifeAct-RFP and Gelsolin-GFP, was recruited to the appressorial pore but the toroidal ring structures were not formed. At 24, both LifeAct-RFP and Gelsolin-GFP showed the standard toroidal organized ring structure at the base of the appressorium. However, 24 h after HU treatment had been applied at 10 h, both LifeAct-RFP and Gelsolin-GFP were completely mis-localised, not showing the typical F-actin ring structure at the appressorium pore. In the case of the septin ring, the results indicated that by 10 h the toroidal ring structure was already formed as expected (Dagdas *et al.,* 2012). However, when observed at 24 h after HU had been applied at 10 h, the septin ring was completely absent, and septin filaments were no longer visible in the appressorial dome. These results suggested that formation of the F-actin ring and maintenance of the septin ring were both S-phase dependent processes during appressorium formation on glass coverslips.

To observe the effect of HU on actin dynamics during plant penetration, a Guy11 strain expressing LifeAct-RFP was inoculated on to 28 day-old CO-39 rice leaf sheath and incubated at 25 ℃ for 10 h until 1 M HU was added. At 30 h, non-HU treated leaf sheath showed formation of primary invasive hyphae showing the presence of actin cables and patches (Fig. 6.11). However after 1 M HU treatment, appressoria were unable to form a penetration peg and LifeAct-RFP was recruited at the pore site but in a disorganized manner. In addition a Guy11 strain expressing Gelsolin-GFP was also used. Guy11 expressing Gelsolin-GFP was inoculated onto a 28 day-old CO-39 rice leaf sheath and incubated at 25 ℃ for 10 h at which time 1 M HU was added. At 30 h, non-HU treated leaf sheath showed formation of primary invasive and Gelsolin-GFP was observed as sub-apical localised patches (Fig. 6.13). However after 1 M HU treatment, appressoria were unable to form a penetration peg and Gelsolin-GFP was recruited at the pore site but in an a disorganized manner.

To observe the effect of HU on septin dynamics during plant penetration, a Guy11 strain expressing Sep5-GFP was inoculated onto 28 day-old CO-39 rice leaf sheath and incubated at 25 ℃ for 10 h when 1 M HU was added. At 30 h, non-HU treated leaf sheath showed the formation of the primary invasive hyphae showing the presence of Sep5-GFP localised at septa (Fig. 6.12). However under 1 M HU treatment, appressoria were unable to form a penetration peg and therefore Sep5-GFP was randomly distributed and disorganized in the appressorium.

After confirming that septin and actin toroidal ring structures were S-phase regulated, we were interested to determine whether the localization of other cytoskeleton related proteins, such as Chm1, Tea1, Rvs167 and Las17, were also S-phase dependent (Dagdas *et al.,* 2012). The septin toroidal ring structure is scaffolded at the base of the appressoria though a PAK kinase called Chm1 (Dagdas

et al., 2012). At the same time the septin ring scaffolds an F-actin toroidal ring structure though a ERM (Ezrin/ Radin/ Myosin) Tea1 protein (Dagdas *et al.,* 2012) that is NADPH oxidase-dependent (Ryder *et al.,* 2013). Rvs167 is an inverse-BAR (*B*im1, *A*mphiphysin, and *R*vs167) proteins which bind to actin and PtdIns (4, 5)P_2 to generate protrusions (Bompard *et al.,* 2005). Las17 is involved in actin nucleation (Urbanek *et al.,* 2013). To investigate this, an *in vitro* appressorial assay was set up using the wild-type strain Guy11 expressing Chm1-GFP, Tea1-GFP, Rvs167-GFP and Las17-GFP. Conidia were harvested and inoculated on hydrophobic glass coverslips and incubated for 10 h at 24 ℃ when 200 mM HU was added. After 24 h post initial inoculation, the coverslips were observed microscopically (Fig. 6.14). The results indicated that by 10 h, Chm1-GFP and Tea1-GFP were recruited to the appressorial pore. Moreover Rvs167-GFP and Las17-GFP showed the standard localization as puncta distributed around the appressorial pore. At 24 h the Chm1-GFP and Tea1-GFP toroidal ring structures were visible around the appressorial pore. However, in HU treated samples, none of the structures were maintained. Both Chm1-GFP and Tea1-GFP were mislocalised and showed random punctate distribution, not central to the appressorial pore. In HU treated cells Rvs167-GFP and Las17-GFP were not visible in the appressorial dome and instead were found localized to the cell periphery. These results suggested that localization of Chm1, Tea1, Rvs167 and Las17 are all S-phase dependent.

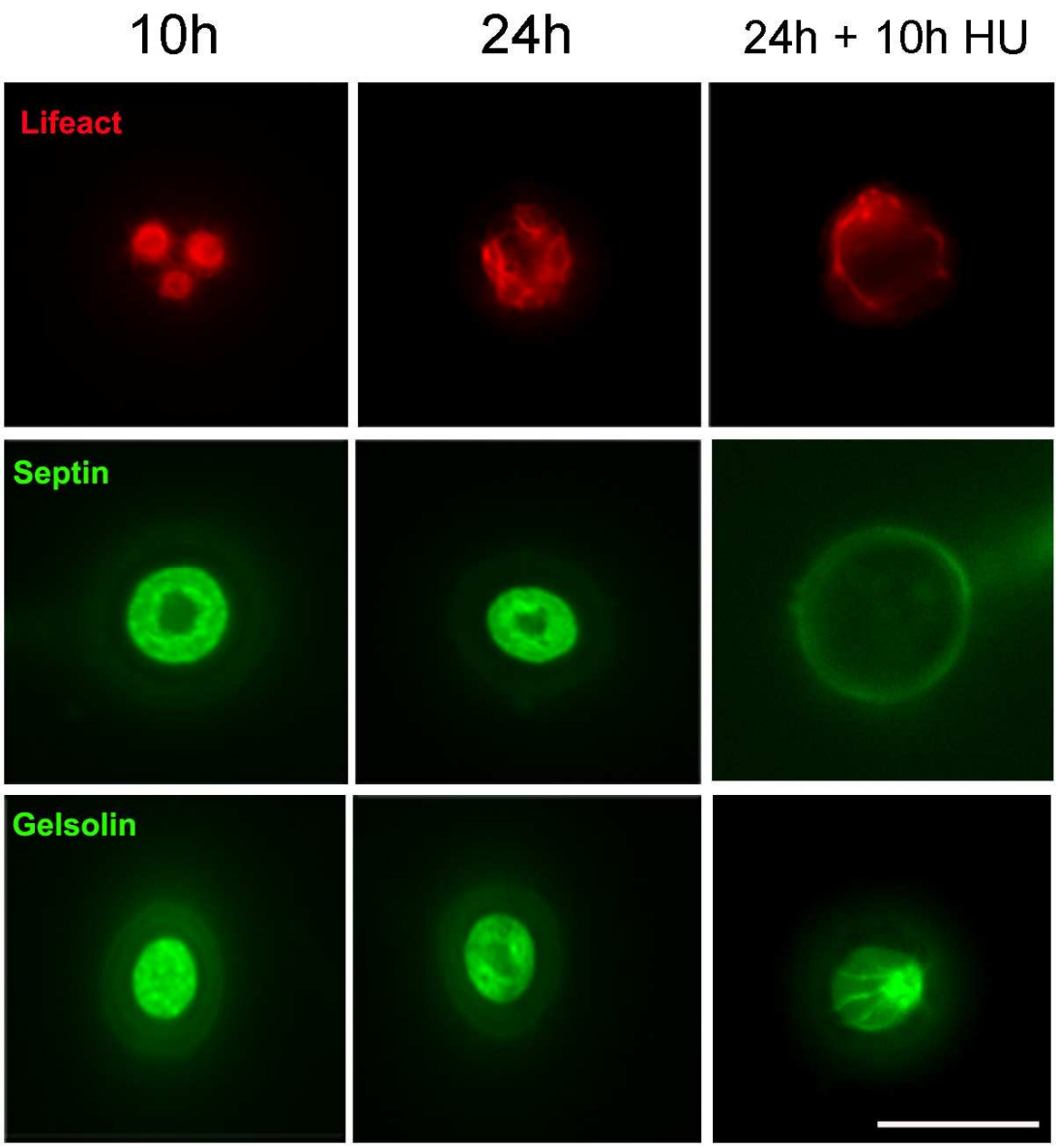

Figure 6.10 HU blocks maintenance of the septin ring and the assembly of F-actin network at the appressorium pore on glass coverslips. Micrographs to show localization of LifeAct-RFP, Sep5-GFP and Gelsolin-GFP during appressorium development at 10 h, 24 h and 24 h following HU addition at 10 h. (bar= 10 µm).

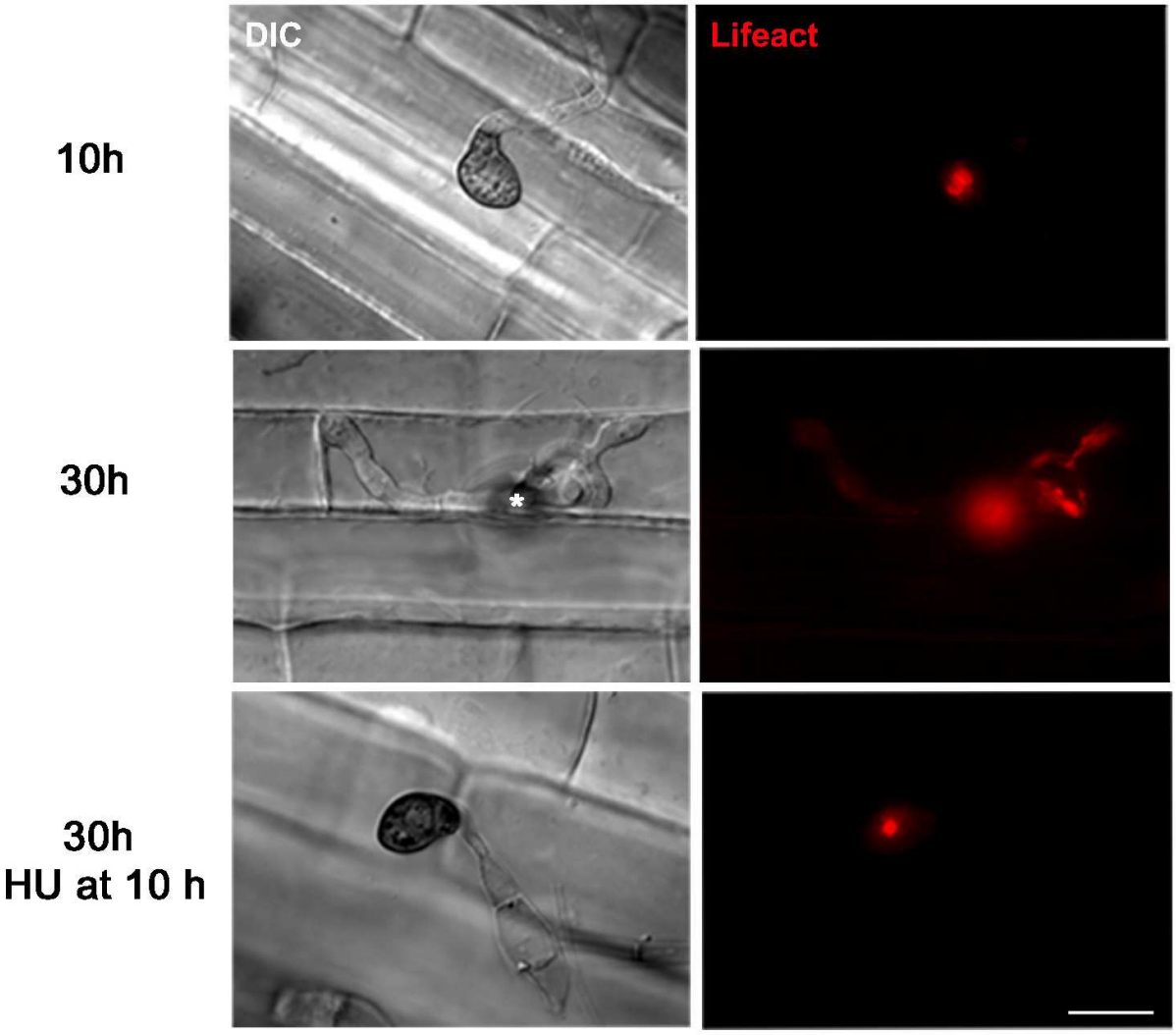

Figure 6.11 HU blocks the F-actin network at the appressorium pore during plant penetration in rice leaf sheath. Micrographs to show localization LifeAct-RFP during plant infection on a rice leaf sheath at 10 h, 24 h and 24 h when HU was added at 10 h. (bar= 10 µm).

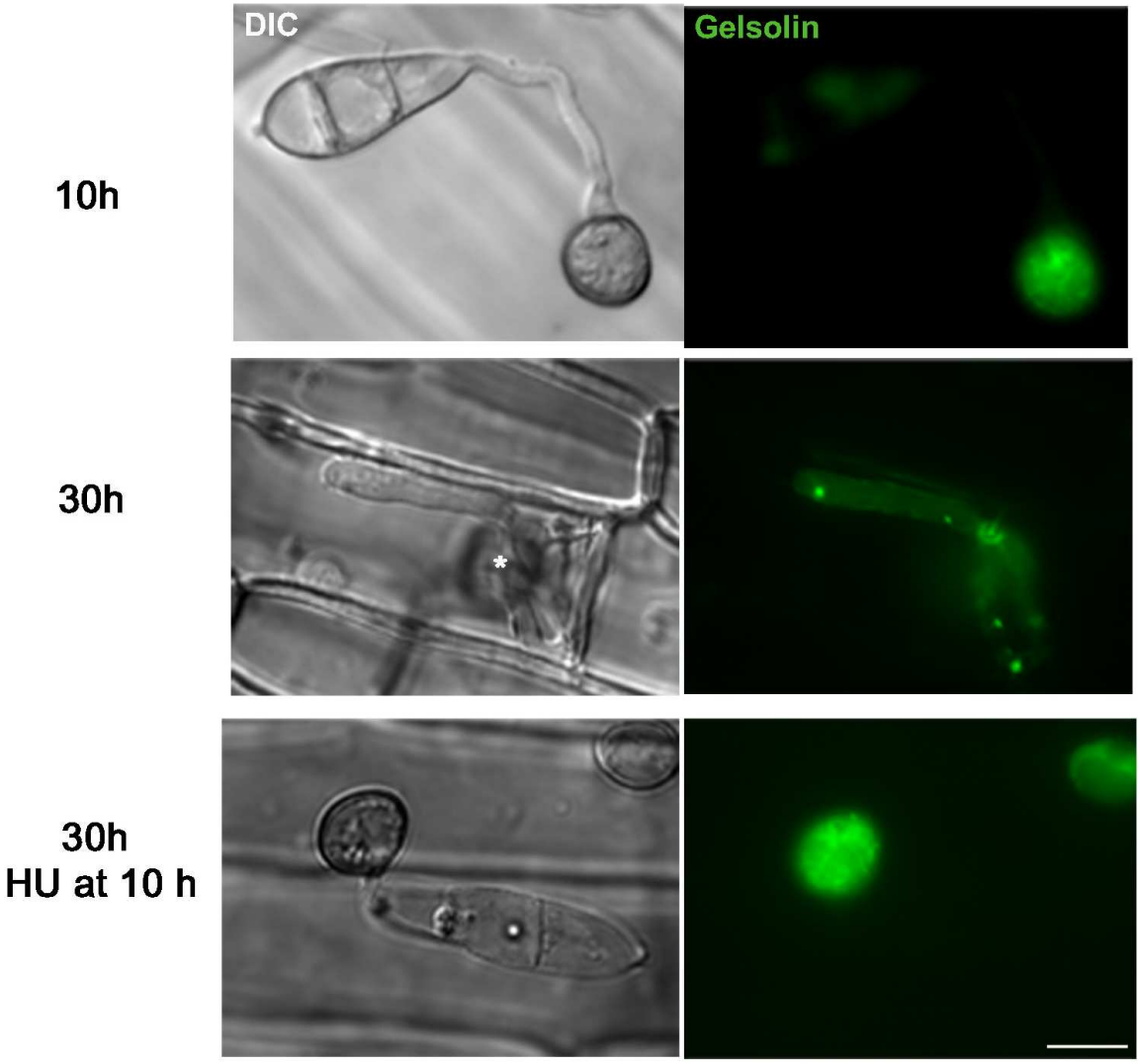

Figure 6.12 HU blocks formation of the gelsolin ring at the appressorium pore during plant penetration in rice leaf sheath. Micrographs to show localization Gelsolin-GFP during plant infection on a rice leaf sheath at 10 h, 24 h and 24 h when HU was added at 10 h. (bar= 10 µm).

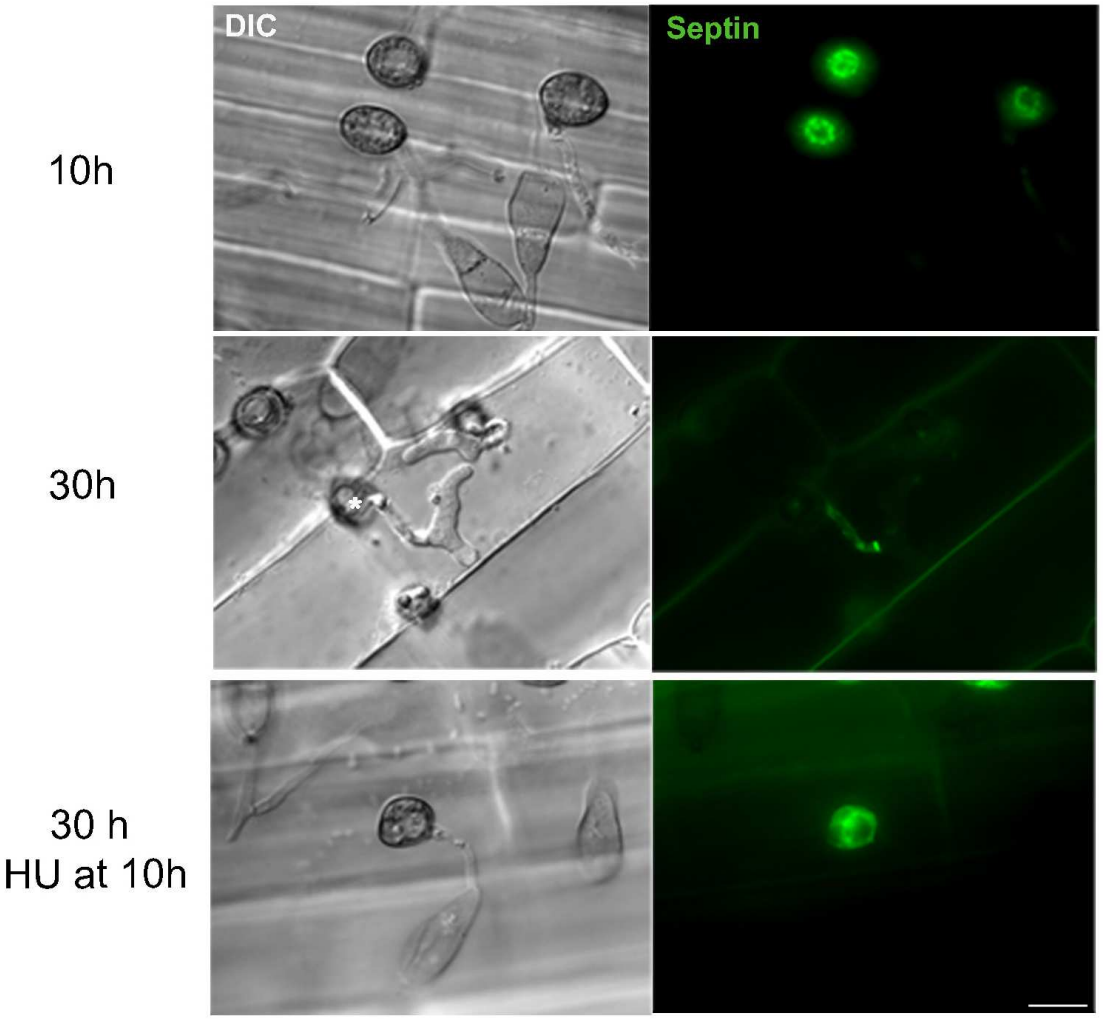

Figure 6.13 HU blocks maintenance of the septin ring at the appressorium pore during plant penetration in rice leaf sheath. Micrographs to show localization of Septin-GFP during plant infection on a rice leaf sheath at 10 h, 24 h and 24 h when HU was added at 10 h. (bar= 10 µm).

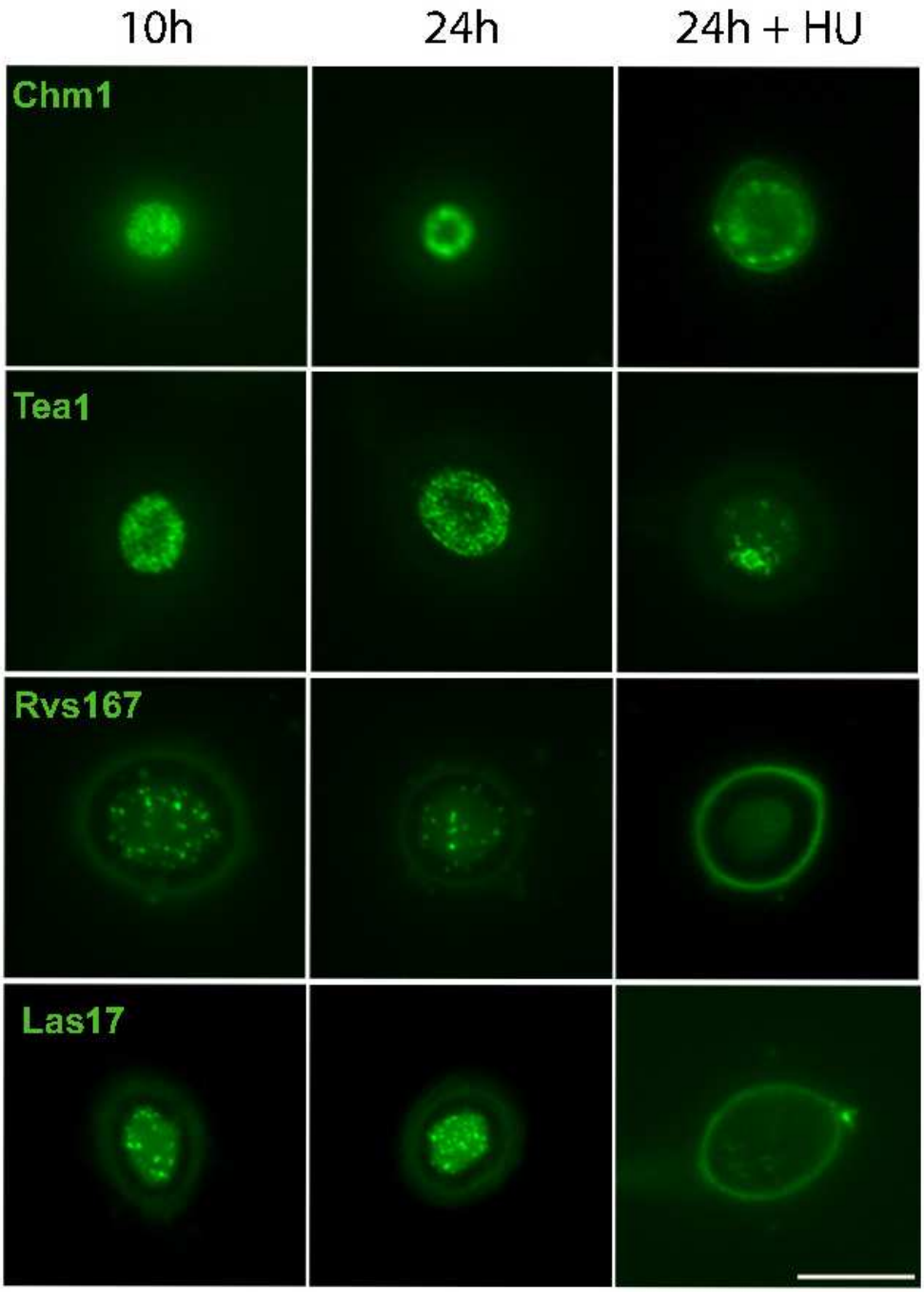

Figure 6.14 HU affects localization of F-actin cytoskeleton-associated proteins during appressorium formation on glass coverslips. Micrographs to show localization Chm1-GFP, Tea1-GFP, Rvs167-GFP and Las17-GFP during appressorium development at 10 h, 24 h and 24 h when HU was added at 10 h. (bar= 10 µm).

6.3.8 Determination of the role of the DNA replication checkpoint in appressorium morphogenesis and plant penetration in the rice blast fungus *M. oryzae*

It was already known from previous research, that successful DNA replication is required for appressorium formation (Saunders *et al.,* 2010a). When germinating conidia are treated with HU, formation of an incipient appressoria is blocked (Saunders *et al.,* 2010a). The formation of an incipient appressoria implies a change from apical growth (anisotropy) to isotropic growth (radial expansion). Once the appressorium is formed and sufficient turgor inside the dome is reached to facilitate plant penetration, re-polarization occurs in which a penetration peg emerges perpendicular to the appressorial dome to breach the tough cuticle of the leaf. It was shown in this study, that the second re-polarization leading to penetration peg formation was blocked upon HU treatment, suggesting that completion of DNA replication is also necessary for appressorium-mediated plant infection.

In all organisms, completion of DNA replication is guaranteed though the DNA replication checkpoint, which is a conserved cellular mechanism in all eukaryotic organisms (Russell, 1998). After DNA damage or un-replicated DNA, cells use the DNA replication checkpoint to arrest the cell cycle and allow replication, or repair, to occur and therefore ensure successful segregation of the genetic material (Russell, 1998). However, it is not known whether the replication checkpoint is active constitutively or becomes activated when a problem in DNA is found within the cell (Elledge, 1996). The DNA damage checkpoint consists of several sensors that immediately send signals to downstream kinases that, ultimately, inhibit entry into mitosis (reviewed in Elledge, 1996). The first kinases in the transduction pathway are the phosphoinositide 3-kinases Tel1 and Mec1, homologues of ataxia telangiectasia

mutated (ATM) and ataxia telangiectasia (ATR) of humans associated with cancer (Kastan and Bartek, 2004; Russell, 1998). Tel1 and Mec1 transduce the signal to the kinases Chk1 and Rad53 to arrest the cell cycle by promoting inhibitory phosphorylation of the cyclin-dependent kinase CDK1 (Russell, 1998). The inhibitory phosphorylation of CDK1 occurs via Wee1 and Mik1 kinases and is removed to allow entry into mitosis through the phosphatase Cdc25 (Russell, 1998).

To determine involvement of the DNA replication checkpoint in monitoring DNA replication and subsequently in controlling morphogenesis in the rice blast fungus *M. oryzae*, I decided to investigate the DNA replication checkpoint by generating targeted gene deletion mutants of the checkpoint kinases and studying their involvement in morphogenesis of *M. oryzae.*

6.3.8.1 Identification, phylogenetic analysis and multiple amino acid sequence alignment of DNA damage checkpoint kinases in *M. oryzae*

To identify the putative DNA checkpoint kinases in *M. oryzae,* BLASTP analysis was performed using the *S. cerevisiae* proteins Chk1 (YBR274W) and Rad53 (YPL153C) and the *S. pombe* proteins Chk1 (SPCC1259.13) and Cds1 (SPCC18B5.11) as query into *M. oryzae* genome v.8.0. (http://www.broad.mit.edu/annotation/fungi/magnaporthe/). A BLASTP search revealed that *M. oryzae* Chk1 corresponded to the protein MGG_03729, containing a protein kinase domain. However, BLASTP searches for Rad53 or Cds1 identified two putative homologues within the *M. oryzae* genome, currently annotated as Rad53, MGG_01596 (e= 0) and MGG_04790 (e= 2.29 e^{-32}), both containing a serine/ threonine protein kinase domain (S/T Pkinase) and a fork head domain (FHA),

characteristic of Cds1 and Rad53 proteins (Perez-Martin, 2009). *S. cerevisiae* possess three protein kinases containing S/T Pkinase and FHA domains which are Mek1, Rad53 and Dun1. To determine the identity of the homology of Rad53 in *M. oryzae*, phylogenetic analysis of the proteins of *M. oryzae* containing both S/T Pkinase and FHA domains was performed (Fig. 6.15). This analysis revealed that the Chk1 homologue in *M. oryzae* corresponded to MGG_03729, the Cds1 homologue in *M. oryzae* corresponded to MGG_04790, and the Dun1 homologue in *M. oryzae* corresponded to MGG_01596. The corresponding protein alignments for Chk1 (Fig. 6.16), Dun1 (Fig. 6.17) and Cds1 (Fig. 6.18) were also analysed to determine the homology with other orthologues in *Neurospora crassa, S. cerevisiae, A. nidulans,* and *Shizosaccharomyces pombe*.

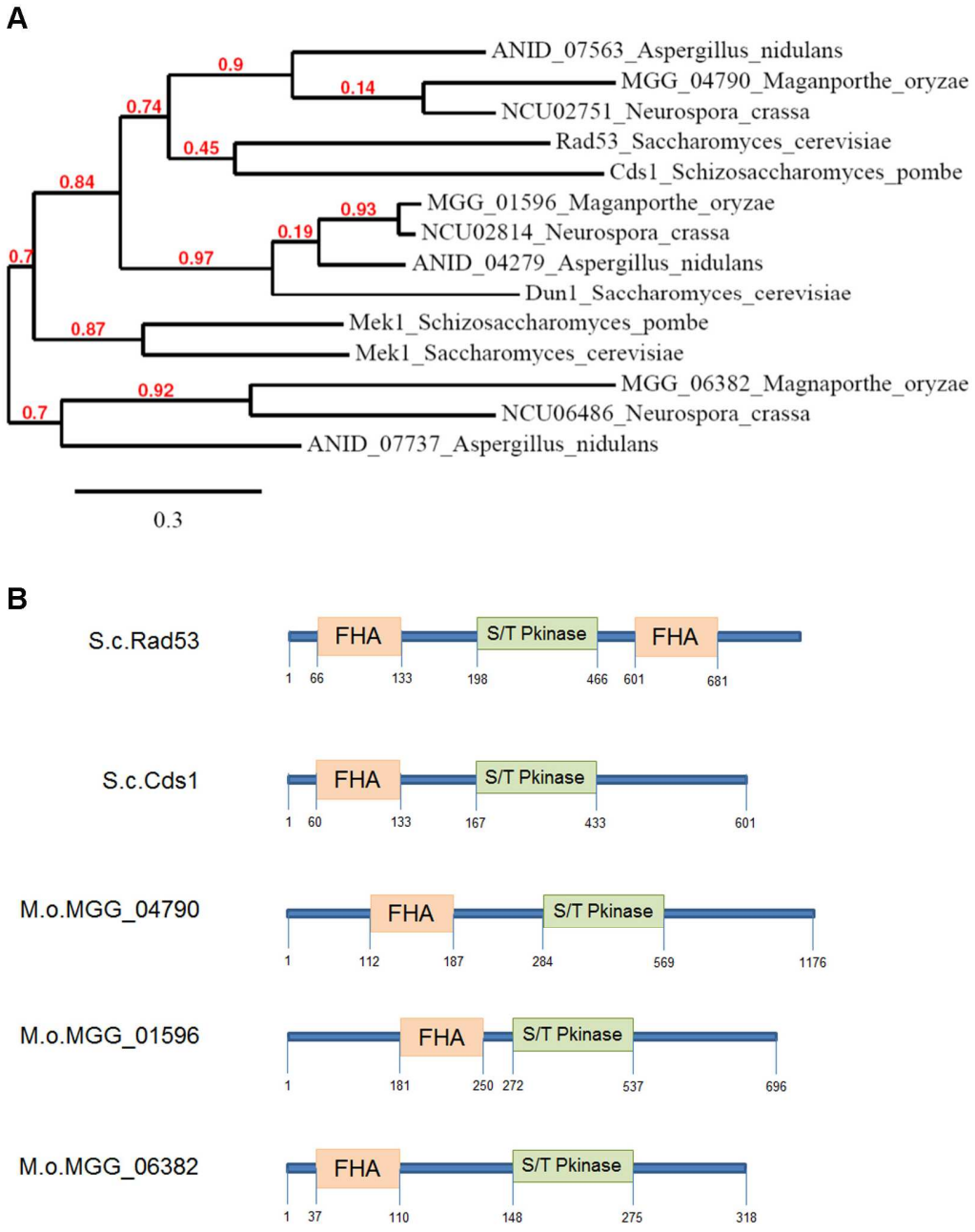

Figure 6.15 Phylogenetic and domain analysis of fork head domain (FHA) and serine threonine protein kinase domain (S/T Pkinase) containing proteins of *M. oryzae*. A) Phylogenetic tree of FHA and S/T Pkinase domain containing proteins was performed by aligning the sequences using MUSCLE software, by performing a curation procedure using G-blocks and the phylogenetic tree was plotted using TreeDyn (http://www.phylogeny.fr) Red numbers represent the approximation of the standard Likehood Ratio Test (Dereeper *et al.,* 2008). **B)** Domain analysis of FHA and S/T Pkinase domain containing proteins compared to Rad53 of *S. cerevisiae* and Cds1 of *S. pombe.*.

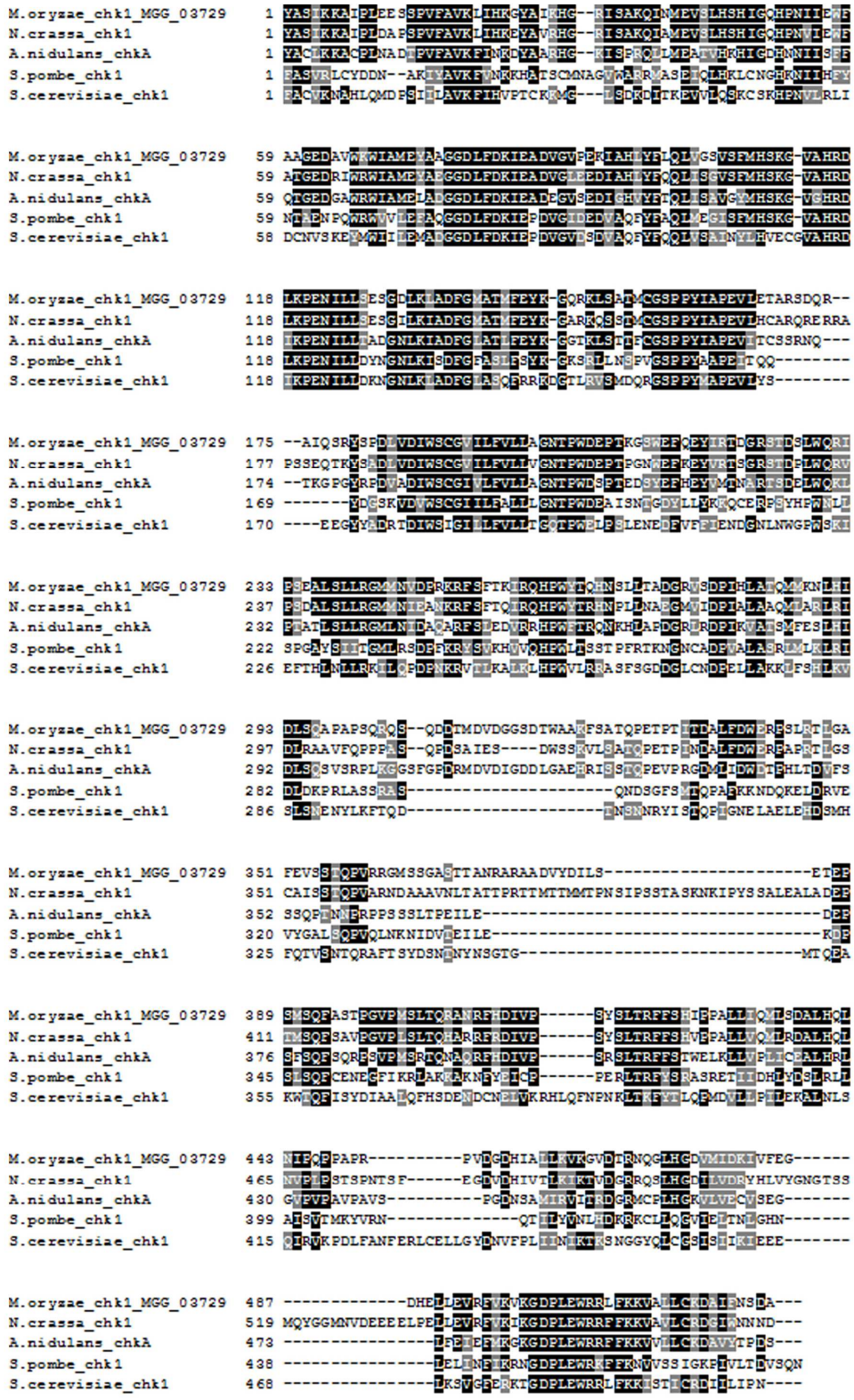

Figure 6.16 Multiple amino acid sequence alignment of Chk1 proteins. Identical amino acids are depicted in black, similar amino acids in grey and non-identical residues as unshaded.

Figure 6.17 Multiple amino acid sequence alignment of Dun1 proteins. Identical amino acids are depicted in black, similar amino acids in grey and non-identical residues as unshaded.

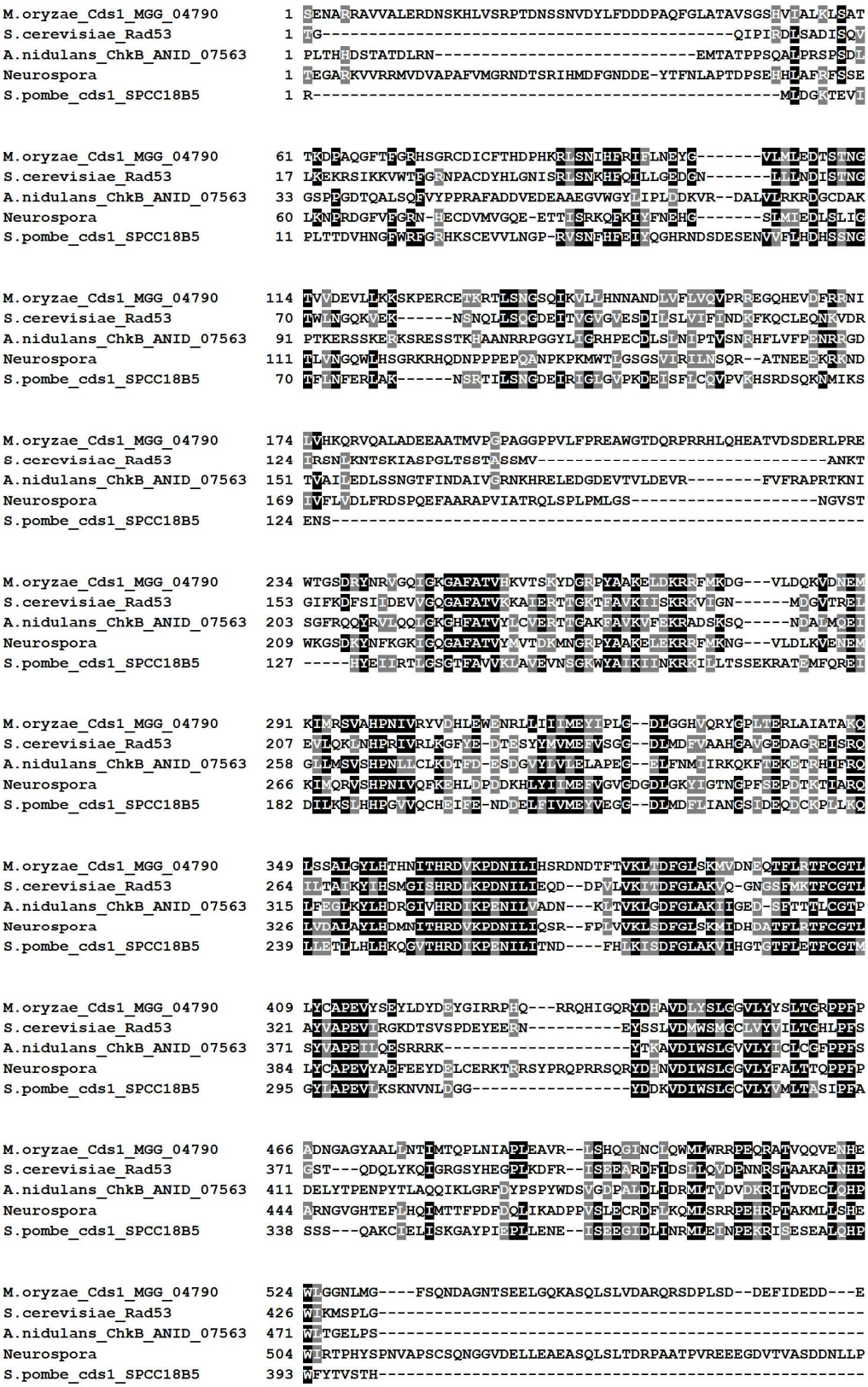
M.oryzae_Cds1_MGG_04790
S.cerevisiae_Rad53
A.nidulans_ChkB_ANID_07563
Neurospora
S.pombe_cds1_SPCC18B5

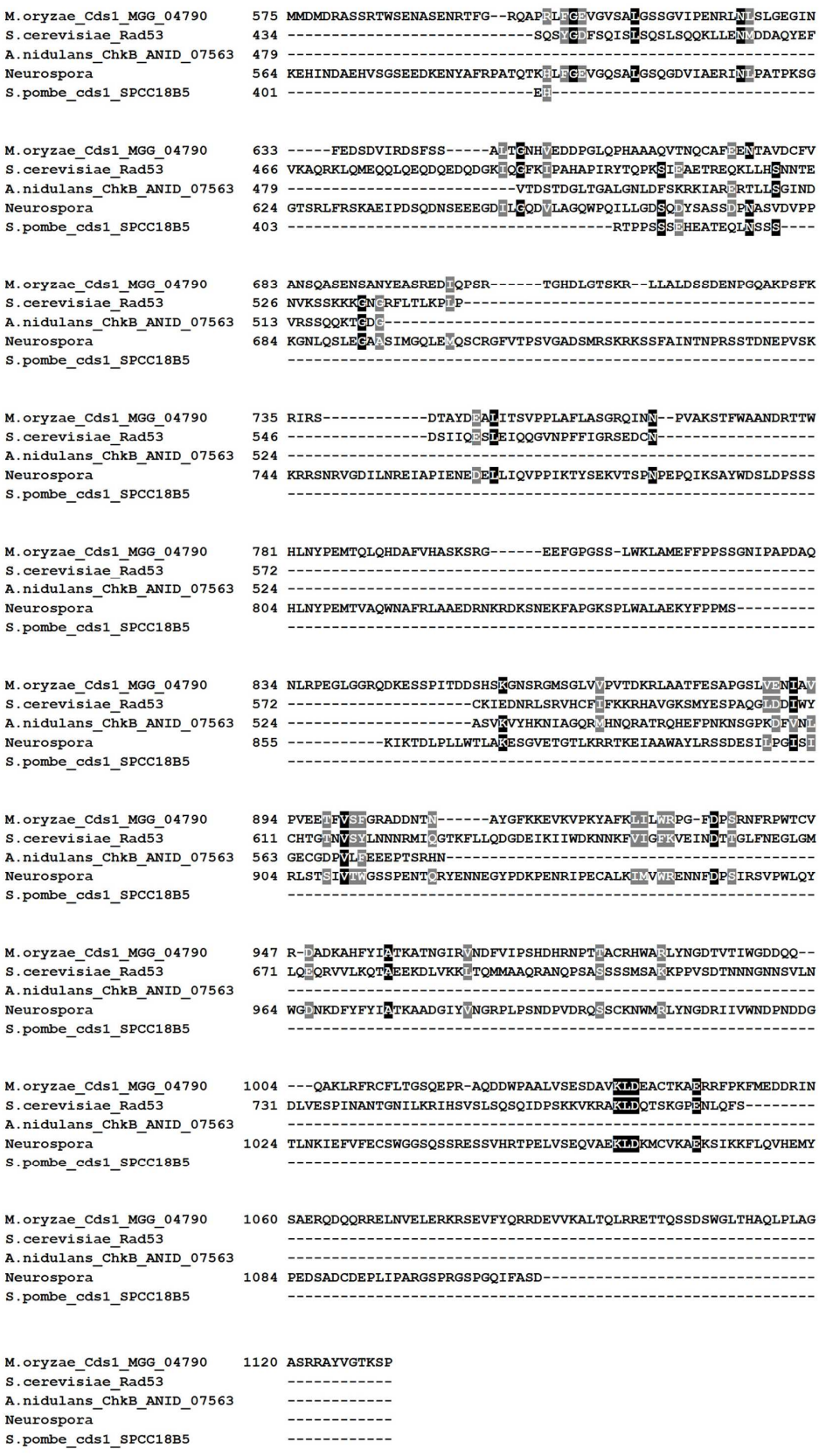

Figure 6.18: Multiple amino acid sequence alignment of Cds1 proteins. Identical amino acids are depicted in black, similar amino acids in grey and non-identical residues as unshaded.

6.3.9 Generation of the *CHK1* targeted gene replacement vector

In order to determine the role of Chk1 in *M. oryzae*, targeted gene replacement of *CHK1* was performed using a PCR-based split marker deletion method, as shown in Figure 6.20 (Kershaw and Talbot, 2009). In a first round PCR, primers were designed to amplify a 1 Kb genomic region both upstream and downstream of the *CHK1* ORF. The primers contained 5' and 3' overhanging regions complementary in sequence to the hygromycin phosphotransferase resistance gene cassette (*Hph*). In a second round PCR, two different fusion fragments were generated. The first PCR fusion was generated between the 1 Kb upstream *CHK1* ORF region and the initial 1.4 Kb fragment of *Hph* cassette through the 3' overhanging region generated in the first round PCR. The second PCR fusion was generated between 1 Kb downstream *CHK1* ORF region and the terminal 0.8 Kb fragment of *Hph* cassette through the 5' overhanging region generated in the first round PCR. The two fused constructs were simultaneously introduced into the *M. oryzae* Guy11 strain to guarantee successful integration at the respective locus. The primers used for the targeted gene replacement of *CHK1* are listed in Table 6.1.

6.3.10 Analysis of putative Δ*chk1* transformants

Putative transformants of Δ*chk1* were selected in the presence of the antibiotic hygromycin B (200 µg mL^{-1}). One-hundred putative transformants were selected and genomic DNA extracted for Southern blot analysis. Two separate Southern blots were prepared in which genomic DNA was digested with *Hin*dIII and *Pvu*II, respectively. The resulting digestions were fractionated by gel electrophoresis before being transferred to Hybond-N (Amersham). The membrane was probed with

the upstream region of *CHK1* which was generated as a 1 Kb first round PCR amplicon. In the Southern blot with DNA digested with *Hin*dIII the probe hybridized to a 1.1 Kb fragment in the Guy11 control lane. However, hybridization was absent in transformant T44 and instead, a 2.4 Kb band was visible as a result of the replacement of the *CHK1* gene by the *Hph* resistance cassette (Fig. 6.21, panel A). In the Southern blot with DNA digested with *Pvu*II the probe hybridized to a 4.4. Kb fragment in the Guy11 control lane. However, hybridization was absent in transformant T44 and instead, a 2.6 Kb band was visible as a result of the replacement of the *CHK1* gene by the resistance cassette (Fig. 6.21, panel B). These results suggested that the *CHK1* gene had been successfully replaced with the *Hph* resistant cassette in transformant T44. T44 was therefore identified as a *Δchk1* null mutant and was selected for further phenotypic analysis.

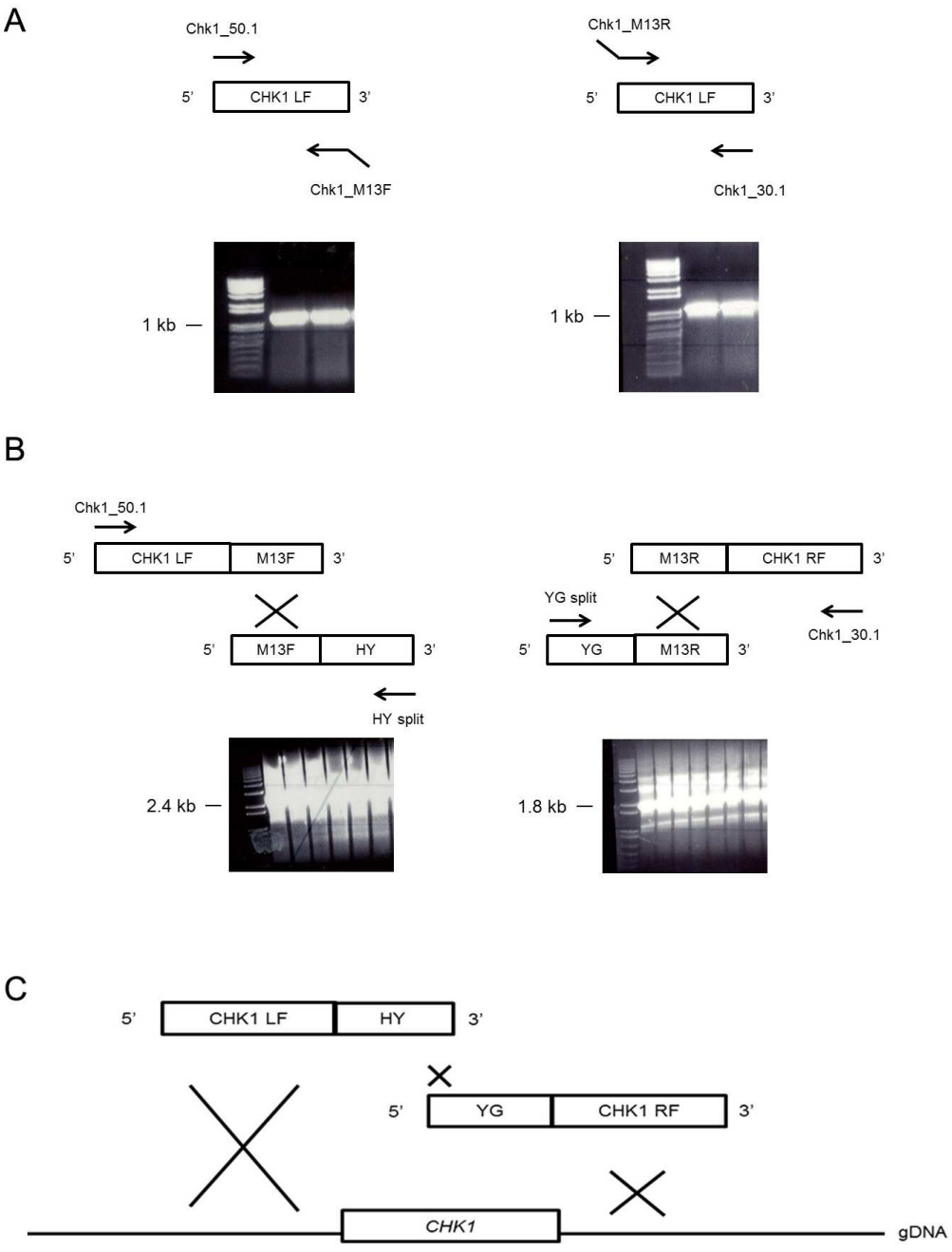

Figure 6.19 Schematic representation of the targeted deletion of *CHK1* using a PCR-based split-marker deletion method. A) First round PCR: amplification of a 1 Kb flanking region either side of the *CHK1* ORF using primers shown. **B)** Second round PCR: fusion of the *CHK1* LF to the initial 1 Kb coding sequence of the *Hph* cassette (HY) and the *CHK1* RF to the terminal 1 Kb coding sequence of the *Hph* cassette (YG). **C)** Fungal transformation of the two constructs into *M. oryzae*, in which homologous recombination occurs resulting in the replacement of the *CHK1* ORF with the *Hph* cassette.

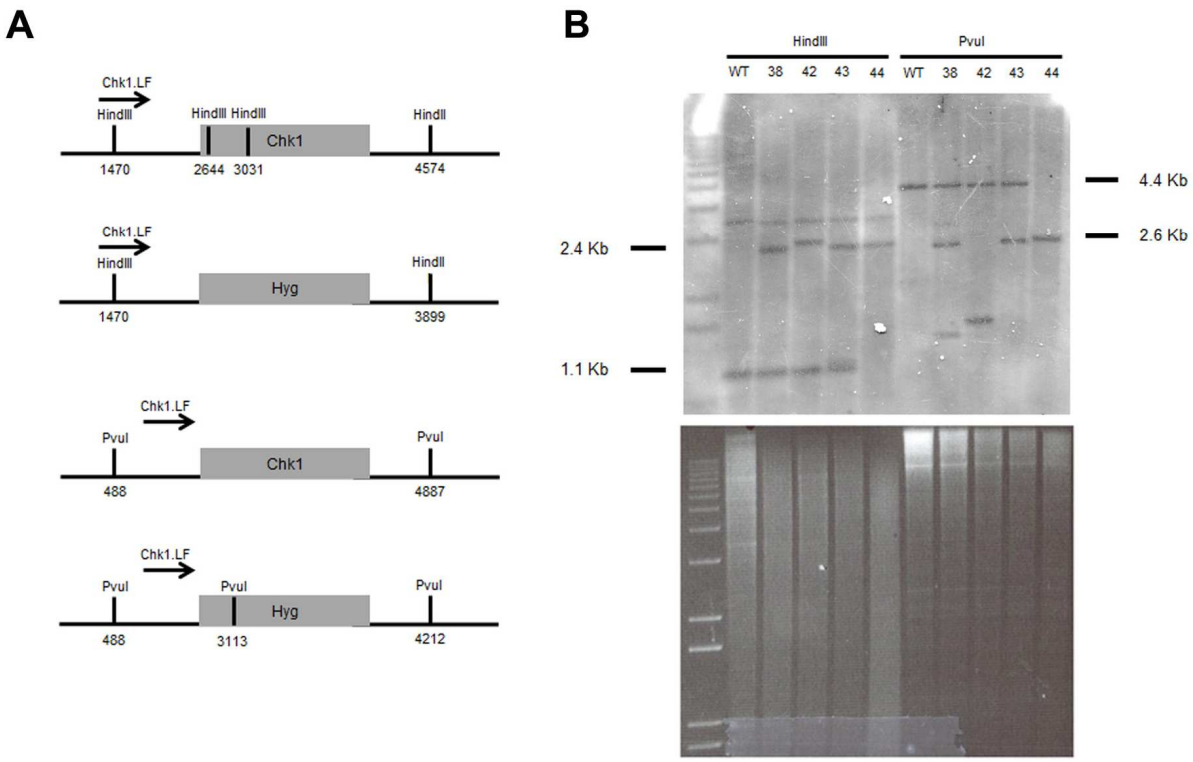

Figure 6.20 Southern Blot analysis to show targeted gene replacement of *CHK1* into Guy11 background. **A)** Schematic representation of the Southern blot analysis carried out to identify*CHK1* targeted gene replacement transformants. The upper scheme represents the strategy using *Hin*dIII and the lower scheme represents the strategy using *Pvu*II. **B)** Southern blot analysis result showing *Hin*dIII and *Pvu*II restriction digestions followed by probing with the 1 Kb upstream region of *CHK1* (Chk1.LF). In the case of *Hin*dIII, the result showed a 1.1 Kb band when no gene replacement had occurred and a 2.4 Kb band when the corresponding resistance cassette was integrated at the *CHK1* locus. The Southern showed a positive result for T44. In the case of *Pvu*II, the result showed a 4.4 Kb band when no gene replacement had occurred and a 2.6 Kb band when the corresponding resistance cassette was integrated at the *CHK1* locus. The Southern confirmed the positive result for T44.

6.3.11 Generation of the *DUN1* targeted gene replacement vector

In order to determine the role of Cds1, targeted gene replacement of *CDS1* was performed using a PCR-based split marker deletion method, as shown in Figure 6.22 (Kershaw and Talbot, 2009). In a first round PCR, primers were designed to amplify a 1 Kb genomic region both upstream and downstream of the *CDS1* ORF. The primers contained 5' and 3' overhanging regions complementary in sequence to the acetolactase synthase-encoding gene cassette (Ilv). In a second round PCR, two different fusion fragments were generated. The first PCR fusion was generated between the 1 Kb upstream *CDS1* ORF region and the initial 1.4 Kb fragment of *Ilv1* cassette through the 3' overhanging region generated in the first round PCR. The second PCR fusion was generated between 1 Kb downstream *CDS1* ORF region and the terminal 1.4 Kb fragment of *Ilv1* cassette through the 5' overhanging region generated in the first round PCR. The two fused constructs were simultaneously introduced into the *M. oryzae* strain Guy11 and into the mutant Δ*chk1* to guarantee a successful integration of the two constructs in the respective locus

6.3.12 Analysis of putative Δ*dun1* transformants

Putative *Δdun1* transformants were selected in the presence of the antibiotic chlorimuron ethyl (50 μg mL^{-1}). One hundred putative transformants for each background were selected and genomic DNA was extracted. For both backgrounds, Southern blot analysis was set up in which the genomic DNA was digested with *Sap*I. The resulting digestions were fractionated by gel electrophoresis before being transferred to a Hybond-N membrane (Amersham). The membranes were probed with the upstream region of *DUN1* generated as a 1 Kb first round PCR amplicon.

(Fig. 6.23 panel A) The probe hybridized to a 5.1 Kb fragment in the Guy11 control lane. However hybridization was absent in transformant T43 and T44. Instead, a 9 Kb band was visible as a result of the replacement of the *DUN1* gene by the selectable marker gene cassette (Fig. 6.23, panel B). T43 and T44 were therefore identified as *Δdun1* null mutants and were selected for further phenotypic analysis

In the case of the Δ*chk1* background, the probe hybridized to a 5.1 Kb fragment into the Guy11 control lane. However, hybridization was absent in transformant T15 and instead, a 9 Kb band was visible as a result of replacement of the *DUN1* gene by the selectable marker gene cassette (Fig. 6.24, panel B). These results suggested that the *DUN1* gene had been replaced correctly with the *Ilv1* resistance gene cassette into T15. T15 was considered to be a *Δdun1*Δ*chk1* null mutant and was selected for further phenotypic analysis.

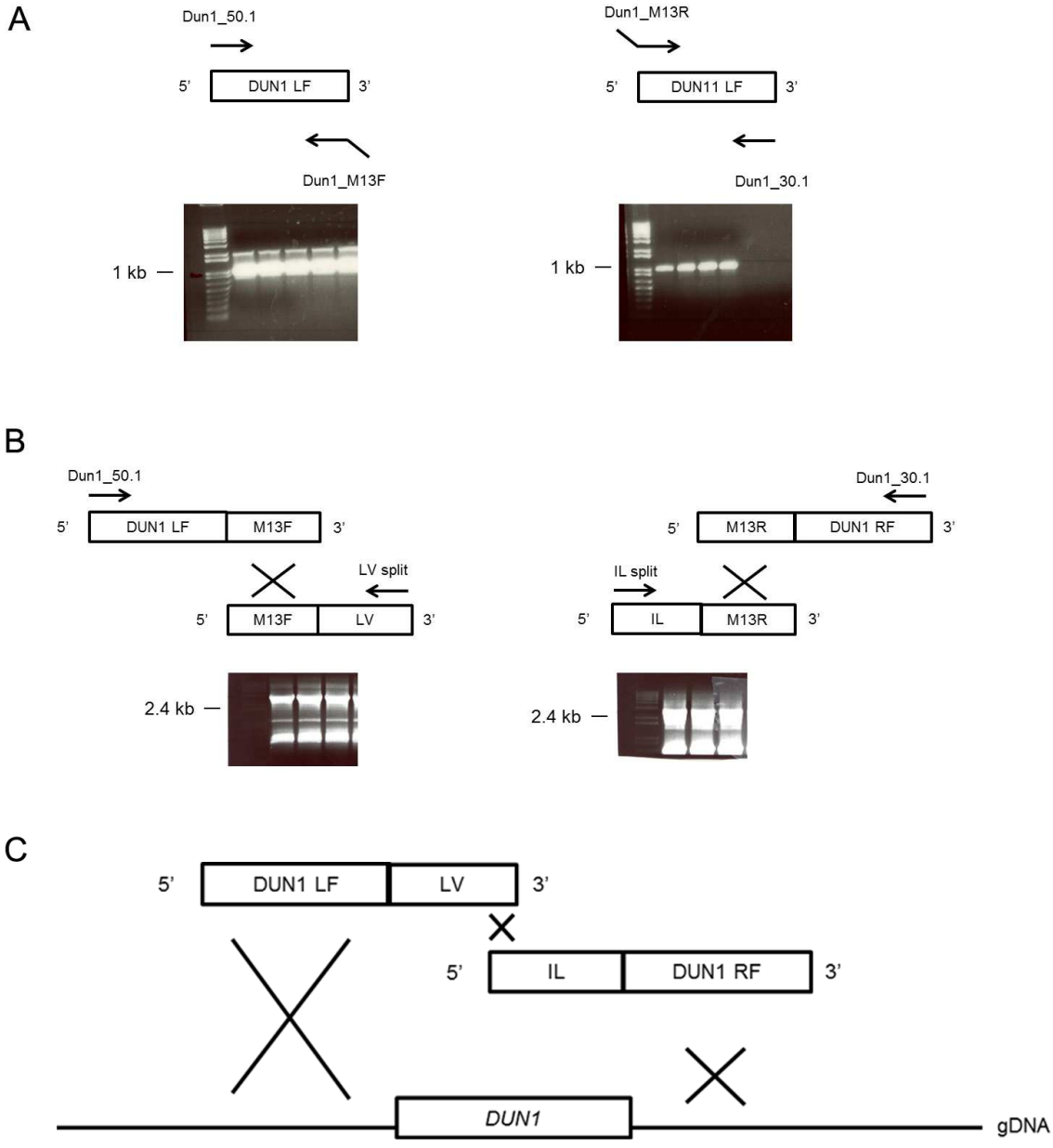

Figure 6.21 Schematic representation of the targeted deletion of *DUN1* using a PCR-based split-marker deletion method. A) First round PCR: amplification of a 1 Kb flanking region either side of the *DUN1* ORF using primers shown. **B)** Second round PCR: fusion of the *DUN1* LF to the terminal 1 Kb coding sequence of the *Ilv1* cassette (LV) and the *CDS1* RF to the initial 1 Kb coding sequence of the *Ilv1* cassette (IL). **C)** Fungal transformation of the two constructs into *M. oryzae*, in which homologous recombination occur resulting in the replacement of the *DUN1* ORF with the *Ilv* cassette

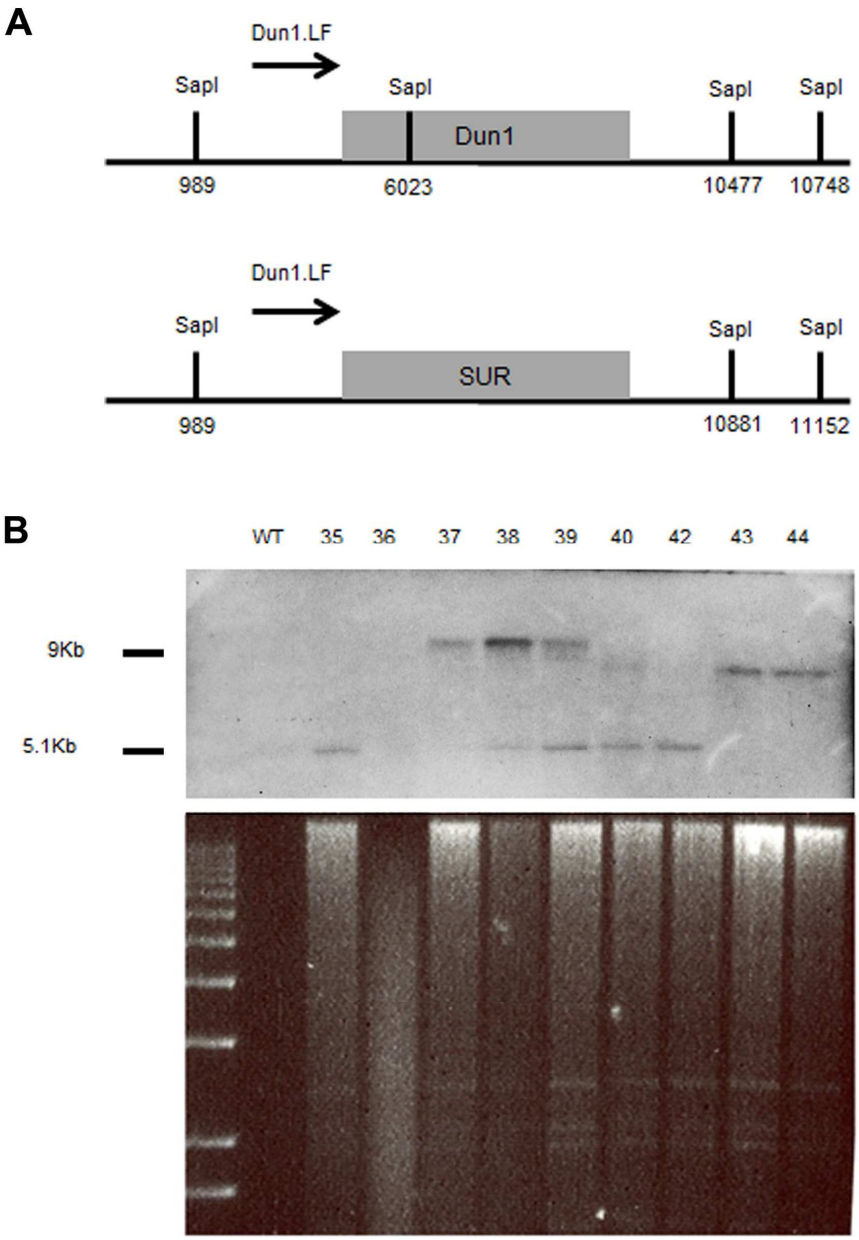

Figure 6.22 Southern Blot analysis for targeted gene replacement of *DUN1* into Guy11 background. **A)** Schematic representation of Southern blot analysis carried out to identify *DUN1* targeted gene replacement transformants. The upper scheme represents the wild type (Guy11) and the lower scheme represents the Δ*dun1* null mutant. **B)** Southern blot analysis showing a *Sap*I enzyme restriction digestion probed with the 1 Kb upstream region of *DUN1* (Dun1.LF) that generated a 5.1 Kb band when no gene replacement had occurred and a 9 Kb band when the corresponding resistance cassette was integrated at the *DUN1* locus. The Southern blot showed a positive result for T43 and T44.

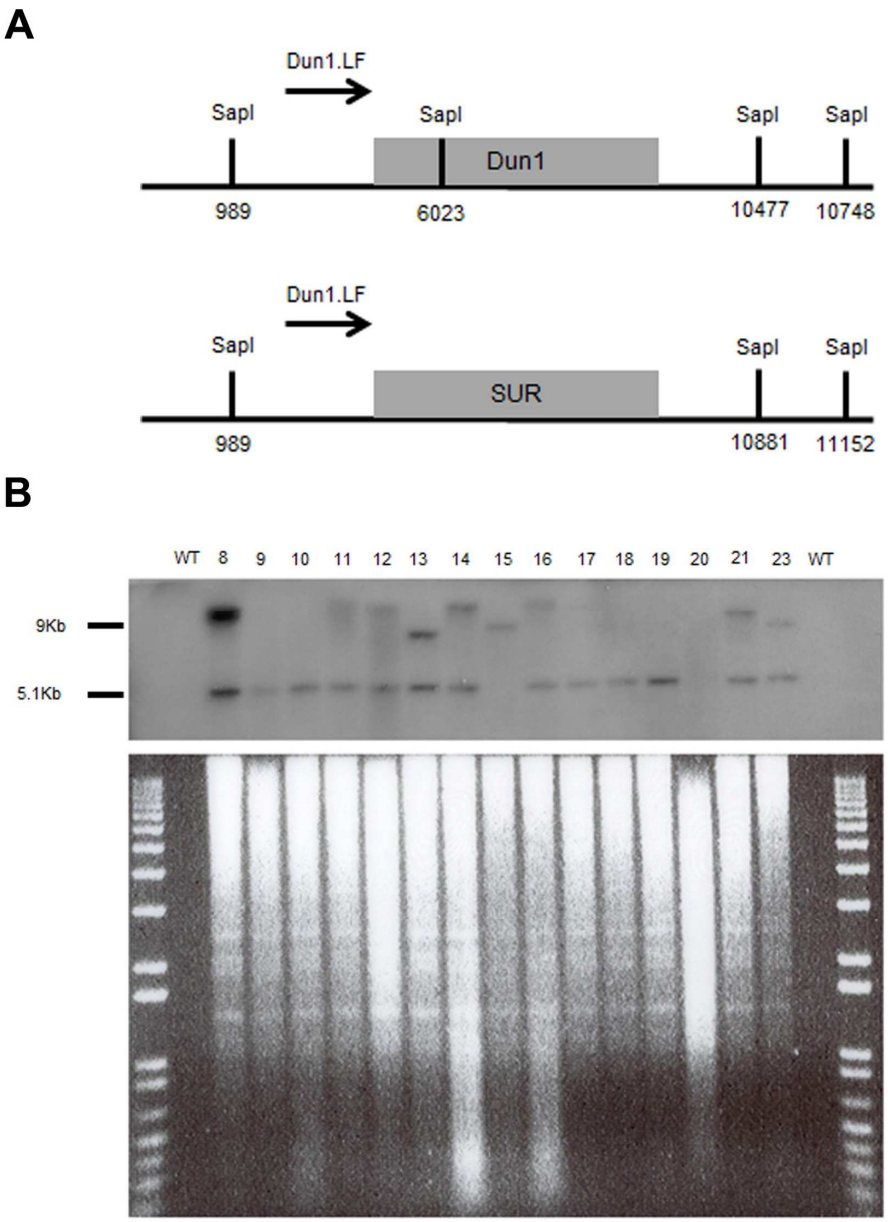

Figure 6.23 Southern Blot analysis for targeted gene replacement of *DUN1* into Δ*chk1* background. **A)** Schematic representation of the Southern blot analysis carried out to identify *DUN1* targeted gene replacement transformants in a Δ*chk1* background. The upper scheme represents the wild type (Guy11) and the lower scheme represents the Δ*dun1* null mutant. **B)** Southern blot analysis showing a *Sap*I enzyme restriction digestion probed with the 1 Kb upstream region of *DUN1* (Dun1.LF) that generated a 5.1 Kb band when no gene replacement had occurred and a 9 Kb band when the corresponding resistance cassette was integrated at the *DUN1* locus. The Southern showed a positive result for T15.

6.3.13 Generation of the *CDS1* targeted gene replacement vector

In order to determine the role of Cds1, targeted gene replacement of *CDS1* was performed using a PCR-based split marker deletion method as shown in Figure 6.25 (Kershaw and Talbot, 2009). In a first round PCR, primers were designed to amplify a 1 Kb genomic region both upstream and downstream of the *CDS1* ORF. The primers contained 5' and 3' overhanging regions complementary in sequence to the bialophos resistance gene cassette (Bar). In a second round PCR, two different fusion fragments were generated. The first PCR fusion was generated between the 1 Kb upstream of the *CDS1* ORF region and the initial 1.4 Kb fragment of *Bar* cassette through the 3' overhanging region generated in the first round PCR. The second PCR fusion was generated between 1 Kb downstream *CDS1* ORF region and the terminal 0.8 Kb fragment of *Bar* cassette through the 5' overhanging region generated in the first round PCR. The two fused constructs were simultaneously introduced into the *M. oryzae* Guy11, Δ*chk1,* Δ*dun1* and Δ*chk1*Δ*dun1* to guarantee successful integration of the two constructs at the respective locus. The primers used for the targeted gene replacement of *CDS1* are listed in Table 1.

6.3.14 Analysis of putative Δ*cds1* transformants

Putative transformants of Δ*cds1* mutants were selected in the presence of the antibiotic glufosinate (30 µg mL^{-1}). One hundred putative *M. oryzae* transformants were selected and genomic DNA was extracted. Transformants generated in the Guy11 background, were analysed by Southern blot analysis in which genomic DNA was digested with *Kpn*I. The resulting digestion was fractionated by gel electrophoresis before being transferred to a Hybond-N (Amersham). The membrane

was probed with the upstream region of *CDS1* generated as a 1 Kb first PCR amplicon. (Fig. 6.26, panel A). The probe hybridized into a 1.8 Kb fragment in the Guy11 control lane. However this hybridization was absent into transformant T13, T19 and T20 and instead, an 8.7 Kb band was visible as a result of the replacement of the *CDS1* gene by the resistance cassette (Figure 6.26, panel B).

For transformants generated in the Δ*chk1* mutant background, Southern blots analysis was set up in which the genomic DNA was digested with *Eco*RI. The resulting digestion was fractionated by gel electrophoresis before being transferred to a Hybond-N membrane (Amersham). The membrane was probed with the upstream region of *CDS1* as above (Fig. 6.27, panel A). The probe hybridized in a 5.7 Kb fragment in the Guy11 control lane. However this hybridization was absent into transformant T2 and T7 and instead, a 10.4 Kb band was visible as a result of the replacement of the *CDS1* gene by the resistance cassette (Fig. 6.27, panel B).

For transformants generated in the Δ*dun1* background, Southern blot analysis was set up in which the genomic DNA was digested with *Eco*RI. The resulting digestion was fractionated by gel electrophoresis before being transferred to Hybond-N (Amersham). The membrane was probed with the 1 Kb upstream region of *CDS1* as above (Fig. 6.28, panel A). The probe hybridized to a 5.7 Kb fragment into the Guy11 control lane. However this hybridization was absent in transformant T10 and instead, a 10.4 Kb band was visible as a result of replacement of the *CDS1* gene by the resistance cassette (Fig. 6.28, panel B).

For transformants generated in the Δ*chk1*Δ*dun1* background, Southern blot analysis was carried out in which genomic DNA was digested with *Kpn*I. The resulting digestion was fractionated by gel electrophoresis before being transferred

to a Hybond-N membrane (Amersham). The membrane was again probed with the 1 Kb upstream region of *CDS1* (Fig. 6.29, panel A). The probe hybridized to a 1.8 Kb fragment into the Guy11 control lane. However, hybridization was absent into transformant T15 and instead, an 8.7 Kb band was visible as a result of the replacement of the *CDS1* gene by the resistance cassette (Figure 6.29, panel B).

For further confirmation of the null mutation of *CDS1* an extra Southern blot analysis was set up in which the genomic DNA from all the positive transformants from the different backgrounds was digested with *Pst*I. The resulting digestion was fractionated by gel electrophoresis before being transferred to a Hybond-N membrane (Amersham). The membrane was also probed with the 1 Kb upstream region of *CDS1* (Fig. 6.30, panel A). The probe hybridized to a 5.5 Kb fragment into the Guy11 control lane. However this hybridization was absent from all the transformants corresponding to T7 from Δ*chk1* background, T15 from Δ*chk1*Δ*dun1* background, and T19 and T20 from Guy11 background showed the expected size band of 2.5 Kb which denotes that *CDS1* replacement had successfully occurred (Fig. 6.30, panel B). Although transformant T2 in the Δ*chk1* background, the wild-type band was absent, it did not have the expected 2.5 Kb band size.

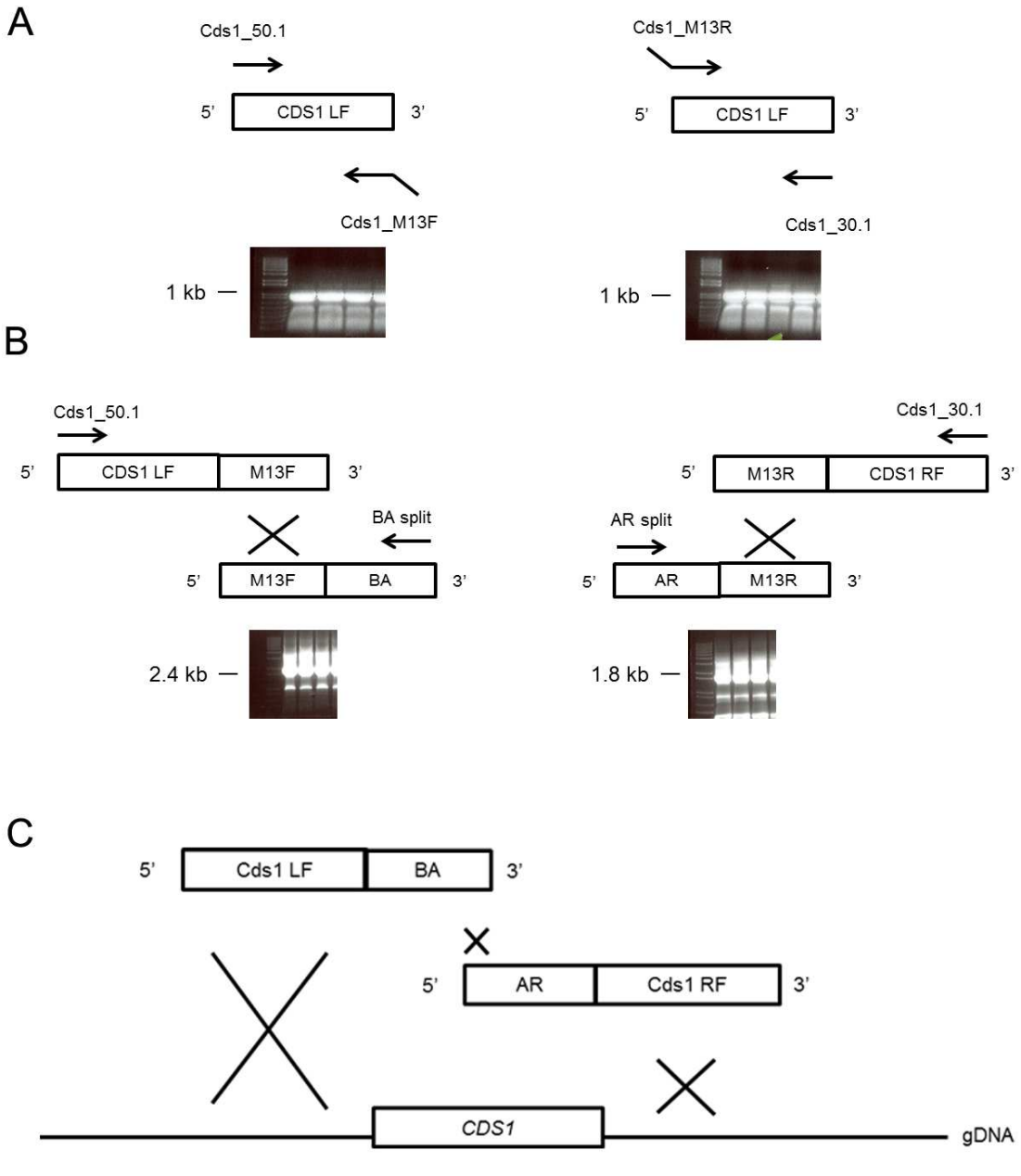

Figure 6.24 Schematic representation of the targeted deletion of *CDS1* using a PCR-based split-marker deletion method. A) First round PCR: amplification of a 1 Kb flanking region either side of the *CDS1* ORF using primers shown. **B)** Second round PCR: fusion of the *CDS1* LF to the initial 1 Kb coding sequence of the *Bar* cassette (BA) and the *CDS1* RF to the terminal 1 Kb coding sequence of the *Bar* cassette (AR). **C)** Fungal transformation of the two constructs into *M. oryzae*, in which homologous recombination occur resulting in the replacement of the *CDS1* ORF with the *Bar* cassette.

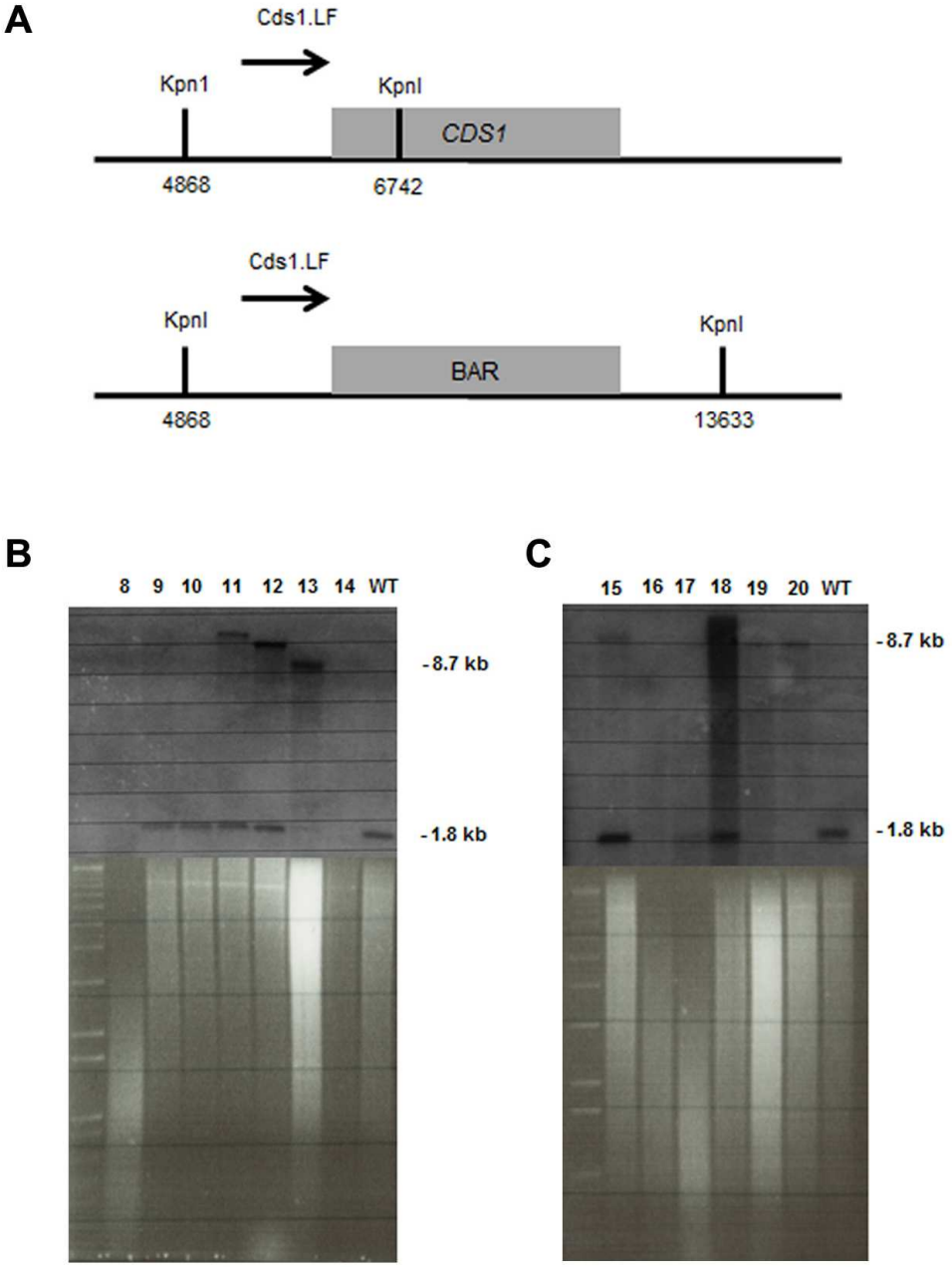

Figure 6.25 Southern Blot analysis for targeted gene replacement of *CDS1* into Guy11 background. **A)** Schematic representation of Southern blot analysis carried out to identify targeted gene replacement of *CDS1.* The upper scheme represents the wild type (Guy11) and the lower scheme represents Δ*chk1* null mutant. **B)** Southern blot analysis result showing a *Kpn*I enzyme restriction digestion followed by probing with the 1 Kb upstream region of *CDS1* (Cds1.LF) that generated a 1.8 Kb band when no gene replacement had occurred and a 8.7 Kb band when the corresponding resistance cassette was integrated at the *CDS1* locus. The Southern showed a positive result for T13, T19 and T20.

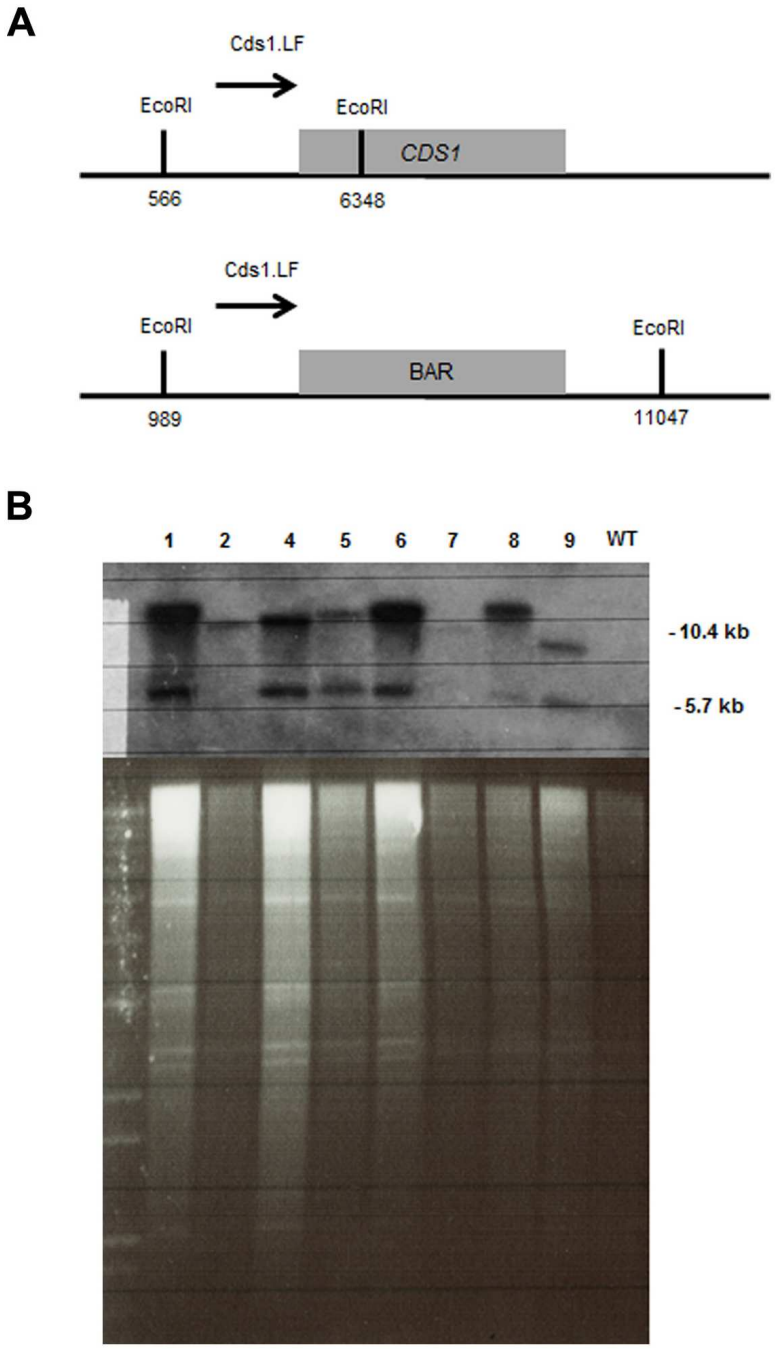

Figure 6.26 Southern Blot analysis for targeted gene replacement of *CDS1* into Δ*chk1* background. **A)** Schematic representation of the Southern blot analysis to identify targeted gene replacement of *CDS1.* The upper scheme represents the wild type (Guy11) and the lower scheme represents Δ*cds1* null mutant*.* **B)** Southern blot analysis result showing a *Eco*RI enzyme restriction digestion followed by probing with the 1 Kb upstream region of *CDS1* (Cds1.LF) that generated a 5.7 Kb band when no gene replacement had occurred and a 10.4 Kb band when the corresponding resistance cassette was integrated at the *CDS1* locus. The Southern showed a positive result for T2 and T7.

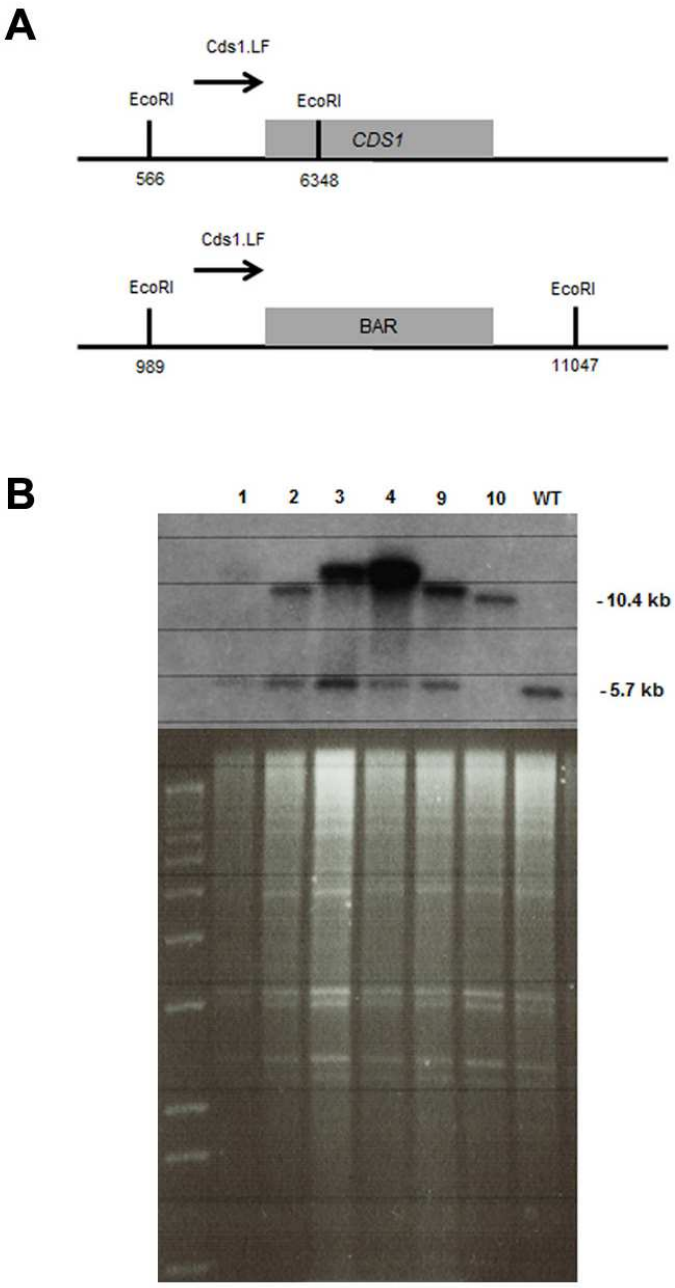

Figure 6.27 Southern Blot analysis for targeted gene replacement of *CDS1* into Δ*dun1* background. **A)** Schematic representation of the Southern blot analysis followed for targeted gene replacement of *CDS1.* The upper scheme represents the wild type (Guy11) and the lower scheme represents Δ*cds1* null mutant. **B)** Southern blot analysis result showing a *Eco*RI enzyme restriction digestion followed by probing with the 1 Kb upstream region of *CDS1* (Cds1.LF) that generated a 5.7 Kb band when no gene replacement had occurred and a 10.4 Kb band when the corresponding resistance cassette was integrated at the *CDS1* locus. The Southern showed a positive result for T10.

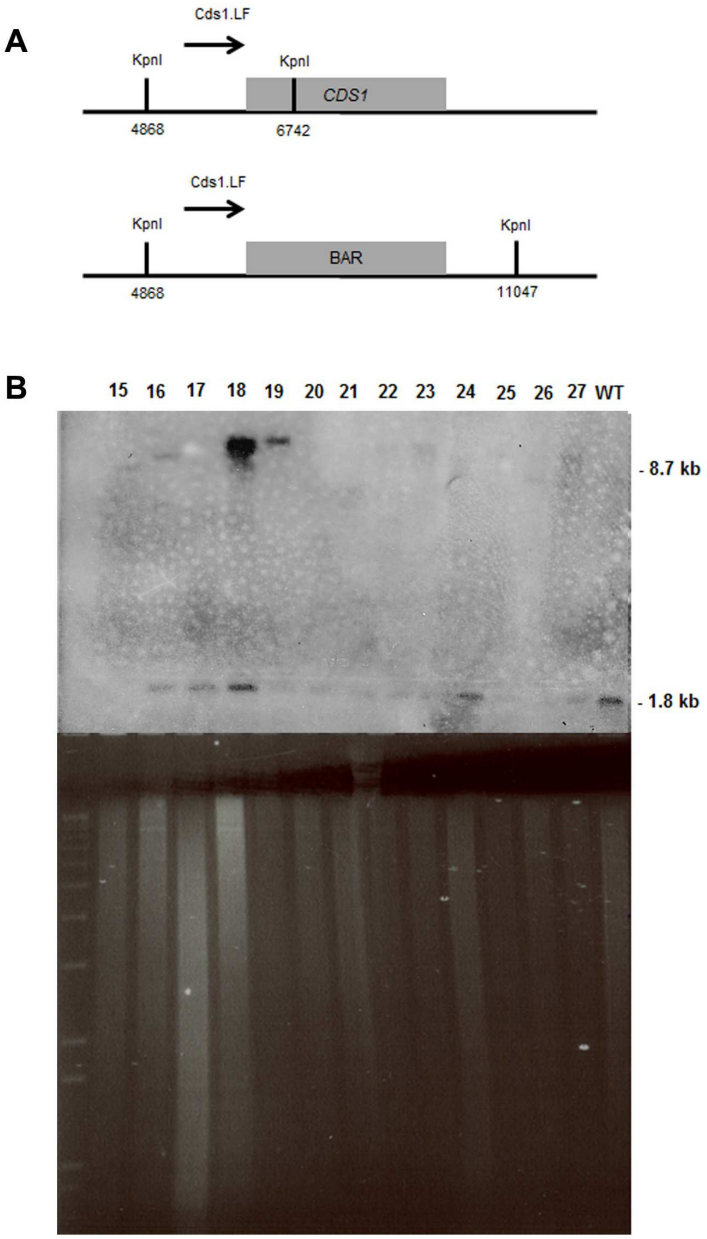

Figure 6.28 Southern Blot analysis for targeted gene replacement of *CDS1* into Δ*chk1*Δ*dun1* background. **A)** Schematic representation of the Southern blot analysis carried out to identify targeted gene replacement of *CDS1.* The upper scheme represents the wild type (Guy11) and the lower scheme represents Δ*cds1* null mutant. **B)** Southern blot analysis result showing a *Kpn*I enzyme restriction digestion followed by probing with the 1 Kb upstream region of *CDS1* (Cds1.LF) that generated a 1.8 Kb band when no gene replacement had occurred and a 8.7 Kb band when the corresponding resistance cassette was integrated at the *CDS1* locus. Southern blot analysis showed a positive result for T15.

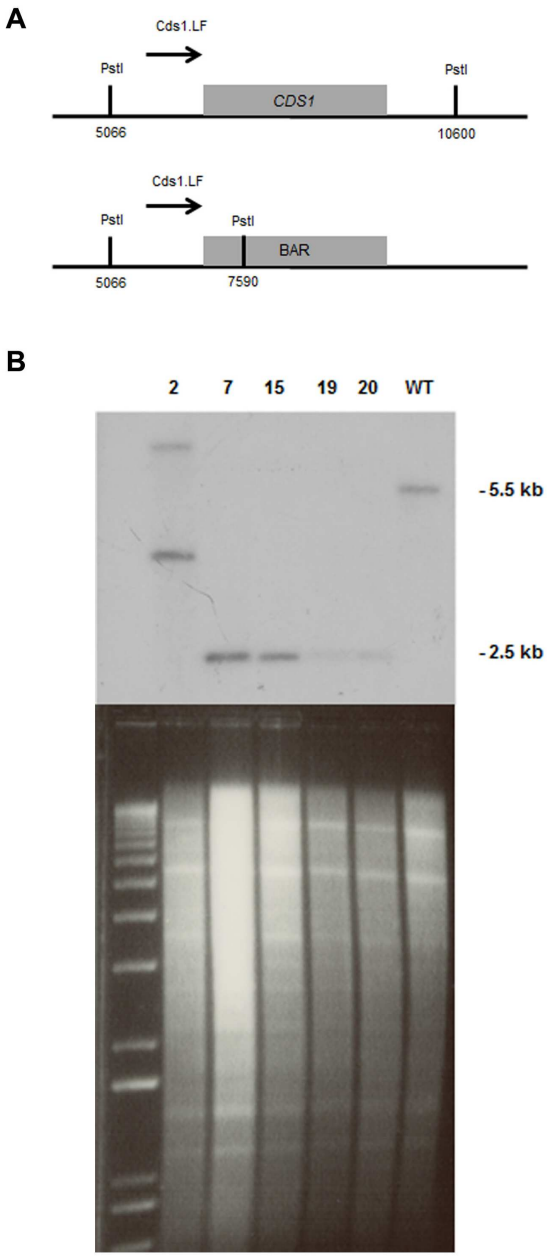

Figure 6.29 Southern Blot analysis for targeted gene replacement of *CDS1* into each genetic backgrounds. A) Schematic representation of the Southern blot analysis followed for targeted gene replacement of *CDS1.* The upper scheme represents the wild type (Guy11) and the lower scheme represents Δ*cds1* null mutant. **B)** Southern blot analysis result showing a *Pst*I enzyme restriction digestion followed by probing with the 1 Kb upstream region of *CDS1* (Cds1.LF) that generated a 5.5 Kb band when no gene replacement had occurred and a 2.5 Kb band when the corresponding resistance cassette was integrated at the *CDS1* locus. Numbers 2 and 7 correspond to Δ*chk1* background, number 15 corresponded to the Δ*chk1*Δ*dun1* background, and number 19 and 20 corresponded to the Guy11 background.

Table 6.1 Oligonucleotide primer list used for targeted gene deletions of *CHK1, DUN1* and *CDS1.*

Primer	Sequence 5'→3'
Dun1_50.1	ACGAAGGAGGTGACAATCTGCTAT
Dun1_M13F	GTCGTGACTGGGAAAACCCTGGCGCACCGTTAAAGAAACATACCCGAG
Dun1_M13R	TCCTGTGTGAAATTGTTATCCGCTGAACAACTACATCCACAACAGATT
Dun1_30.1	GAGGACGGCAACTGCATCTAGC
Chk1_50.1	GGGATGGTATATGGGCGTCTTG
Chk1_M13F	GTCGTGACTGGGAAAACCCTGGCGATTGCTGTACTTCGTAGGTCCGTT
Chk1_M13R	TCCTGTGTGAAATTGTTATCCGCTTCCCATTTCCAGGTCTGTAATAGT
Chk1_30.1	TTCCTCTTCCTCCTTATTTTTGCT
Cds1_50.1	TCAGCAGCCAACACATCTTTTTAC
Cds1_M13F	GTCGTGACTGGGAAAACCCTGGCGTCGTCACCATCCAGTCTAGCCT
Cds1_M13R	TCCTGTGTGAAATTGTTATCCGCTACATCTAAGCCGCGCATTGGAG
Cds1_30.1	TGGTTGCGGCTTATCTGGAGGC
HY split	GGATGCCTCCGCTCGAAGTA
YG split	CGTTGCAAGACCTGCCTGAA
M13F	CGCCAGGGTTTTCCCAGTCACGAG
M13R	AGCGGATAACAATTTCACACAGGA

6.3.15 Phenotypic analysis of *Δchk1*, *Δcds1*, *Δdun1*, *Δchk1Δcds1*, *Δchk1Δdun1*, *Δcds1Δdun1* and *Δchk1Δdun1Δcds1*

In order to study the effect of the DNA replication checkpoint mutation in *M. oryzae*, colony morphology and vegetative growth were studied. The Δ*chk1,* Δ*cds1,* Δ*dun1,* Δ*chk1*Δ*cds1,* Δ*chk1*Δ*dun1,* Δ*cds1*Δ*dun1* and Δ*chk1*Δ*dun1*Δ*cds1* were inoculated alongside the Guy11 as a control, onto CM plates (Fig. 6.31). After ten days post-inoculation Δ*chk1,* Δ*cds1,* Δ*dun1,* Δ*chk1*Δ*cds1,* Δ*chk1*Δ*dun1,* Δ*cds1*Δ*dun1* and Δ*chk1*Δ*dun1*Δ*cds1* displayed normal patterns of vegetative growth with dark concentric rings as a result of growth similar to Guy11.

In many organisms, DNA replication checkpoint mutants show increased sensitivity to DNA damage agents, such as HU or methylmethane sulfonate (MMS) (Bashkirov *et al.,* 2003; Perez-Martin, 2009). To investigate sensitivity of the mutants to DNA damage agents, the DNA-alkylation agent MMS was added at 0.001% onto CM plates in which mycelial plugs of the wild type and mutant strains were inoculated and measurements of colony growth were recorded over the period of ten days and a graph was plotted (Fig. 6.32). Morphology of the colonies of Δ*chk1*Δ*cds1* and Δ*chk1*Δ*dun1*Δ*cds1* was significantly different from the rest of the mutants and to Guy11. The Δ*chk1*Δ*cds1* and Δ*chk1*Δ*dun1*Δ*cds1* colonies showed colonial compact, mycelial growth with a yellowish-brown halo at the edge of the colony. Guy11 and Δ*dun1* showed no differences in growth over the time period (Fig. 6.32). However, Δ*chk1*Δ*cds1* and Δ*chk1*Δ*dun1*Δ*cds1* showed a dramatic reduction in growth compared with the wild type (Fig. 6.32).

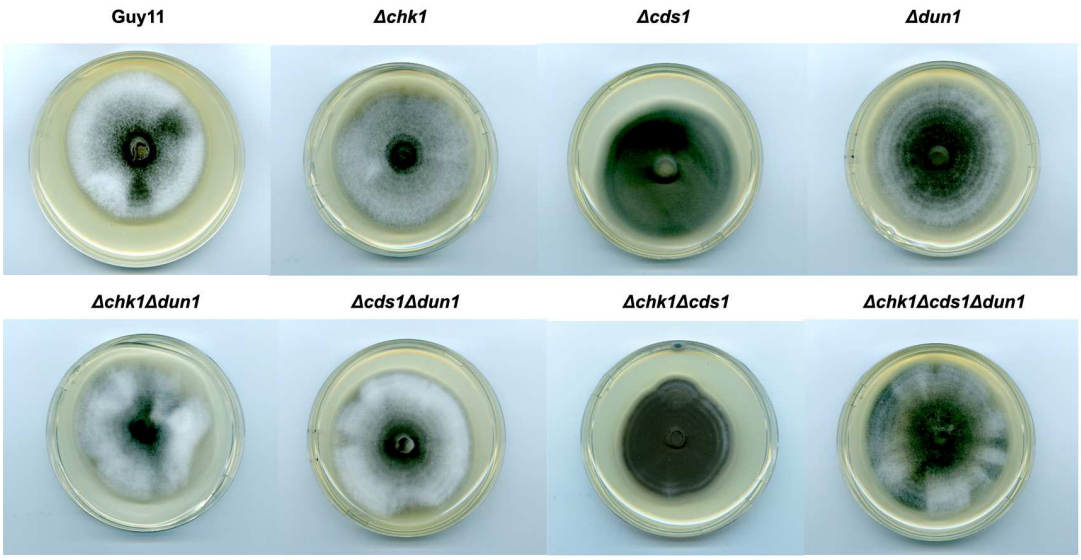

Figure 6.30 Vegetative growth and colony morphology of DNA replication checkpoint mutants. A mycelial plug of Guy11 Δ*chk1*, Δ*cds1*, Δ*dun1*, Δ*chk1*Δ*cds1*, Δ*chk1*Δ*dun1*, Δ*cds1*Δ*dun1 and* Δ*chk1*Δ*dun1*Δ*cds1* were inoculated onto CM plates and incubated over a period of 10 days at 26 ℃. Images were taken by using an Epson Expression 1680 Pro scanner.

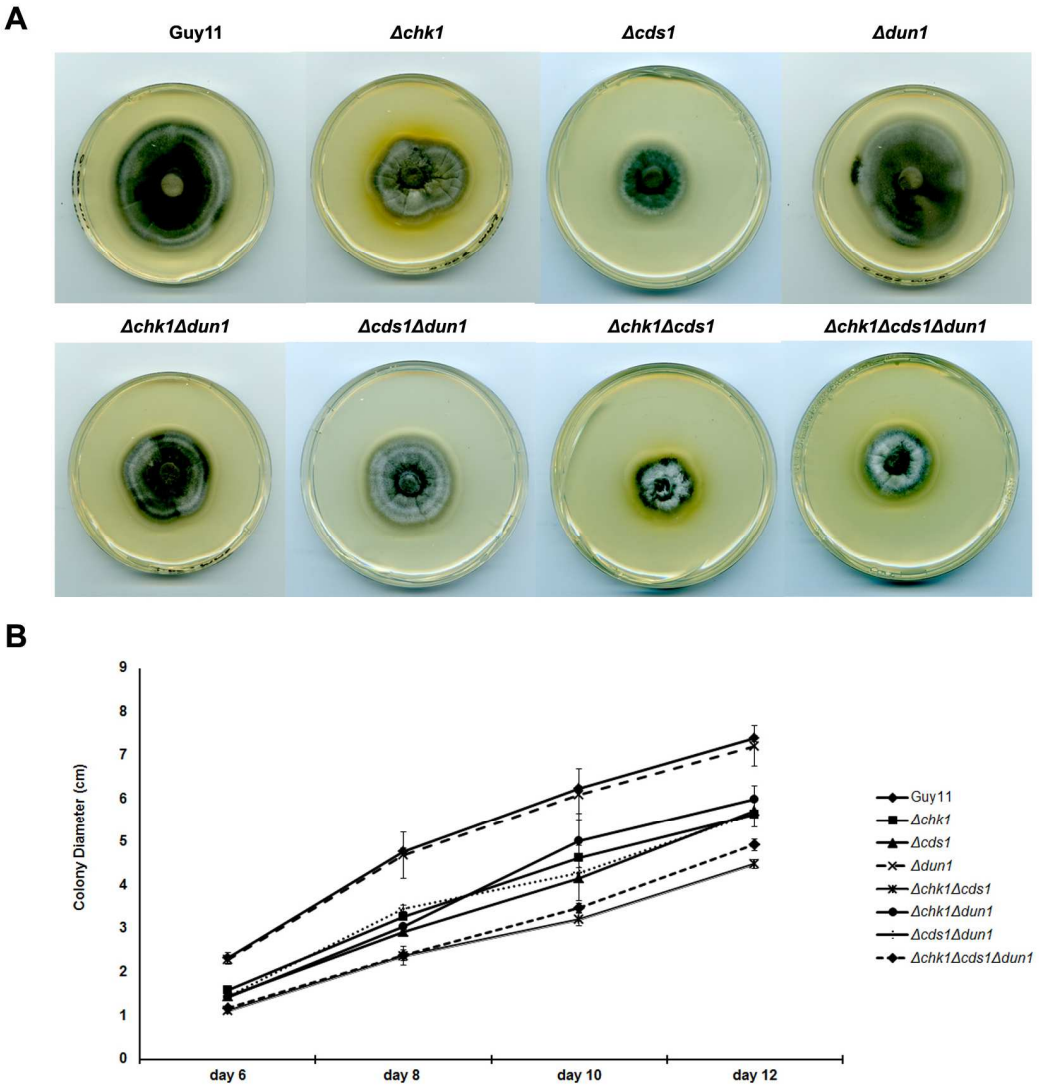

Figure 6.31 Vegetative growth and colony morphology of DNA replication checkpoint mutants. **A)** A mycelial plug of Guy11, Δ*chk1*, Δ*cds1*, Δ*dun1*, Δ*chk1*Δ*cds1*, Δ*chk1*Δ*dun1*, Δ*cds1*Δ*dun1* and Δ*chk1*Δ*dun1*Δ*cds1* were inoculated onto 0.001% MMS in CM plates and incubated during 12 days at 26 ℃. Images were taken by using an Epson Expressi on 1680 Pro scanner after 10 days post inoculation. **B)** Colony growth was measured for the mutants and Guy11 over the period of 12 days. Error bars represented the standard deviation from three independent replicates.

6.3.16 Pathogenicity assay of *Δchk1*, *Δcds1*, *Δdun1, Δchk1Δcds1*, Δchk1Δdun1, *Δcds1Δdun1* and *Δchk1Δdun1Δcds1*

To investigate the ability of the mutants to cause disease in rice, three-week old CO-39 rice plants were spray inoculated with the mutants and the wild-type, Guy11. Symptoms were quantified at 5 days post inoculation by counting the number of lesions every 5 cm of leaf and establishing the percentage of infection compared with Guy11. A statistical analysis using the Student's two-tailed t-test was used to determine any significant differences between each mutant with the wild type by using at least 15 leaves per strain (Fig. 6.33). The results indicated that the percentage infection was slightly reduced for both Δ*cds1* (76%; p=0.047) and *Δchk1Δcds1* (70.9%; p=0.01) compared to Guy11. However the other mutants showed no significant differences in percentage infection compared to Guy11. The results indicated that *CDS1* might be required for full virulence of the fungus, and this effect might be enhanced when *CHK1* is absent. However, when the *CDS1* mutation was combined with *DUN1*, this effect on virulence was attenuated indicating a positive effect of *DUN1* mutation in the ability of the fungus to colonize its host.

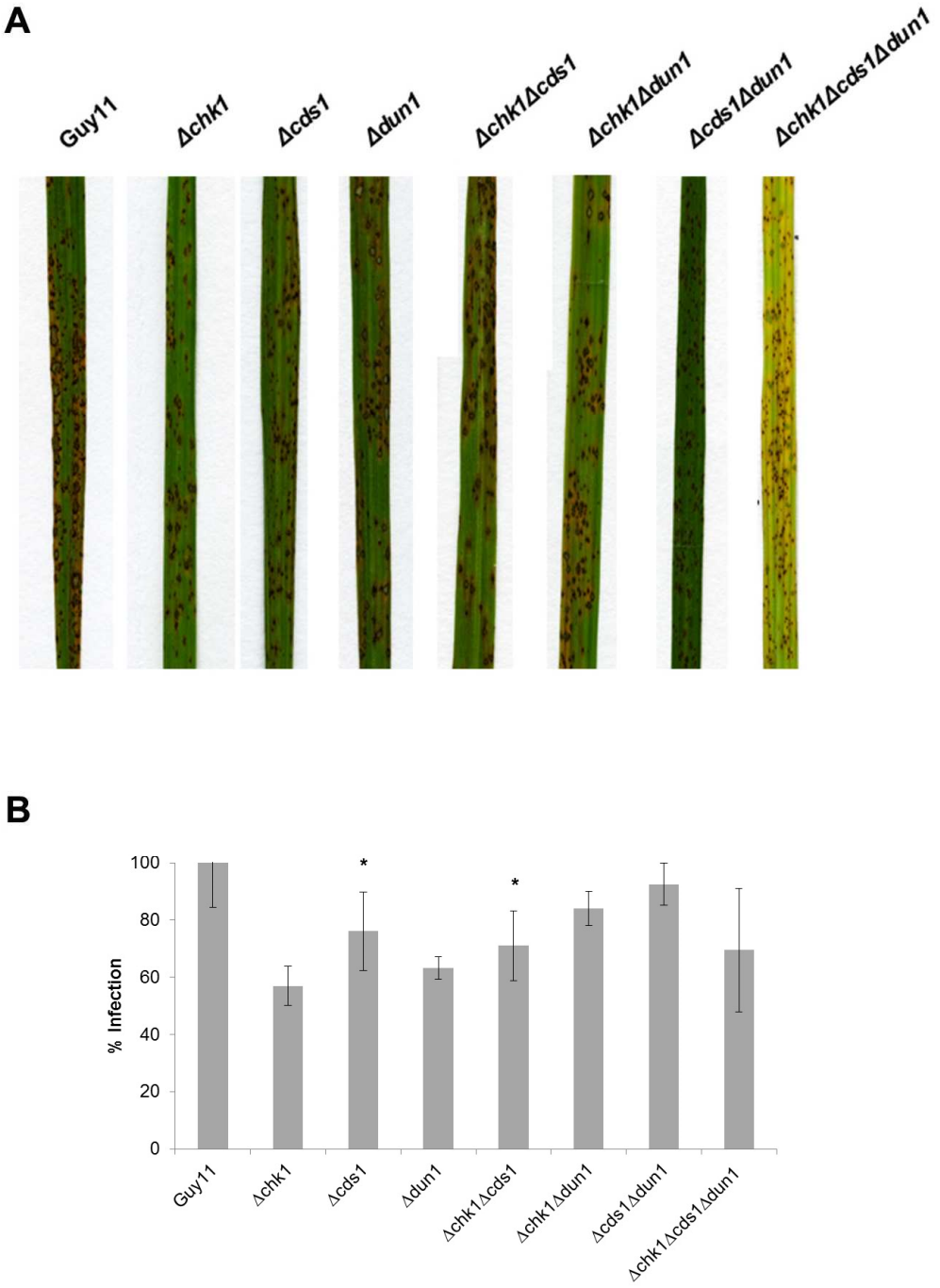

Figure 6.32 Pathogenicity assay of DNA replication checkpoint mutants. A) Three week-old seedlings of CO-39 rice cultivar were sprayed inoculated with Δ*chk1,* Δ*cds1,* Δ*dun1,* Δ*chk1*Δ*cds1,* Δ*chk1*Δ*dun1,* Δ*cds1*Δ*dun1* and Δ*chk1*Δ*dun1*Δ*cds1* and Guy11. Leaves were harvested at 5 days post inoculation. **B)** Bar chart showing the percentage of infection compared to Guy11 of DNA replication checkpoint mutants. Error bars represent the standard deviation.

6.3.17 Investigating the role of the DNA checkpoint kinases in appressorium morphogenesis

To test whether DNA checkpoint kinases are involved in appressorium morphogenesis, an appressorial assay was set up using the wild-type Guy11 strain and the Δ*chk1,* Δ*cds1,* Δ*dun1,* Δ*chk1*Δ*cds1,* Δ*chk1*Δ*dun1,* Δ*cds1*Δ*dun1* and Δ*chk1*Δ*dun1*Δ*cds1* null mutants. All the mutants were able to form appressoria non-distinguishable from the ones of the wild-type Guy11 under standard conditions (data not shown). Conidia were harvested and inoculated onto hydrophobic glass coverslips and incubated at 26 ℃ with 50 µL 200 mM HU added after 1 hour. At 24 h the percentage of germling formation, hooking and appressorium formation was monitored and quantified (Fig. 4.34). The results show that appressorium formation was partially restored in *Δcds1* (73.5% ± 5.91) and *Δchk1Δcds1* (46% ± 4.9%) compared to the wild-type Guy11 (1.4% ± 0.4) indicating that *Δcds1* and *Δchk1Δcds1* were able to overcome the S-phase arrest caused by the HU addition and therefore were impaired in monitoring the DNA damage. The rest of the mutants *Δchk1* (4.34% ± 3.01), *Δdun1* (13.7% ± 7.16), *Δchk1Δdun1* (38% ± 8.22), *Δcds1Δdun1* (38% ± 3.3) and *Δchk1Δdun1Δcds1* (25% ± 6) showed a similar percentage of appressorium formation to the wild type. These results suggest a possible involvement of Cds1 and Chk1 in appressorium morphogenesis in the presence of a DNA replication stress.

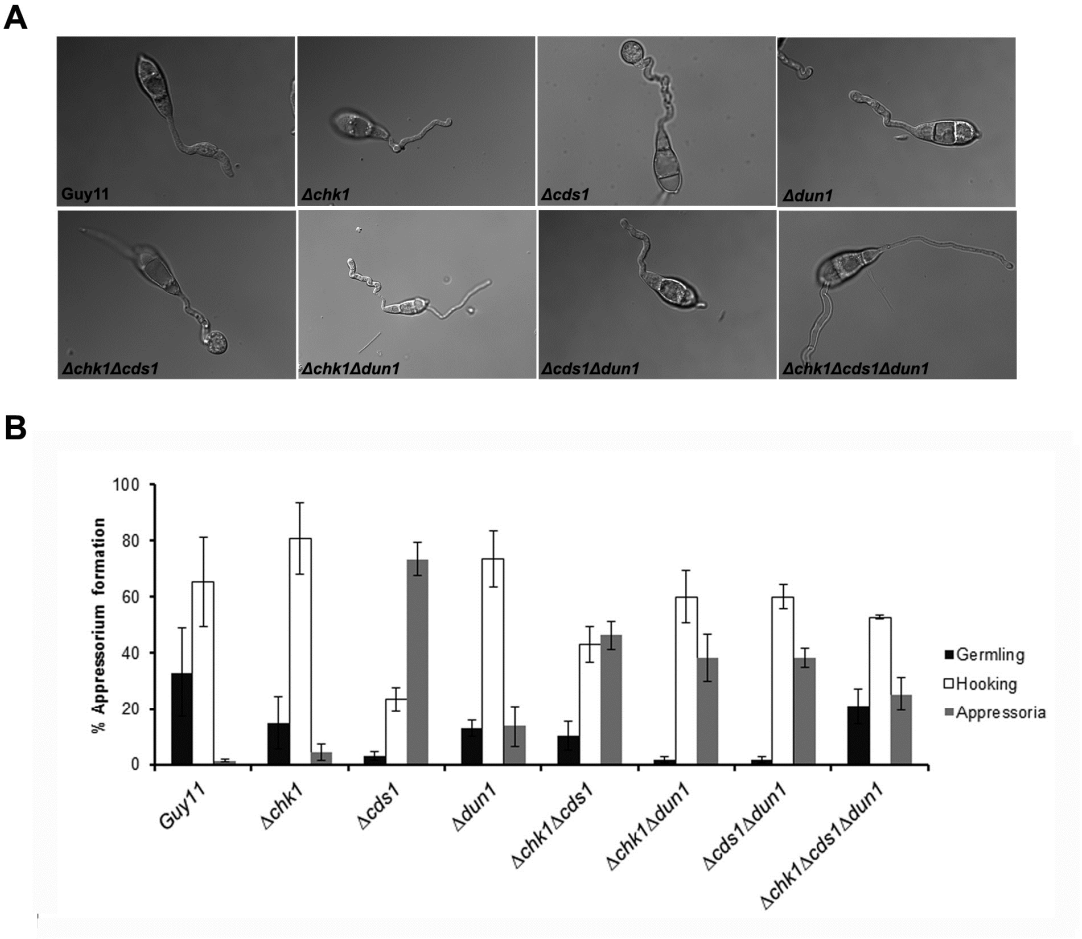

Figure 6.33 Involvement of DNA checkpoint kinases into appressorium morphogenesis. A) Micrographs at 24 h of appressorial assays in which 50 µL of 200 mM HU were added at 1 h post inoculation into Guy11 strain and Δ*chk1,* Δ*cds1,* Δ*dun1,* Δ*chk1*Δ*cds1,* Δ*chk1*Δ*dun1,* Δ*cds1*Δ*dun1* and Δ*chk1*Δ*dun1*Δ*cds1* null mutants . **B)** Bar chart to show the percentage formation of germlings (black), hooking (white) and appressoria (grey) for each of the mutants (bar= 10 µm).

6.3.18 Investigating the role of DNA checkpoint kinases in appressorium-mediated plant penetration

Following the previous result, we decided to investigate whether Cds1 and Chk1 were involved in appressorium-mediated plant infection. To test this the wild-type Guy11 strain, Δ*cds1,* and Δ*chk1*Δ*cds1* mutants were inoculated onto 28 day-old CO-39 rice leaf sheaths and incubated at 25 ℃ for 10 h when 1 M of HU was added covering all the inner part of the leaf sheath (Fig. 6.34). At 30 h, the control leaf sheath for Guy11 strain, Δ*cds1,* and Δ*chk1*Δ*cds1*, showed the formation of the primary invasive hyphae with 77% ± 20, 69% ± 11 and 52% ± 15 percentage of penetration respectively. However, with the addition of 1 M HU, Guy11 was not able to penetrate (0.9% ± 0.49), but this was also the case with Δ*cds1* (1.92% ± 1.92), and Δ*chk1*Δ*cds1* (1.98% ± 0.019) in which an intact appressorium was observed. This suggests that neither Cds1 nor Chk1 are involved in the S-phase checkpoint that governs appressorium mediated plant infection.

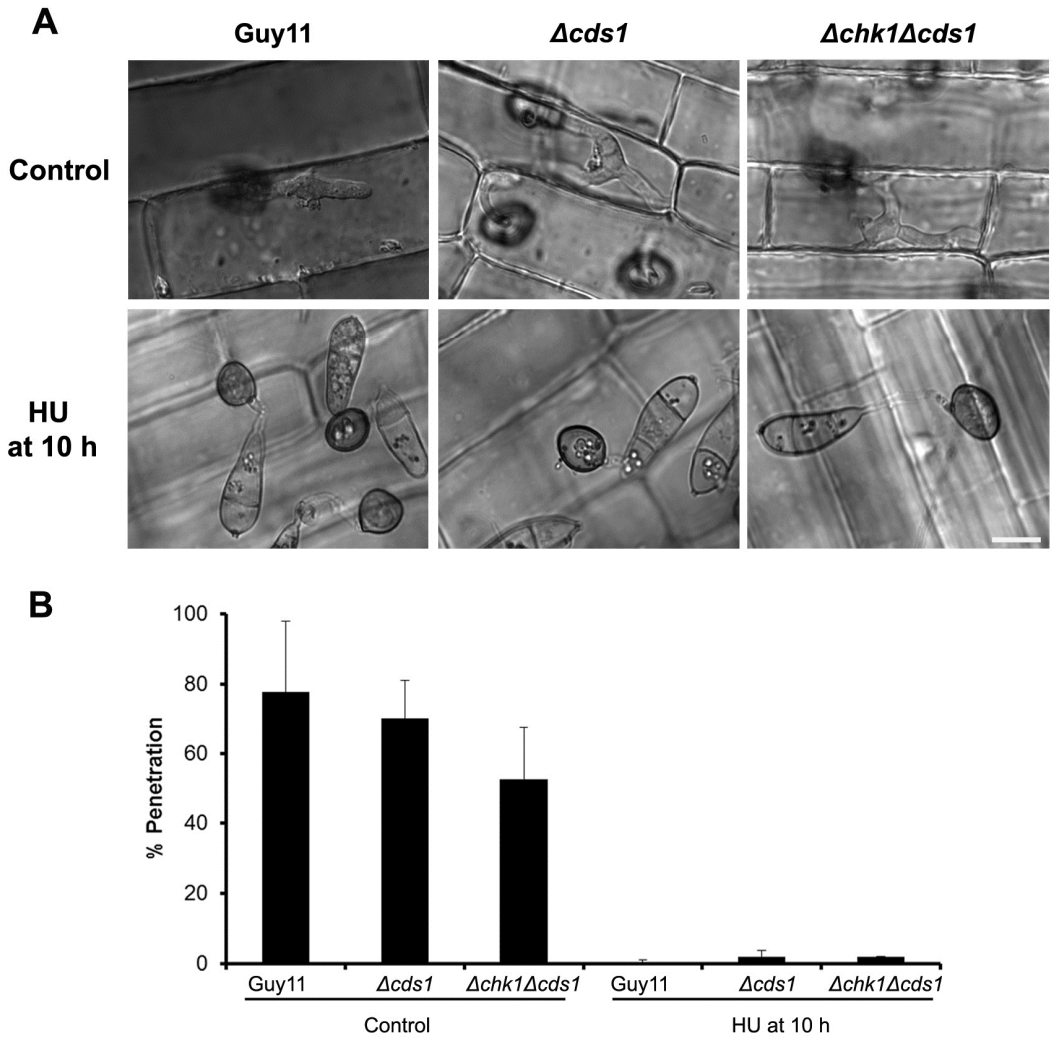

Figure 6.34 Involvement of DNA checkpoint kinases in appressorium-mediated plant penetration. A) CO-39 rice leaf sheath at 30 h inoculated with wild-type Guy11, Δ*cds1 and* Δ*chk1*Δ*cds1* at 30 h without HU (upper panel) and with addition of 1M HU at 10 h (bottom panel). **B)** Bar chart showing the percentage penetration. The graph represents three biological replicates (bar= 10 µm).

6.4 Discussion

In this chapter I have provided evidence that an S-phase checkpoint is required for appressorium–mediated plant penetration in *M. oryzae.* Moreover, the S-phase checkpoint seems to be required for cytoskeleton re-organization at the base of the appressorium but is independent of the DNA replication and damage response.

I have shown that the DNA replication inhibitor, HU, inhibits plant penetration in a reversible and dose-dependent manner. Using a genetic approach, I have shown that the temperature sensitive mutant *Δnim1*^{ts}, impaired in DNA replication, was also unable to form a penetration peg, and therefore failed to cause plant infection. However, in mutants arrested in G2 or at M, plant infection was not prevented. Consistent with this, arresting the cycle at mitosis entry by benomyl treatment did not prevent appressorium-mediated plant infection. Therefore, when considered together these data support the conclusion that completion of a DNA replication phase is necessary for plant penetration, and that an S-phase checkpoint operates to control plant infection.

An S-phase checkpoint in *M. oryzae* is also required for early appressorium morphogenesis and has been suggested to be regulated by Pmk1 MAP kinase pathway (Saunders *et al.,* 2010a). However, not all fungi displaying appressorium formation display this same pattern of regulation. For example, in the obligate biotrophy *Blumeria graminis* HU block did not prevent appressorium morphogenesis, but prevented appressorium maturation (Hansjakob *et al.,* 2012). Interestingly, depending on the *Colletotrichum* species analysed, appressorium formation may be an S-phase dependent process (Nesher *et al.,* 2008), consistent with *M. oryzae*

observations. By analogy to fungal model organisms, we hypothesize that penetration peg emergence represents a similar process to budding in *S. cerevisiae*, in which strong apical polarization occurs during G1 and S phase, with a later switch to isotropic growth occurring during G2 (Howell and Lew, 2012).

In all eukaryotic organisms, a failure or delay in DNA replication causes a cell cycle arrest, mediated through inhibitory phosphorylation of Cdc28, which prevents a catastrophic mitosis (Lew, 2003). In general, surveillance mechanisms of DNA state are mediated through DNA replication or damage responses (Hartwell and Weinert, 1989; Murray, 1992; Russell, 1998). However, there are increasing reports showing that DNA replication and damage responses have extra roles to manipulate cell cycle progression leading to a morphogenetic change (de Sena-Tomas *et al.,* 2011). It has also been shown that the Cds1 homologue in *S. cerevisiae*, Rad53, interacts with septins and Swe1, connecting morphogenetic components with DNA replication and damage responses (Enserink *et al.,* 2006; Smolka *et al.,* 2006). The DNA checkpoint kinases from this response have been also reported to have roles in pathogenicity in, for example, the corn smut fungus *U. maydis* (Mielnichuk *et al.,* 2009).

In this study, we hypothesized that in *M. oryzae,* DNA replication may be directly monitored through the DNA checkpoint damage response, which leads to arrest of the cell cycle. Our data shows that null mutants of DNA checkpoint kinases were able to partly restore appressorium morphogenesis in the presence of HU indicating that they may be involved in monitoring the S-phase at that stage of development, consistent with a conventional S-phase checkpoint governing cellular differentiation during appressorium morphogenesis. However, conversely there was no effect observed on penetration peg formation and appressorium-mediated plant

infection. This suggests that the completion of S-phase during appressorium-mediated plant infection occurs independently of the DNA checkpoint damage response and that, probably, the direct monitoring of the DNA state is not the signal to trigger the formation of the penetration peg. However, it is not known whether the inhibitory phosphorylation of Cdc28 is the only requirement for a sustained cell cycle arrest. In *A. nidulans,* in order to overcome a cell cycle arrest it is necessary not only to remove the inhibitory phosphorylation, but also to promote mitosis (Ye *et al.,* 2014). In *M. oryzae,* it is not known whether removal of the inhibitory phosphorylation of Cdc28 occurs in DNA checkpoint kinase mutants. It will be necessary to confirm this by checking the phosphorylation state of Cdc28 in the presence of HU, in the DNA checkpoint kinase mutants. Another possibility would be to generate a refractory allele of Cdc28 that is insensitive to phosphorylation (reviewed in (Osmani and Ye, 1997)). In addition to this, a thermo sensitive mutation of *BIME* could be generated in those backgrounds in order to promote mitosis. In conclusion, further investigation will be needed to test this hypothesis thoroughly.

It is tempting to speculate in light of this data, that the cell might not be monitoring the state of the DNA per se, but instead is monitoring the morphogenesis of the penetration peg, as is the case with budding in *S. cerevisiae* (Lew and Reed, 1993). In *M. oryzae* formation of the penetration peg depends on a number of factors including cytoskeleton re-organization at the base of the appressorium and turgor generation (Dagdas *et al.,* 2012; Ryder *et al.,* 2013; Xu *et al.,* 1998). Bud formation in *S. cerevisiae* also depends on several factors. *S. cerevisiae* cells in the presence of the actin depolymerizing agent latrunculin are unable to form buds (Harrison *et al.,* 2001). In *M. oryzae* the addition of latrunculin at 16 h to germinating spores results in failure of appressoria to form a penetration peg, and this is also the case in NADPH

oxidases (NOX) null mutants which are impaired in F-actin organization (Ryder *et al.,* 2013). Also null mutants of the master polarization regulator *CDC42* are unable to form a penetration peg (Zheng *et al.,* 2009). Similarly, *CDC42* null mutants in *S. cerevisiae* are unable to form a bud (Lew and Reed, 1995). However *CDC42* null mutants in *M. oryzae* are also impaired in both ROS and turgor generation, indicating some cross talk between these mechanisms in appressorium development (Zheng *et al.,* 2009). The pathway responsible for turgor generation in *M. oryzae* is the cell integrity pathway, involving Mps1, which is the *S. cerevisiae* Slt2 homologue (Xu *et al.,* 1998). Downstream of Mps1 is the transcription factor Swi6, which in *S. cerevisiae* regulates cell cycle genes involved in G1 to S transition, and *SWI6* null mutants in *M. oryzae* are impaired in turgor generation and plant penetration (Qi *et al.,* 2012; Sidorova and Breeden, 1997). Interestingly, preliminary research in our lab suggests that accumulation of turgor in the appressorium is required for cytoskeleton re-organization at the base of appressorium (Y. Dagdas, unpublished). In this current study we have now also shown that a block in cell cycle progression affects cytoskeleton organization at the base of the appressorium, and therefore appressorium-mediated plant penetration cannot occur. I propose as a conclusion that there is likely to be a triple association between turgor generation, cytoskeleton organization and cell cycle progression that is collectively required for appressorium-mediated plant penetration. I hypothesize that if any perturbation occurs to any one of these three factors, it would generate an effect in the other two, leading to impairment in the formation of a penetration peg. I also propose that the master regulator of this interconnection is likely to be the Swe1 kinase. In *S. cerevisiae*, Swe1 has been shown to regulate the cell cycle through Cdc28, to monitor cytoskeleton organization, and it has implicated in monitoring cell size in *S.*

cerevisiae, although this aspect of its function is probably most well studied in fission yeast or in *Xenopus* (Kellogg, 2003; McMillan *et al.,* 1998; Sanchez *et al.,* 1999). To test this hypothesis, it would first be necessary to generate a cell cycle marker to distinguish between G1, S and G2 phase in order to monitor the progression of the cell cycle. Secondly, to generate an analogue-sensitive mutant for Mps1 MAP kinase which would allow manipulation of turgor generation using a drug molecule (PPI), and enable investigation into the effect on both cytoskeleton organization and cell cycle progression, and also, to establish minimal thresholds of activation these mechanisms. Thirdly, to prove that Swe1 is the master regulator of these three processes, it would be necessary to generate a null mutant and/or a stable version of Swe1. It is very tempting to speculate that the interaction and crosstalk between perception of surface signals, cell cycle progression and cytoskeleton re-organisation is necessary for successful appressorium morphogenesis.

7 General Discussion

Research presented in this thesis investigated patterns of gene expression during appressorium development by *M. oryzae* and the role of cell cycle control in appressorium morphogenesis. To investigate the global control of gene expression during infection-related development in *M. oryzae*, I investigated the role of surface hydrophobicity as an inductive signal for appressorium development and the role of two major regulators of morphogenesis. The first, Pmk1, is a MAPK essential for appressoria to develop, and the second, Mst12, is a downstream transcription factor regulated by Pmk1, but with a more specific role in appressorium maturation (Bruno *et al.,* 2004; Park *et al.,* 2002).

Pmk1-dependent gene expression in *M. oryzae*

Global transcriptional profiling using RNA-seq, revealed fundamental differences between the *Δpmk1* mutant and the isogenic wild type strain Guy11, which were apparent from the very early start of germination. At least, 70 putative transcription factors are potentially regulated downstream of Pmk1 at the time of spore germination, highlighting the complexity of initial germ tube formation and the breaking of dormancy. Also, the development of the *Δpmk1* mutant is delayed, and its transcriptome at later stages of development differs significantly from that of Guy11, consistent with the increasing phenotypic differences between them. The fact that the *Δpmk1* transcriptome at 0h is similar to the later stages of appressorium development in Guy11, is also suggestive of a fundamental similarity between appressorium morphogenesis and conidial morphogenesis, both of which require cellular differentiation and development of a non-hyphal, partially de-polarised, or

isotropic cell shape. Fundamental differences from the very start of germination may also correspond to differences in metabolism and its regulation, cellular transport, cellular communication and signal transduction, cell defence and virulence, and interaction with the environment, based on the gene families that are differentially expressed during this time.

MAPK are global regulators and it is known that they regulate large numbers of gene regulators (Dickman and Yarden, 1999). However, MAP kinase signalling has yet not been investigated by whole transcriptome analysis for any filamentous fungal species. In *S. cerevisiae*, at least 106 genes correlated by transcriptional profiling and proteomic analysis (Gygi *et al.,* 1999) have been reported as targets of the Kss1 MAP kinase pathway (Madhani *et al.,* 1999), with many further downstream genes predicted by gene expression patterns.

A total of 5475 putative downstream genes have been identified to be potentially downstream of Pmk1, of which 1690 seem also to be potential downstream targets of Mst12. Among the putative Pmk1 downstream genes, I have identified 172 putative transcription factors, of which 96 were differentially expressed more than 4 fold, suggesting a complex transcriptional response downstream of Pmk1. For example, a group of 9 putative transcription factors may be potentially regulated by Pmk1, directly or indirectly through Mst12. Targeted replacement of some of the corresponding encoding genes, already suggests a role in appressorial morphogenesis. This group of genes, for instance, includes Hox7, which is a regulator of appressorium development (Kim *et al.,* 2009) and which has also here been shown to be potentially regulated by Mst12 during conidial germination suggesting the important and somewhat unexpected potential role of Pmk1 MAP kinase pathway at very early stages of development.

The hierarchical analysis of transcription factor regulation, described in Chapter 5, allowed identification of potential downstream transcription factors, previously unknown to be regulated by Pmk1 (Figure 7.2). Among these, was Swi6 which could probably be involved in the transcription of genes required for the transition of G1 to S phase of the cell cycle (McInerny *et al.,* 1995; Qi *et al.,* 2012) and Stu1, which may be involved in mobilization of lipids towards the appressorium (Nishimura *et al.,* 2009). Among these, the well-known downstream Pmk1 interactor Mst12 was also identified, consistent with its predicted role (Park *et al.,* 2002).

Mst12-dependent gene expression

Mst12 is a zinc finger and homeobox domain containing transcription factor which regulates appressorium maturation and plant penetration in *M. oryzae* (Park *et al.,* 2002). Null mutants of *MST12* make appressoria, but are unable to form a penetration peg and, therefore, to cause rice blast disease (Park *et al.,* 2002). To form a penetration peg and cause disease it is necessary for cytoskeletal re-organisation to occur at the base of the appressorium (Dagdas *et al.,* 2012; Ryder *et al.,* 2013). In Chapter 4, it was shown that cytoskeleton components at the base of the appressorium are completely mislocalised in the *mst12* null mutant, consistent with the inability of the null mutant to form a penetration peg.

Transcriptional profiling highlighted new potential downstream targets of Mst12. Some, very early differences in gene expression, included 44 transcription factors that are affected as early as 0h during spore germination, highlighting the importance of the Pmk1 MAP kinase signalling pathway at early stages of germination, consistent with the data obtained with the *Δpmk1* mutant. In total, 30

putative transcription factors may be dependent on both Mst12 and Pmk1. This suggests a hierarchy of transcriptional regulation during appressorium development in which Pmk1 regulates a very large set of functions including autophagy, Ras signalling, Rho signalling, DNA repair and DNA replication, regulation of cell cycle (specially mitotic exit), polarization, and genes related with peroxisome biology. While Mst12 may regulate a sub-set of functions via at least 30 later-acting transcription factors including cell wall remodelling, effector secretion, cutinase secretion, fasciclin production, peroxisome and appressorium adhesion. Surprisingly, although the most obvious phenotype of the Mst12 null mutant is a lack of penetration by the appressorium, Mst12 appears to exert an effect from the very onset of conidial germination, probably through a sub-set of 44 transcription factors found dramatically down-regulated at very early stages of development.

The Pmk1 MAP kinase cascade may regulate cell cycle functions

Interestingly, Pmk1 may play a role in cell cycle regulation based on gene functions identified in global transcriptional profile analysis, especially functions associated with mitosis exit. The DNA checkpoint kinases, Cds1 and Dun1, for example may be putative, direct or indirect, targets of Pmk1. From previous research, it was known that appressorium morphogenesis is regulated initially by an S-phase checkpoint for initiation of appressorium development and by a G2 to M transition for appressorium maturation (Saunders *et al.,* 2010a). However it was not known how re-polarization of the appressorium and penetration were regulated, or whether this transition also required cell cycle control. Results reported in Chapter 6 suggest that there is an S-phase checkpoint required for re-polarization of the

appressorium that operates independently of the DNA damage and repair checkpoint mediated by the Cds1/Chk1 kinases. Consisted with this idea, gene expression profiling shows a similar pattern of regulation. The DNA damage checkpoint response for example, was identified among differentially regulated processes during early appressorium morphogenesis, consistent with it operating at the S-phase checkpoint during appressorium morphogenesis, but not during re-polarization, when no differences in gene expression were detected. Additionally, and as hypothesised in Chapter 6, it is important to note the importance of the potential regulation of the FHA-RING ubiquitin ligase Dma1 by Pmk1, which could be the connection between the morphogenetic checkpoint described in *S. cerevisiae* and the regulation of MAP kinase signalling pathways (Raspelli *et al.,* 2011).

Principal Conclusions

Appressorium development in *M. oryzae* involves a highly orchestrated process, controlled through a central global signalling pathway directed by the Pmk1 MAP kinase signalling pathway. This influences many gene functions, and at least 5000 genes are altered in expression, controlled in sub-sets by at least 96 transcriptions factors, and possibly as many as 172. These transcription factors include Mst12, Hox7, Swi6 and Stu1. Moreover, Mst12 acts upstream of at least 30 transcriptions factors during appressorium morphogenesis and maturation, which are overwhelmingly dependent on Pmk1, consistent with it being a direct downstream target of the MAP kinase.

Both Pmk1 and Mst12 appears to interact with cell cycle control points for appressorium morphogenesis, which provide control points for the progression of

development and cell differentiation. In future, it will be necessary to integrate these studies by first carrying out RNA-seq experiments for null mutants of each transcription factor and then systematically to classify the downstream patterns of gene expression. In this way a full hierarchical map of transcriptional control of appressorium development can be generated, which should allow precise developmental cascades and processes to be defined in detail. At the same time, it will be necessary to investigate the biochemistry of the protein-protein interactions that mediate both transcriptional control and its integration with cell cycle-mediated checkpoints. Ultimately, a full description of the developmental biology of appressorium formation will be pivotal for the design of novel anti-penetrant fungicides that could prevent cuticle rupture and plant infection by the fungus, providing durable control of rice blast disease.

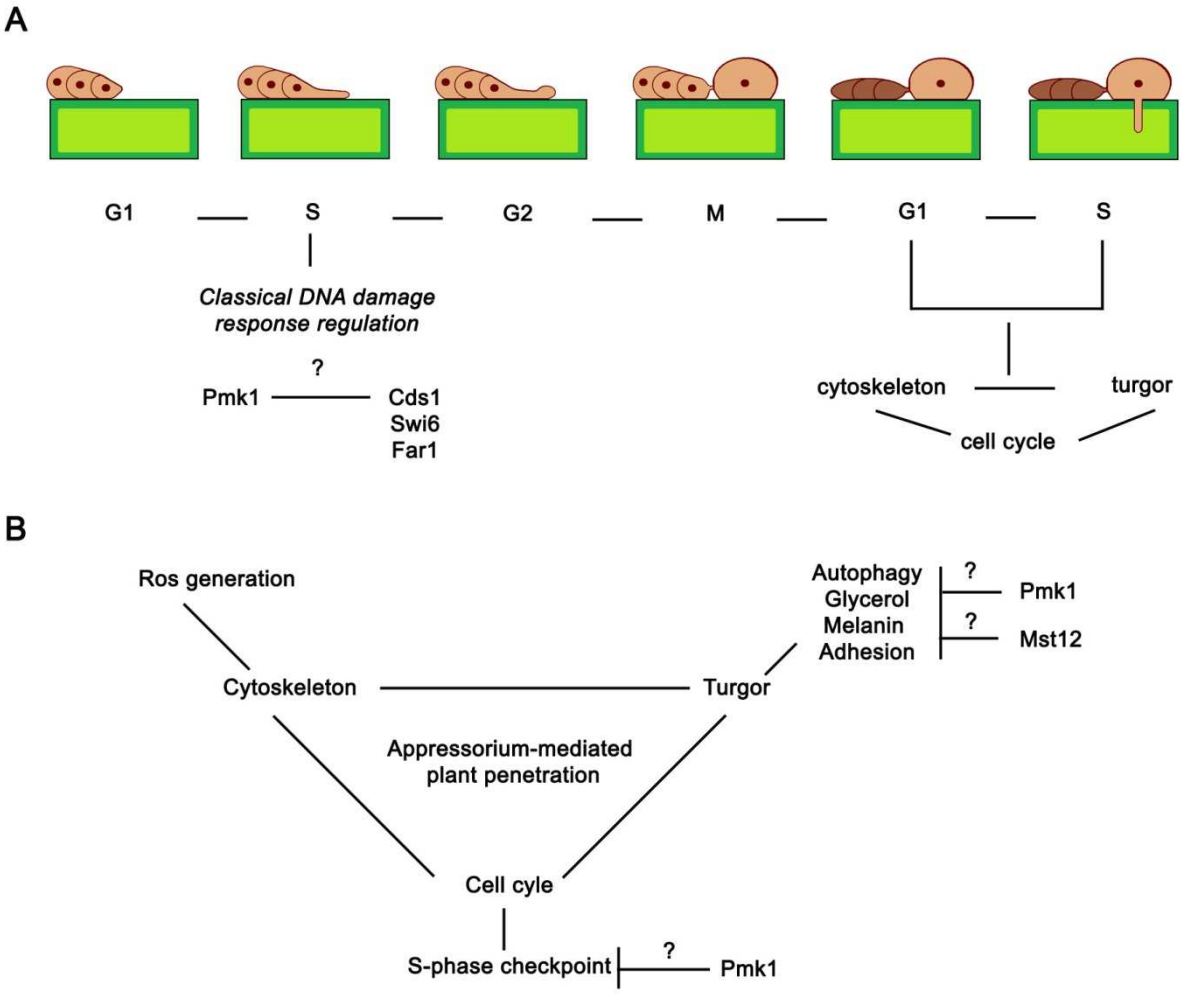

Figure 7.1 Model depicting cell cycle transitions co-ordinated with morphogenetic changes leading to appressorium morphogenesis and appressorium-mediated plant infection in the rice blast fungus *M. oryzae.* A) Both appressorium morphogenesis and re-polarization, leading to penetration peg development depend on S-phase checkpoints. The S-phase checkpoint operating during appressorium morphogenesis depends partially on DNA damage and repair response that might be regulated by Pmk1. The S-phase checkpoint operating during appressorium-mediated plant infection might be dependent on the morphogenetic checkpoint regulating cytoskeleton, turgor generation and cell cycle progression. **B)** Proposed model for appressorium-mediated plant penetration which depends on the interconnection between cytoskeleton, turgor generation and cell cycle progression. ROS generation causes cytoskeleton rearrangements (Ryder *et al.,* 2013), autophagy, glycerol production, melanin and appressorial adhesion are required for turgor generation (Talbot, 2003) and this study hypothesized that autophagy and glycerol are regulated by Pmk1 and Mst12 may also be required for production of melanin and cell adhesion. Cell cycle regulation at S-phase may be regulated by Pmk1.

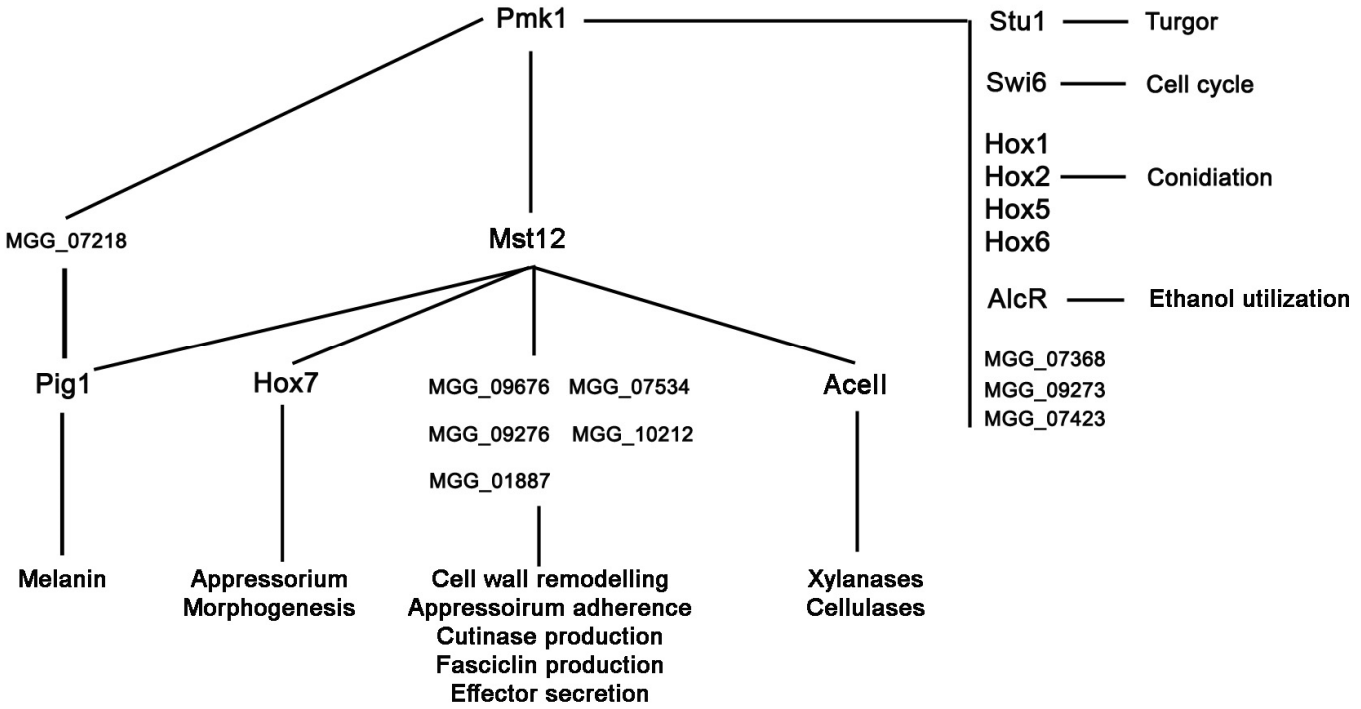

Figure 7.2 Model depicting the possible transcriptional circuitry of the Pmk1 MAP kinase pathway in the rice blast fungus *M. oryzae*. Pmk1 potentially regulates a sub set of transcription factors including Stu1, Swi6, Hoxs, AlcR and other uncharacterized transcription factors to regulate diverse cellular processes necessary for appressorium morphogenesis such as turgor generation, cell cycle progression or conidiation. Pmk1 potentially regulates Mst12 to control the putative transcription factor AceII to potentially regulate the transcription of cell wall degrading enzymes, a subset of unknown transcription factors that might be able to regulate cell wall remodelling processes, appressorium adherence, cutinase and fasciclin production and effector secretion. Mst12 might be also interacting with Hox7 to regulate appressorium morphogenesis from the very early stages of development. Melanin production in appressoria might be regulated through the regulation of MGG_07218 by Pmk1 and Pig1 by Mst12.

8 Bibliography

Adachi, K., and Hamer, J.E. (1998). Divergent cAMP signaling pathways regulate growth and pathogenesis in the rice blast fungus *Magnaporthe grisea*. The Plant cell 10:1361-1374.

Amon, A., Surana, U., Muroff, I., and Nasmyth, K. (1992). Regulation of p34CDC28 tyrosine phosphorylation is not required for entry into mitosis in *S. cerevisiae*. Nature 355:368-371.

Anders, S., and Huber, W. (2010). Differential expression analysis for sequence count data. Genome Biology 11:106.

Andrews, B., and Measday, V. (1998). The cyclin family of budding yeast: abundant use of a good idea. Trends in genetics : TIG 14:66-72.

Aro, N., Saloheimo, A., Ilmen, M., and Penttila, M. (2001). ACEII, a novel transcriptional activator involved in regulation of cellulase and xylanase genes of *Trichoderma reesei*. The Journal of biological chemistry 276:24309-24314.

Audhya, A., and Emr, S.D. (2002). Stt4 PI 4-kinase localizes to the plasma membrane and functions in the Pkc1-mediated MAP kinase cascade. Developmental cell 2:593-605.

Bailey, C., and Arst, H.N., Jr. (1975). Carbon catabolite repression in *Aspergillus nidulans*. European journal of biochemistry / FEBS 51:573-577.

Barr, M.E. (1977). Magnaporthe, Telimenella and Hyponectria (Phycosporellaceae). Mycolgia 69:952-966.

Bashkirov, V.I., Bashkirova, E.V., Haghnazari, E., and Heyer, W.-D. (2003). Direct kinase-to-kinase signaling mediated by the FHA phosphoprotein recognition domain of the Dun1 DNA damage checkpoint kinase. Molecular and Cellular Biology 23:1441-1452.

Bhambra, G.K., Wang, Z.Y., Soanes, D.M., Wakley, G.E., and Talbot, N.J. (2006). Peroxisomal carnitine acetyl transferase is required for elaboration of penetration hyphae during plant infection by *Magnaporthe grisea*. Mol Microbiol 61:46-60.

Blanco, M.A., Sanchez-Diaz, A., de Prada, J.M., and Moreno, S. (2000). APC(ste9/srw1) promotes degradation of mitotic cyclins in G(1) and is inhibited by cdc2 phosphorylation. EMBO J 19:3945-3955.

Bolker, M. (1998). Sex and crime: heterotrimeric G proteins in fungal mating and pathogenesis. Fungal genetics and biology : FG & B 25:143-156.

Bompard, G., Sharp, S.J., Freiss, G., and Machesky, L.M. (2005). Involvement of Rac in actin cytoskeleton rearrangements induced by MIM-B. J Cell Sci 118:5393-5403.

Booher, R.N., Raymond J.Deshaies, and W.Kirschner, a.M. (1993). Properties of *Saccharomyces cerevisiae* wee1 and its differential regulation of p34CDC28 in response to G1 and G2 cyclins. The EMBO Journal 12

Boronenkov, I.V., and Anderson, R.A. (1995). The sequence of phosphatidylinositol-4-phosphate 5-kinase defines a novel family of lipid kinases. The Journal of biological chemistry 270:2881-2884.

Bouquin, N., Johnson, A.L., Morgan, B.A., and Johnston, L.H. (1999). Association of the cell cycle transcription factor Mbp1 with the Skn7 response regulator in budding yeast. Mol Biol Cell 10:3389-3400.

Bourett, T.M.H., R. J. (1990). Invitro development of penetration structures in the rice blast fungus *Magnaporthe grisea*. Can. J. Bot.-Rev. Can. Bot 68:329-342.

Brewster, J.L., de Valoir, T., Dwyer, N.D., Winter, E., and Gustin, M.C. (1993). An osmosensing signal transduction pathway in yeast. Science 259:1760-1763.

Bricmont, P.A., Daugherty, J.R., and Cooper, T.G. (1991). The DAL81 gene product is required for induced expression of two differently regulated nitrogen catabolic genes in *Saccharomyces cerevisiae*. Mol Cell Biol 11:1161-1166.

Bruno, K.S., Tenjo, F., Li, L., Hamer, J.E., and Xu, J.R. (2004). Cellular localization and role of kinase activity of PMK1 in *Magnaporthe grisea*. Eukaryotic cell 3:1525-1532.

Burglin, T.R. (1994). A *Caenorhabditis elegans* prospero homologue defines a novel domain. Trends in biochemical sciences 19:70-71.

Casamayor, A., and Snyder, M. (2003). Molecular dissection of a yeast septin: distinct domains are required for septin interaction, localization, and function. Mol Cell Biol 23:2762-2777.

Casselton, L.A., and Olesnicky, N.S. (1998). Molecular genetics of mating recognition in basidiomycete fungi. Microbiology and molecular biology reviews : MMBR 62:55-70.

Chang, F., and Herskowitz, I. (1990). Identification of a gene necessary for cell cycle arrest by a negative growth factor of yeast: FAR1 is an inhibitor of a G1 cyclin, CLN2. Cell 63:999-1011.

Chant, J., and Stowers, L. (1995). GTPase cascades choreographing cellular behavior: movement, morphogenesis, and more. Cell 81:1-4.

Chen, Z., Franco, C.F., Baptista, R.P., Cabral, J.M.S., Coelho, A.V., Rodrigues, C.R., Melo, E.P. (2007). Purification and identification of cutinases from Colletotrichum kahawae and Colletotrichum gloeosporioides. Appl Microbiol Biotechnol 73:1306–1313.

Choi, W., and Dean, R.A. (1997). The adenylate cyclase gene MAC1 of *Magnaporthe grisea* controls appressorium formation and other aspects of growth and development. The Plant Cell 9:1973-1983.

Chou, S., Lane, S., and Liu, H. (2006). Regulation of mating and filamentation genes by two distinct Ste12 complexes in *Saccharomyces cerevisiae*. Mol Cell Biol 26:4794-4805.

Chu, B., Soncin, F., Price, B.D., Stevenson, M.A., and Calderwood, S.K. (1996). Sequential phosphorylation by mitogen-activated protein kinase and glycogen synthase kinase 3 represses transcriptional activation by heat shock factor-1. The Journal of biological chemistry 271:30847-30857.

Chumley, F.G., and Valent, B. (1990). Genetic analysis of melanin deficient, nonpathogenic mutants of *Magnaporthe grisea*. Molecular Plant-Microbe Interactions: 135–143.

Chung, H., Choi, J., Park, S.Y., Jeon, J., and Lee, Y.H. (2013). Two conidiation-related Zn(II)2Cys6 transcription factor genes in the rice blast fungus. Fungal genetics and biology : FG & B 61:133-141.

Ciosk, R., Zachariae, W., Michaelis, C., Shevchenko, A., Mann, M., and Nasmyth, K. (1998). An ESP1/PDS1 complex regulates loss of sister chromatid cohesion at the metaphase to anaphase transition in yeast. Cell 93:1067-1076.

Couch, B.C., and Kohn, L.M. (2002). A multilocus gene genealogy concordant with host preference indicates segregation of a new species, Magnaporthe oryzae, from M. grisea. Mycologia 94:683-693.

Coudreuse, D., and Nurse, P. (2010). Driving the cell cycle with a minimal CDK control network. Nature 468:1074-1079.

Creaser, E.H., Porter, R.L., Britt, K.A., Pateman, J.A. and Doy, C.H. (1984). Purification and preliminary characterization of alcohol dehydrogenase from *Aspergillus nidulans*. Biochemical Journal 225:449-454.

Dagdas, Y.F., Yoshino, K., Dagdas, G., Ryder, L.S., Bielska, E., Steinberg, G., and Talbot, N.J. (2012). Septin-mediated plant cell invasion by the rice blast fungus, *Magnaporthe oryzae*. Science 336:1590-1595.

Davies, J.R., Osmani, A.H., De Souza, C.P., Bachewich, C., and Osmani, S.A. (2004). Potential link between the NIMA mitotic kinase and nuclear membrane fission during mitotic exit in *Aspergillus nidulans*. Eukaryotic cell 3:1433-1444.

Dawson, J.C., Legg, J.A., and Machesky, L.M. (2006). Bar domain proteins: a role in tubulation, scission and actin assembly in clathrin-mediated endocytosis. Trends in cell biology 16:493-498.

de Jong, J.C., McCormack, B.J., Smirnoff, N., and Talbot, N.J. (1997). Glycerol generates turgor in rice blast. Nature 389:244-244.

de Sena-Tomas, C., Fernandez-Alvarez, A., Holloman, W.K., and Perez-Martin, J. (2011). The DNA damage response signaling cascade regulates proliferation of the phytopathogenic fungus *Ustilago maydis* in planta. The Plant cell 23:1654-1665.

Dean, R., Van Kan, J.A.L., Pretorius, Z.A., Hammond-Kosack, K.E., Di Pietro, A., Spanu, P.D., Rudd, J.J., Dickman, M., Kahmann, R., Ellis, J., et al. (2012). The Top 10 fungal pathogens in molecular plant pathology. Molecular Plant Pathology 13:414-430.

Dean, R.A., Talbot, N.J., Ebbole, D.J., Farman, M.L., Mitchell, T.K., Orbach, M.J., Thon, M., Kulkarni, R., Xu, J.R., Pan, H., et al. (2005). The genome sequence of the rice blast fungus *Magnaporthe grisea*. Nature 434:980-986.

Deising, H.B., Werner, S., and Wernitz, M. (2000). The role of fungal appressoria in plant infection. Microbes and infection / Institut Pasteur 2:1631-1641.

Dementhon, K., Saupe, S.J., and Clave, C. (2004). Characterization of IDI-4, a bZIP transcription factor inducing autophagy and cell death in the fungus *Podospora anserina*. Mol Microbiol 53:1625-1640.

Dereeper, A., Guignon, V., Blanc, G., Audic, S., Buffet, S., Chevenet, F., Dufayard, J.-F., Guindon, S., Lefort, V., Lescot, M., et al. (2008). Phylogeny.fr: robust phylogenetic analysis for the non-specialist. Nucleic Acids Research 36:W465-W469.

DeZwaan, T.M., Carroll, A.M., Valent, B., and Sweigard, J.A. (1999). *Magnaporthe grisea* pth11p is a novel plasma membrane protein that mediates appressorium differentiation in response to inductive substrate cues. The Plant cell 11:2013-2030.

Dickman, M.B., and Yarden, O. (1999). Serine/Threonine protein kinases and phosphatases in filamentious fungi. Fungal Genetics and Biology 26:99-117.

Dixon, K.P., Xu, J.R., Smirnoff, N., and Talbot, N.J. (1999). Independent signaling pathways regulate cellular turgor during hyperosmotic stress and appressorium-mediated plant infection by *Magnaporthe grisea*. The Plant cell 11:2045-2058.

Eliahu, N., Igbaria, A., Rose, M.S., Horwitz, B.A., and Lev, S. (2007). Melanin biosynthesis in the maize pathogen *Cochliobolus heterostrophus* depends on two mitogen-activated protein kinases, Chk1 and Mps1, and the transcription factor Cmr1. Eukaryotic cell 6:421-429.

Elion, E.A., Satterberg, B., and Kranz, J.E. (1993). FUS3 phosphorylates multiple components of the mating signal transduction cascade: evidence for STE12 and FAR1. Mol Biol Cell 4:495-510.

Elkins, T., Hortsch, M., Bieber, A.J., Snow, P.M., and Goodman, C.S. (1990). Drosophila fasciclin I is a novel homophilic adhesion molecule that along with fasciclin III can mediate cell sorting. J Cell Biol 110:1825-1832.

Elledge, S.J. (1996). Cell cycle checkpoints: preventing an identity crisis. Science 274:1664-1672.

Enoch, T., and Nurse, P. (1990). Mutation of fission yeast cell cycle control genes abolishes dependence of mitosis on DNA replication. Cell 60:665-673.

Enserink, J.M., Smolka, M.B., Zhou, H., and Kolodner, R.D. (2006). Checkpoint proteins control morphogenetic events during DNA replication stress in *Saccharomyces cerevisiae*. J Cell Biol 175:729-741.

Evangelista, M., Blundell, K., Longtine, M.S., Chow, C.J., Adames, N., Pringle, J.R., Peter, M., and Boone, C. (1997). Bni1p, a yeast formin linking cdc42p and the actin cytoskeleton during polarized morphogenesis. Science 276:118-122.

Fan, C.-Y., and Köller, W. (1998). Diversity of cutinases from plant pathogenic fungi: differential and sequential expression of cutinolytic esterases by *Alternaria brassicicola*. FEMS microbiology letters 158:33-38.

Fedorova, N.D., Badger, J.H., Robson, G.D., Wortman, J.R., and Nierman, W.C. (2005). Comparative analysis of programmed cell death pathways in filamentous fungi. BMC genomics 6:177.

Feinberg, A.P., and Vogelstein, B. (1983). A technique for radiolabeling DNA restriction endonuclease fragments to high specific activity. Analytical biochemistry 132:6-13.

Felenbok, B., Sequeval, D., Mathieu, M., Sibley, S., Gwynne, D.I., and Davies, R.W. (1988). The ethanol regulon in *Aspergillus nidulans:* characterization and sequence of the positive regulatory gene alcR. Gene 73:385-396.

Fievet, B.T., Gautreau, A., Roy, C., Del Maestro, L., Mangeat, P., Louvard, D., and Arpin, M. (2004). Phosphoinositide binding and phosphorylation act sequentially in the activation mechanism of ezrin. J Cell Biol 164:653-659.

Franck, W.L., Gokce, E., Oh, Y., Muddiman, D.C., and Dean, R.A. (2013). Temporal analysis of the magnaporthe oryzae proteome during conidial germination and cyclic AMP (cAMP)-mediated appressorium formation. Molecular & cellular proteomics : MCP 12:2249-2265.

Froeliger, E.H., and Carpenter, B.E. (1996). NUT1, a major nitrogen regulatory gene in *Magnaporthe grisea*, is dispensable for pathogenicity. Molecular & general genetics : MGG 251:647-656.

Furnari, B., Blasina, A., Boddy, M.N., McGowan, C.H., and Russell, P. (1999). Cdc25 inhibited in vivo and in vitro by checkpoint kinases Cds1 and Chk1. Mol Biol Cell 10:833-845.

Garrenton, L.S., Stefan, C.J., McMurray, M.A., Emr, S.D., and Thorner, J. (2010). Pheromone-induced anisotropy in yeast plasma membrane phosphatidylinositol-4,5-bisphosphate distribution is required for MAPK signaling. Proceedings of the National Academy of Sciences of the United States of America 107:11805-11810.

Garrenton, L.S., Young, S.L., and Thorner, J. (2006). Function of the MAPK scaffold protein, Ste5, requires a cryptic PH domain. Genes Dev 20:1946-1958.

Giraldo, M.C., Dagdas, Y.F., Gupta, Y.K., Mentlak, T.A., Yi, M., Martinez-Rocha, A.L., Saitoh, H., Terauchi, R., Talbot, N.J., and Valent, B. (2013). Two distinct secretion systems facilitate tissue invasion by the rice blast fungus *Magnaporthe oryzae*. Nature communications 4:1996.

Glass, N.L., Rasmussen, C., Roca, M.G., and Read, N.D. (2004). Hyphal homing, fusion and mycelial interconnectedness. Trends Microbiol 12:135-141.

Godfray, H.C.J., Beddington, J.R., Crute, I.R., Haddad, L., Lawrence, D., Muir, J.F., Pretty, J., Robinson, S., Thomas, S.M., and Toulmin, C. (2010). Food Security: The Challenge of Feeding 9 Billion People. Science 327:812-818.

Goley, E.D., and Welch, M.D. (2006). The ARP2/3 complex: an actin nucleator comes of age. Nat Rev Mol Cell Biol 7:713-726.

Gould, K.L., and Nurse, P. (1989). Tyrosine phosphorylation of the fission yeast cdc2+ protein kinase regulates entry into mitosis. Nature 342:39-45.

Govindaraghavan, M., Lad, A.A., and Osmani, S.A. (2014). The NIMA kinase is required to execute stage-specific mitotic functions after initiation of mitosis. Eukaryotic cell 13:99-109.

Gustin, M.C., Albertyn, J., Alexander, M., and Davenport, K. (1998). Map kinase pathways in the yeast *Saccharomyces cerevisiae*. Microbiology and Molecular Biology Reviews 62:1264-1300.

Gygi, S.P., Rochon, Y., Franza, B.R., and Aebersold, R. (1999). Correlation between protein and mRNA abundance in yeast. Molecular and Cellular Biology 19:1720-1730.

Hamer, J.E., Howard, R.J., Chumley, F.G., and Valent, B. (1988). A mechanism for surface attachment in spores of a plant pathogenic fungus. Science 239:288-190.

Hansjakob, A., Riederer, M., and Hildebrandt, U. (2012). Appressorium morphogenesis and cell cycle progression are linked in the grass powdery mildew fungus *Blumeria graminis*. Fungal Biology 116:890-901.

Harashima, H., Dissmeyer, N., and Schnittger, A. (2013). Cell cycle control across the eukaryotic kingdom. Trends in cell biology 23:345-356.

Harrison, J.C., Bardes, E.S., Ohya, Y., and Lew, D.J. (2001). A role for the Pkc1p/Mpk1p kinase cascade in the morphogenesis checkpoint. Nature cell biology 3:417-420.

Hartwell, L.H., and Weinert, T.A. (1989). Checkpoints: controls that ensure the order of cell cycle events. Science 246:629-634.

Herbert, C., Jacquet, C., Borel, C., Esquerre-Tugaye, M.T., and Dumas, B. (2002). A cis-acting sequence homologous to the yeast filamentation and invasion response element regulates

expression of a pectinase gene from the bean pathogen *Colletotrichum lindemuthianum*. The Journal of biological chemistry 277:29125-29131.
Herskowitz, I. (1989). A regulatory hierarchy for cell specialization in yeast. Nature 342:749-757.
Houde, M., Laprise, P., Jean, D., Blais, M., Asselin, C., and Rivard, N. (2001). Intestinal epithelial cell differentiation involves activation of p38 mitogen-activated protein kinase that regulates the homeobox transcription factor CDX2. The Journal of biological chemistry 276:21885-21894.
Howard, R.J., Ferrari, M.A., Roach, D.H., and Money, N.P. (1991). Penetration of hard substrates by a fungus employing enormous turgor pressures. Proceedings of the National Academy of Sciences 88:11281-11284.
Howard, R.J., and Valent, B. (1996). Breaking and entering: host penetration by the fungal rice blast pathogen *Magnaporthe grisea*. Annual review of microbiology 50:491-512.
Howell, A.S., and Lew, D.J. (2012). Morphogenesis and the cell cycle. Genetics 190:51-77.
Huber, O., and Sumper, M. (1994). Algal-CAMs: isoforms of a cell adhesion molecule in embryos of the alga Volvox with homology to Drosophila fasciclin I. Embo j 13:4212-4222.
Jackson, A.L., Pahl, P.M., Harrison, K., Rosamond, J., and Sclafani, R.A. (1993). Cell cycle regulation of the yeast Cdc7 protein kinase by association with the Dbf4 protein. Mol Cell Biol 13:2899-2908.
Jain, A.K. (2009). Data clustering: 50 years beyond K-means. Pattern Recognition Letters 31:651-666.
Jin, K., Han, L., and Xia, Y. (2014). MaMk1, a FUS3/KSS1-type mitogen-activated protein kinase gene, is required for appressorium formation, and insect cuticle penetration of the entomopathogenic fungus *Metarhizium acridum*. Journal of invertebrate pathology 115:68-75.
Johnson, K.L., Jones, B.J., Bacic, A., and Schultz, C.J. (2003). The fasciclin-like arabinogalactan proteins of Arabidopsis. A multigene family of putative cell adhesion molecules. Plant physiology 133:1911-1925.
Kadota, J., Yamamoto, T., Yoshiuchi, S., Bi, E., and Tanaka, K. (2004). Septin ring assembly requires concerted action of polarisome components, a PAK kinase Cla4p, and the actin cytoskeleton in *Saccharomyces cerevisiae*. Mol Biol Cell 15:5329-5345.
Kaksonen, M., Sun, Y., and Drubin, D.G. (2003). A pathway for association of receptors, adaptors, and actin during endocytic internalization. Cell 115:475-487.
Kamada, K. (2012). The GINS complex: structure and function. Sub-cellular biochemistry 62:135-156.
Kamper, J., Reichmann, M., Romeis, T., Bolker, M., and Kahmann, R. (1995). Multiallelic recognition: nonself-dependent dimerization of the bE and bW homeodomain proteins in *Ustilago maydis*. Cell 81:73-83.
Kastan, M.B., and Bartek, J. (2004). Cell-cycle checkpoints and cancer. Nature 432:316-323.
Kellogg, D.R. (2003). Wee1-dependent mechanisms required for coordination of cell growth and cell division. J Cell Sci 116:4883-4890.
Kershaw, M.J., and Talbot, N.J. (2009). Genome-wide functional analysis reveals that infection-associated fungal autophagy is necessary for rice blast disease. Proceedings of the National Academy of Sciences of the United States of America 106:15967-15972.
Kim, S., Park, S.Y., Kim, K.S., Rho, H.S., Chi, M.H., Choi, J., Park, J., Kong, S., Park, J., Goh, J., et al. (2009). Homeobox transcription factors are required for conidiation and appressorium development in the rice blast fungus *Magnaporthe oryzae*. PLoS genetics 5:e1000757.
Kleemann, J., Rincon-Rivera, L.J., Takahara, H., Neumann, U., Ver Loren van Themaat, E., van der Does, H.C., Hacquard, S., Stuber, K., Will, I., Schmalenbach, W., et al. (2012). Sequential delivery of host-induced virulence effectors by appressoria and intracellular hyphae of the phytopathogen *Colletotrichum higginsianum*. PLoS pathogens 8:e1002643.
Koch, C., Moll, T., Neuberg, M., Ahorn, H., and Nasmyth, K. (1993). A role for the transcription factors Mbp1 and Swi4 in progression from G1 to S phase. Science 261:1551-1557.
Kolattukudy, P.E. (1985). Enzymatic penetration of the plant cuticle by fungal pathogens Ann. Rev. Phytopathol 23:223-250.

Koller, W. (1991). The plant cutile: a barrier to be overcome by fungal plant pathogens New York: Plenum press.

Kulkarni, R.D., and Dean, R.A. (2004). Identification of proteins that interact with two regulators of appressorium development, adenylate cyclase and cAMP-dependent protein kinase A, in the rice blast fungus *Magnaporthe grisea*. Molecular genetics and genomics : MGG 270:497-508.

Kulkarni, R.D., Thon, M.R., Pan, H., and Dean, R.A. (2005). Novel G-protein-coupled receptor-like proteins in the plant pathogenic fungus *Magnaporthe grisea*. Genome Biol 6:R24.

Kulmburg, P., Judewicz, N., Mathieu, M., Lenouvel, F., Sequeval, D., and Felenbok, B. (1992). Specific binding sites for the activator protein, ALCR, in the alcA promoter of the ethanol regulon of *Aspergillus nidulans*. The Journal of biological chemistry 267:21146-21153.

Kusari, A.B., Molina, D.M., Sabbagh, W., Jr., Lau, C.S., and Bardwell, L. (2004). A conserved protein interaction network involving the yeast MAP kinases Fus3 and Kss1. J Cell Biol 164:267-277.

Latterell, F.M.R., A. E. (1986). Longevity and pathogenic stability of *Pyricularia oryzae*. Phytopathology 76:231-235.

Lee, I.H., Kumar, S., and Plamann, M. (2001). Null mutants of the neurospora actin-related protein 1 pointed-end complex show distinct phenotypes. Mol Biol Cell 12:2195-2206.

Lee, N., D'Souza, C.A., and Kronstad, J.W. (2003). Of smuts, blasts, mildews, and blights: cAMP signaling in phytopathogenic fungi. Annu Rev Phytopathol 41:399-427.

Lee, Y.H., and Dean, R.A. (1993). cAMP regulates infection structure formation in the plant pathogenic fungus *Magnaporthe grisea*. The Plant cell 5:693-700.

Lefrancois, P., Euskirchen, G.M., Auerbach, R.K., Rozowsky, J., Gibson, T., Yellman, C.M., Gerstein, M., and Snyder, M. (2009). Efficient yeast ChIP-Seq using multiplex short-read DNA sequencing. BMC genomics 10:37.

Lew, D.J. (2003). The morphogenesis checkpoint: how yeast cells watch their figures. Curr Opin Cell Biol 15:648-653.

Lew, D.J., and Kornbluth, S. (1996). Regulatory roles of cyclin dependent kinase phosphorylation in cell cycle control. Curr Opin Cell Biol 8:795-804.

Lew, D.J., and Reed, S.I. (1993). Morphogenesis in the yeast cell cycle: regulation by Cdc28 and cyclins. J Cell Biol 120:1305-1320.

Lew, D.J., and Reed, S.I. (1995). A cell cycle checkpoint monitors cell morphogenesis in budding yeast. The Journal of Cell Biology 129:739-749.

Li, G., Zhou, X., Kong, L., Wang, Y., Zhang, H., Zhu, H., Mitchell, T.K., Dean, R.A., and Xu, J.R. (2011). MoSfl1 is important for virulence and heat tolerance in *Magnaporthe oryzae*. PloS one 6:e19951.

Liu, F., Stanton, J.J., Wu, Z., and Piwnica-Worms, H. (1997). The human Myt1 kinase preferentially phosphorylates Cdc2 on threonine 14 and localizes to the endoplasmic reticulum and Golgi complex. Molecular and Cellular Biology 17:571-583.

Liu, S., and Dean, R.A. (1997). G protein alpha subunit genes control growth, development, and pathogenicity of *Magnaporthe grisea*. Molecular plant-microbe interactions : MPMI 10:1075-1086.

Liu, T.B., Chen, G.Q., Min, H., and Lin, F.C. (2009). MoFLP1, encoding a novel fungal fasciclin-like protein, is involved in conidiation and pathogenicity in *Magnaporthe oryzae*. Journal of Zhejiang University. Science. B 10:434-444.

Lundgren, K., Walworth, N., Booher, R., Dembski, M., Kirschner, M., and Beach, D. (1991). mik1 and wee1 cooperate in the inhibitory tyrosine phosphorylation of cdc2. Cell 64:1111-1122.

Maciel, J.L., Ceresini, P.C., Castroagudin, V.L., Zala, M., Kema, G.H., and McDonald, B.A. (2014). Population structure and pathotype diversity of the wheat blast pathogen *Magnaporthe oryzae* 25 years after its emergence in Brazil. Phytopathology 104:95-107.

MacRae, W.D., Buxton,F.P., Sibley, S., Garvon, S., Gwynne, D.I., Davies, R.W. (1988). A phosphate-repressible acid phosphatase gene from *Aspergillus niger*: its cloning, sequencing and transcriptional analysis. Gene 71:339–384.

Madhani, H.D., Galitski, T., Lander, E.S., and Fink, G.R. (1999). Effectors of a developmental mitogen-activated protein kinase cascade revealed by expression signatures of signaling mutants. Proceedings of the National Academy of Sciences of the United States of America 96:12530-12535.

Maeda H, Y.Y., Abe K, Hasegawa F, Machida M, Ishioka R, Gomi K, Nakajima T. (2005). Purification and characterization of a biodegradable plastic‐degrading enzyme from *Aspergillus oryzae*

Appl Microbiol Biotechnol 67:778‐788.

Malavazi, I., Semighini, C.P., Kress, M.R., Harris, S.D., and Goldman, G.H. (2006). Regulation of hyphal morphogenesis and the DNA damage response by the *Aspergillus nidulans* ATM homolog AtmA. Genetics 173:99-109.

Mathieu, M., and Felenbok, B. (1994). The *Aspergillus nidulans* CREA protein mediates glucose repression of the ethanol regulon at various levels through competition with the ALCR-specific transactivator. Embo j 13:4022-4027.

McGinnis, W., and Krumlauf, R. (1992). Homeobox genes and axial patterning. Cell 68:283-302.

McInerny, C.J., Kersey, P.J., Creanor, J., and Fantes, P.A. (1995). Positive and negative roles for cdc10 in cell cycle gene expression. Nucleic Acids Res 23:4761-4768.

McKinney, J.D., Chang, F., Heintz, N., Cross, F. . (1993). Negative regulation of FAR1 at the start of the yeast cell cycle. Genes Dev 7:833–843.

McMillan, J.N., Sia, R.A., and Lew, D.J. (1998). A morphogenesis checkpoint monitors the actin cytoskeleton in yeast. J Cell Biol 142:1487-1499.

McMillan, J.N., Theesfeld, C.L., Harrison, J.C., Bardes, E.S., and Lew, D.J. (2002). Determinants of Swe1p degradation in *Saccharomyces cerevisiae*. Mol Biol Cell 13:3560-3575.

Mehrabi, R., Ding, S., and Xu, J.R. (2008). MADS-box transcription factor mig1 is required for infectious growth in *Magnaporthe grisea*. Eukaryotic cell 7:791-799.

Mentlak, T.A., Kombrink, A., Shinya, T., Ryder, L.S., Otomo, I., Saitoh, H., Terauchi, R., Nishizawa, Y., Shibuya, N., Thomma, B.P., et al. (2012). Effector-mediated suppression of chitin-triggered immunity by magnaporthe oryzae is necessary for rice blast disease. The Plant cell 24:322-335.

Merlini, L., Fraschini, R., Boettcher, B., Barral, Y., Lucchini, G., and Piatti, S. (2012). Budding yeast Dma proteins control septin dynamics and the spindle position checkpoint by promoting the recruitment of the Elm1 kinase to the bud neck. PLoS genetics 8:e1002670.

Mielnichuk, N., Sgarlata, C., and Pérez-Martín, J. (2009). A role for the DNA-damage checkpoint kinase Chk1 in the virulence program of the fungus *Ustilago maydis*. Journal of Cell Science 122:4130-4140.

Miki, S., Matsui, K., Kito, H., Otsuka, K., Ashizawa, T., Yasuda, N., Fukiya, S., Sato, J., Hirayae, K., Fujita, Y., et al. (2009). Molecular cloning and characterization of the AVR-Pia locus from a Japanese field isolate of *Magnaporthe oryzae*. Mol Plant Pathol 10:361-374.

Millar, J.B., McGowan, C.H., Lenaers, G., Jones, R., and Russell, P. (1991). p80cdc25 mitotic inducer is the tyrosine phosphatase that activates p34cdc2 kinase in fission yeast. Embo j 10:4301-4309.

Mitchell, T.K., and Dean, R.A. (1995). The cAMP-dependent protein kinase catalytic subunit is required for appressorium formation and pathogenesis by the rice blast pathogen *Magnaporthe grisea*. The Plant Cell Online 7:1869-1878.

Moriwaki, A., Ueno, M., Arase, S., and Kihara, J. (2007). RNA-mediated gene silencing in the phytopathogenic fungus *Bipolaris oryzae*. FEMS microbiology letters 269:85-89.

Mosquera, G., Giraldo, M.C., Khang, C.H., Coughlan, S., and Valent, B. (2009). Interaction transcriptome analysis identifies *Magnaporthe oryzae* BAS1-4 as Biotrophy-associated secreted proteins in rice blast disease. The Plant cell 21:1273-1290.

Murakami, H., and Okayama, H. (1995). A kinase from fission yeast responsible for blocking mitosis in S phase. Nature 374:817-819.

Murphy, C., Powlowski, J., Wu, M., Butler, G., and Tsang, A. (2011). Curation of characterized glycoside hydrolases of fungal origin. Database : the journal of biological databases and curation 2011:bar020.

Murray, A.W. (1992). Creative blocks: cell-cycle checkpoints and feedback controls. Nature 359:599-604.

Nesher, I., Barhoom, S., and Sharon, A. (2008). Cell cycle and cell death are not necessary for appressorium formation and plant infection in the fungal plant pathogen *Colletotrichum gloeosporioides*. BMC Biology 6:9.

Nishimura, M., Fukada, J., Moriwaki, A., Fujikawa, T., Ohashi, M., Hibi, T., and Hayashi, N. (2009). Mstu1, an APSES transcription factor, is required for appressorium-mediated infection in *Magnaporthe grisea*. Bioscience, Biotechnology, and Biochemistry 73:1779-1786.

Nishimura, M., Park, G., and Xu, J.R. (2003). The G-beta subunit MGB1 is involved in regulating multiple steps of infection-related morphogenesis in *Magnaporthe grisea*. Mol Microbiol 50:231-243.

Noguchi, E., Noguchi, C., Du, L.-L., and Russell, P. (2003). Swi1 prevents replication fork collapse and controls checkpoint kinase Cds1. Molecular and Cellular Biology 23:7861-7874.

O'Connell, R.J., Thon, M.R., Hacquard, S., Amyotte, S.G., Kleemann, J., Torres, M.F., Damm, U., Buiate, E.A., Epstein, L., Alkan, N., et al. (2012). Lifestyle transitions in plant pathogenic Colletotrichum fungi deciphered by genome and transcriptome analyses. Nature genetics 44:1060-1065.

Ogawa, N., and Mori, K. (2004). Autoregulation of the HAC1 gene is required for sustained activation of the yeast unfolded protein response. Genes to cells : devoted to molecular & cellular mechanisms 9:95-104.

Ogi, H., Wang, C.-Z., Nakai, W., Kawasaki, Y., and Masumoto, H. (2008). The role of the *Saccharomyces cerevisiae* Cdc7–Dbf4 complex in the replication checkpoint. Gene 414:32-40.

Ohtaki S, M.H., Takahashi T, Yamagata Y, Hasegawa F, Gomi K, Nakajima T, Abe K. (2006). Novel hydrophobic surface binding protein, HsbA, produced by *Aspergillus oryzae*. Applied Environmental Microbiology 72:2407‑2413.

Osmani, S.A., Engle, D.B., Doonan, J.H., and Morris, N.R. (1988). Spindle formation and chromatin condensation in cells blocked at interphase by mutation of a negative cell cycle control gene. Cell 52:241-251.

Osmani, S.A., and Ye, X.S. (1997). Targets of checkpoints controlling mitosis: lessons from lower eukaryotes. Trends in cell biology 7:283-288.

Ou, S.H. (1985). Rice Disease.

Papadopoulos, D.K., Skouloudaki, K., Adachi, Y., Samakovlis, C., and Gehring, W.J. (2012). Dimer formation via the homeodomain is required for function and specificity of Sex combs reduced in Drosophila. Developmental Biology 367:78-89.

Park, G., Bruno, K.S., Staiger, C.J., Talbot, N.J., and Xu, J.R. (2004). Independent genetic mechanisms mediate turgor generation and penetration peg formation during plant infection in the rice blast fungus. Mol Microbiol 53:1695-1707.

Park, G., Xue, C., Zheng, L., Lam, S., and Xu, J.R. (2002). MST12 regulates infectious growth but not appressorium formation in the rice blast fungus *Magnaporthe grisea*. Molecular plant-microbe interactions : MPMI 15:183-192.

Parker, L.L., Atherton-Fessler, S., and Piwnica-Worms, H. (1992). p107wee1 is a dual-specificity kinase that phosphorylates p34cdc2 on tyrosine 15. Proceedings of the National Academy of Sciences 89:2917-2921.

Parsons, R., Li, G., Longley, M., Modrich, P., Liu, B., Berk, T., Hamilton, Kinzler, K., and Vogelstein, B. (1995). Mismatch repair deficiency in phenotypically normal human cells. Science 268:738-740.

Pasero, P., Duncker, B.P., Schwob, E., and Gasser, S.M. (1999). A role for the Cdc7 kinase regulatory subunit Dbf4p in the formation of initiation-competent origins of replication. Genes Dev 13:2159-2176.

Perez-Martin, J. (2009). DNA-damage response in the basidiomycete fungus *Ustilago maydis* relies in a sole Chk1-like kinase. DNA repair 8:720-731.

Perez-Nadales, E., Almeida Nogueira, M.F., Baldin, C., Castanheira, S., El Ghalid, M., Grund, E., Lengeler, K., Marchegiani, E., Mehrotra, P.V., Moretti, M., et al. (2014). Fungal model systems and the elucidation of pathogenicity determinants. Fungal genetics and biology : FG & B 70c:42-67.

Pruyne, D., and Bretscher, A. (2000). Polarization of cell growth in yeast. J Cell Sci 113 (Pt 4):571-585.

Purdy, R.E., and Kolattukudy, P.E. (1975). Hydrolysis of plant cuticle by plant pathogens. Purification, amino acid composition, and molecular weight of two isoenzymes of cutinase and a nonspecific esterase from *Fusarium solani* f. pisi. Biochemistry 14:2824-2831.

Qi, Z., Wang, Q., Dou, X., Wang, W., Zhao, Q., Lv, R., Zhang, H., Zheng, X., Wang, P., and Zhang, Z. (2012). MoSwi6, an APSES family transcription factor, interacts with MoMps1 and is required for hyphal and conidial morphogenesis, appressorial function and pathogenicity of *Magnaporthe oryzae*. Mol Plant Pathol 13:677-689.

Raspelli, E., Cassani, C., Lucchini, G., and Fraschini, R. (2011). Budding yeast Dma1 and Dma2 participate in regulation of Swe1 levels and localization. Molecular Biology of the Cell 22:2185-2197.

Rhind, N., and Russell, P. (1998). Mitotic DNA damage and replication checkpoints in yeast. Curr Opin Cell Biol 10:749-758.

Rispail, N., Soanes, D.M., Ant, C., Czajkowski, R., Grunler, A., Huguet, R., Perez-Nadales, E., Poli, A., Sartorel, E., Valiante, V., et al. (2009). Comparative genomics of MAP kinase and calcium-calcineurin signalling components in plant and human pathogenic fungi. Fungal genetics and biology : FG & B 46:287-298.

Roman, E., Arana, D.M., Nombela, C., Alonso-Monge, R., and Pla, J. (2007). MAP kinase pathways as regulators of fungal virulence. Trends Microbiol 15:181-190.

Russell, P., and Nurse, P. (1986). cdc25+ functions as an inducer in the mitotic control of fission yeast. Cell 45:145-153.

Russell, N.R.a.P. (1998). Tyrosine phosphorylation of Cdc2 is required for the replication checkpoint in *Schizosaccharomyces pombe*. Mol Cell Biol. 18:3782–3787.

Ryder, L.S., Dagdas, Y.F., Mentlak, T.A., Kershaw, M.J., Thornton, C.R., Schuster, M., Chen, J., Wang, Z., and Talbot, N.J. (2013). NADPH oxidases regulate septin-mediated cytoskeletal remodeling during plant infection by the rice blast fungus. Proceedings of the National Academy of Sciences of the United States of America 110:3179-3184.

Sambrook, J., Fritsch, E.F., and Maniatis, T. (1989). Molecular Cloning - a laboratory manual, second edition.: Cold Spring Harbour Laboratory press.

Sanchez, Y., Bachant, J., Wang, H., Hu, F., Liu, D., Tetzlaff, M., and Elledge, S.J. (1999). Control of the DNA damage checkpoint by Chk1 and Rad53 protein kinases through distinct mechanisms. Science 286:1166-1171.

Sanchez, Y., Desany, B.A., Jones, W.J., Liu, Q., Wang, B., and Elledge, S.J. (1996). Regulation of RAD53 by the ATM-like kinases MEC1 and TEL1 in yeast cell cycle checkpoint pathways. Science 271:357-360.

Santocanale, C., and Diffley, J.F.X. (1998). A Mec1- and Rad53-dependent checkpoint controls late-firing origins of DNA replication. Nature 395:615-618.

Santos-Rosa, H., Leung, J., Grimsey, N., Peak-Chew, S., and Siniossoglou, S. (2005). The yeast lipin Smp2 couples phospholipid biosynthesis to nuclear membrane growth. Embo j 24:1931-1941.

Sardar, H.S., and Showalter, A.M. (2007). A cellular networking model involving interactions among glycosyl-phosphatidylinositol (GPI)-anchored plasma membrane arabinogalactan proteins (AGPs), microtubules and F-actin in tobacco BY-2 Cells. Plant signaling & behavior 2:8-9.

Saunders, D.G., Aves, S.J., and Talbot, N.J. (2010a). Cell cycle-mediated regulation of plant infection by the rice blast fungus. The Plant Cell 22:497-507.

Saunders, D.G., Dagdas, Y.F., and Talbot, N.J. (2010b). Spatial uncoupling of mitosis and cytokinesis during appressorium-mediated plant infection by the rice blast fungus *Magnaporthe oryzae*. The Plant Cell 22:2417-2428.

Schrettl, M., Beckmann, N., Varga, J., Heinekamp, T., Jacobsen, I.D., Jochl, C., Moussa, T.A., Wang, S., Gsaller, F., Blatzer, M., et al. (2010). HapX-mediated adaption to iron starvation is crucial for virulence of *Aspergillus fumigatus*. PLoS pathogens 6:e1001124.

Seifert, G.J., and Roberts, K. (2007). The biology of arabinogalactan proteins. Annual review of plant biology 58:137-161.

Shah, R., Jensen, S., Frenz, L.M., Johnson, A.L., and Johnston, L.H. (2001). The Spo12 protein of *Saccharomyces cerevisiae*: a regulator of mitotic exit whose cell cycle-dependent degradation is mediated by the anaphase-promoting complex. Genetics 159:965-980.

Sheu, Y.J., Santos, B., Fortin, N., Costigan, C., and Snyder, M. (1998). Spa2p interacts with cell polarity proteins and signaling components involved in yeast cell morphogenesis. Mol Cell Biol 18:4053-4069.

Sidorova, J.M., and Breeden, L.L. (1997). Rad53-dependent phosphorylation of Swi6 and down-regulation of CLN1 and CLN2 transcription occur in response to DNA damage in *Saccharomyces cerevisiae*. Genes Dev 11:3032-3045.

Siniossoglou, S., Santos-Rosa, H., Rappsilber, J., Mann, M., and Hurt, E. (1998). A novel complex of membrane proteins required for formation of a spherical nucleus. Embo j 17:6449-6464.

Skamnioti, P., Furlong, R.F., and Gurr, S.J. (2008). Evolutionary history of the ancient cutinase family in five filamentous Ascomycetes reveals differential gene duplications and losses and in *Magnaporthe grisea* shows evidence of sub- and neo-functionalization. The New phytologist 180:711-721.

Skamnioti, P., and Gurr, S.J. (2007). *Magnaporthe grisea* Cutinase2 mediates appressorium differentiation and host penetration and is required for full virulence. The Plant Cell Online 19:2674-2689.

Smolka, M.B., Chen, S.H., Maddox, P.S., Enserink, J.M., Albuquerque, C.P., Wei, X.X., Desai, A., Kolodner, R.D., and Zhou, H. (2006). An FHA domain-mediated protein interaction network of Rad53 reveals its role in polarized cell growth. J Cell Biol 175:743-753.

Soanes, D.M., Chakrabarti, A., Paszkiewicz, K.H., Dawe, A.L., and Talbot, N.J. (2012). Genome-wide transcriptional profiling of appressorium development by the rice blast fungus *Magnaporthe oryzae*. PLoS pathogens 8:e1002514.

Soanes, D.M., Kershaw, M.J., Cooley, R.N., and Talbot, N.J. (2002). Regulation of the MPG1 hydrophobin gene in the rice blast fungus *Magnaporthe grisea*. Molecular plant-microbe interactions : MPMI 15:1253-1267.

Sorger, P.K., and Murray, A.W. (1992). S-phase feedback control in budding yeast independent of tyrosine phosphorylation of P34cdc28. Nature 355:365-368.

Southern, E.M. (1975). Detection of specific sequences among DNA fragments separated by gel electrophoresis. Journal of molecular biology 98:503-517.

Steinberg, G. (1997). A kinesin-like mechanoenzyme from the zygomycete *Syncephalastrum racemosum* shares biochemical similarities with conventional kinesin from *Neurospora crassa*. European journal of cell biology 73:124-131.

Strahl, T., and Thorner, J. (2007). Synthesis and function of membrane phosphoinositides in budding yeast, *Saccharomyces cerevisiae*. Biochimica et biophysica acta 1771:353-404.

Strange, R.N., and Scott, P.R. (2005). Plant disease: a threat to global food security. Annu Rev Phytopathol 43:83-116.

Su, T.C., Tamarkina, E., and Sadowski, I. (2010). Organizational constraints on Ste12 cis-elements for a pheromone response in *Saccharomyces cerevisiae*. The FEBS journal 277:3235-3248.

Sun, L.L., Li, M., Suo, F., Liu, X.M., Shen, E.Z., Yang, B., Dong, M.Q., He, W.Z., and Du, L.L. (2013). Global analysis of fission yeast mating genes reveals new autophagy factors. PLoS genetics 9:e1003715.

Sun, M., and Fasullo, M. (2007). Activation of the budding yeast securin Pds1 but not Rad53 correlates with double-strand break-associated G2/M cell cycle arrest in a mec1 hypomorphic mutant. Cell Cycle 6:1896-1902.

Sweigard, J.A., Carroll, A.M., Farrall, L., Chumley, F.G., and Valent, B. (1998). *Magnaporthe grisea* pathogenicity genes obtained through insertional mutagenesis. Molecular plant-microbe interactions : MPMI 11:404-412.

Sweigard, J.A., Chumley, F.G., and Valent, B. (1992). Disruption of a *Magnaporthe grisea* cutinase gene. Molecular & general genetics : MGG 232:183-190.

Takahashi T, M.H., Yoneda S, Ohtaki S, Yamagata Y, Hasegawa F, Gomi K, Nakajima T, Abe K. . (2005). The fungal hydrophobin RolA recruits polyesterase and laterally moves on hydrophobic surfaces. Mol Microbiol 57:1780‐1796.

Takano, Y., Kikuchi, T., Kubo, Y., Hamer, J.E., Mise, K., and Furusawa, I. (2000). The *Colletotrichum lagenarium* MAP kinase gene CMK1 regulates diverse aspects of fungal pathogenesis. Molecular plant-microbe interactions : MPMI 13:374-383.

Takano, Y., Kubo, Y., Kuroda, I., and Furusawa, I. (1997). Temporal transcriptional pattern of three melanin biosynthesis genes, PKS1, SCD1, and THR1, in appressorium-differentiating and nondifferentiating conidia of *Colletotrichum lagenarium*. Applied and environmental microbiology 63:351-354.

Takeshita, N., Manck, R., Grun, N., de Vega, S.H., and Fischer, R. (2014). Interdependence of the actin and the microtubule cytoskeleton during fungal growth. Curr Opin Microbiol 20:34-41.

Talbot, N.J. (2003). On the trail of a cereal killer: Exploring the biology of *Magnaporthe grisea*. Annual review of microbiology 57:177-202.

Talbot, N.J., Ebbole, D.J., and Hamer, J.E. (1993). Identification and characterization of MPG1, a gene involved in pathogenicity from the rice blast fungus *Magnaporthe grisea*. The Plant cell 5:1575-1590.

Talbot, N.J., Kershaw, M.J., Wakley, G.E., De Vries, O., Wessels, J., and Hamer, J.E. (1996). MPG1 encodes a fungal hydrophobin involved in surface interactions during infection-related development of *Magnaporthe grisea*. The Plant cell 8:985-999.

Thines, E., Weber, R.W., and Talbot, N.J. (2000). MAP kinase and protein kinase A-dependent mobilization of triacylglycerol and glycogen during appressorium turgor generation by *Magnaporthe grisea*. The Plant cell 12:1703-1718.

Thinlay, X., Finckh, M.R., Bordeos, A.C., and Zeigler, R.S. (2000). Effects and possible causes of an unprecedented rice blast epidemic on the traditional farming system of Bhutan. Agriculture, Ecosystems & Environment 78:237-248.

Todd, R.B., and Andrianopoulos, A. (1997). Evolution of a fungal regulatory gene family: the Zn(II)2Cys6 binuclear cluster DNA binding motif. Fungal genetics and biology : FG & B 21:388-405.

Trapnell, C., Williams, B.A., Pertea, G., Mortazavi, A., Kwan, G., van Baren, M.J., Salzberg, S.L., Wold, B.J., and Pachter, L. (2010). Transcript assembly and quantification by RNA-Seq reveals unannotated transcripts and isoform switching during cell differentiation. Nature biotechnology 28:511-515.

Tsuji, G., Fujii, S., Tsuge, S., Shiraishi, T., and Kubo, Y. (2003). The *Colletotrichum lagenarium* Ste12-Like gene CST1 is essential for appressorium penetration. Molecular Plant-Microbe Interactions 16:315-325.

Tsuji, G., Kenmochi, Y., Takano, Y., Sweigard, J., Farrall, L., Furusawa, I., Horino, O., and Kubo, Y. (2000). Novel fungal transcriptional activators, Cmr1p of *Colletotrichum lagenarium* and

pig1p of *Magnaporthe grisea*, contain Cys2His2 zinc finger and Zn(II)2Cys6 binuclear cluster DNA-binding motifs and regulate transcription of melanin biosynthesis genes in a developmentally specific manner. Mol Microbiol 38:940-954.

Tucker, S.L., and Talbot, N.J. (2001). Surface attachment and pre-penetration stage development by plant pathogenic fungi. Annu Rev Phytopathol 39:385-417.

Turunen, O., Wahlstrom, T., and Vaheri, A. (1994). Ezrin has a COOH-terminal actin-binding site that is conserved in the ezrin protein family. J Cell Biol 126:1445-1453.

Urban, M., Kahmann, R., and Bolker, M. (1996). Identification of the pheromone response element in *Ustilago maydis*. Molecular & general genetics : MGG 251:31-37.

Urbanek, Agnieszka N., Smith, Adam P., Allwood, Ellen G., Booth, Wesley I., and Ayscough, Kathryn R. (2013). A novel actin-binding motif in Las17/WASP nucleates actin filaments independently of Arp2/3. Current Biology 23:196-203.

Valent, B., and Chumley, F.G. (1991). Molecular genetic analysis of the rice blast fungus, *Magnaporthe grisea*. Annu Rev Phytopathol 29:443-467.

Van Peij, N.N.M.E., Visser, J., and De Graaff, L.H. (1998). Isolation and analysis of xlnR, encoding a transcriptional activator co-ordinating xylanolytic expression in *Aspergillus niger*. Molecular Microbiology 27:131-142.

Veneault-Fourrey, C., Barooah, M., Egan, M., Wakley, G., and Talbot, N.J. (2006). Autophagic fungal cell death is necessary for infection by the rice blast fungus. Science 312:580-583.

Wakabayashi, M., Ishii, C., Inoue, H., and Tanaka, S. (2008). Genetic analysis of CHK1 and CHK2 homologues revealed a unique cross talk between ATM and ATR pathways in *Neurospora crassa*. DNA repair 7:1951-1961.

Walworth, N., Davey, S., and Beach, D. (1993). Fission yeast chk1 protein kinase links the rad checkpoint pathway to cdc2. Nature 363:368-371.

Wang, H., Liu, D., Wang, Y., Qin, J., and Elledge, S.J. (2001). Pds1 phosphorylation in response to DNA damage is essential for its DNA damage checkpoint function. Genes & Development 15:1361-1372.

Wang, Z.Y., Soanes, D.M., Kershaw, M.J., and Talbot, N.J. (2007). Functional analysis of lipid metabolism in *Magnaporthe grisea* reveals a requirement for peroxisomal fatty acid beta-oxidation during appressorium-mediated plant infection. Molecular plant-microbe interactions : MPMI 20:475-491.

Watts, H.J., Very, A.A., Perera, T.H., Davies, J.M., and Gow, N.A. (1998). Thigmotropism and stretch-activated channels in the pathogenic fungus *Candida albicans*. Microbiology 144 (Pt 3):689-695.

Wild, A.C., Yu, J.W., Lemmon, M.A., and Blumer, K.J. (2004). The p21-activated Protein Kinase-related Kinase Cla4 Is a coincidence detector of signaling by Cdc42 and phosphatidylinositol 4-Phosphate. Journal of Biological Chemistry 279:17101-17110.

Wilson, R.A., Gibson, R.P., Quispe, C.F., Littlechild, J.A., and Talbot, N.J. (2010). An NADPH-dependent genetic switch regulates plant infection by the rice blast fungus. Proceedings of the National Academy of Sciences 107:21902-21907.

Wilson, R.A., and Talbot, N.J. (2009). Under pressure: investigating the biology of plant infection by *Magnaporthe oryzae*. Nat Rev Micro 7:185-195.

Woloshuk, C.P., Sisler, H.D., and Vigil, E.L. (1983). Action of the antipenetrant, tricyclazole, on appressoria of *Pyricularia oryzae*. Physiological Plant Pathology 22:245-IN221.

Wong Sak Hoi, J., Herbert, C., Bacha, N., O'Connell, R., Lafitte, C., Borderies, G., Rossignol, M., Rouge, P., and Dumas, B. (2007). Regulation and role of a STE12-like transcription factor from the plant pathogen *Colletotrichum lindemuthianum*. Mol Microbiol 64:68-82.

Xu, J.-R., Staiger, C.J., and Hamer, J.E. (1998). Inactivation of the mitogen-activated protein kinase Mps1 from the rice blast fungus prevents penetration of host cells but allows activation of plant defense responses. Proceedings of the National Academy of Sciences 95:12713-12718.

Xu, J.R., and Hamer, J.E. (1996). MAP kinase and cAMP signaling regulate infection structure formation and pathogenic growth in the rice blast fungus *Magnaporthe grisea*. Genes Dev 10:2696-2706.

Xue, C., Park, G., Choi, W., Zheng, L., Dean, R.A., and Xu, J.R. (2002). Two novel fungal virulence genes specifically expressed in appressoria of the rice blast fungus. The Plant cell 14:2107-2119.

Yang, S.-H., Sharrocks, A.D., and Whitmarsh, A.J. (2003). Transcriptional regulation by the MAP kinase signaling cascades. Gene 320:3-21.

Yarbro, J.W. (1992). Mechanism of action of hydroxyurea. Seminars in oncology 19:1-10.

Ye, W., Chen, X., Zhong, Z., Chen, M., Shi, L., Zheng, H., Lin, Y., Zhang, D., Lu, G., Li, G., et al. (2014). Putative RhoGAP proteins orchestrate vegetative growth, conidiogenesis and pathogenicity of the rice blast fungus *Magnaporthe oryzae*. Fungal genetics and biology : FG & B 67:37-50.

Yoshida, K., Saitoh, H., Fujisawa, S., Kanzaki, H., Matsumura, H., Yoshida, K., Tosa, Y., Chuma, I., Takano, Y., Win, J., et al. (2009). Association genetics reveals three novel avirulence genes from the rice blast fungal pathogen *Magnaporthe oryzae*. The Plant cell 21:1573-1591.

Yoshida, S., Ohya, Y., Nakano, A., and Anraku, Y. (1994). Genetic interactions among genes involved in the STT4-PKC1 pathway of *Saccharomyces cerevisiae*. Molecular & general genetics : MGG 242:631-640.

Zeng, Y., Forbes, K.C., Wu, Z., Moreno, S., Piwnica-Worms, H., and Enoch, T. (1998). Replication checkpoint requires phosphorylation of the phosphatase Cdc25 by Cds1 or Chk1. Nature 395:507-510.

Zhang, H., Xue, C., Kong, L., Li, G., and Xu, J.R. (2011). A Pmk1-interacting gene is involved in appressorium differentiation and plant infection in *Magnaporthe oryzae*. Eukaryotic cell 10:1062-1070.

Zhao, X., Kim, Y., Park, G., and Xu, J.R. (2005). A mitogen-activated protein kinase cascade regulating infection-related morphogenesis in *Magnaporthe grisea*. The Plant cell 17:1317-1329.

Zhao, X., and Xu, J.R. (2007). A highly conserved MAPK-docking site in Mst7 is essential for Pmk1 activation in *Magnaporthe grisea*. Mol Microbiol 63:881-894.

Zheng, W., Zhao, X., Xie, Q., Huang, Q., Zhang, C., Zhai, H., Xu, L., Lu, G., Shim, W.B., and Wang, Z. (2012). A conserved homeobox transcription factor Htf1 is required for phialide development and conidiogenesis in *Fusarium* species. PloS one 7:e45432.

Zheng, W., Zhao, Z., Chen, J., Liu, W., Ke, H., Zhou, J., Lu, G., Darvill, A.G., Albersheim, P., Wu, S., et al. (2009). A Cdc42 ortholog is required for penetration and virulence of *Magnaporthe grisea*. Fungal genetics and biology : FG & B 46:450-460.

Zhou, B.-B.S., and Elledge, S.J. (2000). The DNA damage response: putting checkpoints in perspective. Nature 408:433-439.

Zhou, X., Liu, W., Wang, C., Xu, Q., Wang, Y., Ding, S., and Xu, J.R. (2011). A MADS-box transcription factor MoMcm1 is required for male fertility, microconidium production and virulence in *Magnaporthe oryzae*. Mol Microbiol 80:33-53.